THE DEVELOPMENT OF PRECAST CONCRETE BEAM-COLUMN CONNECTION JOINT USING ULTRA-HIGH PERFORMANCE CONCRETE (UHPC)

KRAIRERK AIAMSRI

A Thesis Submitted in Partial Fulfillment of the Requirements for the Degree of
Doctor of Philosophy in Civil Engineering and Construction Management
Suranaree University of Technology
Academic Year 2025

การพัฒนาจุดต่อองค์อาคารคาน-เสาคอนกรีตสำเร็จรูป ที่ใช้คอนกรีตสมรรถนะสูงพิเศษ

นายไกรฤกษ์ เอี่ยมศรี

วิทยานิพนธ์นี้เป็นส่วนหนึ่งของการศึกษาตามหลักสูตรปริญญาปรัชญาดุษฎีบัณฑิต
สาขาวิชาวิศวกรรมโยธาและการบริหารงานก่อสร้าง
มหาวิทยาลัยเทคโนโลยีสุรนารี
ปีการศึกษา 2568

THE DEVELOPMENT OF PRECAST CONCRETE BEAM-COLUMN CONNECTION JOINT USING ULTRA-HIGH PERFORMANCE CONCRETE (UHPC)

Suranaree University of Technology has approved this thesis submitted in partial fulfillment of the requirements for the Degree of Doctor of Philosophy

Thesis Examining Committee

.....

(Assoc. Prof. Dr.Cherdsak Suksiripattanapong)
Chairperson

.....

(Prof. Dr.Suksun Horpibulsuk)
Member (Thesis Advisor)

.....

(Dr.Teerasak Yaowarat)
Member (Thesis Co-Advisor)

.....

(Assoc. Prof. Dr.Menglim Hoy)
Member

.....

(Dr.Apichat Suddeepong)
Member

.....

(Dr.Apinun Buritatum)
Member

.....

(Dr.Kongsak Akkharawongwhatthana)
Member

.....

(Assoc. Prof. Dr.Yupaporn Ruksakulpiwat)
Vice Rector for Academic Affairs
and Quality Assurance

.....

(Assoc. Prof. Dr.Pornsiri Jongkol)
Dean of institute of Engineering

ไกรฤกษ์ เอี่ยมศรี : การพัฒนาจุดต่อองค์อาคารคาน-เสาคอนกรีตสำเร็จรูปที่ใช้คอนกรีตสมรรถนะสูงพิเศษ (THE DEVELOPMENT OF PRECAST CONCRETE BEAM-COLUMN CONNECTION JOINT USING ULTRA-HIGH PERFORMANCE CONCRETE (UHPC))
อาจารย์ที่ปรึกษา : ศาสตราจารย์ ดร.สุขสันติ์ หอพิบูลสุข, 154 หน้า

คำสำคัญ : คอนกรีตสมรรถนะสูงพิเศษ/กำลังยึดเหนียว/คอนกรีตสำเร็จรูป

วิทยานิพนธ์ฉบับนี้มีจุดประสงค์เพื่อพัฒนาจุดต่อองค์อาคารคาน-เสาคานสำเร็จรูป ซึ่งทำการทดสอบเปรียบเทียบกำลังยึดเหนียวของเหล็กเสริมในกรีตธรมมดา (NC) และคอนกรีตสมรรถนะสูงพิเศษ (UHPC) ที่ประกอบไปด้วยการทดสอบดึงออก การทดสอบแบบทาบของเหล็กเสริมแบบหักงอและไม่หักงอ ซึ่งมีประโยชน์อย่างยิ่งในการลดปริมาณเหล็กเสริมบริเวณจุดต่อองค์อาคารคาร-เสาคอนกรีตสำเร็จรูป รวมทั้งช่วยลดระยะเวลาในก่อสร้าง แต่คงไว้ซึ่งความแข็งแรง

บทที่หนึ่งและบทที่สองจะกล่าวถึงความเป็นมาของปัญหาและจุดประสงค์หลักของงานวิจัย สรุปข้อดีและข้อเสียของการก่อสร้างอาคารคอนกรีตสำเร็จรูป รวมทั้งผลงานวิจัยในอดีตที่เกี่ยวข้องกับคอนกรีตสมรรถนะสูงพิเศษ เส้นใยเหล็ก การรับแรงยึดเหนียวของเหล็กเสริมในคอนกรีต และกลไกการถ่ายแรงที่จุดต่อองค์อาคารคาน-เสาคอนกรีต

บทที่สามศึกษากำลังรับแรงยึดเหนียวจากทดสอบแบบดึงออก ของเหล็กเสริม DB12, 16 20 และ 25 ที่พารามิเตอร์ต่างๆ ได้แก่ เส้นผ่านศูนย์กลางเหล็กเสริม (D) ระยะห่างระหว่างเหล็กเสริม (s) ความยาวของระยะทาบ (L_1) และความยาวของระยะงอ (L_2) การศึกษาได้นำเสนอสมการในการคำนวณแรงยึดเหนียวของเหล็กเสริมที่ไม่ระยะทาบ ($s=\infty$) คือ $\tau_{bond} = 11.64\sqrt{(fc'/D)}$ ที่ระยะห่างระหว่างเหล็กเสริมได้พบว่าแรงยึดเหนียวเพิ่มขึ้นตามระยะห่างที่เพิ่มขึ้น โดยค่าแรงยึดเหนี่ยวสูงสุดที่เกิดที่ระยะห่างเหล็กเสริม S = 3 และต่ำสุดที่ระยะห่างเหล็กเสริม S = 1 จึงได้กำหนดตัวคูณลดสำหรับเหล็กเสริมที่มีการทาบสำหรับสมการข้างต้น 0.75 สำหรับคอนกรีตสมรรถนะสูงพิเศษ และ 0.6 สำหรับคอนกรีตทั่วไป การหักงอเสร็กเสริม พบว่ากำลังยึดเหนียวของเหล็กเสริมจะเพิ่มขึ้นเมื่อระยะห่างระหว่างเหล็กเสริม ความยาวระยะทาบ และความยาวของระยะหักงอ ที่เพิ่มขึ้น ที่ระยะทาบ $L_1 \geq 4D$ และระยะหักงอ $L_2 \geq 3D$ ให้ค่ากำลังยึดเหนียวของเหล็กเสริมมากกว่าแบบการทาบเหล็กเสริมแบบไม่หักงอ เนื่องจากระยะหักงอที่ยาวกว่า ทำให้มีผิวสัมผัสคอนกรีตที่มาก จึงลดความเข้มข้นของความเครียด จึงเกิดแรงยึดเหนียวที่เพิ่มขึ้น

บทที่สี่นำเสนอการทดสอบตัวอย่างเท่าขนาดจริงของจุดต่อคาน-เสาที่ก่อสร้างด้วยคอนกรีตสมรรถนะสูงพิเศษ (UHPC) โดยมีวัตถุประสงค์เพื่อยืนยันสมการแรงยึดเหนี่ยวและแนวทางออกแบบความยาวทาบของเหล็กเสริมดังที่เสนอไว้ในบทที่ 3 การทดสอบดำเนินการกับจุดต่อคาน-เสา 6 แบบภายใต้แรงกระทำแบบสถิตย์ โดยเปลี่ยนค่าความยาวทาบ (L_1 = 4D ถึง 9D) และความยาวหักงอ.(L_2 = 3D ถึง 4D) ผลการทดลองพบว่าจุดต่อที่มี $L_1 \geq 8D$ และระยะหักงอเพียงพอสามารถพัฒนาให้เหล็กเสริมเกิดการครากและขาดได้โดยไม่เกิดการวิบัติจากหน่วยแรงยึดเหนี่ยว แสดงถึงพฤติกรรมการวิบัติแบบเหนียว ขณะที่รอยต่อที่มีระยะทาบสั้นหรือไม่มีหักงอที่เพียงพอเกิดการวิบัติแบบเปราะก่อนเวลาตัวอย่างที่มีสมรรถนะดีที่สุดคือ LS9 (L_1 = 9D) ซึ่งสามารถยืนยันความถูกต้องของแบบจำลองได้ การศึกษานี้แสดงให้เห็นว่าหลักการออกแบบจากคอนกรีตเสริมเหล็กแบบทั่วไปไม่สามารถนำมาใช้กับคอนกรีตสมรรถนะสูงพิเศษได้โดยตรง และเน้นถึงความสำคัญของการออกแบบเฉพาะสำหรับจุดต่อที่ใช้คอนกรีตสมรรถนะสูงพิเศษเป็นวัสดุเชื่อมต่อเพื่อความปลอดภัยและประสิทธิภาพในการใช้งานจริง

บทที่ห้านำเสนอข้อสรุปของการศึกษาในครั้งนี้ รวมถึงข้อเสนอแนะสำหรับการศึกษาต่อในอนาคต การใช้คอนกรีตสมรรถนะสูงพิเศษ (UHPC) ในจุดต่อระหว่างคานและเสา แสดงให้เห็นถึงประโยชน์ในด้านประสิทธิภาพทางวิศวกรรม ความคุ้มค่าทางเศรษฐกิจในการก่อสร้าง และความทนทานของโครงสร้างในระยะยาว

สาขาวิชา วิศวกรรมโยธาและการบริหารงานก่อสร้าง ลายมือชื่อนักศึกษา .....

ปีการศึกษา 2568 ลายมือชื่ออาจารย์ที่ปรึกษา .....

ลายมือชื่ออาจารย์ที่ปรึกษาร่วม.....

KRAIRERK AIAMSRI : THE DEVELOPMENT OF PRECAST CONCRETE BEAM-COLUMN CONNECTION JOINT USING ULTRA-HIGH PERFORMANCE CONCRETE (UHPC). THESIS ADVISOR : PROF. SUKSUN HORPIBULSUK, Ph.D., 154 PP.

Keyword: ULTRA-HIGH PERFORMANCE CONCRETE (UHPC)/BOND STRENHTH/PRECAST

The objective of this thesis is to develop of precast concrete beam-column connections joint. This test compares the bond strength of reinforcement in normal concrete (NC) and ultra-high performance concrete (UHPC) with pull-out tests, lap-splice tests with and without hooks. This is especially useful in reducing the amount of reinforcing steel at the connection points of prefabricated concrete building elements and columns. Including reducing construction time but maintains strength.

The first and second chapters present the statement of the problems and the objectives of this study. Summary of advantages and disadvantages of precast concrete building construction. Including past research results related to ultra-high performance concrete, steel fibers, bond strength of reinforcement in concrete. and the force transfer mechanism at the concrete beam-column building member connection.

The third chapter studies the bond strength from pull-out tests. of reinforcement DB12, 16 20 and 25 where the parameters are rebar diameter (D), spacing (s), lap-splice length (L_1), and hook length (L_2). The study presents an equation for calculating the bond strength of pull-out test ($s=\infty$) which is $\tau_{bond} = 11.64\sqrt{(fc'/D)}$. At the distance between the reinforcement bars, it was found that the cohesive strength increased with increasing distance. The highest bond strength occurred at the reinforcement spacing S = 3 and the lowest at the reinforcement spacing S = 1 . The reduction factor for spacing reinforcement has been determined for the above equation to be 0.75 for ultra-high performance concrete and 0.6 for normal concrete. The hook length of the reinforcement revealed that the bond strength of the reinforcement increases with the spacing the reinforcement lap-splice length (L_1) and

the hook length (L_2) increased. At the lap-splice length $L_1 \geq 4D$ and hook length $L_2 \geq 3D$, the bond strength of the reinforcement is higher than that of the pull-out test ($s=\infty$). Due to the longer bend distance, there is a greater surface contact with the concrete. Thus, reducing the concentration of stress. As a result, the cohesive strength increases.

Fourth chapter presents a full-scale experimental study on beam-column joints constructed with ultra-high-performance concrete (UHPC) to validate a proposed bond strength equation and splice length design scheme. Six connection configurations were tested under static loading, with varying lap splice lengths (L_1 = 4D to 9D) and hook lengths (L_2 = 3D to 4D). The results demonstrated that joints with $L_1 \geq 8D$ and sufficient hook length could develop yielding and even bar rupture without slippage, indicating ductile failure. In contrast, joints with short splices or inadequate hook anchorage experienced premature bond failure. The best performance was observed in the LS9 specimen (L_1 = 9D), which confirmed the model's accuracy. This investigation highlights that RC-based design principles cannot be directly applied to UHPC due to different bond characteristics, and confirms that UHPC-specific detailing is essential for ensuring safe and efficient structural connections.

The fifth chapter presents the conclusions of this study. The recommendations for future work were also presented in this chapter. The use of Ultra-High-Performance Concrete (UHPC) in beam-column joint applications proves to be beneficial in terms of engineering efficiency, construction economy, and long-term structural durability.

School of Civil Engineering and Construction Management
Academic Year 2025

Student's Signature .....
Advisor's Signature .....
Co-advisor's Signature .....

ACKNOWLEDGEMENTS

First and foremost, I wish to express my sincere and profound gratitude to my advisor, Professor Dr.Suksun Horpibulsuk, and co-advisor, Dr.Teerasak Yaowarat, for their unwavering support, insightful guidance, and consistent encouragement throughout my Ph.D. studies. Their exceptional expertise, academic discipline, and leadership in the fields of structural and geotechnical engineering have been a constant source of inspiration to me, both professionally and personally. It has been a distinct honor and privilege to conduct my research under their mentorship. I firmly believe that pursuing a Ph.D. in Civil Engineering and Construction Management at Suranaree University of Technology has been one of the most rewarding and impactful decisions of my academic and professional life.

I would also like to sincerely thank the members of my thesis examination committee, Associate Professor Dr.Cherdsak Suksiripattanapong, Associate Professor Dr.Menglim Hoy, Dr.Apinun Buritatum, Dr.Apichat Suddeepong, and Dr.Kongsak Akkharawongwhatthana, for their thoughtful comments, constructive feedback, and valuable suggestions that strengthened the quality of this thesis. Special appreciation is extended to Suranaree University of Technology for providing the academic environment, facilities, equipment, and financial support that made this research possible. I am also grateful for the scholarship and resources offered by the university throughout the course of my study.

This research was generously funded by Concrete Products and Aggregate Co., Ltd. (CPAC), a distinguished subsidiary of the Siam Cement Group (SCG), renowned for its commitment to excellence in the production and supply of high-quality concrete products in Thailand. I wish to express my deepest appreciation to CPAC for their

invaluable financial support, which significantly contributed to the successful execution of the experimental program and the overall advancement of this study.

My thanks also go to the laboratory staff, technical officers, and fellow researchers, particularly Mr.Nantipat Pongsri for their assistance, collaboration, and encouragement during the experimental and analytical phases of the research.

Finally, I would like to express my heartfelt thanks to my beloved family. Their unconditional love, endless patience, and unwavering support were my source of strength through every challenge. Without their encouragement and understanding, this journey would not have been possible.

Krairerk Aiamsri

TABLE OF CONTENTS

Page

TABLE OF CONTENTS (Continued)

Page

TABLE OF CONTENTS (Continued)

Page

LIST OF TABLES

Table **Page**

LIST OF FIGURES

Figure **Page**

LIST OF FIGURES (Continued)

Figure **Page**

LIST OF FIGURES (Continued)

Figure **Page**

LIST OF FIGURES (Continued)

Figure **Page**

LIST OF ABBREVIATIONS

DB12, DB16, DB20, DB25	Deformed bars with diameters of 12, 16, 20, and 25 mm
D	Diameter of reinforcing bar (mm)
s	Spacing between reinforcing bars (center-to-center)
L_1	Lap splice length of rebar
L_2	Hook length of rebar
L_e	Embedment length of rebar into concrete
τ_{bond}	Bond strength between rebar and concrete (MPa)
f'_c	Compressive strength of concrete (MPa)
f_s	Tensile stress in reinforcing steel (MPa)
f_u	Ultimate tensile strength of rebar (MPa)
A_s	Cross-sectional area of rebar
$A_{surface}$	Bond surface area of embedded rebar (πDL)
L_d	Development length (required embedment length for full stress transfer)
σ_{av}	Average tensile stress in rebar
E	Elastic modulus of concrete (GPa)
Poisson's ratio	Lateral strain ratio of concrete
V_n	Nominal shear strength (kN)
V_c	Concrete contribution to shear strength
V_s	Shear strength contribution from stirrups
RB6, RB9	Stirrups with 6 mm and 9 mm diameter
PC-UP01, Type D	Chemical admixtures used in UHPC mix
UHPC	Ultra-High-Performance Concrete
NC	Normal Concrete

LIST OF ABBREVIATIONS (Continued)

TCIP	Traditional Cast-In-Place concrete joint
LS8, LS9	Lap splice lengths of 8D and 9D, respectively
LE4	Embedment length of 4D
H3, H4	Hook lengths of 3D and 4D, respectively
k	Reduction factor due to hook length

CHAPTER I

INTRODUCTION

1.1 Statement of the problem

Over the past 30 years, there has been a significant increase in the use of precast concrete for structural components in buildings in Thailand. This trend can be attributed primarily to the high quality control of precast elements, reduction in on-site formwork, decreased site possession time, and a notable increase in construction speed. The mid to late 1980s marked a significant turning point with substantial growth in the utilization of precast concrete in moment resisting frames and structural walls. Presently, precast seismic frames, walls, and flooring systems have become the standard practice for building construction throughout Thailand.

Outside of thailand, there have been reports indicating poor performance of moment resisting frames and structural walls incorporating precast concrete elements during earthquakes (Hall, 1994; Wyllie and Filson, 1989). It is widely believed that the inadequate seismic performance of these precast frames and walls is attributed to several factors. These include the brittle (non-ductile) behavior of connection details between precast concrete elements, insufficient detailing of components, and outdated design concepts.

The capacity design for monolithic concrete structures, which ensures the achievement of adequate ductility, was developed by Thailand engineers and researchers. This design approach was summarized in a report by the Thailand National Society for Earthquake Engineering in the 1970s (Park, 2002). The main goal of implementing the capacity design in structures for earthquake resistance is to ensure that the structure possesses a reliable capacity to accommodate significant displacements caused by earthquakes and, thereby, prevent collapse even under severe seismic events.

During the 1980s, there was a gradual shift from cast-in-place construction to precast construction in New Zealand. The precast construction method adopted in New Zealand largely emulates the characteristics of monolithic (cast-in-place) construction, with the placement of Plastic Hinge (PH) zones at the beam-ends, away from precast connections.

The recent earthquakes, such as Northridge 1994 and Kobe 1995, have not only confirmed the effectiveness of capacity design techniques in preventing structural collapse but have also revealed the potential for extensive damage. As a result of the significant damage to buildings and infrastructure, substantial economic losses were incurred due to repair work and downtime. This has led to an increased demand from clients and the public for engineers to prioritize structural systems that are designed to prioritize life-safety as the primary objective. There is also a strong emphasis on limiting the cost of repairing or reinstating the damaged structures.

In 1990, research on the prestress seismic structure system (PRESSS) was initiated in the United States. Early findings of the PRESSS, as reported by Cheok and Lew (1993), Stone et al. (1995), Priestley and MacRae (1996), and Priestley et al. (1999), demonstrated that precast concrete frames constructed from prestressed segmental elements exhibited significantly better performance than conventional frames when subjected to lateral loading. Structural deformations were accommodated through gap openings at the joints of precast components. Despite achieving similar strength and interstorey drift capacities, the damage to structural elements was considerably reduced, and the frames demonstrated re-centring capabilities that resulted in negligible residual displacement.

In 1997, Mander and Chang introduced the concepts of rapid jointed precast construction and Damage Avoidance Design (DAD). They proposed innovative techniques to enhance the performance of precast structures. One key aspect was the use of steel armoring at the member ends, which effectively mitigated high stress concentrations in the concrete and prevented crushing and splitting. Experimental studies on rocking bridge columns confirmed that this approach significantly reduced damage. Additionally, the presence of unbonded prestress allowed for re-centering of

the system, further enhancing its performance and resilience during cyclic loading. These advancements in precast construction and the implementation of DAD principles contributed to the avoidance of extensive damage and improved the overall performance of precast structures.

Applying the principles of Damage Avoidance Design (DAD) to jointed building frames, Davies (2004) and Arnold (2004) conducted studies demonstrating that specially designed steel-to-steel connections at the beam-to-column interface can effectively prevent damage to precast components even at high drift levels of up to 3%. These connections are designed to allow for safe transfer of high contact forces from the end steel plate into the concrete during rocking action. However, the design of these connections often necessitates extensive welding to secure the steel end plates to the reinforcing bars. Additionally, there is little room for tolerance in the manufacturing process of these precast segments, as precise lengths are required to ensure adequate force transfer through the jointed connection.

1.2 Objectives of the study

1.2.1 To investigate the bond strength of steel rebars in both Normal Concrete (NC) and Ultra-High Performance Concrete (UHPC).

1.2.2 To conduct an investigation on the bond strength of lap-spliced rebars, comparing those with and without hooks, in both Normal Concrete (NC) and Ultra-High Performance Concrete (UHPC).

1.2.3 To undertake a comprehensive examination of the connection performance in precast concrete beam-column members utilizing Ultra-High-Performance Concrete (UHPC) on a full-scale level, subject to static loading conditions.

1.3 Organization of the dissertation

This thesis consists of four chapters and outlines of each chapter are presented as follows:

Chapter I presents an overview of the research by addressing the problem statement, stating the study objectives, and outlining the organization of the dissertation.

Chapter II presents a comprehensive review of Ultra-High Performance Concrete (UHPC), steel fibers, the bonding behavior of steel in concrete, and the behavior of buildings, beams-columns, and concrete.

Chapter III presents an The tests include pull-out tests, lap-splice tests with and without hooks, and an analysis of various parameters such as rebar diameter (D), spacing (s), lap-splice length (L1), and hook length (L2) using steel DB12, 16, 20, and 25 mm.

Chapter IV concludes the findings of the present study and offers suggestions for potential topics of further investigation.

1.4 References

Arnold, D.M (2004). Development and Experimental Testing Of a Seismic Damage Avoidance Designed Beam to Column Connection Utilising Draped Unbonded PostTensioning Masters, Thesis, Department of civil Engineering, University of Canterbury, Christchurch, New Zealand.

Cheok, G.S. and Lew, H.S. (1991), Performance of precast concrete beam to column connections subject to cyclic loading. PCI journal, Vol. 36, No.3, pp56-67.

Cheok, G.S, Stone, W.C. and Kunnath, S.K (1998), Seismic Response of Precast Concrete Frames with Hybrid Connections. ACI Structural Journal, V.95, No5, pp527- 539.

Davies, M.N (2004) Seismic Damage Avoidance Design of Beam-Column Joints using Unbonded Post-Tensioning: Theory, Experiments and Design Example. Masters, Thesis, Department of civil Engineering, University of Canterbury, Christchurch, New Zealand.

EI-Sheikh, M., Sause, R., Pessiki, S. and Lu, L.-W. (1999), Seismic Behaviour and Design of Unbonded Post-Tensioned Precast Concrete Frames. PCI journal, v44, No3 1999, P54-71.

Elgawady, M., Ma, Q., Ingham, J., and Butterworth, J. (2005) Experimental Investigation of Rigid Body Rocking The New Zealand Concrete Industry Conference, Auckland, NewZealand.

Hall, J.F.(Editor) "Northridge Earthquake of January 17, 1994, Reconnaissance Report Vol.2." Supplement to Vol.11, Earthquake Spectra, 1995.

Holden, T.J., Restrepo, J.I., Mander, J.B. (2003). Seismic Performance of Precast Reinforced and Prestressed Concrete Walls, Journal of Structural Engineering, Vol.129, No. 3, pp 286-296.

Houser, G.W (1963). "The Behaviour of Inverted Pendulum Structure during Earthquakes, Bulletin of the Seismological Society of America, vol. 53, No.2, pp. 403- 417, February 1963.

Kurama, Y., Sause, R., Pessiki, S., and Lu, W-L (1999) Lateral load Behaviour and Seismic Design of Unbonded Post-Tensioned Precast Concrete Walls. ACI structural Journal, vol.96, No.4, pp622-632.

Ma, Q.T. Wight, G.D. Butterworth, J.W. and. Ingham, J.M. (2005), Predicting the InPlane Rocking Behaviour of Post-Tensioned Concrete Walls Subjected to Earthquake Excitations, The New Zealand Concrete Industry Conference, Auckland 2005.

Mander, J.B., and Cheng, C.T. (1997). Seismic Resistance of Bridge Piers Based on Damage Avoidance Design, Technical Report NCEER-97-0014, Department of Civil, Structural and Environmental Engineering, State University of New York at Buffalo, New York, USA.

Meek, J.W. (1975). Effects of Foundation Tipping on Dynamic Response, Journal of the Structure Division ASCE, vol.101, No. ST 7, July 1975, pp 1297-1311.

Morgen, B.G. and Kurama, Y.C. (2004) A Friction Damper For Post-Tensioned Precast Concrete Moment Frames, PCI journal, v49, n 4, July/August, , p112-133.

Murahidy, A.G, Carr, A.J, Spieth, H.A, Mander, J.B and Bull (2004), D.K. Design, construction and dynamic testing of a post-tensioned precast reinforced concrete frame building with rocking beam-column connections and ADAS elements. Paper 31, 2004 NZSEE conference.

Park, R (2002) Seismic Design and Construction of Precast Concrete Buildings in New Zealand, PCI journal vol.47,no.5, September/October,pp60-75.

Pampanin, S., Priestley, N.J., and Sritharan, S. (2001). Analytical modelling of the Seismic Behaviour of Precast Concrete Frames Designed with Ductile Connections, Journal of Earthquake Engineering, Vol.5, No.3, pp329-367.

Pampanin, S., Pagani, C., and Zambelli, S.,(2004) Cable-Stayed and Suspended posttensioned Solution for Precast Concrete Frames: The Brooklyn System. Proc of NZ Concrete Industry Conference, Queenstown.

Percassi, S.J.(2002). Rocking column Structures with Supplementary Damping Device, M.S.Thesis, State University of New York at Buffalo, New York, USA. Priestley, M.J.N. and MacRae, G.A., (1996). Seismic Tests of Precast Beam-to-Column Joint Subassemblages with Unbonded Tendons, PCI Journal, January/February, 1996, pp. 64-81.

Priestley, M.J.N., Sritharan, S., Conley, J.R., Pampanin, S. (1999). Preliminary Results and Conclusions from the PRESSS Five-Storey Precast Concrete Test Building, PCI Journal, Vol. 44, No. 6, pp 43-67.

Priestley, M.J.N. and Tao, J.R.T. (1993). Seismic Response of Precast Prestressed Concrete Frames with Partially Debonded Tendons, PCI Journal, vol. 38, no.1, p.58-69.

Rahman, A. and Restrepo, J.I., (2000) Earthquake Resistant Precast Concrete Buildings: Seismic Performance of Cantilever Walls Prestressed Using Unbonded Tendons. Research Report 2005-5, Department of Civil Engineering, University of Canterbury, New Zealand.

Surdarno, I., (2003). Performance of Thin Precast Concrete Wall Panels under Dynamic Loadings, ME thesis, University of Canterbury, New Zealand.

Spieth, H.A, Arnold, D. Davies, M., Mander, J.B, and Carr, A.J (2004). Modelling of post-tensioned precast reinforced concrete frame structure with rocking beam-column connections. Paper 32 2004 NZSEE conference.

Stanton, J.F., Stone, W.C. and Cheok, G.S. (1997). A Hybrid Reinforced Precast Frame for Seismic Regions, PCI Journal, vol. 42, pp. 20-32.

Tone, W.C., Cheok, G.S., and Stanton, J.F. (1995), Performance of hybrid momentresisting precast beam-column concrete connection subjected to cyclic loading, ACI Journal, Vol. 91, No, 2 March-April.

Toranzo-Dianderas,L.A.(2002). The use of rocking walls in Confined Masonry Structures: a Performance Based Approach, PHD. Thesis, Department of Civil Engineering, University of Canterbury, Christchurch, New Zealand.

Wyllie, L.A., and Filson, J.R., “Armenia Earthquake Reconnaissance Report” Earthquake Spectra, Special Supplement, EERI Pub. 89-101, Aug.1989, 175pp.

CHAPTER II

LITERATURE REVIEW

2.1 Introduction

The beam-column joints play a crucial role in transferring forces between beams and columns in a structure, particularly in reinforced concrete (RC) buildings. These joints are located at the intersections where portions of columns are shared by beams. Proper design and detailing of beam-column joints are essential for moment resisting frames, especially when the structure is subjected to earthquake loads. In a moment resisting frame, the beam-column joints are vital components that require careful attention. The exterior joint connects one beam to a vertical face of the column, while two other beams frame into the joint from perpendicular directions. Therefore, beam-column joints must be designed to effectively withstand the effects of earthquakes.

Figure 2.1 presents an example of the structural damage observed in beam-column joints of typical reinforced concrete (RC) framed buildings during the Kocaeli earthquake in 1999. The image illustrates that both the beam and column elements remained intact, while the joints suffered significant damage. A closer examination of the beam-column joint in **Figure 2.1.(b)** reveals inadequate anchorage length for the beam reinforcement within the joint area and the absence of transverse reinforcement. Conversely, **Figure 2.1.(c)** depicts a building under construction where transverse reinforcement in the joint region proves beneficial. The presence of horizontal ties in this scenario has helped preserve the integrity of the joint.

(a) Failure of beam-column joint (b) Close-up of beam-column joint failure
(Image source: http://nisee.berkeley.edu/elibrary/Image/IZT-673)

(c) Damage to beam-column joint of building under construction in Adapazari, Turkey
(Image source: http://nisee.berkeley.edu/elibrary/Image/IZT-749)

Figure 2.1. Damage to reinforced concrete moment framed building after Kocaeli earthquake, 1999 (Sezen et al. 2003 (Sezen, Whittaker, Elwood and Mosalam, 2003))

The incorporation of steel fibers in concrete can have significant positive effects on the strength, ductility, and energy absorption capacity of flexural members, especially in the context of earthquake effects. Steel Fiber Reinforced Ultra-High-Performance Concrete (SFRUHPC) exhibits higher tensile strain, even at the microstructure level, compared to conventional Fiber Reinforced Concrete (FRC). In

recent decades, there has been a growing emphasis on developing structural systems that are more efficient and better equipped to resist the effects of earthquakes. This has resulted in the adoption of the "strong column weak beam" theory, which highlights the importance of designing beam-column joints with earthquake effects in mind.

2.2 Ultra-High-Performance Concrete (UHPC)

Despite concrete being widely used in construction, it does have limitations, including low tensile strength and brittleness. However, there is a potential solution in the form of Ultra-High-Performance Concrete (UHPC), an advanced concrete technology that addresses these concerns. According to the Federal Highway Administration (FHWA), UHPC is a cementitious material that consists of Portland cement, fine silica sand, silica fume, quartz flour, high-range water reducer, and discontinuous internal steel or organic fibers. It has a water-to-cement (W/C) ratio of less than 0.25. UHPC offers exceptional compressive strength exceeding 21.7 ksi (150 MPa) and sustained post-cracking tensile strength surpassing 0.72 ksi (5 MPa) (Russell, Graybeal and Russell, 2013). The unique pore structure of UHPC minimizes liquid ingress, leading to significantly improved durability compared to conventional concrete (Graybeal, 2011).

Wille et al. (Wille, Naaman and Parra-Montesinos, 2011) conducted a study to investigate the mechanical properties of Ultra-High Performance Concrete (UHPC), both plain and fiber reinforced, using commercially available materials. In their research, they utilized silica fume, fine sand, and silica powder (glass powder) to enhance reactivity. Under moist curing conditions at 20°C, the highest compressive strength achieved for 2x2x4-inch (50x50x100 mm) size cubes was 29 ksi (201 MPa) for steel fiber reinforced UHPC and 27.8 ksi (192 MPa) for plain UHPC (**Figure 2.2**). For measuring flexural strength, they tested 4x4x16-inch (100x100x400 mm) prisms, and the highest flexural strength recorded was 2 ksi (13.95 MPa) for fiber reinforced UHPC and 1.1 ksi (7.5 MPa) for plain UHPC. Notably, specimens without fibers exhibited immediate

flexural failure after the first crack, highlighting the influence of fibers on the ductility of UHPC.

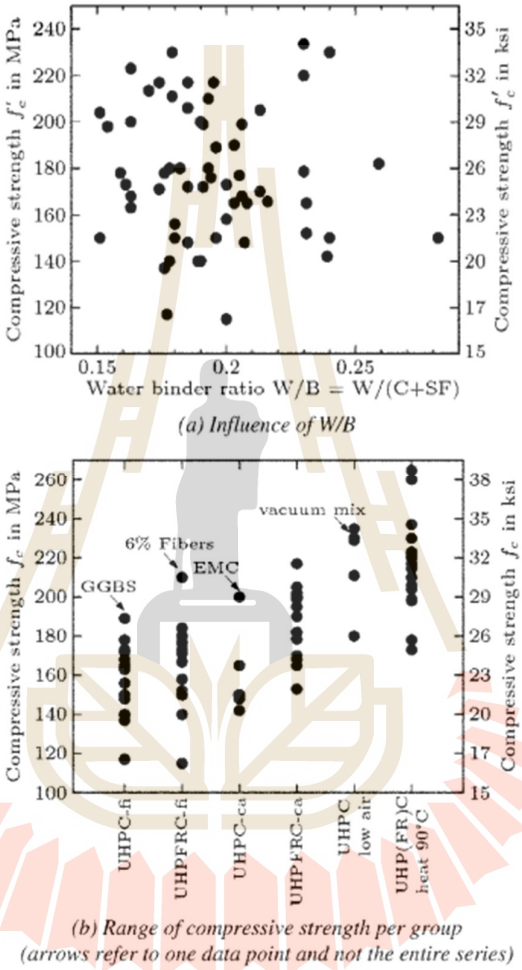

Figure. 2.2 Overview of UHPC compressive strength fc′, summarized from different authors (Wille et al. 2011)

Dili and Santhanam (Dili and Santhanam, 2004) conducted a study comparing the mechanical properties of Ultra-High Performance Concrete (UHPC) and High-Performance Concrete (HPC). For compressive strength testing, 2-inch (50 mm) cubes were subjected to wet curing at 90°C. The maximum compressive strength observed

for UHPC was 29 ksi (200 MPa). The researchers also investigated the flexural behavior of 1.6x1.6x6.4-inch (40x40x160 mm) prisms, both plain and fiber reinforced, in UHPC and HPC. The flexural strength of the fiber reinforced UHPC and HPC prisms was found to be higher than that of the plain prisms. Notably, the flexural strength of UHPC prisms was significantly greater than that of HPC prisms.\

2.3 Steel Fibers

Steel fibers (**Figure 2.3**) are commonly employed in concrete to enhance its ductility compared to conventional concrete. By incorporating fibers into the concrete mixture, the cracking behavior can be effectively controlled, and permeability can be reduced. The primary purpose of using fibers in concrete is to mitigate plastic shrinkage cracking and drying shrinkage cracking. By adding steel fibers, the concrete's resistance to cracking is increased, and the width of cracks is reduced.

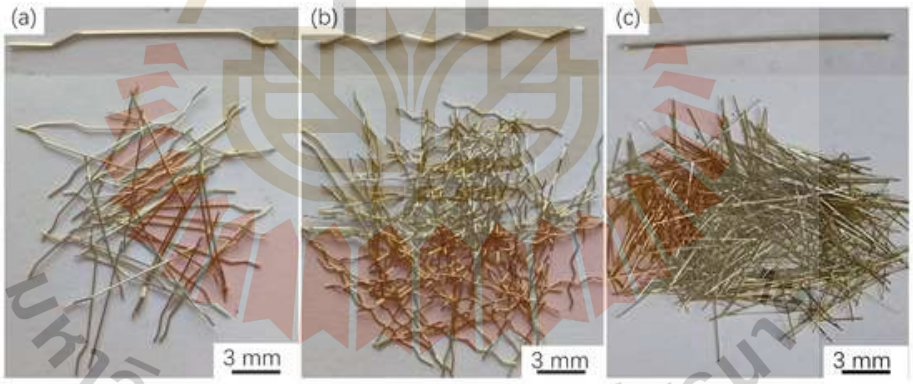

Figure 2.3 Types of the brass-coated steel fibers: (a) Hooked fibers, (b) Corrugated fiber, (c) Straight fiber. (Jiang et al. 2023, (Jiang, Yan, Li, Cao, Yu and Qi, 2023))

2.3.1 Uses of steel fibers

Steel fibers offer excellent resistance to cracking and crack propagation in concrete structures by increasing the tensile strength. They effectively reduce the occurrence of cracks under normal service conditions and enhance the structure's ability to withstand various forms of material deterioration, including fatigue, impact, shrinkage, and thermal stresses. By preventing or delaying the propagation of cracks from microcracks to larger cracks, steel fibers significantly improve the durability of concrete. Moreover, steel fibers exhibit exceptional resistance to repeated and shock loading. This makes them highly suitable for applications that involve frequent or sudden impact, such as pavements, tunnel linings, airport pavements, and repairs of bridge deck slabs.

In a study conducted by Beglarigale and Yalçınkaya (2014) (Beglarigale and Yalçınkaya, 2014), it was discovered that steel micro-fibers in Reactive Powder Concrete (RPC) serve to control the growth and delay the propagation of micro-cracks in bridge structures. Brass-coated steel micro-fibers exhibit strong adherence to the cement paste even with a low water-to-binder ratio. Furthermore, the tensile strength of brass-coated steel micro-fibers surpasses that of steel macro fibers. As the size of the steel fiber decreases, the number of fibers crossing a cracked section of concrete increases, illustrating the bridging effect of fibers under flexural loading, as depicted in **Figure 2.4**. Visual observations indicated that an increase in steel fiber dosage led to a higher number of ruptured fibers. In other words, the presence of steel fibers enhanced the bond between the fiber and the matrix.

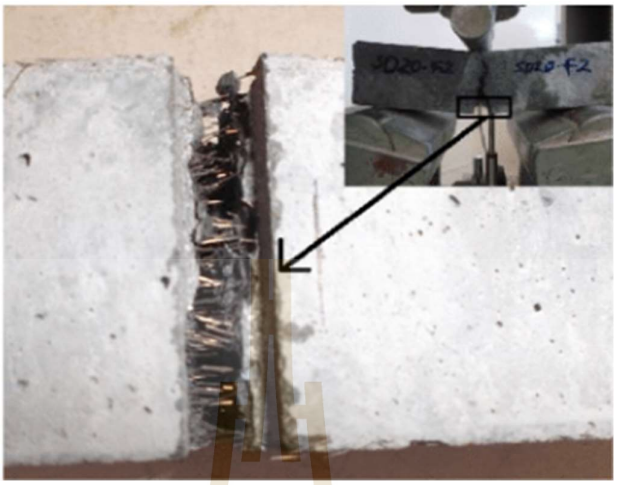

Figure 2.4 Crack bridging of steel micro-fibers (Beglarigale and Yalçınkaya, 2014)

2.3.2 Advantages of steel fibers

Steel fibers offer several advantages when used in concrete:

1) Increased tensile strength: Steel fibers enhance the tensile strength of concrete, making it more resistant to cracking and improving its overall structural integrity.

2) Improved ductility: Steel fibers increase the ductility of concrete, allowing it to deform and absorb energy without sudden failure. This makes the concrete more capable of withstanding loads and dynamic forces, such as those experienced during earthquakes or impact events.

3) Enhanced crack resistance: The presence of steel fibers helps to control crack propagation and reduce crack width in concrete. This improves the durability and longevity of structures by minimizing the effects of cracking, such as moisture ingress and corrosion of embedded reinforcement.

4) Better impact and fatigue resistance: Steel fibers significantly improve the resistance of concrete to impact loads and cyclic loading, such as those caused by heavy traffic or repeated loading/unloading. This makes it suitable for applications such as pavements, industrial floors, and structures subjected to dynamic loading.

5) Improved fire resistance: Steel fibers can enhance the fire resistance of concrete by providing additional reinforcement. They can help prevent spalling and maintain the structural integrity of the concrete under high-temperature conditions.

6) Increased construction speed: The use of steel fibers in concrete can accelerate the construction process by reducing the need for traditional reinforcement, such as steel bars or mesh. This can result in faster construction, cost savings, and reduced labor requirements.

Overall, the incorporation of steel fibers in concrete offers numerous advantages, including increased tensile strength, improved ductility, enhanced crack resistance, better impact and fatigue resistance, improved fire resistance, and potential construction efficiency gains.

2.4 Bonding Mechanisms of steel rebar and concrete

2.4.1 Steel rebar Embedded in Concrete

In Ultra-High-Performance Concrete (UHPC) structures, the bonding mechanism is expected to experience improvements proportional to the increase in tensile strength, corresponding to that of the compressive strength of the concrete. The incorporation of steel fibers further enhances the bonding mechanism by delaying crack opening and providing continued tensile strength once cracking initiates. As a result, the concrete maintains its bearing strength against lugs, even after the concrete enclosing lap splices splits. This behavior can be observed in **Figure 2.5.** In such cases, the bonding strength is predominantly reliant on the bearing strength of the concrete.

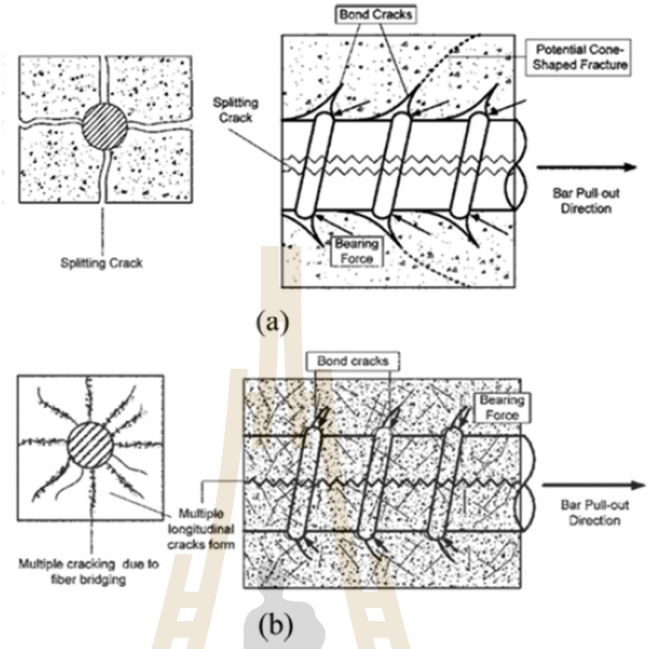

Figure 2.5. Comparison of Bonding Mechanisms (Chao et al., 2009 (Chao, Naaman and Parra-Montesinos, 2009)): (a) Conventional Concrete, (b) Fiber-reinforced Concrete

The bond relationship between concrete and steel bar reinforcement is a critical aspect of all reinforced concrete structures. However, the understanding of this behavior in Ultra-High Performance Concrete (UHPC) is currently limited, which poses a significant obstacle to the widespread adoption of this material. To address this research gap, the experimental program presented in this paper aimed to quantify the bond strength between UHPC and steel bar reinforcement across various influential design parameters. The findings of this study will contribute valuable insights towards advancing the understanding and application of UHPC in structural engineering.

The simple bar pull-out test is commonly employed to assess the bond capacity of concrete due to its simplicity and ease of implementation. However, it is recognized as the least accurate testing method by ACI Committee 408 (408, 1990), as it tends to overestimate the bond capacity. In the traditional pull-out test, the steel bar placed under tension induces compressive forces in the surrounding concrete as

it reacts against the rigid support surface of the specimen holder. In contrast, in most reinforced concrete structures subjected to flexural loading, both the steel bar reinforcement and concrete are under tension.

To mitigate the influence of the compressive region during testing, a modified method of supporting the concrete was implemented, as depicted in **Figure 2.6**. This approach, proposed by De Larrard and Sedran (De Larrard and Sedran, 1994), deviates from the traditional bar pull-out setup by utilizing the high bearing strength of UHPC to minimize the required support surface area. Four small steel plates were used to support the specimen, effectively isolating the concrete directly adjacent to the bar from any compressive struts that may form during loading. It is important to acknowledge that the distribution of bond stress between the rebar and concrete is not consistently uniform along the entire embedment length. However, to simplify the analysis, the average bond stress (τ_{av}) is calculated using Eq. (1) under the assumption of a uniform bond stress distribution.

$$\tau_{av} = \frac{P}{\pi D L} \quad \text{.....(1)}$$

where P is the pull-out load

D is the diameter of rebar

L is the embedment length of rebar (Yoo, Kwon, Park and Yoon, 2015).

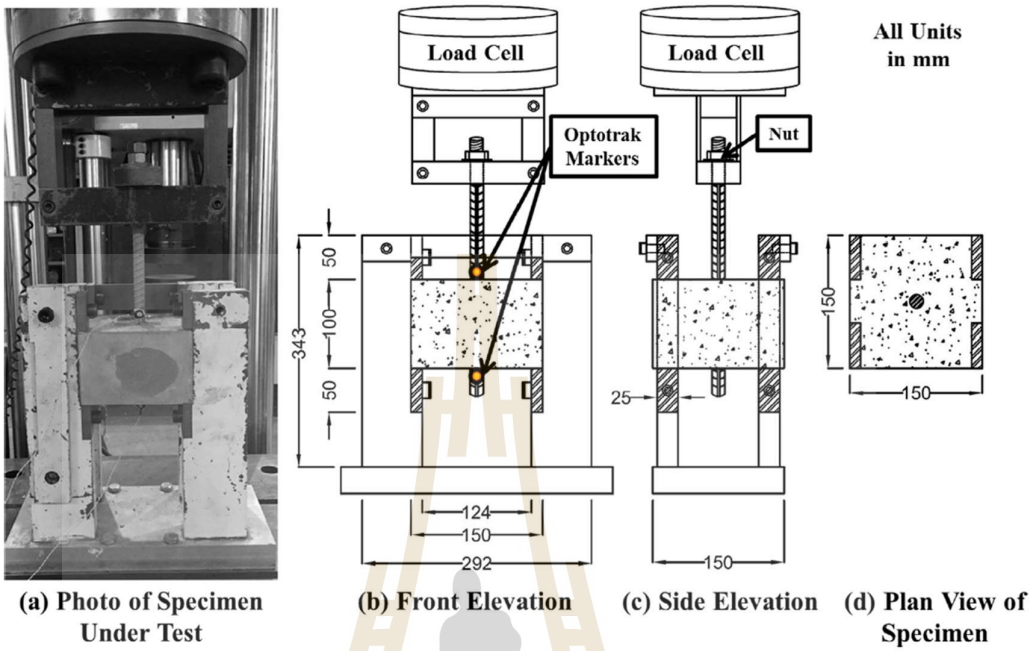

Figure 2.6 Test Set Up Details proposed by De Larrard and Sedran, 1994 (De Larrard and Sedran, 1994)

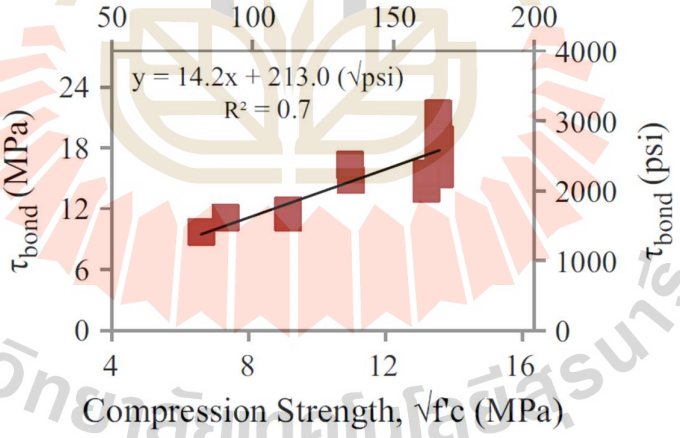

Figure 2.7 τ_{bond} vs. Square Root of Compression Strength of Concrete (Alkaysi and El-Tawil, 2017).

The UHPC composite demonstrates approximately 75% of its pull-out strength after a 7-day period. In **Figure 2.7**, the plot illustrates the bond stress (τ_{bond}) for all tests conducted with 16 mm epoxy bars, embedded at a depth of 6.4 times the

bar diameter (D), at 1, 3, 7, and 28 days. It is observed that τ_{bond} in the specimens increases linearly with the square root of the compressive strength (Alkaysi and El-Tawil, 2017 (Alkaysi and El-Tawil, 2017)). However, it is important to note that this correlation diminishes when compared to other bar diameters. Nonetheless, this valuable information can contribute to the development of future provisions for UHPC design.

Ahmed et al. (Ahmed, Shahjalal, Siddique and Keng, 2021) observed two distinct failure modes during the bond test of pull-out test in concrete. These modes were identified as rebar rupture and splitting failure, further classified as V-notch failure and concrete rupture. The respective failure modes of various concrete specimens are presented in **Figure 2.8**. For clarity, rebar failure can be categorized as either rebar rupture or rebar yielding, as depicted in **Figure 2.8(a1 and a2).** This phenomenon arises when there is adequate embedment of the reinforcing steel in the concrete, leading to failures predominantly occurring within the steel reinforcement itself**.** V-notch or cone failures were observed in multiple samples, as illustrated in **Figure 2.8(b)**. This phenomenon is attributed to insufficient embedment of the steel reinforcement within the concrete, resulting in the detachment of the conical concrete section attached to the reinforcing steel. Additionally, concrete cracking or splitting was evident in several tested samples, as shown in **Figure 2.8(c).** The occurrence of withdrawal failure is attributed to inadequate insertion of the reinforcing bar into the concrete. Disaster scenarios b, and c should be avoided due to their abrupt nature, as the occurrence of such failures in a structure can pose a significant risk with potentially severe consequences.

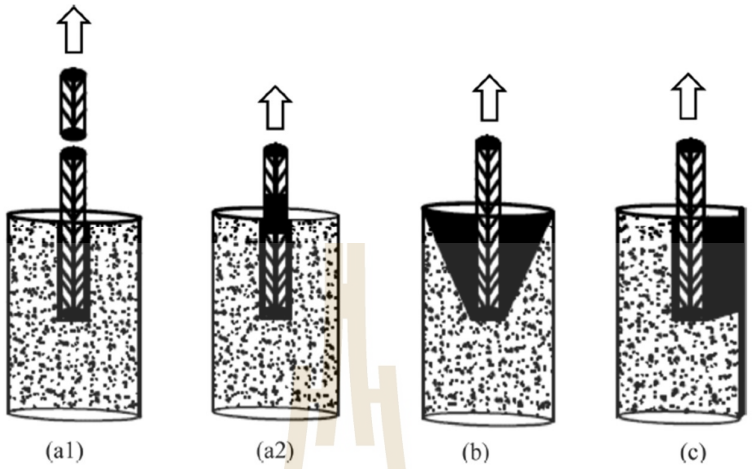

Figure 2.8. Failure modes of pull-out test in concrete under tensile loading; (a1) and (a2) rebar rupture and rebar yielding, respectively; (b) v-notch failure of concrete; (c) concrete cracking or rupture failure. (Ahmed et al. (Ahmed, Shahjalal, Siddique and Keng, 2021))

Garcia-Taengua et al. (Garcia-Taengua, Martí-Vargas and Serna, 2016) provide an explanation regarding the bond between reinforcement and concrete. The bond is quantified as a shear stress, or bond stress, distributed over the surface of the embedded rebar along its length. According to their definition, bond stress is the ratio of the rate of change in axial force along the rebar to the area of the rebar surface over which this change occurs. In the case of deformed, ribbed rebars, there are additional factors to consider. This is depicted in **Figure 2.9**, where the tensile load pulling the rebar out of the concrete results in reaction forces exerted on the surrounding concrete. The ribbed geometry causes these reactions to have two components: (a) a shear component parallel to the rebar axis, and (b) a radial component affecting the surrounding concrete. Thus, bond encompasses both bond stresses and radial stresses.

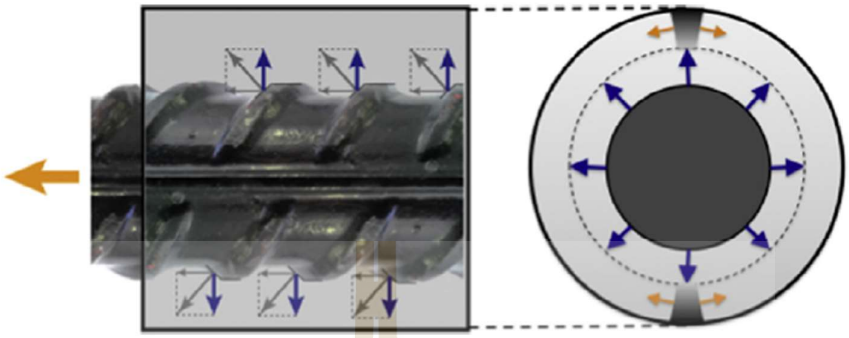

Figure 2.9. Bond stresses and radial stresses generated at the rebar–concrete interface. (Garcia-Taengua et al. 2016 (Garcia-Taengua, Martí-Vargas and Serna, 2016))

The concrete located between the ribs experiences a multiaxial stress state due to the shear component of the bond stresses. As the axial load increases, pulling the rebar outwards, the wedging action intensifies, leading to the crushing of the concrete between the ribs. Simultaneously, radial stresses increase until the tensile strength of the concrete surrounding the rebar is reached. Consequently, transverse microcracking occurs, causing a loss of strain compatibility between the rebar and the concrete, resulting in progressive rebar slippage facilitated by these microcracks. The initiation and progression of this slippage activate the bond. As long as sufficient confinement is maintained and the cracks do not cause complete failure of the concrete surrounding the rebar, bond stresses continue to increase until reaching the ultimate value known as bond strength. After reaching this peak, bond stress–slip curves exhibit a softening behavior.

In UHPC, According to FIB (2000) (FIB, 2000), the splice strength between a steel bar and UHPC is primarily influenced by the splitting of UHPC. When the steel bar is subjected to tension, the circumferential contraction caused by the Poisson effect leads to a reduction in outward pressure, resulting in a decrease in bond stress. This effect becomes more pronounced after the yielding of the bars. As illustrated in **Figure 2.10**, the bond stress in the elastic domain is relatively high due to the effective confinement provided by the surrounding UHPC. However, in the plastic domain, the confinement diminishes due to the circumferential contraction of the steel bar and

the localized damage to the UHPC surrounding the plastic zone of the steel bar. This further contributes to a decrease in bond stress. Therefore, it is necessary to consider separate calculations for the bond stress in the elastic and plastic domains during the post-yield phase.

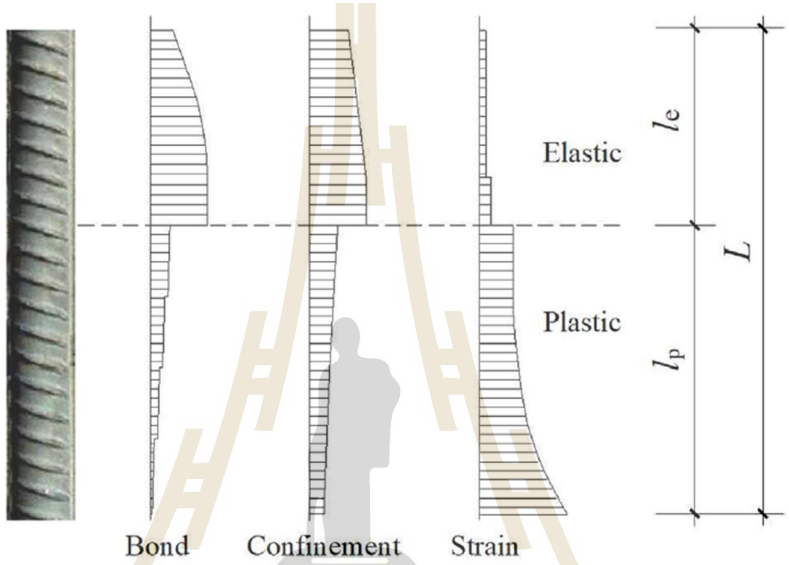

Figure 2.10 Behavior of bond in the post-yield phase (FIB, 2000).

Garcia-Taengua et al. (2016) (Garcia-Taengua, Martí-Vargas and Serna, 2016) conducted an analysis and presented plots illustrating the effects of various variables on bond strength (**Figure 2.11)**. The solid lines in the plots represent the average trends, while the gray bands indicate the 95% confidence limits for these estimates. Through these plots, the researchers assessed the relative importance of different variables on bond strength. It was observed that concrete compressive strength emerged as the most influential factor affecting bond strength, which aligns with previous literature on the subjec. In bond failures where splitting did not occur, the critical process was identified as the crushing of concrete wedges between ribs under multiaxial compression. This explains why concrete compressive strength played a crucial role in determining bond strength. On the other hand, the slightly positive impact of fiber reinforcement and concrete cover on bond strength was attributed to

their influence at the material level, specifically in enhancing the strength of concrete under compression, rather than at a structural level.

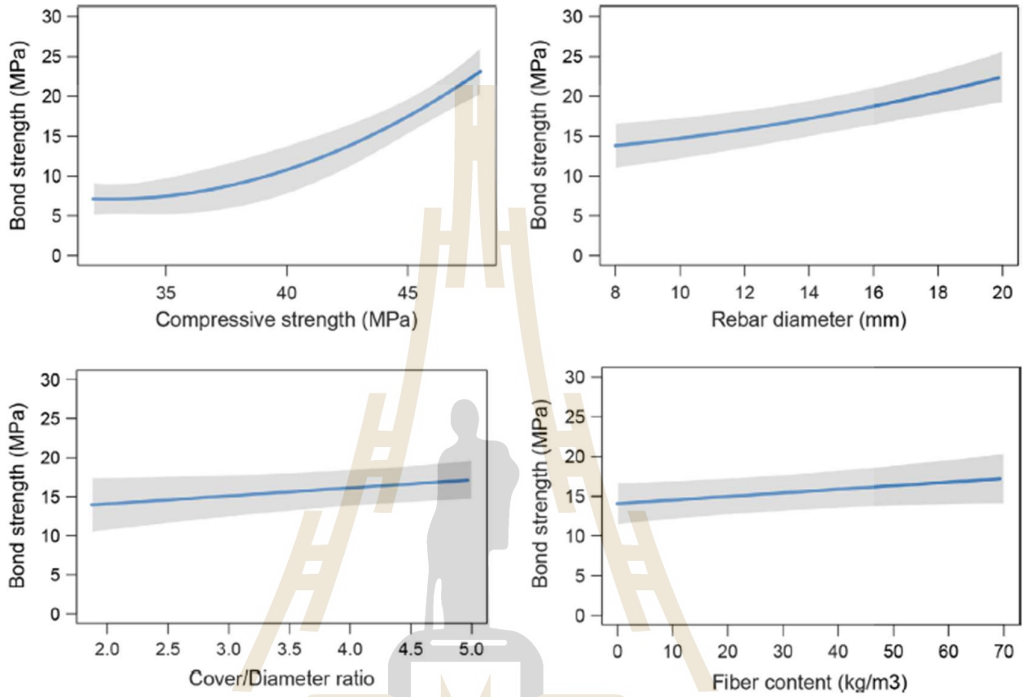

Figure 2.11 Bond strength: average trends with respect to the factors considered (Garcia-Taengua et al. 2016).

Furthermore, it was noted that higher rebar diameters resulted in increased bond strength values. However, this should not be interpreted as the rebar itself enhancing the bond capacity of the interface. Instead, larger rebar diameters with bigger ribs induce higher bond stresses at the rebar-concrete interface, effectively balancing the axial load that tends to pull the rebar out of the concrete. The enhancement of passive confinement, achieved by increasing the cover/diameter ratio or fiber content, demonstrated a slight increase in bond strength. This was attributed to the fact that, at the point where the bond strength is reached, the extent of microcracking is not yet significant enough to activate the sewing effect of fibers or the confinement provided by the concrete cover.

Additionally, **Figure 2.12** illustrates the correlation between bond strength and fiber content, considering different fiber lengths and slenderness values. The findings

indicated that, for a given fiber content, shorter fibers were found to be more favorable in terms of their influence on bond strength. This observation can be attributed to the fact that the full potential contribution of longer fibers is not fully activated until the surrounding microcracking near the rebar becomes more pronounced than at the point where bond strength is achieved. Regarding the effect of slenderness, its impact is directly associated with the cross-sectional area of the fibers.

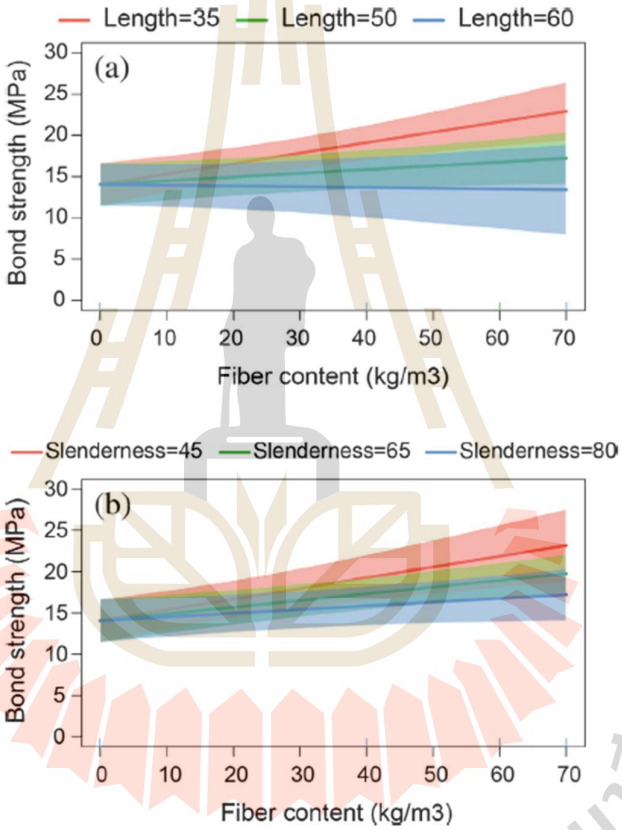

Figure 2.12 Effect of fiber length (a) and slenderness (b) on bond strength (Garcia-Taengua et al. 2016).

Pour and Alam (2016) (Pour and Alam, 2016) conducted a study on the effect of concrete cover on bond strength and observed several significant findings. They found that, in general, larger diameter cylinder specimens exhibited improved bond resistance due to higher confinement. This trend was consistent across the majority of push-out specimens as well. **Figure 2.13** illustrates a noteworthy increase

of up to 50% in bond resistance for 15M rebar when the concrete cover increased from 42.5 mm to 67.5 mm. Similar results have been reported in the existing literature. The variation in bond strength due to concrete cover for 10M rebar was consistent across different mixes. The smaller concrete cover to bar diameter ratios for 10M bars were found to provide satisfactory bond conditions. Furthermore, the influence of various factors on the bond behavior of concrete made with Recycled Concrete Aggregate (RCA) was found to be similar to that of conventional concrete. A previous study by Li et al. (Li, Deeks and Su, 2013), which involved push-out tests on conventional concrete, reported similar factors affecting bond strength.

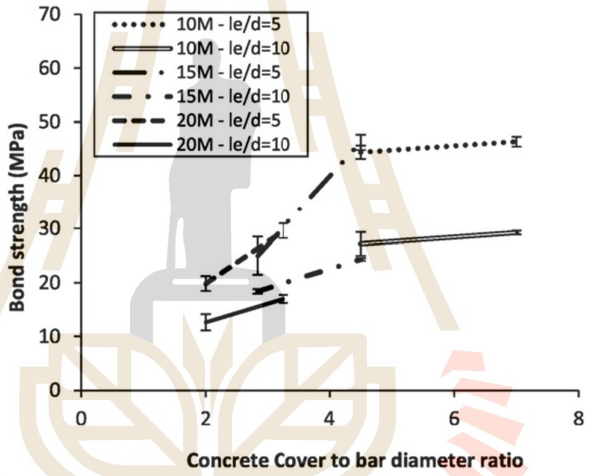

Figure 2.13 Relationship between bond strength and concrete cover with 30% RCA (Pour and Alam. 2016)

2.4.2 Lap splicing of steel rebars embedded in concrete

Lagier et al. (2016) (Lagier, Massicotte and Charron, 2016) highlighted that in the absence of transverse reinforcement, the radial pressure exerted by bar ribs can only be balanced by the hoop stresses developed in the concrete cover surrounding the bars (**Figure 2.14b**). The anchorage capability of reinforcing bars depends on the tensile strength and post-cracking energy of the concrete. Plain concrete tends to fail when the hoop stresses reach the tensile strength of the

material, resulting in the splitting of the concrete cover due to its limited post-cracking energy. This sudden failure leads to a significant reduction in bond resistance.

However, the inclusion of steel fibers in concrete significantly enhances the bond performance of deformed reinforcing bars, particularly when combined with Ultra-High-Performance Fiber-Reinforced Concrete (UHPFRC) matrices. A comparison between typical normal strength concrete (NSC) and UHPFRC demonstrates their respective direct tensile stress-strain properties (**Figure 2.14a**). Notably, UHPFRC exhibits a 2-4 times increase in maximum tensile strength, displays strain-hardening behavior after the initial cracking, and greatly improves post-cracking performance. These remarkable tensile properties induce high and relatively uniform tensile stresses in the concrete surrounding the reinforcing bars (**Figure 2.14c**). As a result, they effectively counteract the radial bursting pressure, leading to significantly improved bond performance for the same concrete cover thickness.

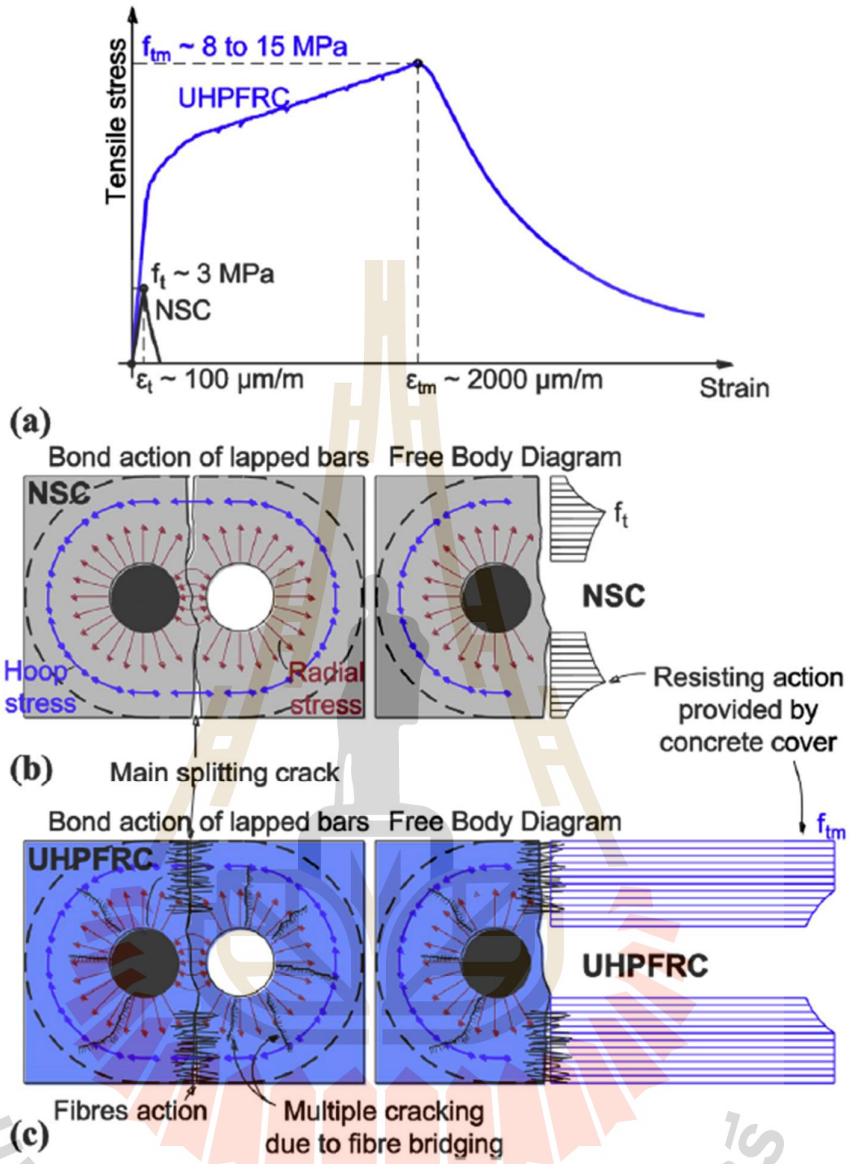

Figure 2.14 Concrete cover tensile stresses, (a) typical stress-strain curve, (b) Normal Strength Concrete, (c) Ultra-High Performance Fibre Reinforced Concrete (Lagier et al., 2016)

Lee (2016) (Lee, 2016) conducted a study on the flexural testing of UHSC beam specimens. The test setup and instrumentation used are presented in **Figure 2.15(a)**. The results of the study indicate that the traditional assumption of uniformly distributed bonding strength over a splice length is not reasonable for UHSC with steel fibers. The bonding strength did not increase proportionally with the lap splice length,

as observed in **Figure 2.15(b)**. Specifically, for UHSC beams without steel fibers, the bonding strength did not significantly increase when the splice length was elongated from 5 db to 15 db. This discrepancy can be attributed to the superior bonding characteristics of UHSC and the bonding enhancement provided by the steel fibers. The bonding mechanism observed in UHSC allows for a shorter splice length, but its effectiveness is compromised once concrete splitting occurs, unless delayed by the presence of steel fibers. Additionally, due to the short splice length, the bonding strength cannot be redistributed over a longer distance.

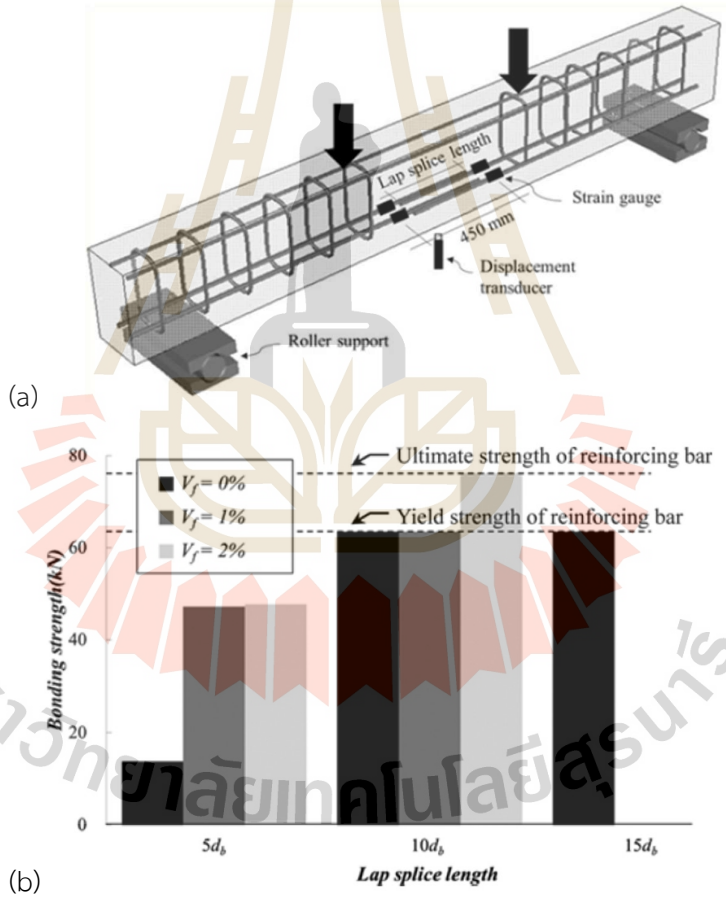

Figure 2.15 (a) Test Set-up and (b) Comparison of the Bonding Strengths of Lap-spliced Bars Embedded in UHSC Beams (Lee., 2016)

McMullen and Haber (2019) (McMullen and Haber, 2019) conducted experimental testing to develop design guidance for UHPC-rebar lap splices. Their research aimed to quantify the impact of various factors, including concrete cover, bar type, bar yield strength, and bar diameter, on the bond strength between UHPC and reinforcing bars (**Figure 2.15)**. The findings indicated that epoxy-coatings have a more significant effect on stress development in smaller diameter bars compared to larger diameter bars. The presence of an epoxy-coating resulted in a reduction of peak stress for bars with full embedment and a smaller bond area (**Figure 2.16)**. Moreover, bars with higher yield stress demonstrated the ability to achieve higher peak stresses compared to similar bars with lower yield stresses. This observation is likely due to the yield plateau exhibited in lower yield strength bars. The influence of yield stress was more pronounced in larger diameter bars with longer embedment lengths. Decreasing the clear cover led to a reduction in the tensile capacity of connections involving larger diameter bars.

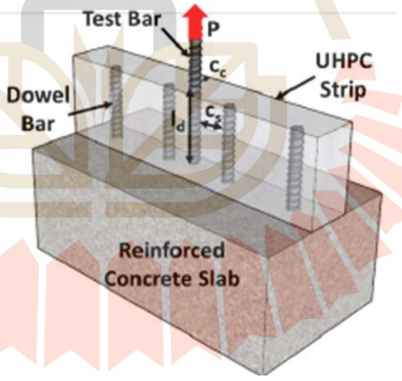

Figure 2.16 Schematic of Test Parameters (McMullen and Haber, 2019)

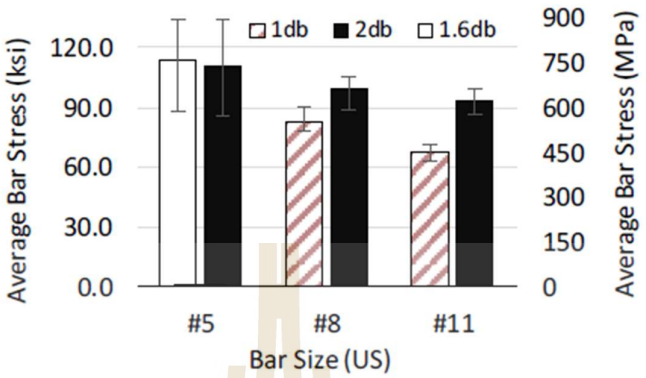

Figure 2.17 Effect of Cover for Uncoated Gr. 120 Bars- Bars Stress vs. Bar Size (McMullen and Haber, 2019)

Minor and Jirsa (1975) (Minor and Jirsa, 1975) conducted pullout tests on bent reinforcing bars and derived three key conclusions. Firstly, at a given load level, the amount of anchorage slip increases with the bend angle and decreases with the bend radius. This behavior can be attributed to the radial movement of the reinforcing bar caused by the radial compressive stress at the bend intrados (refer to **Figure 2.17**). Secondly, the strength of straight and bent anchorages with the same length is generally comparable, except in cases where the bend radius is exceptionally small or the anchorage length is insufficient. Under these circumstances, the bent anchorage exhibits greater strength. This distinction arises because the bending moment effect on the bent reinforcing bar becomes insignificant when the anchorage length is sufficient for yielding to occur. Thirdly, during a pullout test, the initial stiffness of the force-slip relationship is unaffected by the anchorage length. This is due to the fact that, for small pullout forces, the bond stress is significant at the pulled end of the reinforcing bar but negligible elsewhere.

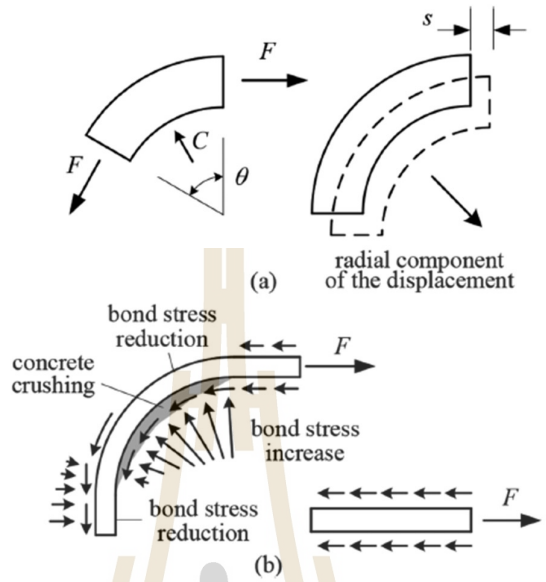

Figure 2.18 (a) Slip due to radial movement of reinforcing bar and (b) bond and normal stresses in straight and bent reinforcing bars. (Minor and Jirsa 1975)

Hwang et al. (2017) (Hwang, Park and Yi, 2017) investigated the bond and bearing stress distributions in 90-degree and 180-degree hook anchorages, as depicted in **Figure 2.18**. When subjected to tensile forces, the bearing stress along the inner radius of the 90-degree hook induces relative deformation (or slip) between the reinforcing bar and concrete, ultimately leading to concrete crushing. As the compressive deformation of the concrete increases in the inner zone of the hook, the bond stress in the outer zone decreases, resulting in kickout stress at the tail of the hook. Similarly, in the case of the 180-degree hooked bar, bond and bearing stresses occur in the inner zone of the hook, mirroring the behavior observed in the 90-degree hooked bar. The bearing effect of the hook enhances the pullout resistance in the hooked bars. Therefore, when evaluating the development length of a hooked bar, the anchorage effect of the hook must be taken into consideration.

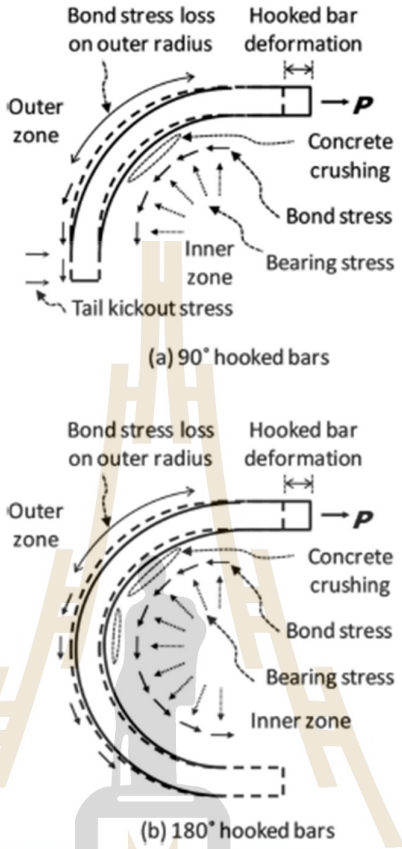

Figure 2.19 Bearing and bond stress distribution along hook length (Hwang et al. 2017)

The findings of Goto (1971) (Goto, 1971) and Tepfers (1979) (Tepfers, 1979) highlight that the bond strength is influenced by the effectiveness of chemical adhesion, friction resistance, and, most significantly, mechanical interlocking, which has been experimentally observed to be closely linked to the development of internal multiscale cracks (**Figure 2.20(a)**). However, in practical applications, the bond strength is often compromised due to a combination of high stress excursions and stress reversals resulting from various severe loadings. In response to this concern, several engineering approaches, such as bending up deformed bars or welding small steel blocks as depicted in **Figure 2.20(b)** and **(c)**, have been successfully implemented to enhance the bond strength. Nonetheless, excessive use of such anchorage techniques

can be labor-intensive and may lead to reinforcement congestion, which is detrimental to concrete compaction.

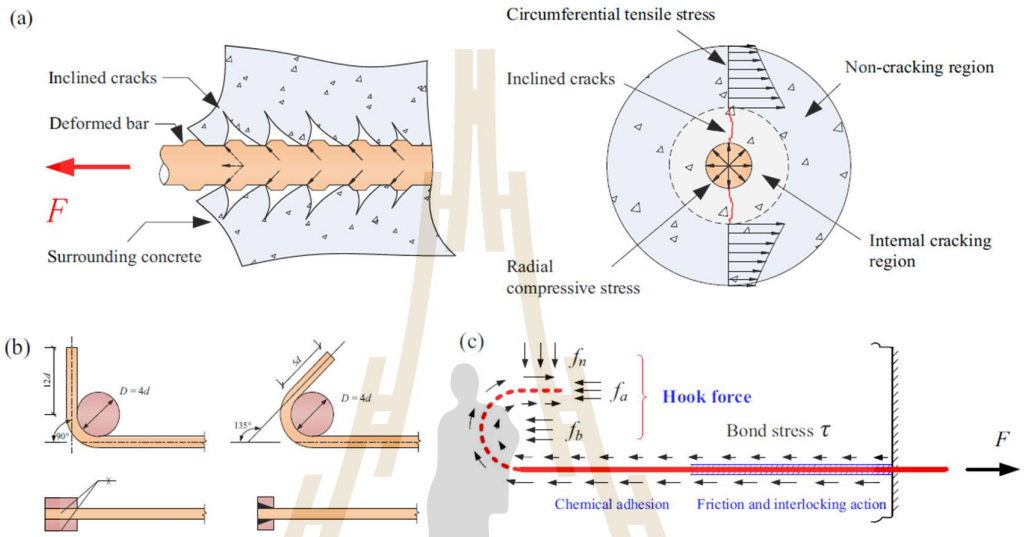

Figure 2.20 Schematic representation of the bond action. (a) crack pattern; (b) engineering approaches to increase bond strength; and (c) components of bond resistance (Huang et al. 2019, (Huang, Xu, Chi, Deng and Zhang, 2019)).

2.5 Connecting Joint of the precast concrete beam-column

The connection between precast concrete beams and columns is of utmost importance in constructing structures using prefabricated components. The behavior of the structure utilizing precast concrete elements depends on the behavior of the connection. The forces from working loads and seismic events are transmitted to other parts of the structure through the connections. The types of connections in a moment resisting frame can be categorized into two forms: 1) Equivalent monolithic system and 2) Jointed system. Each of which will have the following details.

1. In the equivalent monolithic system, or wet joint, the connection between the precast concrete beam and column can be further categorized into two subtypes:

connections of limited ductility and ductile connections. And ductile connection is designed to have sufficient strength and stiffness to accommodate plastic deformation primarily at the beam-column. While the point of connection with high rigidity will be designed to have a plastic hinge behavior at the beam-column interface during seismic events, the rest of the structure will act as a rigid body. Plastic deformation will occur only at the connection point.

2. In a jointed system, these connection points will be weaker compared to the adjacent structural members. This system will have a different performance compared to a monolithic structure made of the same material. The subdivision can be categorized into limited rigidity connections and flexible connections. Limited rigidity connections, in general, are often dry joints that are connected using welding or bolting methods. While limited rigidity connections generally involve welding or bolting, but will be used unbonded post-tensioned tendons at connection points. When a building undergoes deformation beyond the elastic range, the connection point at the beam-face where it meets the column will deflect. However, it will return to its original position once the applied forces decrease. This behavior is due to the presence of unbonded post-tensioned tendons that act as pulling elements, keeping the components connected within the elastic range. These tendons remain in a state of tension and play a role in restoring the connection to its original position during the elastic deformation phase.

2.5.1 Mechanism for Force Transfer at Beam-Column Joints in Monolithic Concrete Structures

When a rigid framework is subjected to vertical loads, internal forces act on the beam-column joint. However, shear forces at the joint are minimal or nonexistent (unlike in the horizontal direction, such as during seismic forces). On the other hand, the beam-column joint that carries horizontal loads experiences shear forces due to the internal forces and moments transmitted from the beam and column. As a result, the beam-column joint may exhibit diagonal cracks, as shown in Figure 2.21

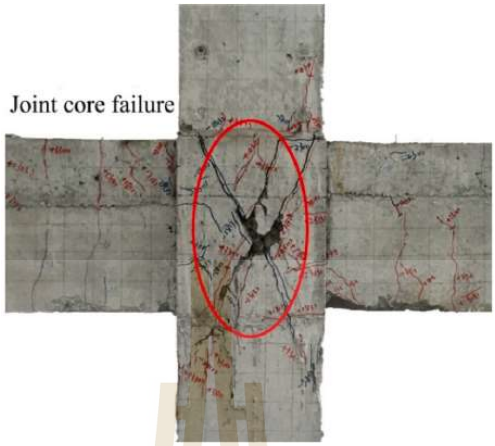

Figure 2.21 Diagonal cracks at the joint in a slanted direction. (Deng et al., 2020)

The theories related to the resistance mechanism and moment capacity of beam-column joints when subjected to horizontal forces are as 1) Strut mechanism 2) Truss mechanism and 3) Bond failure mechanism. Strut Mechanism: This theory assumes that the compressive forces from the beam and column act along a diagonal path, forming a strut mechanism as shown in Figure 2.22. The horizontal force in the joint is generated by the tension force in the longitudinal reinforcement of the beam. The direction of the resultant force is diagonal, as shown in Figure 2.23. When the point of connection loses the gripping force of the reinforcement steel, the strength of the connection relies solely on the Strut mechanism. The Bond failure mechanism theory is used to explain the behavior of a structural element subjected to horizontal forces. It involves tensile and moment forces acting on the connection point, generating both compressive and tensile forces in the reinforcement steel, resulting in the development of bond stress. When the gripping force is lost, the cross-sectional area and the resistance to moment capacity are compromised.

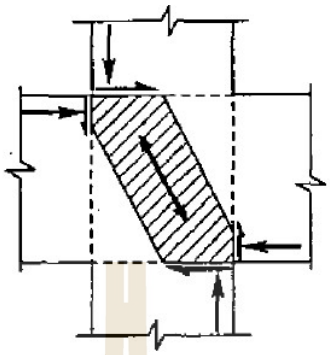

Figure 2.22 Strut mechanism (Park, 2002)

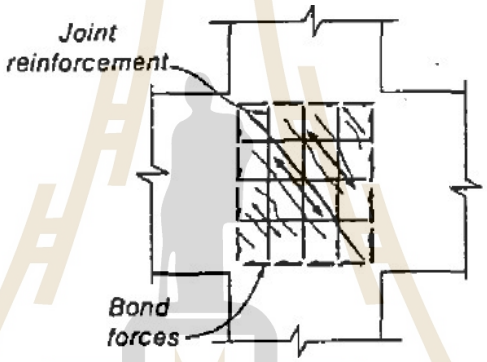

Figure 2.23 Truss mechanism (Park, 2002)

2.6 References

ACI Committee 408, A. C. (1990). "Suggested Development, Splice, and Standard Hook Provisions for Deformed Bars in Tension (ACI 408.1 R–90)." American Concrete Institute, Farmington Hills Michigan,, USA.

Ahmed, K. S., Shahjalal, M., Siddique, T. A., and Keng, A. K. (2021). "Bond strength of post-installed high strength deformed rebar in concrete." Case Studies in Construction Materials, 15, e00581.

Alkaysi, M., and El-Tawil, S. (2017). "Factors affecting bond development between Ultra High Performance Concrete (UHPC) and steel bar reinforcement." Construction and Building Materials, 144, 412-422.

Beglarigale, A., and Yalçınkaya, Ç. (2014). "Autoclaved reactive powder concrete: the effects of steel micro-fibers and silica fume dosage on the mechanical properties." Usak University Journal of Material Sciences, 3(1), 7-14.

Chao, S.-H., Naaman, A. E., and Parra-Montesinos, G. J. (2009). "Bond behavior of reinforcing bars in tensile strain-hardening fiber-reinforced cement composites." ACI Structural Journal, 106(6), 897.

De Larrard, F., and Sedran, T. (1994). "Optimization of ultra-high-performance concrete by the use of a packing model." Cement and concrete research, 24(6), 997-1009.

Dili, A., and Santhanam, M. (2004). "Investigations on reactive powder concrete: A developing ultra high-strength technology." Indian concrete journal, 78(4), 33-38.

FIB (2000). "Bond of reinforcement in concrete." FIB Bulletin 10.

Garcia-Taengua, E., Martí-Vargas, J. R., and Serna, P. (2016). "Bond of reinforcing bars to steel fiber reinforced concrete." Construction and Building Materials, 105, 275-284.

Goto, Y. "Cracks formed in concrete around deformed tension bars." Proc., Journal Proceedings, 244-251.

Graybeal, B. (2011). "Ultra-high performance concrete."

Huang, L., Xu, L., Chi, Y., Deng, F., and Zhang, A. (2019). "Bond strength of deformed bar embedded in steel-polypropylene hybrid fiber reinforced concrete." Construction and Building Materials, 218, 176-192.

Hwang, H.-J., Park, H.-G., and Yi, W.-J. (2017). "Development length of standard hooked bar based on non-uniform bond stress distribution." ACI structural journal, 114(6), 1637-1649.

Jiang, Y., Yan, Y., Li, T., Cao, X., Yu, L., and Qi, H. (2023). "Comparison of the Mechanical Properties and Crack Expansion Mechanism of Different Content and Shapes of Brass-Coated Steel Fiber-Reinforced Ultra-High-Performance Concrete." Materials, 16(6), 2257.

Lagier, F., Massicotte, B., and Charron, J.-P. (2016). "Experimental investigation of bond stress distribution and bond strength in unconfined UHPFRC lap splices under direct tension." Cement and Concrete Composites, 74, 26-38.

Lee, J.-K. (2016). "Bonding behavior of lap-spliced reinforcing bars embedded in ultra-high strength concrete with steel fibers." KSCE Journal of Civil Engineering, 20, 273-281.

Li, H.-t., Deeks, A. J., and Su, X.-z. (2013). "Experimental study on compressive bond anchorage properties of 500 MPa steel bars in concrete." Journal of Structural Engineering, 139(12), 04013005.

McMullen, K. F., and Haber, Z. "Effect of Steel Reinforcement Type and Diameter on the Strength of Non-Contact Lap Splice Connections using UHPC." Proc., International Interactive Symposium on Ultra-High Performance Concrete, Iowa State University Digital Press.

Minor, J., and Jirsa, J. O. "Behavior of bent bar anchorages." Proc., Journal Proceedings, 141-149.

Pour, S. M., and Alam, M. S. "Investigation of compressive bond behavior of steel rebar embedded in concrete with partial recycled aggregate replacement." Proc., Structures, Elsevier, 153-164.

Russell, H. G., Graybeal, B. A., and Russell, H. G. (2013). "Ultra-high performance concrete: A state-of-the-art report for the bridge community." United States. Federal Highway Administration. Office of Infrastructure ....

Sezen, H., Whittaker, A., Elwood, K., and Mosalam, K. (2003). "Performance of reinforced concrete buildings during the August 17, 1999 Kocaeli, Turkey earthquake, and seismic design and construction practise in Turkey." Engineering Structures, 25(1), 103-114.

Tepfers, R. (1979). "Cracking of concrete cover along anchored deformed reinforcing bars." Magazine of concrete research, 31(106), 3-12.

Wille, K., Naaman, A. E., and Parra-Montesinos, G. J. (2011). "Ultra-High Performance Concrete with Compressive Strength Exceeding 150 MPa (22 ksi): A Simpler Way." ACI materials journal, 108(1).

Yoo, D.-Y., Kwon, K.-Y., Park, J.-J., and Yoon, Y.-S. (2015). "Local bond-slip response of GFRP rebar in ultra-high-performance fiber-reinforced concrete." Composite Structures, 120, 53-64.

CHAPTER III

BONDING BEHAVIOR OF LAP-SPLICED REINFORCING BARS EMBEDDED IN ULTRA-HIGH-PERFORMANCE CONCRETE WITH STEEL FIBERS

3.1 Introduction

The precast concrete structures possess several advantages over their cast-in-place counterparts, including shorter design and construction time, cost-effectiveness, quality assurance, and improved aesthetics. Frame structures are particularly suitable for the precast concrete industry due to their standardization, prefabrication, and easy assembly. As a result, the use of precast structures in infrastructure systems has garnered increasing interest in recent years. However, under seismic attack, precast concrete structures are prone to losing their bearing capacity due to brittle failure at the connections when the plastic deformations of the frame components have not been fully developed, thereby impeding effective dissipation of seismic energy (Belleri, Brunesi, Nascimbene, Pagani and Riva, 2015). Analysis of collapsed and damaged precast buildings has shown that prefabricated beams or columns usually suffer minimal damage. Instead, structural failure primarily results from the destruction of connections between the structural components.

The integrity of connections in precast concrete structures is critical in ensuring their stability during seismic events. Hence, the development of beam-column connections that exhibit satisfactory seismic performance has become a significant research focus in the field. Furthermore, lessons learned from previous earthquakes underscore the need for beam-to-column connections that are specifically designed to enhance the safety of precast concrete structures. In line with this, ACI 318-19 (Committee, 2019) promotes the "Strong joints and weak members" principle and sets a minimum anchorage length requirement for tensile reinforcing

steel in ordinary concrete, which should be no less than 20 times its diameter. However, the installation of connection joints for precast concrete members remains a complex and challenging process in contemporary construction practices. In Europe, America, and Japan, grout sleeves are often utilized to ensure continuity of reinforcing steel at connection joints, as reported by Einea et al. (1995) (Einea, Yamane and Tadros, 1995). However, such methods necessitate high precision, and verifying the quality of grout in joints can be arduous. This may introduce potential hazards that may remain concealed within the structure, underscoring the need for safer and more efficient alternatives.

Ultra-high performance concrete (UHPC) is a cement-based composite material possessing remarkable mechanical properties and workability, including ultra-high compressive and flexural strength, high toughness, excellent durability, and high self-compacting factor, making it an attractive option for structural applications that require resistance to heavy loads, large spans, seismic events, explosions, and impact. Notably, UHPC exhibits distinctive behavior compared to conventional reinforced concrete, as it enables the shortening of steel bars through lap splicing, thereby offering superior performance in structural applications. The outstanding bond strength between deformed steel bars and UHPC is the primary driver behind its exceptional behavior, which leads to a significant reduction in required splice length (Yuan and Graybeal, 2015). This attribute has paved the way for the development of innovative connection specifications for precast concrete bridges (Graybeal, 2014, Shafieifar, Farzad and Azizinamini, 2017) and buildings (Aarup and Jensen, 1998), highlighting the immense potential of UHPC in pushing the boundaries of structural engineering. Moreover, these connections have simplified construction procedures and minimized on-site work requirements, thanks to the significantly reduced splice length (Tosa and Salha, 2016, Ye, Jiang, Chen, Zhou and Song, 2021).

From the literature survey, the bonding mechanism in UHPC is expected to be positively correlated with the increase in tensile strength, which corresponds to that of the compressive strength (Alkaysi and El-Tawil, 2017, Pour and Alam, 2016, Shen, Shi, Zhang, Duan and Jiang, 2016). Moreover, the incorporation of steel fibers in UHPC

can significantly enhance the bonding mechanism by delaying crack opening and providing tensile strength post-cracking (Lee, 2016, Yoo, Kwon, Park and Yoon, 2015). This leads to the preservation of the concrete's bearing strength against lugs even after splitting at the lap splices. It is worth noting that the concrete's bearing strength in this case is primarily influenced by the delayed crack opening induced by the steel fibers. In addition, the utilization of UHPC for joint construction provides enhanced shear capacity and reduces the necessary length of reinforcing steel within the joint. This also facilitates the attainment of greater homogeneity between columns and beams during construction, and lap-splicing utilizing UHPC represents a noteworthy characteristic of precast concrete structures (Bae, Choi and Choi, 2016, Garcia-Taengua, Martí-Vargas and Serna, 2016).

Despite the widespread success of UHPC as a connection material for precast concrete members in other countries (Elliott, 2000), Thailand has yet to establish a standard for the design of beam-column connections utilizing UHPC. Moreover, previous research conducted in foreign countries has not taken into account the variations in material standards utilized in Thailand, such as the size and quality of reinforcing steel, and the quality of cement. As a result, the adoption of UHPC for precast concrete beam-column connections in Thailand remains limited, despite the demonstrated engineering, economic, and environmental benefits as evidenced by academic research conducted abroad. Thus, there is a pressing need to investigate and establish the applicability of UHPC in the context of Thailand's unique material standards and construction practices, to fully realize the potential benefits of this innovative technology.

The primary aim of this study is to investigate the impact of embedment length and lap-splice length in both normal concrete and UHPC, using four different sizes of reinforcing steel. The splice-lengths under varying conditions were evaluated through pull-out tests, and theoretical calculation methods for splice strength and splice length in the pre- and post-yield phases were proposed. Based on the study results, an optimal connection model that accounts for engineering, environmental, and economic factors was developed. The use of UHPC as the connection point for

precast concrete beam-column structures represents a sustainable innovation that significantly enhances the design of beam-column connections. The incorporation of UHPC also reduces the need for detailed construction plans, simplifies construction processes, and ultimately leads to lower construction costs.

3.2 Materials and methods

3.2.1 Material Characteristics of Normal concrete and Steel-fiber-reinforced UHPC

The normal concrete (NC) used as a comparison to UHPC employed Type 1 Portland cement as the binding material. Sand with a grain size lower than 4.75 mm was used as fine aggregate according to ASTM C33 "Standard Specification for Concrete Aggregates", whereas coarse aggregates were excluded from the mixture (Standard, 2003). The design goal for the normal concrete was to attain a compressive strength exceeding 38 MPa after 28 days, achieved through the mixing weight ratio (job mix formula) of cement: sand: water in a ratio of 1:2:0.275, while maintaining a slump value within the range of 7.5±2.5 cm.

Figure 3.1 Micro steel fibers.

The UHPC mixture (ready-mix) utilized for constructing the specimens was provided by Concrete Products and Aggregate Co., Ltd. (CPAC), which is a subsidiary of SCG Cement-Building Materials and a reputable supplier of high-quality concrete products in Thailand. The maximum size of the fine aggregate was 1 mm, and the water-to-binder ratio was 0.175. Using this mix design, a 28-day compressive strength (f_c') of more than 130 MPa was achieved, while the elastic modulus was found to be 26,455 MPa. The straight steel fiber used in the study had a diameter of 0.22 mm and a length of 13 mm (**Figure 3.1**), and exhibited an ultimate tensile strength of 2,800 MPa. The test items include slump flow test, compressive test, Poisson's ratio, and elastic modulus measurement of NC and UHPC specimens, and are shown in **Table 3.**. Following the concrete casting, all test specimens were immediately covered with plastic sheets and allowed to cure at room temperature for 48 hours before being demolded. Subsequently, the specimens were stored at room temperature until the testing process.

Table 3.1 Test contents of normal concrete and UHPC specimens.

Test item	Specimen size	Test age	Test standard
Slump flow test	Slump cone	Fresh concrete	ASTM C230
Initial and Final Setting Time	-	Fresh concrete	ASTM C403
Compressive Strength test	Φ15 cm × 30 cm	1, 3, 7, 14 and 28 days	ASTM C39
Poisson's ratio, and elastic modulus test	Φ15 cm × 30 cm	7 and 28 days	ASTM C469

Reinforcing bars with four different diameters (12, 16, 20, and 25 mm) were utilized, and an uncoated deformed steel bar was chosen for this purpose. The average yield and ultimate strength of the four different diameter bars were measured as 522.24 MPa and 636.10 MPa, respectively, while the elastic modulus

was determined to be higher than 190,000 MPa. The mechanical properties of the steel bars are listed in **Table 3.2**

Table 3.2 Mechanical properties of steel bars.

Diameter (mm)	Grade	Yield tensile strength (MPa)	Ultimate tensile strength (MPa)
12	SD40	536.15	645.09
16	SD40	565.94	658.14
20	SD40	504.79	611.54
25	SD40	482.06	629.73

3.2.2 Test setup and procedure

3.2.2.1 Pull-out test

The bar pull-out test, despite its simplicity and ease of implementation, is considered the least accurate testing method for measuring bond capacity in concrete, according to ACI Committee 408 (Bond, 2003). This is due to the fact that it tends to overestimate bond capacity. In the traditional pull-out test, the load applied to the steel bar in tension generates compressive forces in the surrounding concrete as it reacts against the rigid support surface holding the specimen. However, in reinforced concrete structures under flexural loading, both the steel bar reinforcement and concrete are under tension during loading, which differs from the traditional pull-out test method.

To reduce the impact of the compressive area during the testing process, a modified method of concrete support was employed in accordance with the Alkaysi and El-Tawil recommendation (Alkaysi and El-Tawil, 2017), as illustrated in **Figure 3.2** Steel rebars with nominal diameters of 12, 16, 20, and 25 mm were utilized in the experiment. A mold with a square cross-section of 150 mm and a height ranging from 150 to 300 mm was utilized to fabricate the pull-out specimen, which consisted of a single steel bar embedded vertically along the central axis. The

embedment length of steel rebars with diameters of 12 mm was determined to be 40, 50, 75, and 100 mm, while for those with diameters of 16, 20, and 25 mm, the embedment length was determined to be 50, 75, 100, 125, 150, 175, and 200 mm. During the testing, a Universal Testing Machine (UTM) with a maximum load capacity of 5000 kN was used to apply a pull-out load via displacement control. The rate of load increase was maintained at 0.5 mm/min. In this research, the pull-out test and lap-splice test were conducted on NC and UHPC when they attained a 7-day compressive strength.

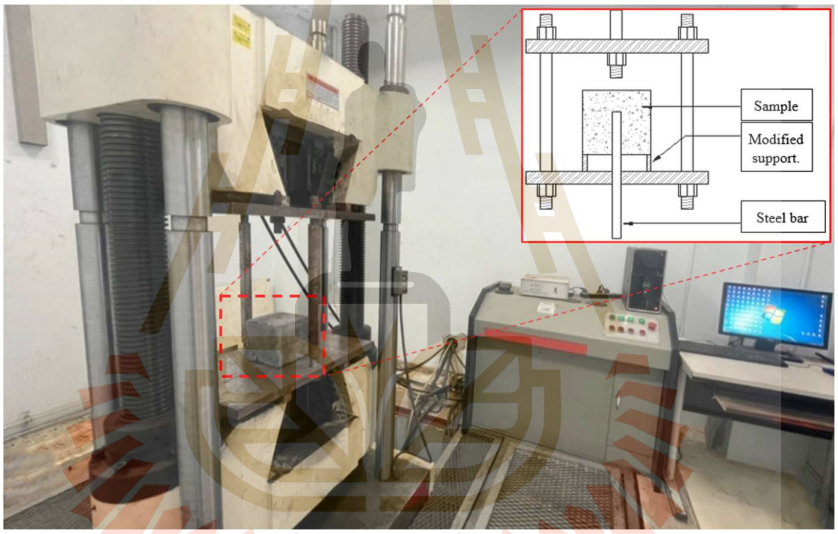

Figure 3.2 Test setup details.

3.2.2.2 Lap-Splice Test

Table 3.3 presents two groups of lap-splice specimens designed with different parameters of splice lengths and longitudinal bar end shape (straight or hooked). The experimental test setup employed in this study was consistent with the configuration utilized by McMullen and Haber (2019) (McMullen and Haber, 2019) and Yuan and Graybeal (2015) (Yuan and Graybeal, 2015). To achieve various failure modes, the range of splice length is set between 2 to 12 times the bar diameter. The varied splice lengths (L_1) of the steel bars in the concrete

specimens aimed to achieve either bonding failure or steel bar rupture. The lengths of the hooked bar ends (L_2) were designed to explore better strengthening measures for the continuity of steel bars. The clear spacing of the two longitudinal steel bars (s) was varied from 1 to 3 times the bar diameter. The lap-splice specimen was subjected to loading using a 500 kN center hole jack, as depicted in **Figure 3.3** The steel bars were anchored using a steel anchorage system. The magnitude of the tension force was measured using a digital display meter mounted on the jack. To measure the slippage between the concrete specimen and the steel bars at the loaded end, an LVDT was utilized. During the loading process, the appearance and load values were recorded until the specimen developed visible cracks.

Figure 3.3 Test loading device for lap-splice test.

Table 3.3 Parameters and test results of lap-splice specimens.

Graphic expression (mm)	Diameter (mm)	L_1	L_2	s
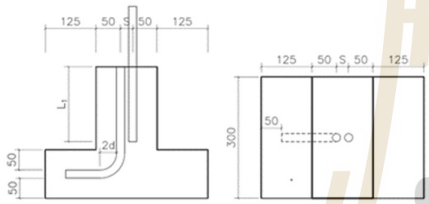	12	4d, 6d, 8d, 10d, 12d	-	1d, 1.5d, 2d, 3d
	16	3d, 4.5d, 6d, 8d, 10d, 12d		
	20	3d, 6d, 8d, 10d, 12d		
	25	3d, 4d, 6d, 8d, 10d, 12d		
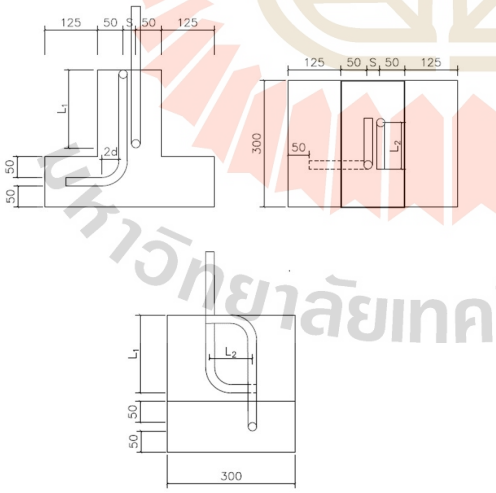	12	2d	1.5d, 2d	1d, 1.5d, 2d, 3d
		4d	1.5d, 2d, 3d, 4d	
	16	3d	1.5d, 3d	1d, 1.5d, 2d, 3d
		4d	1.5d, 3d, 4d	
		5d	1.5d, 3d, 4d, 6d	
		6d	1.5d, 3d, 4d, 6d	
	20	3d	1.5d, 3d	1d, 1.5d,
		4d	1.5d, 3d, 4d	

Graphic expression (mm)	Diameter (mm)	L_1	L_2	s
		5.5d	1.5d, 3d, 4d, 6d	2d, 3d
		6d	1.5d, 3d, 4d, 6d	
	25	3d	1.5d, 3d	1d, 1.5d, 2d, 3d
		4d	1.5d, 3d, 4d	
		6d	1.5d, 3d, 4d, 6d	

3.3 Test results

3.3.1 Mechanical Strength of NC and UHPC

The results of the Initial and Final Setting Time tests, conducted according to ASTM C403 "Standard Test Method for Time of Setting of Concrete Mixture by Penetration Resistance" (Standard, 2009), are presented in **Figure 3.4** In this test, the initial and final setting times are determined by measuring the compression resistance per area of 500 psi (3.5 MPa) and 4000 psi (27.6 MPa), respectively. The test results indicate that the NC has an initial and final setting time of 4 hours 46 minutes and 8 hours 22 minutes, respectively, while the UHPC exhibits a longer initial and final setting times of 8 hours 37 minutes and 14 hours 16 minutes, respectively.

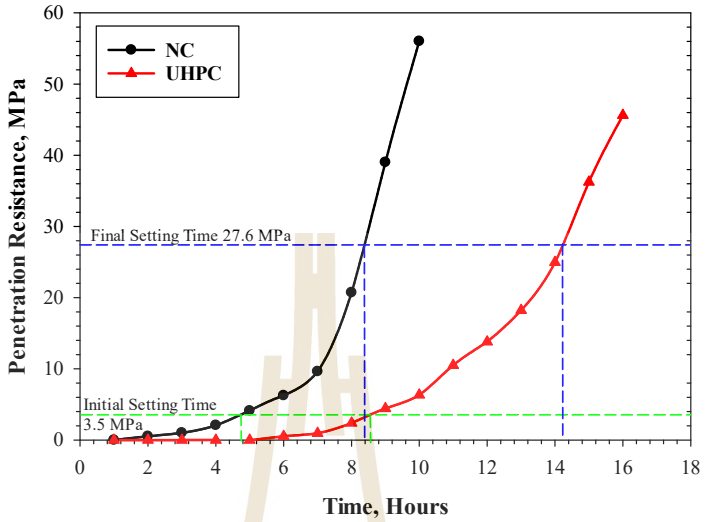

Figure 3.4 Initial and Final Setting Time of Normal concrete (NC) and UHPC

Figure 3.5 illustrates the compressive strength of NC and UHPC specimens at various curing times of 1, 3, 7, 14, and 28 days, in accordance with ASTM C39 (Standard, 2001) testing standards. The test results indicate that the NC exhibited compressive strength values of 2.169, 16.16, 29.10, 35.48, and 43.91 MPa after curing for 1, 3, 7, 14, and 28 days, respectively. Conversely, the UHPC specimens displayed compressive strength values of 5.25, 54.06, 93.86, 111.76, and 132.84 MPa for the corresponding curing periods. These findings suggest that UHPC specimens cured for 3 days possess a higher compressive strength than NC cured for 28 days. The results of the Young's modulus and Poisson's ratio tests, conducted in accordance with the ASTM C469 standard (Standard, 2009), are presented in **Table 3.4** The obtained data indicate that there is an increase in the values of both Young's modulus and Poisson's ratio as curing time is prolonged for both NC and UHPC. These findings are consistent with the research conducted by Huang et al. (2022) (Huang, Lee, Kan, Wang, Wang and Pan, 2022).

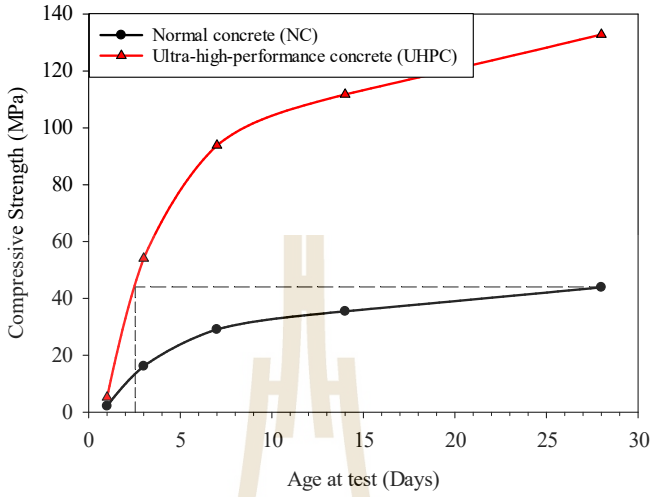

Figure 3.5 Compressive strength of Normal concrete and UHPC

Table 3.4 Poisson's ratio and elastic modulus of UHPC and NC.

Age (days)	Average Poisson's ratio (ν) and elastic modulus (E)			
	Normal concrete (NC)		UHPC	
	ν	E (GPa)	ν	E (GPa)
7	0.198	10.765	0.212	12.191
28	0.205	19.545	0.219	26.455

3.3.2 Pull-out test results

Based on the pull-out test results, it was observed that the failure mode of NC was the complete pull-out of all rebar steel, as shown in **Figure 3.6(a)**. On the other hand, UHPC exhibited two distinct failure modes, namely the rebar steel pull-out (bond failure) as depicted in **Figure 3.6(b)**, and steel rebar rupture illustrated in **Figure 3.6(c)**. The bonding equations for each size of rebar steel were generated, however, they did not take into account the tensile forces generated by the rebar steel rupture (**Figure 3.6(c)**). The relationship between the pull-out force and embedment lengths of the rebar steel was depicted in **Figure 3.7**, where **Figure 3.7(a)** represents all the pull-out forces including rebar rupture, while **Figure 3.7(b)** shows only the pull-out forces resulting from rebar steel pull-out. The results indicate

that, for both NC and UHPC, an increase in the embedment length led to an increase in the pull-out force. However, in the case of UHPC, the pull-out force continued to increase until it reached the ultimate tensile strength (f_u) of the steel rebar, resulting in steel rebar rupture. Specifically, steel rebar ruptured at an embedment length of 0.05, 0.10, 0.15, and 0.175 m for DB12, DB16, DB20, and DB25, respectively.

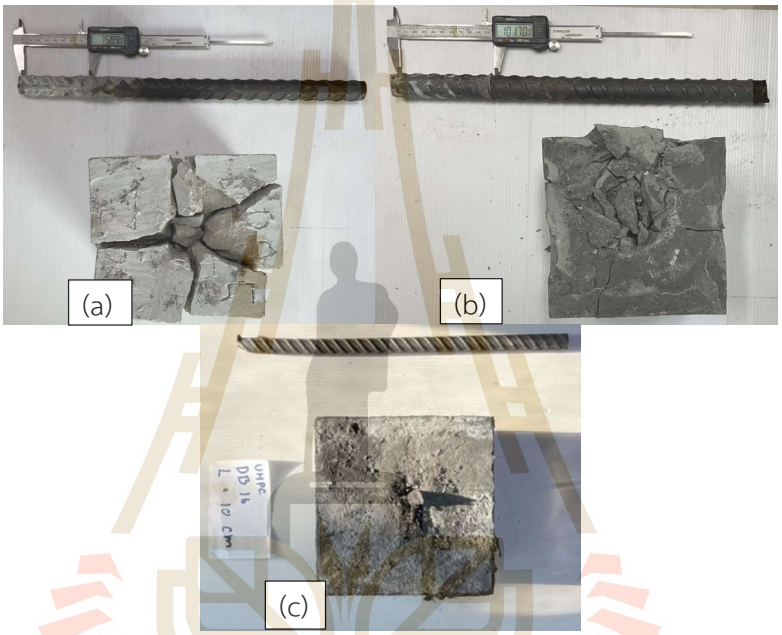

Figure 3.6. Failure modes of (a) Normal concrete, (b) UHPC with bond failure and (c) UHPC with steel bar rupture

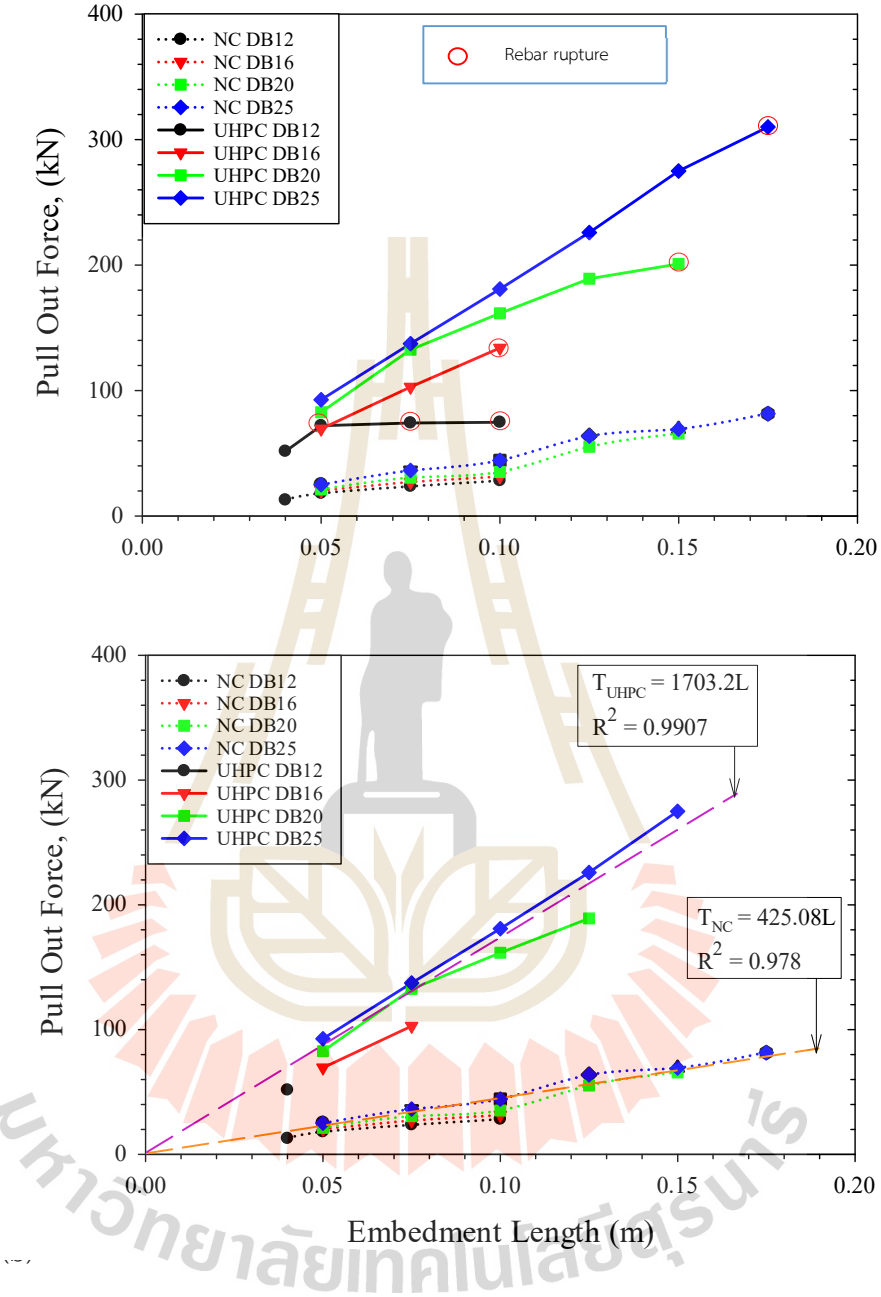

Figure 3.7. Relationship between the pull-out force and embedment lengths at 7-day of fc' (a) considering all types of failures and (b) considering only types of pull-out failure.

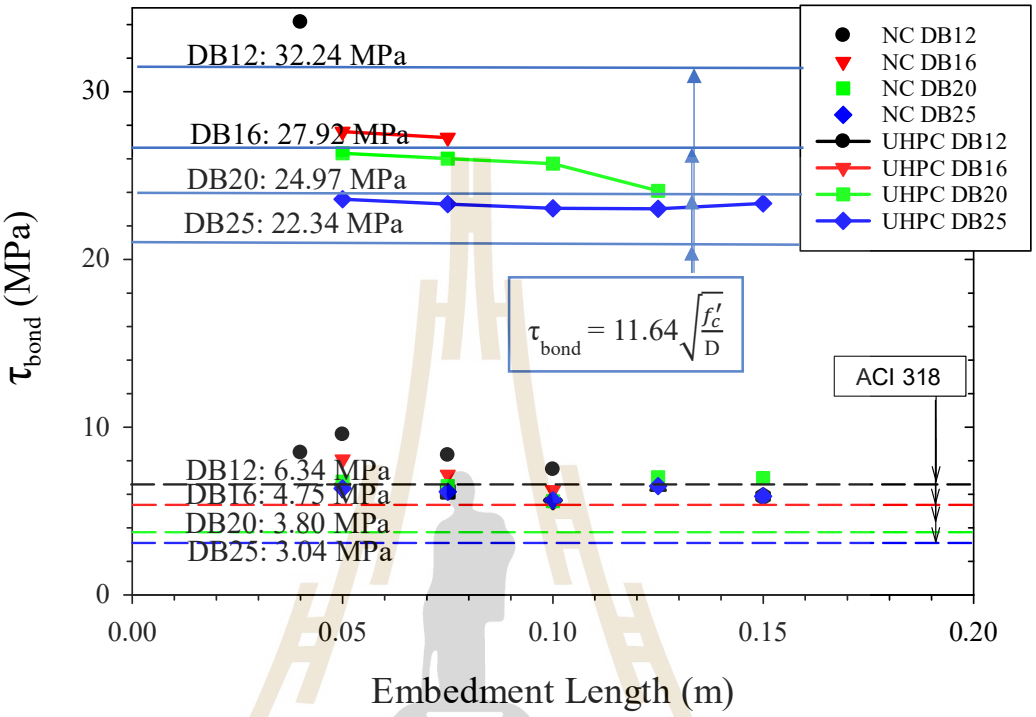

Figure 3.8. Bond strength of steel rebar in NC and UHPC at 7-day of f_c'.

Figure 3.8 displays the bond strength between steel rebars and both NC and UHPC at varying steel rebar diameters. The bond strength obtained from the pull-out test was assumed to represent the bond strength at infinite spacing ($s=\infty$), as this bond strength is not affected by the presence of neighboring rebars. The experimental results of NC revealed bond strengths of 8.46, 7.17, 6.56, and 6.07 MPa for DB12, DB16, DB20, and DB25, respectively. The ACI-318 (2011) bond strength equation can predict the ultimate bond strength of NC at 6.34, 4.75, 3.80, and 3.04 MPa for DB12, DB16, DB20, and DB25, respectively. However, the equation slightly underestimates the experimental results by 25.7%, 33.7%, 42.1%, and 49.9% for DB12, DB16, DB20, and DB25, respectively. The bond strength equation proposed by ACI-318 is not capable of accurately predicting the ultimate bond strength for UHPC, as the compressive strength of concrete is limited to 70 MPa (Bae, Choi and Choi,

2016) in ACI-318's bond strength prediction (2011). Consequently, this research proposes a new equation for predicting the bond strength of UHPC, given by:

$$\tau_{bond,\ UHPC} = 11.64\sqrt{\frac{f_c'}{D}} \quad \text{.....(3.1)}$$

where $\tau_{bond,\ UHPC}$ is predicted ultimate bond strength for UHPC [MPa],

f_c' is compressive strength of UHPC [MPa] and

D is the diameter of steel rebar [mm]

The predicted ultimate bond strength of UHPC was determined using equation (1) and found to be 32.24, 27.92, 24.97, and 22.34 MPa for DB12, DB16, DB20, and DB25, respectively. The experimental results showed bond strengths of 34.14, 27.44, 25.53, and 23.26 MPa, which resulted in error percentages of 5.56%, -1.74%, 2.21%, and 3.96% for DB12, DB16, DB20, and DB25, respectively. Additionally, a comparison between the predicted values of the ultimate bond strength of UHPC using equation (1) and the experimental results at varying f_c' is presented in **Figure 3.9** The findings revealed that the predicted bond strengths obtained from equation (1) were highly accurate when the *fc'* of UHPC exceeded 70 MPa. However, when the *fc'* of UHPC was lower than 70 MPa, the bond strength equation proposed by ACI-318 was capable of predicting not only the bond strength of UHPC but also the bond strength of NC.

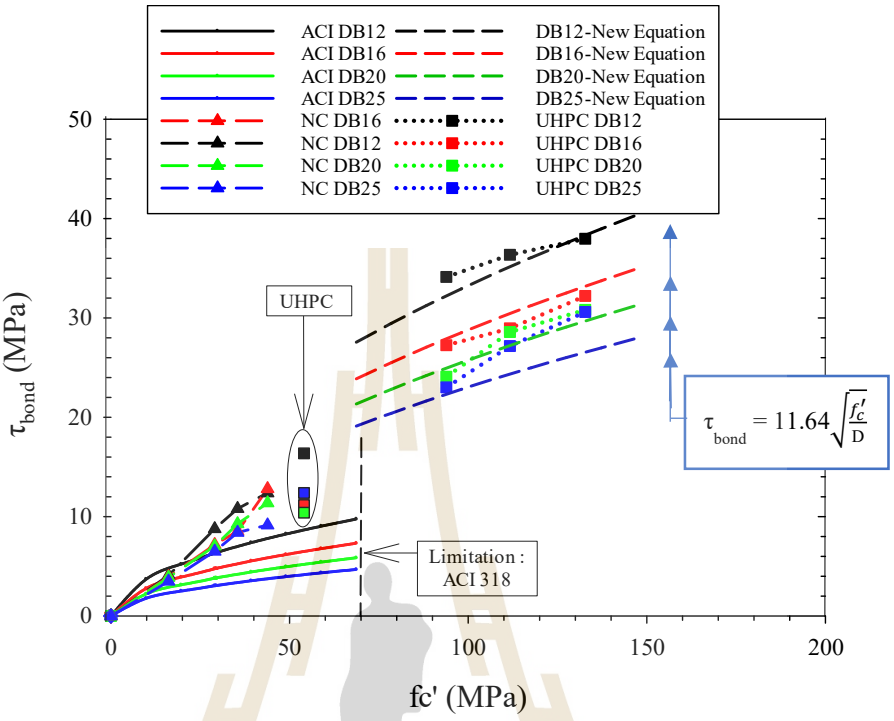

Figure 3.9. Bond strength of steel rebar in NC and UHPC at varied f_c'.

In addition, this study proposed an equation to predict the safe steel embedding length (development length) based on the bond strength and tension stress in the steel bar (f_s). To derive this equation, the maximum force at rebar rupture was assumed to be equal to the maximum force of bonding (Max. Tensile force = Max. Bonding force), and the relevant equations were applied accordingly. The resulting equation for safe steel implantation length is as follows:

$$\text{Max. Tensile force } (A_b f_s) = \text{Max. Bonding force } (\tau_{bond} A_{surface})$$

$$\tau_{bond} = \frac{f_s}{4\left(\frac{L}{D}\right)} \quad \text{.....(3.2)}$$

where τ_{bond} is bond strength,

f_s is tensile stress in rebar

A_b is cross-section area of rebar ($\frac{\pi}{4}D^2$),

$A_{surface}$ is the initial surface area of the embedded portion of the rebar (πDL),

L/D is the embedment length to diameter ratio.

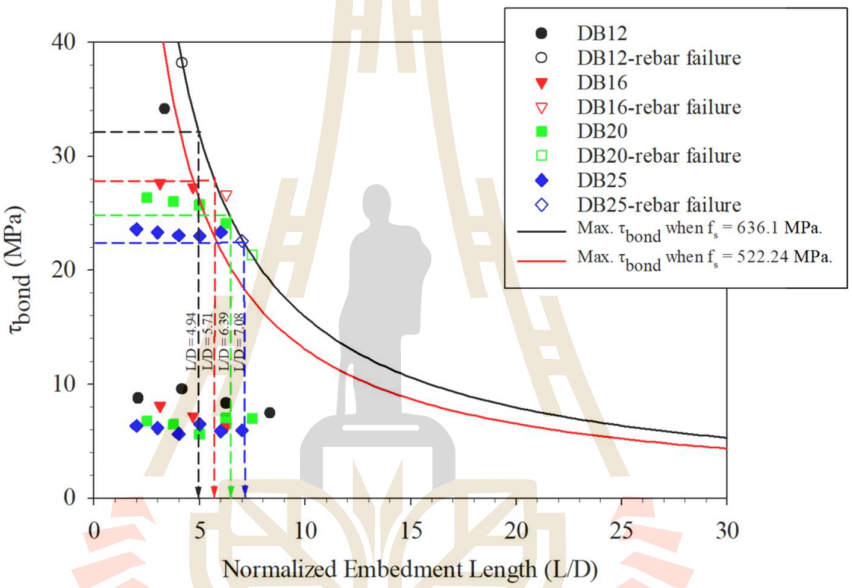

Figure 3.10. Failure boundary of steel rebars of different sizes in both NC and UHPC

The equation (2) can be utilized to determine the boundary of the required embedment length necessary to achieve the desired bond strength between the steel and concrete. In **Figure 3.10**, the boundary of the required embedment length is shown in terms of the embedment length to diameter ratio (L/D). The tension stress in the rebar (f_s) was considered at two values: 522.24 MPa for the average yield stress and 636.1 MPa for the average ultimate stress of the rebar. Furthermore, the bond strength of the rebar can be estimated using equation (1) for UHPC. It should be noted that while using equation (1) with fs = 636.1 MPa, the predicted required L/D ratios were 4.94, 5.71, 6.39 and 7.08 for DB12, DB16, DB20, and

DB25, respectively. However, the experimental results revealed embedment length to diameter ratios of 4.52, 5.89, 6.74 and 6.92 at the point of rebar rupture, which were lower than the predicted values by approximately 9.29%, -3.05%, -5.19% and 2.31% for the respective bar sizes.

3.3.3 Lap-Splice Test results

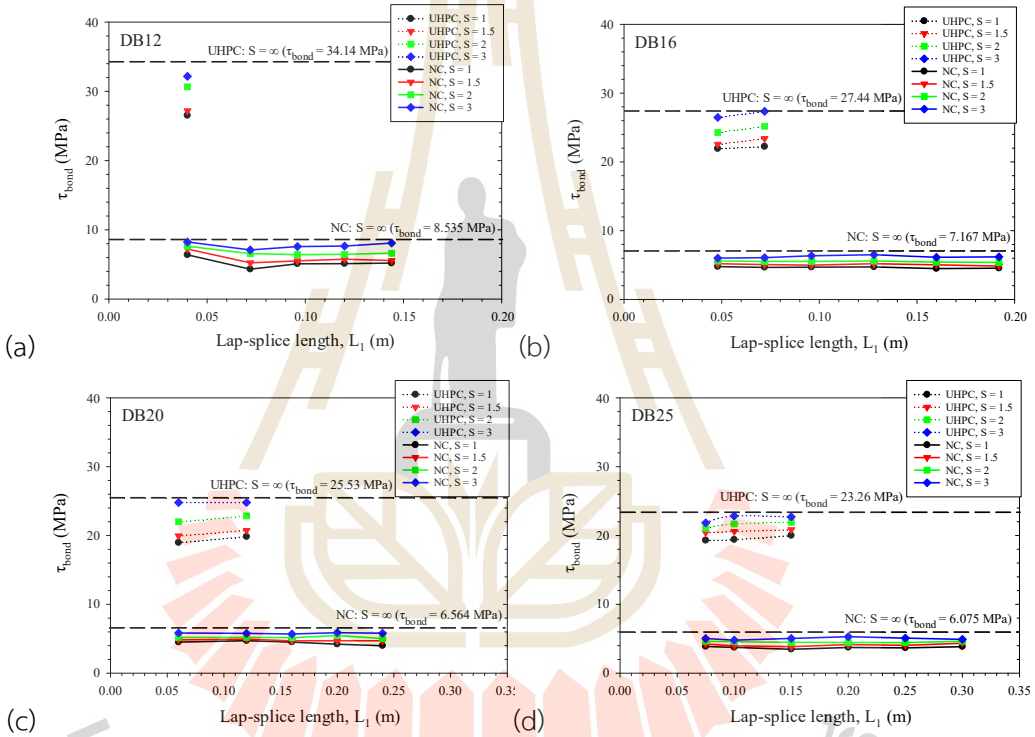

Figure 3.11. Bond strength of lap-spliced bars without hook in NC and UHPC at 7-day of fc' for (a) DB12, (b) DB16, (c) DB20 and (d) DB25

The findings from the bond strength tests for lap-spliced bars without hook in NC and UHPC, with varying rebar diameter and spacing (*s*) and lap-splice lengths (L_1), are presented in **Figure 3.11**. It was observed that the bond strength of lap-spliced bars increased with an increase in s for all the tested rebars, with the highest bond strength recorded at *s*=3 and the lowest at *s*=1. As an example, the

average bond strength of DB12 (**Figure 3.11(a)**) in NC was observed to be 5.22, 5.92, 6.72, and 7.72 MPa for the *s* values of 1, 1.5, 2, and 3, respectively. However, these values were found to be lower than the bond strength obtained from the pull-out test ($s=\infty$) by approximately 38.84%, 30.64%, 21.27%, and 9.55%, respectively. The lap-spliced bars in UHPC exhibited average bond strength values of 26.52, 27.19, 30.66 and 32.18 MPa for the *s* values of 1, 1.5, 2, and 3, respectively. However, these values were observed to be lower than the bond strength obtained from $s=\infty$ by approximately 22.34%, 20.36%, 10.19%, and 5.74%, respectively.

In a similar manner, the highest bond strength was observed at $s=3$ for DB16, DB20, and DB25 in both NC and UHPC (**Figure 3.11(b-d)**). The average bond strengths in NC were 6.21, 6.42, and 5.03 MPa for DB16, DB20, and DB25, respectively, and in UHPC were 26.91, 24.80, and 22.47 MPa for DB16, DB20, and DB25, respectively. Conversely, when the spacing was set to 1, the average bond strength in NC was 4.65, 4.38, and 3.73 MPa for DB16, DB20, and DB25, respectively, while the average bond strength in UHPC was 22.08, 19.40, and 19.70 MPa for DB16, DB20, and DB25, respectively. The observed increase in bond strength for lap-spliced bars in concrete with an increase in rebar spacing can be attributed to a higher level of lateral confinement forces acting on the bars. As the spacing between the bars increases, the confinement forces also increase, which reduces the lateral deformation and crack formation in the surrounding concrete. This phenomenon results in the development of mechanical interlocks between the bars and the surrounding concrete, leading to an increase in bond strength (Harajli, Hamad and Rteil, 2004, Wang, Wu, Guo and Song, 2018, Yoo, Shin, Yang and Yoon, 2014).

The normalized bond strength of lap-spliced bars without hooks is presented in **Figure 3.12**, demonstrating that a decrease in the spacing between rebars results in a reduction in bond strength for both NC and UHPC when compared to $s=\infty$ for their respective concrete types. In NC, the normalized bond strength of lap-spliced bars ranged from 0.61 to 0.66, 0.67 to 0.72, 0.74 to 0.79, and 0.82 to 0.89 for *s* values of 1, 1.5, 2, and 3, respectively. Meanwhile, in UHPC, the normalized bond strength of lap-spliced bars ranged from 0.77 to 0.84, 0.79 to 0.88, 0.87 to 0.92,

and 0.94 to 0.98 for *s* values of 1, 1.5, 2, and 3, respectively. However, it is important to acknowledge that in practical construction, lapped splice bars are typically positioned close together, corresponding to a spacing of *s*=1. Therefore, this study recommends the use of reduction factors (ϕ) of 0.6 and 0.75 for NC and UHPC, respectively, to adjust the bond strength obtained from pull-out tests ($s=\infty$) to approximate the actual bond strength of lap-spliced bars. This approach offers a safer method for calculating bond strength and designing lap-splice lengths (L_1).

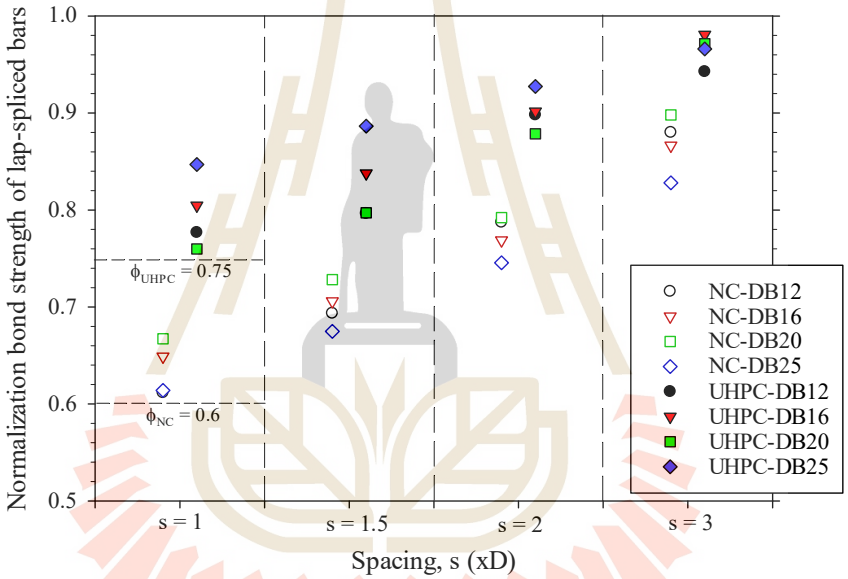

Figure 3.12. Normalization of bond strength of lap-spliced bars without hook

The bond strength tests for lap-spliced bars with hook in NC and UHPC, with varying rebar diameter and spacing (*s*), lap-splice length (L_1) and hook length (L_2) are presented in **Figure 3.13**. The green dashed line in the graph represents the theoretical upper limit of bond strength, which is obtained by dividing the ultimate tensile strength of the steel rebar (f_u) by the surface area calculated at a specific lap-splice length ($A_{surface} = \pi D L_1$) (Ma, Deng, Fan, Yang and Sun, 2020). The results reveal that both NC and UHPC exhibit an increase in bond strength as the spacing, lap-splice

length, and hook length increase. When $L_1 \geq 4D$, in conjunction with $L_2 \geq 3D$, a notable enhancement in bond strength is observed, surpassing the bond strength obtained from the pull-out test ($s=\infty$). This effect is particularly pronounced in UHPC, where a significant improvement in bond strength occurs as L_2 increases, resulting in its convergence towards the theoretical upper limit of bond strength.

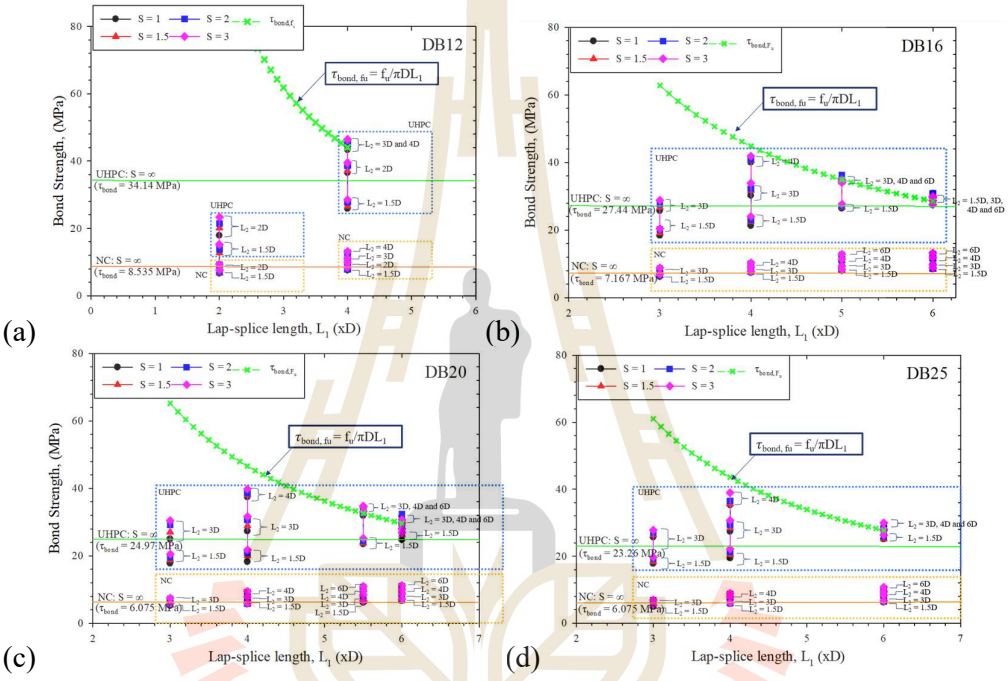

Figure 3.13. Bond strength of lap-spliced bars with hook in NC and UHPC at 7-day of fc' for (a) DB12, (b) DB16, (c) DB20 and (d) DB25

For example, in the case of UHPC, when s = 1 and L_1 = 4D, the bond strength values of DB12 are 25.79, 36.5, 43.31, and 45.93 MPa for hook lengths (L_2) of 1.5D, 2D, 3D, and 4D, respectively. Conversely, for NC, the bond strength values are 7.52, 9.27, 10.47, and 12.2 MPa for L_2 of 1.5D, 2D, 3D, and 4D, respectively. When comparing these values to the bond strength obtained at $s=\infty$ for each concrete type, it is observed that the bond strength of UHPC experiences increases of -24.45%, 6.91%, 26.85%, and 34.53% for L_2 of 1.5D, 2D, 3D, and 4D, respectively. For NC, the bond strength exhibits increase of -11.89%, 8.61%, 22.67%, and 42.94% for the same

respective L_2. Similar to DB16, DB20, and DB25, in the case of UHPC with s=1, L_1= 4D, L_2=3D, the bond strength values are 30.22, 27.32, and 27.35 MPa, respectively. Comparing these values to the bond strength obtained at s=∞, it is observed that there is an increase of approximately 10.13%, 9.41%, and 17.58% for DB16, DB20, and DB25, respectively. Moreover, with an increase in L_2 to 4D while keeping s and L_1 constant, the bond strength values for DB16, DB20, and DB25 exhibit further increments of 46.02%, 49.97%, and 51.67%, respectively.

The bond strength of rebar with hooks is generally higher than that of lap-spliced bars due to several reasons. Firstly, the presence of hooks creates additional surface area for bond development between the rebar and concrete, enhancing the mechanical interlock. This increased contact area allows for a greater transfer of forces and improves the bond strength (Goksu, Yilmaz, Chowdhury, Orakcal and Ilki, 2014, Mousa, 2016, Xia, Mackie, Saleem and Mirmiran, 2011). Secondly, the hooks act as anchorage devices by resisting the pull-out forces exerted on the rebar. The curved shape of the hooks helps to distribute the applied load more evenly along the length of the rebar, reducing stress concentrations and preventing premature bond failure (Mousa, 2015, Sulaiman, Ma, Apandi, Chin, Awang, Mansur and Omar, 2017, Yin, Xu and Lv, 2014, Yu and Tan, 2013). Furthermore, the hooks provide a better confinement effect on the surrounding concrete compared to lap-spliced bars due to their curved shape and ability to engage with the concrete more effectively. The presence of hooks generates localized pressure, resulting in improved confinement of the concrete in their vicinity. This localized confinement effectively restrains lateral deformation and minimizes crack formation within the concrete, ultimately leading to a notable enhancement in bond strength (Bournas and Triantafillou, 2011, Bousias, Spathis and Fardis, 2007, Ghosh and Sheikh, 2007, Tariverdilou, Farjadi and BARKHOURDARI, 2009).

The normalized bond strength of lap-spliced bars with hooks is presented in **Figure 3.14**. In this study, the selection of L_1 = 4D was based on its observed highest effectiveness in strengthening the bond strength of lap-spliced bars with hooks, as demonstrated in **Figure 3.13**. The findings indicate that the bond strength of lap-

spliced bars with hooks increases with an increase in both the spacing (*s*) and the hook length to diameter ratio (L_2/D). For instance, in UHPC with *s*=1 (**Figure 3.14(a)**), the bond strength of lap-spliced bars with hooks is 1.06, 1.15, and 1.52 times higher than the bond strength obtained at s=∞ for L_2/D values of 2, 3, and 4, respectively. Similarly, at s=3, the bond strength of lap-spliced bars with hooks further increases to 1.15, 1.30, and 1.63 times higher than the bond strength obtained at s=∞ for L_2/D values of 2, 3, and 4, respectively. However, in contrast to UHPC, the effectiveness of lap-spliced bars with hooks in strengthening the bond strength in NC is comparatively lower. At *s*=1 (**Figure 3.14(b)**), the bond strength of lap-spliced bars with hooks is 1.03, 1.06, 1.18, and 1.37 times higher than the bond strength obtained at s=∞ for L_2/D values of 1.5, 2, 3, and 4, respectively. Similarly, at *s*=3, the bond strength of lap-spliced bars with hooks is 1.10, 1.14, 1.26, and 1.47 times higher than the bond strength obtained at s=∞ for L_2/D values of 1.5, 2, 3, and 4, respectively.

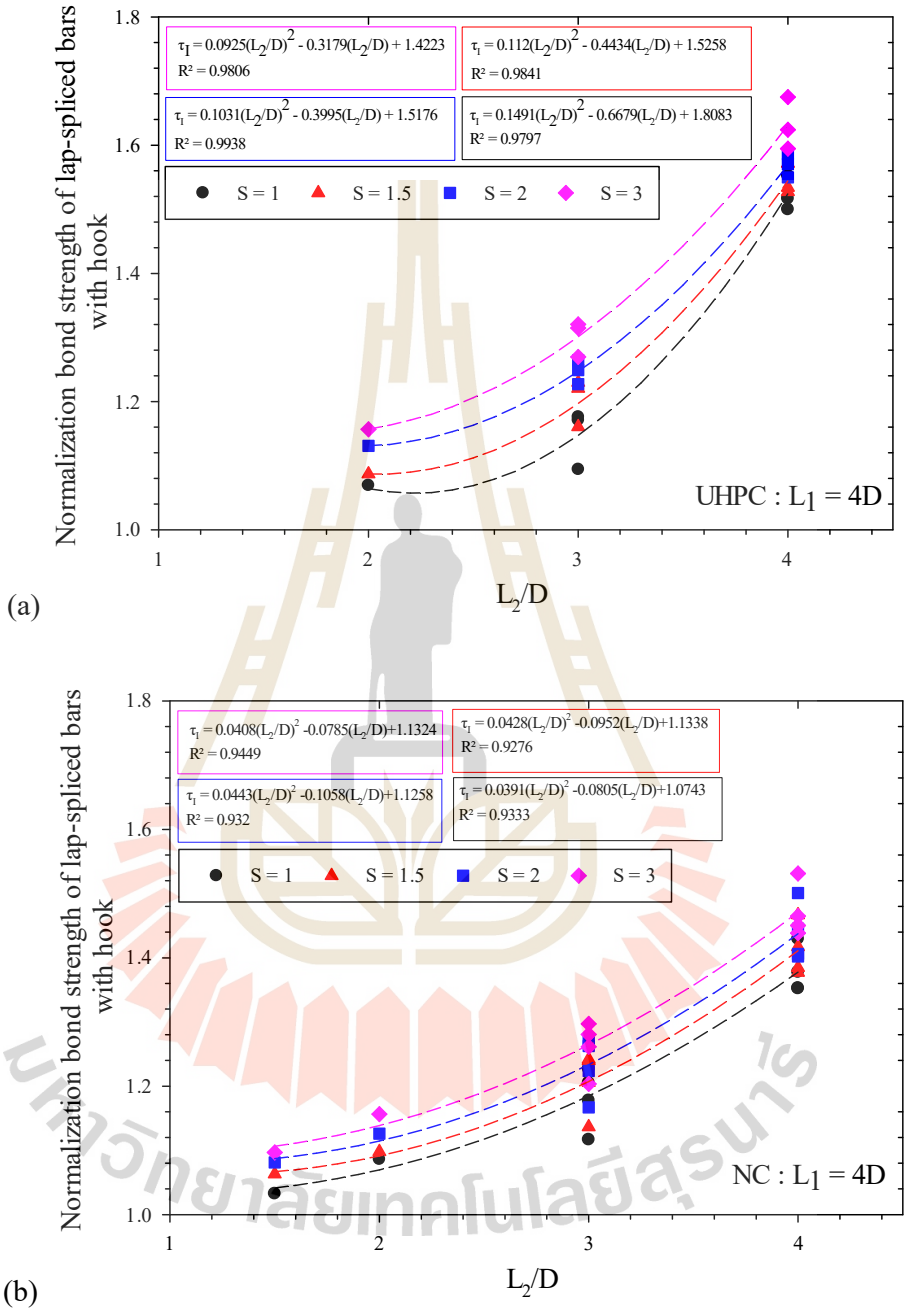

Figure 3.14. Normalization of bond strength of lap-spliced bars with hook

The higher bond strength of lap-spliced bars with hooks in UHPC compared to NC can be attributed to the superior mechanical properties exhibited

by UHPC. With its higher compressive strength, greater tensile strength, and enhanced durability, UHPC inherently provides a stronger bond between the rebar and the surrounding concrete (Zhou and Qiao, 2018). The presence of steel fibers in UHPC further enhances this bond by creating an interconnected network of fibers that effectively interlock with the rebar and the concrete matrix. This improved interlocking mechanism promotes a more efficient transfer of forces, resulting in a higher bond strength (Li, Tan and Yang, 2018, Song, Yu, Shui, Rao, Wang, Sun and Jiang, 2018, Li, Tan and Yang, 2019). Moreover, the steel fibers act as effective crack bridging elements, effectively distributing stresses and impeding crack propagation, thereby contributing to the overall bond performance (Zhang, Stang and Li, 2000, Leung and Shapiro, 1999). Additionally, the inclusion of steel fibers enhances the ductility of the concrete, allowing it to deform and absorb greater energy before experiencing failure (Oh, 1992, Balendran, Zhou, Nadeem and Leung, 2002, Mohod, 2012), ultimately leading to a higher bond strength.

3.4 Conclusions

Based on the experiments conducted in this study, the following conclusions may be drawn:

1) In both NC and UHPC, an increase in the embedment length during the pull-out test resulted in a corresponding increase in the pull-out force. This research introduces a novel equation, denoted as $\tau_{bond} = 11.64\sqrt{(f_c'/D)}$ (MPa), which offers an effective means of estimating the bond strength and the corresponding required embedment length in terms of L/D. The proposed equation demonstrates a remarkable level of accuracy, exhibiting an error margin of less than ±10%.

2) The study observed an increase in bond strength for lap-spliced bars as the spacing (s) between the bars increased, with the highest strength at s=3 and the lowest at s=1. However, in practical construction, bars are often closely spaced (s=1). To estimate the actual bond strength in such cases, reduction factors (ϕ) of 0.6 for NC and 0.75 for UHPC are recommended. These factors adjust the bond strength

obtained from infinite spacing (s=∞) pull-out tests to approximate real-work lap-spliced bar strength.

3) The bond strength of lap-spliced bars with hooks in both NC and UHPC increases with an increase in s, L_1, and L_2. When $L_1 \geq 4D$ and $L_2 \geq 3D$, a significant improvement in bond strength is observed, exceeding the bond strength obtained from the pull-out test (s=∞). This is because a longer hook provides a larger contact area for interaction with the concrete, resulting in a stronger bond. It also allows for a more gradual transfer of forces, reducing stress concentration and minimizing the risk of localized failure or bond slippage.

4) The superior bond strength of lap-spliced bars with hooks in UHPC compared to NC can be attributed to UHPC's higher compressive strength, as well as the presence of steel fibers. The steel fibers in UHPC create an interconnected network that enhances interlocking between the rebar and the concrete, resulting in improved force transfer. Additionally, these fibers act as crack bridging elements, effectively distributing stresses and impeding crack propagation, thereby enhancing the overall bond performance.

5) This study presents a promising opportunity for the utilization of short-distanced lap splices embedded in UHPC structures. The experimental findings provide valuable insights into the required parameters for achieving the desired bond strength, including the embedment length, lap-spliced length, and hook length expressed in terms of L/D, L1/D, and L2/D, respectively. Furthermore, this study emphasizes the potential benefits of using UHPC in combination with short-distanced lap splices, opening up possibilities for the optimization of construction processes and the realization of more efficient and sustainable structural solutions.

3.5 References

(2011). "ACI Committee 318, Building Code Requirements for Structural Concrete (ACI318-11) and Commentary." American Concrete Institute, Farmington Hills, Mich., 391 p.

Aarup, B., and Jensen, B. (1998). "Bond properties of high-strength fiber reinforced concrete." Special Publication, 180, 459-472.

Alkaysi, M., and El-Tawil, S. (2017). "Factors affecting bond development between Ultra High Performance Concrete (UHPC) and steel bar reinforcement." Construction and Building Materials, 144, 412-422.

Bae, B.-I., Choi, H.-K., and Choi, C.-S. (2016). "Bond stress between conventional reinforcement and steel fibre reinforced reactive powder concrete." Construction and Building Materials, 112, 825-835.

Balendran, R., Zhou, F., Nadeem, A., and Leung, A. (2002). "Influence of steel fibres on strength and ductility of normal and lightweight high strength concrete." Building and environment, 37(12), 1361-1367.

Belleri, A., Brunesi, E., Nascimbene, R., Pagani, M., and Riva, P. (2015). "Seismic performance of precast industrial facilities following major earthquakes in the Italian territory." Journal of Performance of Constructed Facilities, 29(5), 04014135.

Bond, A. (2003). "Development of Straight Reinforcing Bars in Tension." ACI 408R-03.

Bournas, D., and Triantafillou, T. (2011). "Bond strength of lap-spliced bars in concrete confined with composite jackets." Journal of Composites for Construction, 15(2), 156-167.

Bousias, S., Spathis, A.-L., and Fardis, M. N. (2007). "Seismic retrofitting of columns with lap spliced smooth bars through FRP or concrete jackets." Journal of Earthquake Engineering, 11(5), 653-674.

Committee, A. (2019). "Building code requirements for structural concrete and commentary (ACI 318-19)." American Concrete Institute: Farmington Hills, MI, USA, 623.

Einea, A., Yamane, T., and Tadros, M. K. (1995). "Grout-filled pipe splices for precast concrete construction." PCI journal, 40(1), 82-93.

Elliott, K. S. (2000). "Research and development in precast concrete framed structures." Progress in structural engineering and materials, 2(4), 405-428.

Garcia-Taengua, E., Martí-Vargas, J. R., and Serna, P. (2016). "Bond of reinforcing bars to steel fiber reinforced concrete." Construction and Building Materials, 105, 275-284.

Ghosh, K. K., and Sheikh, S. A. (2007). "Seismic upgrade with carbon fiber-reinforced polymer of columns containing lap-spliced reinforcing bars." ACI structural journal, 104(2), 227.

Goksu, C., Yilmaz, H., Chowdhury, S., Orakcal, K., and Ilki, A. (2014). "The effect of lap splice length on the cyclic lateral load behavior of RC members with low-strength concrete and plain bars." Advances in Structural Engineering, 17(5), 639-658.

Graybeal, B. (2014). "Design and construction of field-cast UHPC connections." United States. Federal Highway Administration.

Harajli, M. H., Hamad, B. S., and Rteil, A. A. (2004). "Effect of confinement of bond strength between steel." ACI Structural Journal, 101(5), 595-603.

Huang, Y., Lee, M.-G., Kan, Y.-C., Wang, W.-C., Wang, Y.-C., and Pan, W.-B. (2022). "Reinforced concrete beams retrofitted with UHPC or CFRP." Case Studies in Construction Materials, 17, e01507.

Lee, J.-K. (2016). "Bonding behavior of lap-spliced reinforcing bars embedded in ultra-high strength concrete with steel fibers." KSCE Journal of Civil Engineering, 20, 273-281.

Leung, C. K., and Shapiro, N. (1999). "Optimal steel fiber strength for reinforcement of cementitious materials." Journal of Materials in Civil Engineering, 11(2), 116-123.

Li, Y., Tan, K. H., and Yang, E.-H. (2018). "Influence of aggregate size and inclusion of polypropylene and steel fibers on the hot permeability of ultra-high performance concrete (UHPC) at elevated temperature." Construction and Building Materials, 169, 629-637.

Li, Y., Tan, K. H., and Yang, E.-H. (2019). "Synergistic effects of hybrid polypropylene and steel fibers on explosive spalling prevention of ultra-high performance concrete at elevated temperature." Cement and Concrete Composites, 96, 174-181.

Ma, F., Deng, M., Fan, H., Yang, Y., and Sun, H. (2020). "Study on the lap-splice behavior of post-yield deformed steel bars in ultra high performance concrete." Construction and Building Materials, 262, 120611.

McMullen, K. F., and Haber, Z. "Effect of Steel Reinforcement Type and Diameter on the Strength of Non-Contact Lap Splice Connections using UHPC." Proc., International Interactive Symposium on Ultra-High Performance Concrete, Iowa State University Digital Press.

Mohod, M. V. (2012). "Performance of steel fiber reinforced concrete." International Journal of Engineering and Science, 1(12), 1-4.

Mousa, M. I. (2015). "Flexural behaviour and ductility of high strength concrete (HSC) beams with tension lap splice." Alexandria Engineering Journal, 54(3), 551-563.

Mousa, M. I. (2016). "Effect of bond loss of tension reinforcement on the flexural behaviour of reinforced concrete beams." HBRC journal, 12(3), 235-241.

Oh, B. H. (1992). "Flexural analysis of reinforced concrete beams containing steel fibers." Journal of structural engineering, 118(10), 2821-2835.

Pour, S. M., and Alam, M. S. "Investigation of compressive bond behavior of steel rebar embedded in concrete with partial recycled aggregate replacement." Proc., Structures, Elsevier, 153-164.

Shafieifar, M., Farzad, M., and Azizinamini, A. (2017). "Alternative ABC connection utilizing UHPC."

Shen, D., Shi, X., Zhang, H., Duan, X., and Jiang, G. (2016). "Experimental study of early-age bond behavior between high strength concrete and steel bars using a pull-out test." Construction and Building materials, 113, 653-663.

Song, Q., Yu, R., Shui, Z., Rao, S., Wang, X., Sun, M., and Jiang, C. (2018). "Steel fibre content and interconnection induced electrochemical corrosion of Ultra-High Performance Fibre Reinforced Concrete (UHPFRC)." Cement and Concrete Composites, 94, 191-200.

Standard (2001). "ASTM C39: Standard test method for compressive strength of cylindrical concrete specimens." ASTM international West Conshohocken, PA, USA.

Standard (2003). "ASTM C33: Standard Specification for Concrete Aggregates." ASTM international West Conshohocken, PA, USA.

Standard (2009). "ASTM C469: Standard Test Method for Static Modulus of Elasticity and Poisson's Ratio of Concrete in Compression." ASTM international West Conshohocken, PA, USA.

Standard (2009). "C403: Standard Test Method for Time of Setting of Concrete Mixtures by Penetration Resistance." ASTM international West Conshohocken, PA, USA.

Sulaiman, M. F., Ma, C.-K., Apandi, N. M., Chin, S., Awang, A. Z., Mansur, S. A., and Omar, W. "A review on bond and anchorage of confined high-strength concrete." Proc., Structures, Elsevier, 97-109.

Tariverdilou, S., Farjadi, A., and BARKHOURDARI, M. (2009). "Fragility curves for reinforced concrete frames with lap-spliced columns."

Tosa, F. V., and Salha, R. (2016). "The behavior of different precast concrete structures under seismic action." Procedia Technology, 22, 235-242.

Wang, F., Wu, X., Guo, C., and Song, W. (2018). "Experimental study on bond strength of deformed steel bars in recycled glass aggregate concrete." KSCE Journal of Civil Engineering, 22, 3409-3418.

Xia, J., Mackie, K. R., Saleem, M. A., and Mirmiran, A. (2011). "Shear failure analysis on ultra-high performance concrete beams reinforced with high strength steel." Engineering Structures, 33(12), 3597-3609.

Ye, M., Jiang, J., Chen, H., Zhou, H., and Song, D. (2021). "Seismic behavior of an innovative hybrid beam-column connection for precast concrete structures." Engineering Structures, 227, 111436.

Yin, S., Xu, S., and Lv, H. (2014). "Flexural behavior of reinforced concrete beams with TRC tension zone cover." Journal of Materials in Civil Engineering, 26(2), 320-330.

Yoo, D.-Y., Kwon, K.-Y., Park, J.-J., and Yoon, Y.-S. (2015). "Local bond-slip response of GFRP rebar in ultra-high-performance fiber-reinforced concrete." Composite Structures, 120, 53-64.

Yoo, D.-Y., Shin, H.-O., Yang, J.-M., and Yoon, Y.-S. (2014). "Material and bond properties of ultra high performance fiber reinforced concrete with micro steel fibers." Composites Part B: Engineering, 58, 122-133.

Yu, J., and Tan, K.-H. (2013). "Experimental and numerical investigation on progressive collapse resistance of reinforced concrete beam column sub-assemblages." Engineering Structures, 55, 90-106.

Yuan, J., and Graybeal, B. (2015). "Bond of Reinforcement in Ultra-High-Performance Concrete." ACI Structural Journal, 112(6).

Zhang, J., Stang, H., and Li, V. C. (2000). "Experimental study on crack bridging in FRC under uniaxial fatigue tension." Journal of Materials in Civil Engineering, 12(1), 66-73.

Zhou, Z., and Qiao, P. (2018). "Bond behavior of epoxy-coated rebar in ultra-high performance concrete." Construction and Building Materials, 182, 406-417.

CHAPTER IV

PERFORMANCE OF CONNECTION JOINTS OF BEAM-COLUMN STRUCTURE USING ULTRA-HIGH-PERFORMANCE CONCRETE UNDER FULL-SCALE TESTS

4.1 Introduction

The use of precast concrete technology has revolutionized modern construction practices, providing significant advantages in terms of construction speed, quality control, and cost-effectiveness (Chan 2011; Parskiy et al. 2017). Precast concrete involves casting concrete elements in a controlled factory environment and then transporting them to the construction site for assembly. This method ensures that each component is produced under optimal conditions, leading to high-quality, consistent products (Hong et al. 2018). The precast approach allows for rapid assembly on-site, reducing construction time and labor costs (Anvari et al. 2016; Wang et al. 2018). Additionally, the ability to produce components in a factory setting allows for better resource management and waste reduction, contributing to more sustainable construction practices (Cai and Waldmann 2019; Garetti and Taisch 2012; Sev 2009). However, despite its many benefits, precast concrete technology faces several challenges, particularly concerning the performance of joints in precast column-beam structures (Choi 2020; Ghayeb et al. 2020; Xue et al. 2021; Zhang et al. 2020; Zhong et al. 2019).

One of the main issues with precast concrete structures is the performance of the joints that connect the various elements. These joints are critical to the structural integrity and overall stability of the structure. They must efficiently transfer loads,

including axial loads, shear forces, and bending moments, between the connected elements (Cabral-Fonseca et al. 2018; Engindeniz et al. 2005; Mousavi and Dehestani 2022). Poorly designed or constructed joints can become weak points in the structure, leading to potential failure under load. Common problems include inadequate bonding between the precast elements, insufficient load transfer capabilities, and susceptibility to cracking and other forms of deterioration over time (Lowes and Altoontash 2003; Shishesaz and Hosseini 2020). Addressing these issues is crucial for ensuring the long-term durability and safety of precast concrete structures.

In addition to the common challenges found in precast systems, reinforced concrete (RC) beam-column joints in traditional construction also have important weaknesses, especially when the design details are not carefully considered. These joints must transfer different types of forces such as shear and tension within a small area, making the force transfer process quite complicated. If the steel rebars inside the joint are not properly anchored or if there is insufficient reinforcement, the joint can fail early, even under normal loading conditions. Supaviriyakit and Pimanmas (2008) found that joints without horizontal reinforcement or with weak rebar connections failed in brittle ways, like cracking along diagonals or splitting the beam, and they could not absorb much energy. Their research also showed that simply adding more reinforcement does not always improve performance if the joint's shape or detailing is still poor. Similarly, Somma et al. (2015) pointed out that problems like weak concrete confinement, short rebar anchorage, and poor coordination between the concrete and steel parts of the joint can also lead to failure. They explained that these parts need to work together, and if one fails, the others may not work properly either. For example, when stirrups (the small steel loops) inside the joint give way, the joint quickly loses its ability to resist shear forces. These issues highlight the importance of using well-rounded design approaches that consider all key factors like bonding, support, and shear resistance to ensure RC joints are strong and reliable.

Ultra-High-Performance Concrete (UHPC) has emerged as a promising solution to the challenges associated with joints in precast concrete structures. UHPC is an advanced cementitious material known for its exceptional mechanical properties and durability. It typically exhibits compressive strengths exceeding 150 MPa, significantly higher than conventional concrete (Du et al. 2021; Fehling et al. 2014; Ullah et al. 2022). UHPC's dense microstructure provides excellent resistance to environmental degradation, such as freeze-thaw cycles, chemical attacks, and abrasion (Bahmani and Mostofinejad 2022). Additionally, UHPC includes steel fibers, which enhance its tensile strength and ductility, allowing it to absorb and dissipate energy more effectively (Wen et al. 2022; Yoo and Kim 2019; Yoo et al. 2019; Yoo et al. 2020). These properties make UHPC an ideal material for improving the performance of precast concrete joints, addressing the weaknesses that commonly arise in these critical areas.

The high compressive strength of UHPC has a significant impact on the bond strength between rebar and concrete (Alkaysi and El-Tawil 2017; Farzad et al. 2019; Pokorný et al. 2020). UHPC's superior bonding capabilities ensure that the rebar can effectively anchor within the concrete, providing enhanced load transfer and structural stability (Huang et al. 2022; Hung et al. 2021). This characteristic is particularly beneficial for the design of joints in precast concrete structures, where effective load transfer is essential for maintaining the overall integrity of the structure. The enhanced bond strength provided by UHPC helps prevent issues such as slippage or pull-out of the reinforcing bars, which can compromise the joint's performance (Khayat and Meng 2014; Maya and Graybeal 2017; Zhou and Qiao 2018).

Aiamsri et al. (Aiamsri et al. 2024) conducted a laboratory test and proposed a new equation to predict the bond strength of rebar in UHPC:

$$\tau_{bond} = \phi 11.64\sqrt{\frac{f'_c}{D}} \quad \text{.....(4.1)}$$

where τ_{bond} is the bond strength for UHPC [MPa], ϕ is the reduction factor due to a spacing (s) between rebars (s = 1, 2, 3 and ≥ 4D, ϕ = 0.75, 0.87, 0.94 and 1, respectively), f_c' is the compressive strength of UHPC [MPa] and D is the diameter of steel rebar [mm].

Therefore, the development length of rebars in UHPC can be determined:

$$\frac{L_d}{D} = \frac{f_s}{4\,(\tau_{bond})} \quad \text{.....(4.2)}$$

where f_s is tensile stress in rebar, L_d/D is the development length to diameter ratio.

Furthermore, Aiamsri et al. [35] proposed an equation to determine the bond force of lap-splice rebar with hook (F_{bond}) could be expressed as follows:

$$F_{bond} = (\phi_1 L_1 + k\phi_2 L_2)\tau_{bond}\pi D \quad \text{.....(4.3)}$$

where ϕ_1 and ϕ_2 are the reduction factors due to the spacing (s) between lap-spliced rebars and hooks, respectively (if s = 1, 2, 3 and ≥ 4D, ϕ_1 and ϕ_2 = 0.75, 0.87, 0.94 and 1, respectively), L_1 and L_2 are lap-splice length and hook length, respectively, and k = reduction factor due to hook length (for simplicity and safety in design, the reduction factor was recommended as 0.2). τ_{bond} can be obtained from Equation (1).

To thoroughly evaluate the performance of UHPC in precast concrete joints, full-scale testing under loading conditions is essential. Static load tests involve applying gradual, controlled loads to the structure to assess its behavior under typical service conditions (Aktan et al. 1997; Alampalli et al. 2021; Küntz et al. 2006). This type of testing provides valuable insights into the structural performance of the joints, including their load-carrying capacity, deformation characteristics, and failure modes. These tests are crucial for validating theoretical models and ensuring that the joints perform as expected in real-world applications (Contento et al. 2024; Meoni et al. 2024; Molinari et al. 2009).

In this research, two types of lap-spliced rebars embedded in UHPC are investigated: lap-splice without hook (L_1) and lap-splice with a 90-degree hook. Lap splicing is a common method of connecting rebars in concrete structures, where the ends of two bars overlap for a certain length to transfer load between them. The inclusion of a 90-degree hook (L_2) provides additional anchorage (Baek et al. 2018; Tack 2019), potentially enhancing the bond strength and overall performance of the joint. Comparing the performance of these two configurations under static load conditions will provide insights into the most effective reinforcement strategies for UHPC joints in precast concrete structures. A key objective of this research is to validate the rebar length predicted by previous equations (Aiamsri et al. 2024) for use in UHPC joints at full scale. The failure behavior at the connection joint would moreover be investigated. Understanding this failure behavior is crucial for designing joints that have comparable or superior performance to the conventional concrete joints. The research finally aimed to establish guidelines for determining the required embedment length of rebars in UHPC, ensuring effective load transfer and maintaining structural integrity under service conditions.

Integrating UHPC into precast concrete joints holds substantial significant for enhancing the performance of the precast concrete elements. The superior mechanical properties of UHPC address many common issues associated with precast concrete joints, such as inadequate bonding and load transfer. The full-scale testing under static load conditions provides essential data to validate the effectiveness of UHPC in the connection application, thereby informing the development of improved design practices and standards. By exploring various configurations of lap-splice rebars and determining the optimal embedment length, this research seeks to advance the understanding of UHPC's role in strengthening the structural integrity of precast column-beam assemblies, ultimately contributing to more resilient and reliable construction practices.

4.2 Materials and methods

4.2.1 Material Characteristics of Normal Concrete and UHPC

The normal concrete (NC), used as a benchmark for UHPC, employed ordinary Portland cement as its binding agent. Fine aggregate consisted of sand with a grain size smaller than 4.75 mm, adhered to the ASTM C33 (Standard 2003). The NC achieved a compressive strength exceeding 38 MPa after 28 days, using a mix ratio (job mix formula) of cement to sand to water at 1:2:0.275, while maintaining a slump value within the range of 50 to 100 mm.

The UHPC mixture (ready-mix) used for casting the concrete specimens was supplied by Concrete Products and Aggregate Co., Ltd. (CPAC), a subsidiary of Siam Cement Group (SCG), a well-known provider of high-quality concrete products in Thailand. The mixing procedure for UHPC began by adding CPAC Cement Grout into the mixer and mixed it for 2 minutes. Next, water and the admixture PC-UP01 were added, followed by an additional 1 minute of mixing. Then, the Type D admixture was introduced, and the mixing continued for another 5 minutes. Steel fibers were gradually added to the mix by sprinkling them in with a scoop to prevent clumping, and the mixing proceeded for an additional 3 minutes. Finally, the flowability of the UHPC was checked either visually or by measuring the flow diameter, which should range between 80 and 95 cm.

Table 4.1 The mix design for UHPC.

UHPC		Materials per 1 cubic meter, kg
Cement Grout CPAC	Cement Grout	1143
	Sand	1130
Additional admixtures PC-UP01		31
Additional admixtures Type D		22
Steel fiber		155
Water		200

Table 4.1 presents the constituent material proportions per cubic meter for UHPC, offering a detailed reference for its mix design. The fine aggregate had a maximum size of 1 mm, and the water-to-binder ratio was 0.175. This mix design achieved compressive strengths (f_c') of 92.05, 111.76 and 132.84 MPa at 7, 14 and 28 days, respectively. The corresponding tensile strengths, as illustrated in **Figure 4.1**, were 3.87 MPa, 4.66 MPa, and 5.49 MPa. The elastic modulus was 19.54 and 26.46 GPa at 7 and 28 days of curing, respectively, The straight steel fibers in the UHPC measured 0.22 mm in diameter and 13 mm in length **(Figure 4.2)** and had an ultimate tensile strength of 2,800 MPa.

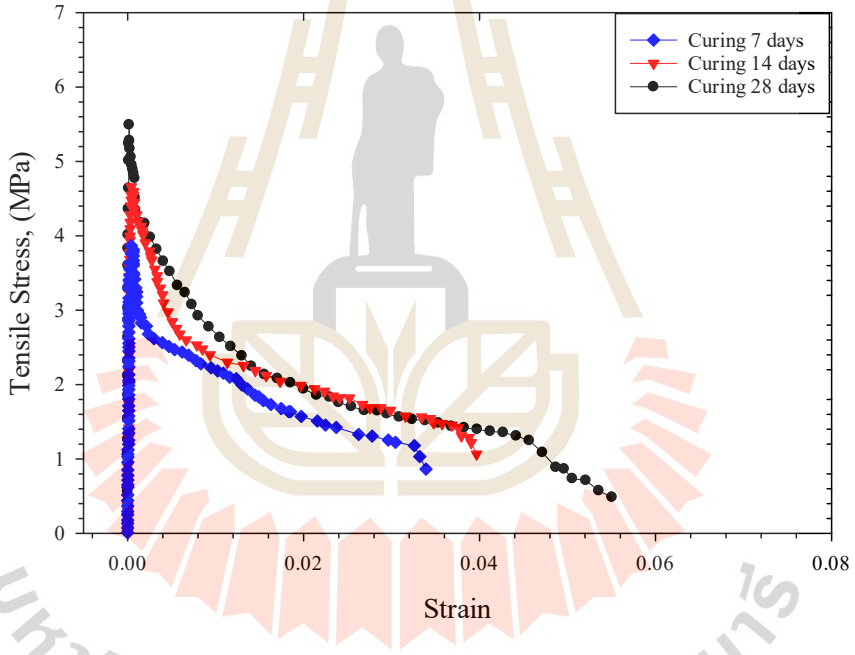

Figure 4.1 Tensile stress–strain behavior of UHPC at various curing ages.

The relatively low modulus of elasticity (26.46 GPa) observed in this study's UHPC mix can be attributed to the absence of coarse aggregate, as the mixture was composed solely of fine aggregate (maximum size 1 mm) and a high binder content. Although UHPC typically exhibits superior compressive strength compared to conventional concrete, its elastic modulus is more strongly influenced by the stiffness

and volume fraction of the aggregates than by compressive strength alone. Previous studies have shown that UHPC containing only fine quartz sand can have a modulus of around 48 GPa, while the inclusion of stiffer coarse aggregates such as basalt or bauxite split can increase the modulus by approximately 21% to 46%, reaching up to 70 GPa (Ma et al. 2004). Thus, the use of only fine aggregate in the current mix resulted in a more deformable matrix, explaining the lower measured elastic modulus.

Figure 4.2. Steel fibers in the UHPC

16-mm deformed rebars (DB16) were used to manufacture the beam. The average yield and ultimate loads for this rebar were measured at 108.63 kN and 126.33 kN, respectively. The average yield stress (f_y) and ultimate stress (f_u) were thus 565.94 MPa and 658.13 MPa, respectively, with an elastic modulus equal to 201,830 MPa.

4.2.2 Preparation of full-scale samples

The full-scale test involved evaluating the connection joints of precast concrete beam-column members under static loads. The test began with the casting of a column specimen and 2 cantilever beam specimens. The column had a cross-

section of 0.20 x 0.20 m^2 and a height of 0.40 m, and the beam had a cross-section of 0.20 x 0.40 m^2, extending 2.00 m from the column, as illustrated in **Figure 4.3**. The test comprised six connection conditions, including one with a traditional beam-column concrete connection and five with specialized UHPC connections, as summarized in **Table 4.2**

(a)

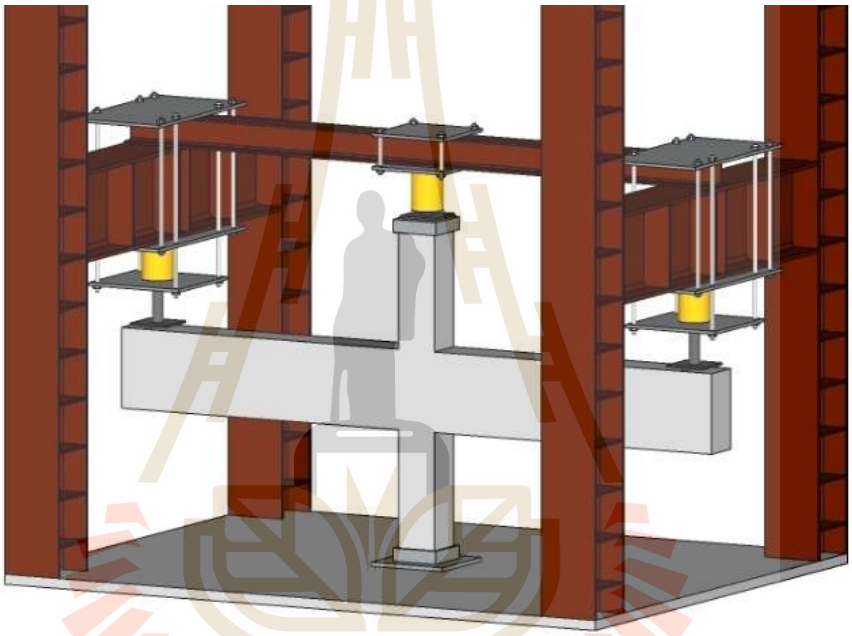

(b)

Figure 4.3. Depicts (a) the Full-Scale Test Model and (b) the Actual Test Conditions.

Table 4.2 Summary of Test Specimens and Connection Configurations

No.	Name	Concrete at joint	Embedment length (L_e)	Splice length (L_1)	Hook length (L_2)	Remark
1	Traditional cast-in-place beam-column joint (**TCIP**)	Normal Concrete		-	-	Strong joint
2	Non-overlapping without hook joint (**LE4**)	UHPC	4*D*	-	-	Weak joint
3	Non-overlapping with hook joint (**LE4+H3**)	UHPC	4*D*	-	3*D*	Weak joint
4	Lap-splicing without hook joint (**LS8**)	UHPC	-	8*D*	-	Strong joint
5	Lap-splicing with hook joint (**LS8+H4**)	UHPC	-	8*D*	4*D*	Strong joint
6	Lap-splicing without hook joint (**LS9**)	UHPC	-	9*D*	-	Strong joint

TCIP: Traditional Cast-In-Place, **LE4**: Embedment length with 4D, **LS8 / LS9**: Lap Splice with 8D or 9D, **H3 / H4**: Hook with 3D or 4D

For the five UHPC connection conditions, after casting the beam and column specimens by normal concrete, all test specimens were immediately covered with plastic sheets and cured at room temperature for 48 hours before being demolded. The specimens were then stored at room temperature until the target curing time was reached. The beam and column specimens were cured more for 19 days using water sprinkling before being assembled at connections filled with UHPC. The entire assembly was then cured for an additional 7 days, ensuring that the beam-column specimens were cured for a total of 28 days and the UHPC was cured for 7

days. The rebars of the beam specimens embedded in the UHPC connection joints were configured with varying lap-splice lengths (L_1) and hook lengths (L_2), maintaining a spacing (s) of 1 (measured as the center-to-center distance between bars). In cases where the rebars are non-overlapping ($s \geq 4D$), the embedment length (L_e) was evaluated both with and without hook lengths (L_2). Variations in the L_e, L_1 and L_2 configurations resulted in different failure modes, which were classified into two categories: Weak Joint (Samples No. 2-3) and Strong Joint (Samples No. 4-6). Weak Joints are characterized by insufficient lap-splice and hook lengths, leading to premature bond failure and reduced load-carrying capacity. In contrast, Strong Joints exhibit adequate lap-splice and hook lengths, providing superior bond performance and enabling the rebars to reach their failure tensile strength before failure.

For the full-scale tests, strain gauges were installed on the upper and lower rebars at the beam-column interface, with four points on each side. These gauges were used in every test to measure strain variations, which were then converted into tensile stresses to calculate the flexural moment capacity of the cross-section, as detailed in ACI-318 (ACI Committee 2008). The steel rebars exhibited an average failure tensile strength (f_u) of 658.13 MPa. The test procedure involved the application of vertical static loads simultaneously at both ends of the cantilever beams using two 500 kN hydraulic jacks, each precisely controlled to increment the load by approximately 1 kN. As shown in **Figure 3**, the experimental setup included three hydraulic jacks. The two side jacks were actively engaged in applying the test loads, while the central 200 kN hydraulic jack, positioned above the column, functioned solely as a support mechanism to stabilize the specimen and maintain the vertical alignment of the beam-column assembly under its self-weight. This central jack did not apply any active load during the test, thereby allowing the structural response of the beam-column connections to be assessed under well-defined loading conditions. The deliberate omission of axial loading on the column was intended to isolate the mechanical behavior and failure mechanisms of the connection itself, independent of axial force

effects (Bjorhovde et al. 1999). Following each load increment, the test was paused for approximately one minute to allow strain readings to stabilize and for data acquisition to be completed. This controlled, step-by-step loading protocol ensured accurate and consistent monitoring of strain distribution within the reinforcement. The following comparisons were then made:

1) The actual flexural moment obtained from the test (calculated as force multiplied by the distance from the edge of the column to the point of loading) was compared with the flexural moment calculated from the tensile force of the rebars, as measured by the strain gauges.

2) The bond strength of the rebars obtained from the full-scale test was compared with the predicted bond strength calculated using Equations (1), (2) and (3).

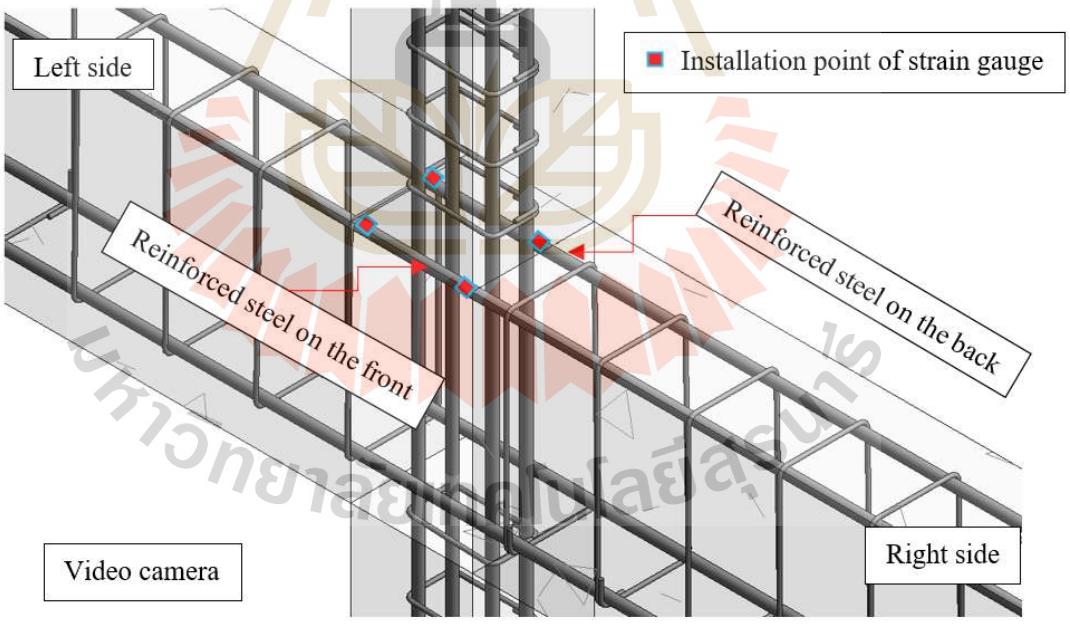

Figure 4.4. Detailed specifications of the steel reinforcement and locations of strain-gauge installation.

The beam-column connection test comprised six samples, defined as follows:

1) **Sample No.1-TCIP:** Traditional cast-in-place beam-column joint

The sample was fabricated by casting beam-column specimens in a standard construction manner, with the beam's rebars passing through the column. The sample was constructed from concrete cast uniformly through the entire sample. Following a 28-day curing period, testing commenced. Details of the steel reinforcement and strain-gauge installation are illustrated in **Figure 4.4.**

2) **Sample No. 2-LE4:** Non-overlapping without hook joint (Weak joint, L_e = 4*D*)

A full-scale test sample was cast and assembled, without any lap-splicing in the joint area (rebars embedded in the joint were shorter than half of the column width). The embedded length of the beam's rebars in the joint (L_e) was 64 mm (4*D* of DB16). Details are shown in **Figure 4.5(a).**

3) **Sample No. 3-LE4+H3:** Non-overlapping with hook joint (Weak joint, L_e = 4*D* and L_2 = 3*D*)

The test sample was prepared by casting separate beam and column components and then assembling them, with hook rebars embedded into the beam-column joint area. The embedded straight length of the beam's rebars (L_e) was 64 mm (4*D* of DB16), and the hook length (L_2) was 48 mm (3*D* of DB16). Details are shown in **Figure 5(b).**

4) **Sample No. 4-LS8:** Lap-splicing without hook joint (Strong joint, L_1 = 8*D*)

The test sample was cast and assembled with straight lap-splicing of the rebars in the joint area. The lap splice length of the beam's rebars was 128 mm (8*D* of DB16). Details are shown in **Figure 4.5(c).**

5) **Sample No. 5-LS8+H4:** Lap-splicing with hook joint (Strong joint, L_1 = 8*D* and L_2 = 4*D*)

The samples were cast and assembled with lap-splice and hook rebars in the joint area. The lap splice length of the beam's rebars (L_1) was 128 mm (8*D* of DB16), and the hook length (L_2) was 64 mm (4*D* of DB16). Details of the reinforcement and lap-splicing are shown in **Figure 4.5(d).**

6) Sample No. 6-LS9: Lap-splicing without hook joint (Strong joint, L_1 = 9*D*)

The test sample was prepared by casting separate beam and column components and then assembling them with straight lap-splicing of the rebars in the beam-column joint area. The lap splice length of the beam's rebars (L_1) was 144 mm (9*D* of DB16). Details of the reinforcement are shown in **Figure 4.5(e).**

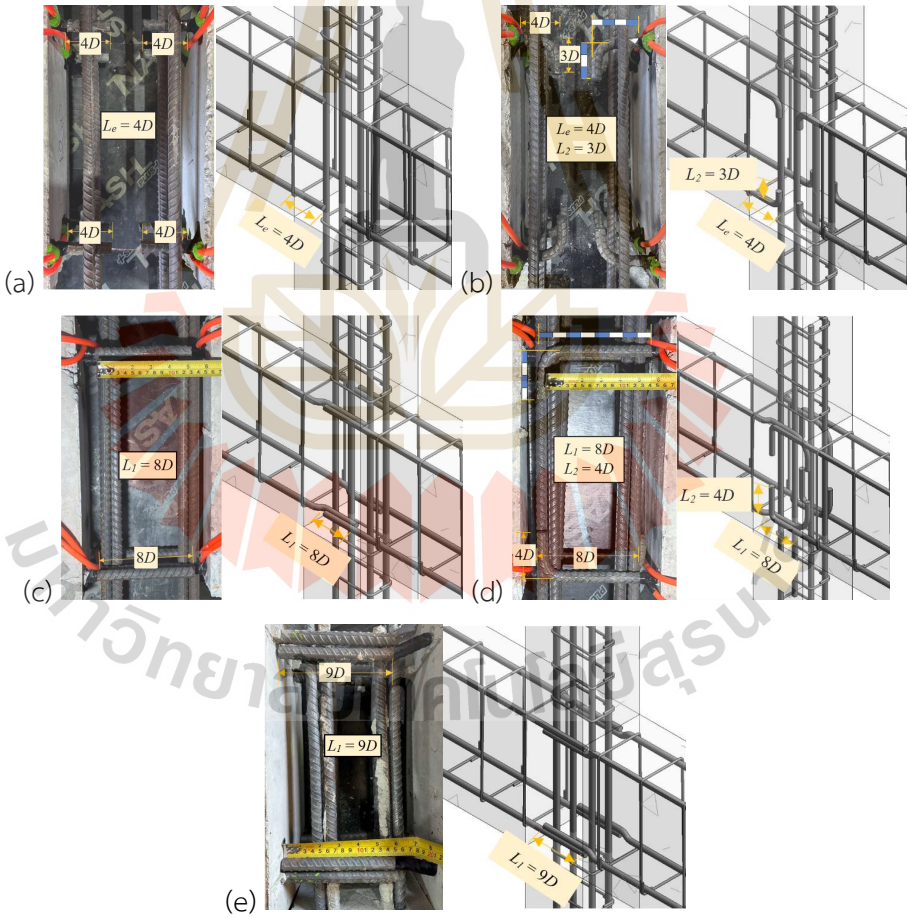

Figure 4.5 The type of joint for each sample (a) LE4, (b) LE4+H3, (c) LS8, (d) LS8+H4 and (e) LS9

In the UHPC joint **(Figure 4.5)**, specific portions of the rebars were either embedded without overlapping or lap spliced, while other sections were intentionally insulated using black Scotch VM Tape. This insulation ensures that no bond occurs between the rebars and the surrounding UHPC in the taped regions. By isolating these areas, the study focused on the bond performance only in the designated sections, allowing for a controlled and accurate analysis of the bond behavior as scheduled. This approach prevented unintended bonding outside the target area and ensured the reliability of the experimental results. The reinforcement arrangement details for the beam-column samples No. 1-5 are shown in **Figure 4.6(a)**, featuring RB6 stirrups spaced at 0.15 m for both the beam and column. In contrast, **Figure 4.6(b)** depicts the reinforcement arrangement to prevent shear failure in the beams of sample No. 6, with RB6 stirrups at 0.15 m for the column and RB9 stirrups at 0.10 m for the beam.

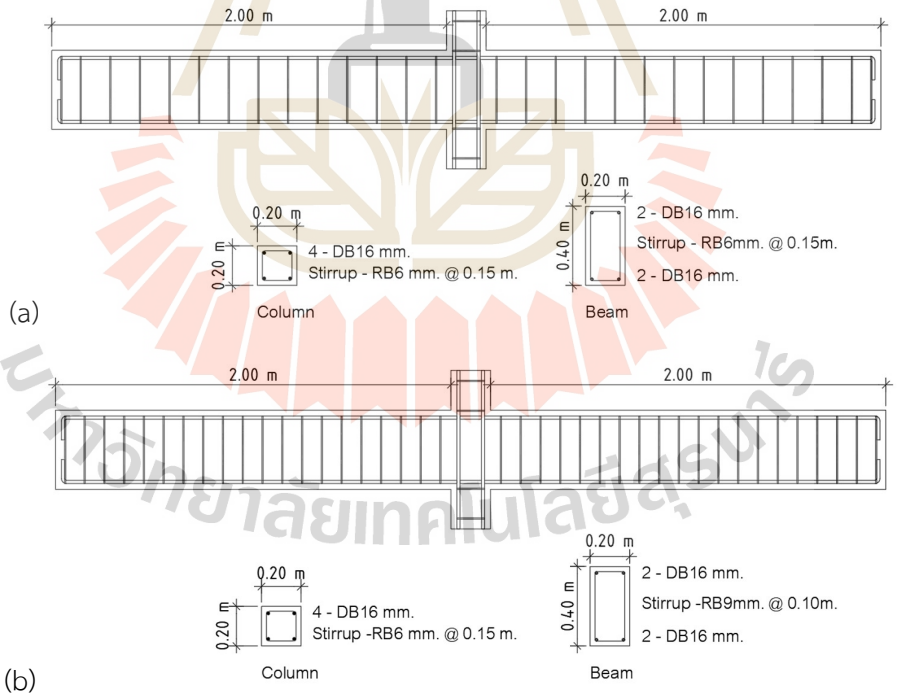

Figure 4.6 The reinforcement arrangement details for the beam-column of (a) TCIP, LE4, LE4+H3, LS8, LS8+H4 and (b) LS9

4.3 Results

Table 4.3 Measured parameters from full-scale sample

Parameter	Position	No.1 TCIP	No. 2 LE4	No. 3 LE4+H3	No. 4 LS8	No. 5 LS8+H4	No. 6 LS9
Applied Load (kN)	At the Left side	47.37	25.11	22.37	45.7	45.11	47.27
	At the Right side	46.09	25.70	22.17	45.6	47.37	47.76
Moment Calculated from the Applied Load (kN-m)	At the Left side	94.44	51.70	46.39	91.2	91.01	94.24
	At the Right side	96.4	52.78	45.99	91.01	94.44	95.12
Strain value	Strain front at the Left side	6073	663	762	9737	17872	13380
	Strain behind at the Left side	12404	625	437	9735	18293	3404
	Strain front at the Right side	16906	444	430	15400	14716	20277
	Strain behind at the Right side	16630	507	482.5	22230	18532	20126
Stress value, f_s (MPa)	Stress front at the Left side	588.14	379.57	435.86	610.97	643.6	622.46
	Stress behind at the Left side	617.9	357.81	250.56	599.75	645.58	575.6
	Stress front at the Right side	639.06	254.19	306.29	658.18	649.83	658.18
	Stress behind at the Right side	637.76	290.25	246.17	658.18	625.63	658.18

Parameter	Position	No.1 TCIP	No. 2 LE4	No. 3 LE4+H3	No. 4 LS8	No. 5 LS8+H4	No. 6 LS9
Average Stress, σ_{av} (MPa)	At the Left side	603.01	368.69	343.21	605.35	644.58	599.03
	At the Right side	638.4	272.22	276.23	658.14	637.72	658.14
Moment Calculated from the Average Strain Gauge (kN-m)	At the Left side	77.77	47.56	44.33	78.16	83.16	77.28
	At the Right side	82.38	35.11	35.6	83.65	82.28	84.44

Table 4.3 provides a comprehensive summary of the measured parameters from all full-scale samples (Samples No. 1-6), including applied loads, tensile strains, and bending moments calculated from applied loads and strains. The moment calculated from the maximum applied load indicates the corresponding maximum bending moment at the critical section of the beam-column connection. Measured strains using stain gauges display the deformation in the tested rebars, and the corresponding stresses in the rebars are converted from the measured strain. Finally, the bending moments were calculated using the ACI equation (ACI Committee 2008); they provides valuable insights into the structural behavior of the connections under applied loads, enhancing the understanding of the integrity and failure mechanisms for each test condition.

4.3.1 Traditional cast-in-place beam-column joint (Sample No. 1-TCIP)

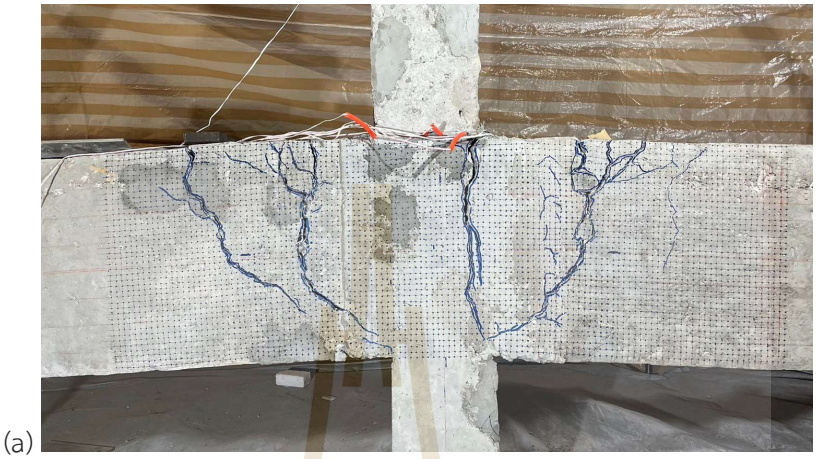

(a)

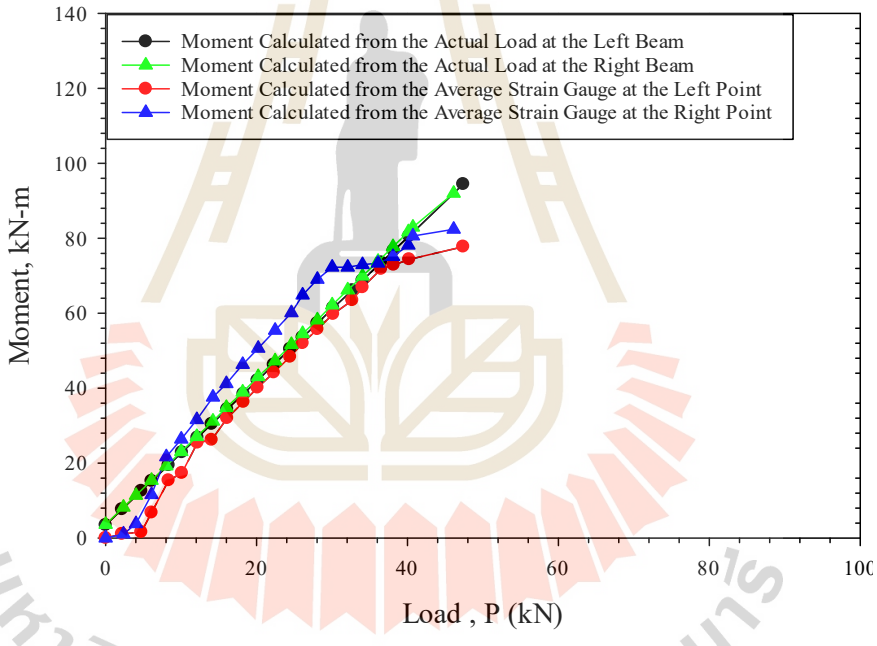

(b)

Figure 4.7 The traditional cast-in-place beam-column joint (TCIP) sample: (a) Failure of the sample, (b) Relationship between the moment calculated from the average strain gauge and the applied load.

The failure at the connection, depicted in **Figure 4.7(a)**, was notably attributed to flexural moment with no track of shear failure, due to insufficient number of tensile rebars. The comparison of moments calculated from the applied loads and strain

measurements, from the initial application of the loads to their maximum, is depicted in **Figure 7(b)**. The results revealed that the average maximum flexural moments calculated from the maximum load and strain were 93.25 kN-m and 80.10 kN-m, respectively. Though the rupture of rebars were not observed, the tensile stress in all four rebars exceeded the yield point with large deformation. This indicates that the test beam was designed under under-reinforced condition (Kartal et al. 2021; Liu et al. 2022; Mohammadhassani et al. 2014; Said et al. 2021), where failure did not occur due to the compression rupture of concrete, but rather due to the large elongation of the rebars beyond their yield limit. This caused the concrete above the top rebars, which has a low tensile strength, to crack and ultimately fail.

4.3.2 Strong joint configuration

4.3.2.1 Lap-splicing without hook joint (Sample No. 4-LS8)

For lap-splicing without hook joint (Strong joint, $L_1 = 8D$) sample, the observed failure after the test and the moments calculated from the applied loads and measured strains during the test are depicted in **Figure 4.8**. One of the tensile rebars was found to fail, while another had slipped out. Since the test was conducted until the rebars failed, the tensile stress used in calculating the threshold lap-splice length without hook joint is the value at the rupture (f_u = 658.13 MPa). Using Equation (1) with s = 1, ϕ = 0.75, and τ_{bond} = 0.75 x 27.92 = 20.94 MPa and applying Equation (2), the threshold lap-splicing length of rebars at rupture state was determined as follows:

$$\frac{L_1}{D} = \frac{f_s}{4(\tau_{bond})} = \frac{658.18}{4(20.94)} = 7.86$$

In this experiment, L_1/D = 8 was used, which is close to the value obtained from Equation (2). This length resulted in slippage and rupture of rebars

occurring simultaneously. It was evident that this calculation was consistent with the failure of the joint, where one rebar slipped out and another one fractured.

(a)

(b)

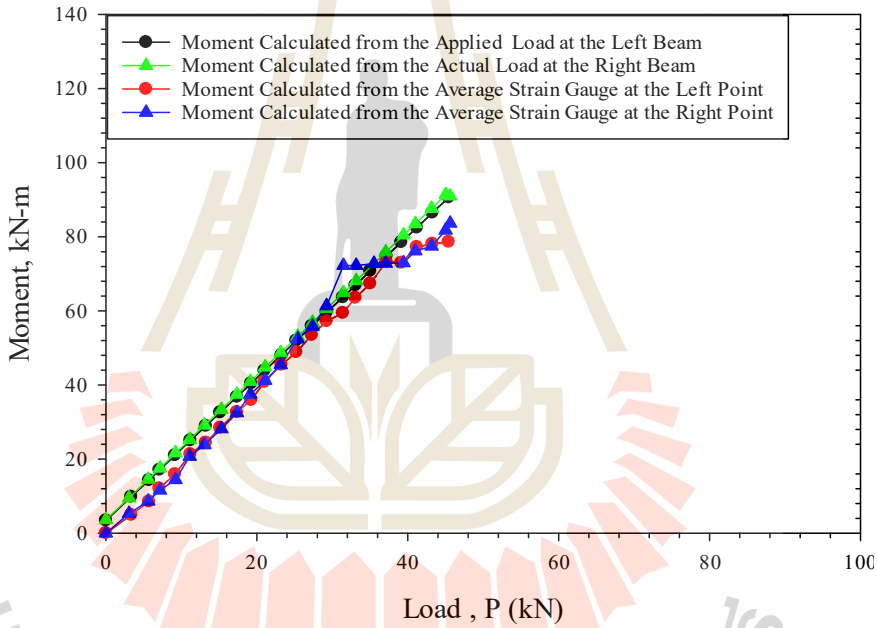

Figure 4.8 The lap-splicing without hook joint (LS8: Strong joint, L_1 = 8*D*) sample: (a) Failure of the sample, (b) Relationship between the moment calculated from the average strain gauge and the applied load.

4.3.2.2 Lap-splicing with hook joint (Sample No. 5-LS8+H4)

For lap-splicing with hook joint (Strong joint, L_1 = 8*D* and L_2 = 4*D*), the observed failure after the test and the bending moments generated at the joint interface during the test are depicted in **Figure 4.9**. Unlike the previous

observations, the failure occurred in the beam rather than at the joint interface, attributed to the shear failure. The failure initiated with a shear at the junction between the beam and column, which was subsequently followed by the failure of the stirrups. The inclusion of the hook (L_2) in this case where the lap splice length exceeded the development length would typically indicate the rupture failure of rebars if the bending moment was dominant. In other words, in this experiment, shear failure was observed to be dominant without the rupture of rebars. The shear resistance of the beam can be calculated using the ACI (Standard 2011) equation as follows:

$$V_n = V_c + V_s = 0.53bd\sqrt{fc'} + A_v f_y d/s$$

The properties of the stirrups used in the research, RB6-SR24, included a cross-sectional area of 28.2 mm², a yield tensile stress (f_y) of 240 MPa, and a stirrup spacing (s) of 150 mm.

Thus, $V_n = 0.17(200)(361)(\sqrt{43.91}) + (2)(28.2)(240)(361)/(150)$

$V_n = 81.33 + 32.58 = 113.91$ kN

The calculated shear resistance was greater than the shear force applied at the beam-column interface, which was 45.62 kN. Initial shear failure occurred at the beam-column joint, followed by stirrup failure (**Figure 4.9(a)**). This implied that the ACI's equation to calculate the shear resistance was overestimated. This might be because the ACI's equation assumes monolithic casting of beams and columns, which does not account for the weakness at the joint. This suggests that using UHPC for beam connections requires stirrups with approximately 2.5 times greater cross-sectional area than what is calculated using the ACI equation.

(a)

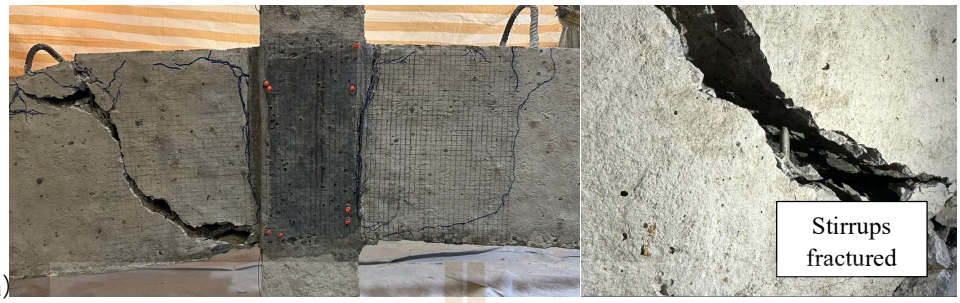

(b)

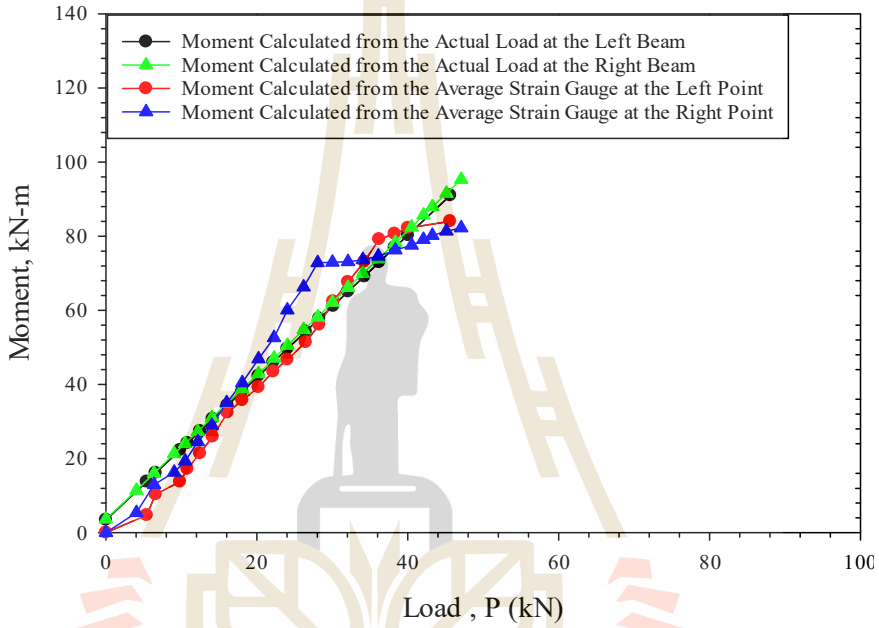

Figure 4.9 The lap-splicing with a hook joint (LS8+H4: Strong joint, L_1 = 8*D* and L_2 = 4*D*) sample: (a) Failure of the sample, (b) Relationship between the moment calculated from the average strain gauge and the applied load.

4.3.2.3 Lap-splicing without hook joint (Sample No. 6-LS9)

In this test, the size of the stirrups was increased to RB9 and the spacing was reduced to 100 mm. The lap splice length (L_1) was 144 mm (9*D* of DB16). After completing the test, the observed failure, shown in **Figure 4.10(a)**, indicated that both top rebars fractured under tensile stress without any stirrup failure. According to Equation (1), the bond strength of the rebar (ϕ_1= 0.75) could be calculated as follows:

$$\tau_{bond} = 0.75 \times 11.64 \sqrt{\frac{f'_c}{D}} = 0.75 \times 11.64 \sqrt{\frac{92.05}{16}} = 20.94 \text{ MPa}$$

Therefore, the maximum bond force was:

$$\text{Bond force } (F_{bond}) = \tau_{bond} \pi D L = (20.94)(\pi)(16)(16x9) = 151.35 \text{ kN}$$

which was greater than the tensile force at the point of failure of the rebars:

$$\text{Tensile force } (F_s) = f_s \frac{\pi}{4} D^2 = (658.13)(201) = 132.29 \text{ kN}$$

This calculation is consistent with the test results, indicating that the reinforcement failed without slipping out of the concrete.

(a)

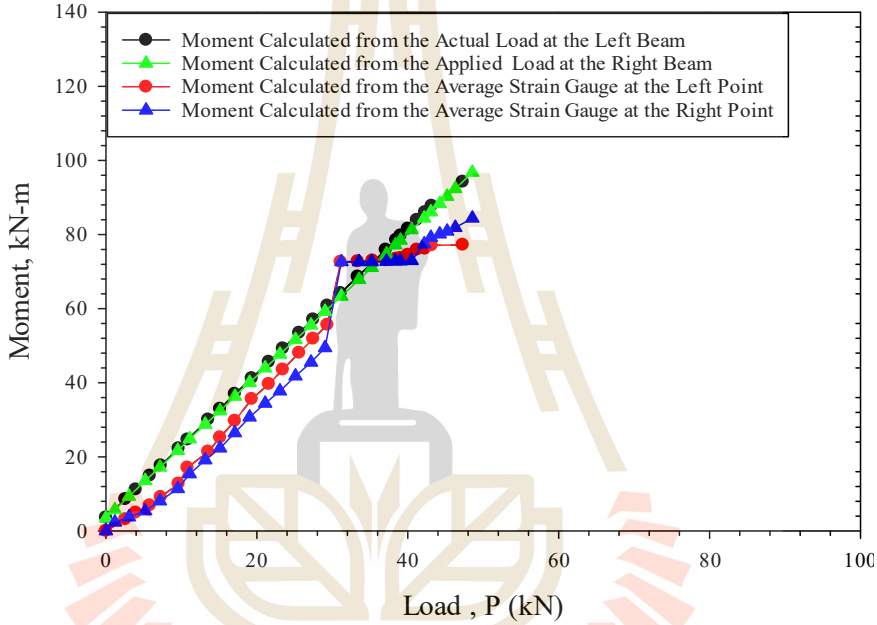

(b)

Figure 4.10 The lap-splicing without hook joint (LS9: Strong joint, L_1 = 9*D*) sample: (a) Failure of the sample, (b) Relationship between the moment calculated from the average strain gauge and the applied load.

4.3.3 Weak joint configuration

4.3.3.1 Non-overlapping without hook joint (Sample No. 2-LE4)

For non-overlapping without hook joint (Weak joint, L_e = 4D) sample, failure occurred at the interface between the column and beam (**Figure 11(a)**), where both top rebars slipped out from the UHPE connection. In other words, the

failure was due to insufficient embedment length of the rebars. The comparison of moments derived from the applied loads and measured strains, spanning from the initial loading to the peak load, is illustrated in **Figure 11(b)**. To verify the applicability of the bond strength equation, the tensile force (F_s) in the rebars calculated from the measured strain (data from **Table 3**) was compared with the maximum bond force (F_{bond}) calculated using Equation (1). At a measured maximum f_s = 379.57 MPa, and with a cross-sectional area of the rebars during applied loading being assumed to be constant and equal to 201 mm², F_s was then calculated as:

$$\text{Tensile force } (F_s) = f_s \frac{\pi}{4} D^2 = (379.57)(201) = 76.34 \text{ kN}$$

τ_{bond} predicted from Equation (1) was 27.92 MPa (f_c' of UHPC at 7-day = 92.05 MPa) using an L_e/D ratio of 3.5, instead of 4.0. This reduction in input L_e/D was the correction due to the placement of the column's rebars passing through the beam's rebars at the joint caused the beam's rebars on either side to be positioned closer to the column's rebars, resulting in a reduced bonding surface between the beam's rebars and the UHPC. Therefore,

$$\text{Bond force } (F_{bond}) = \tau_{bond}\, \pi\, D\, L_e = (27.92)(\pi)(16)(16\text{x}3.5) = 78.58 \text{ kN}$$

It was observed that the F_{bond} predicted by Equation (1) was very close to the F_s calculated from the measured strain, with a discrepancy of only 2.93%. In addition, the predicted F_{bond} was found to be less than the rupture tensile force of the rebars (126.33 kN), indicating the reinforcement being failed by slipping out due to insufficient bond resistance.

(a)

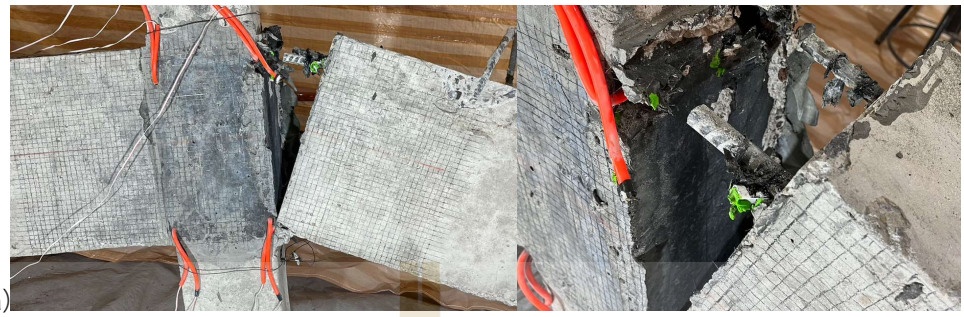

(b)

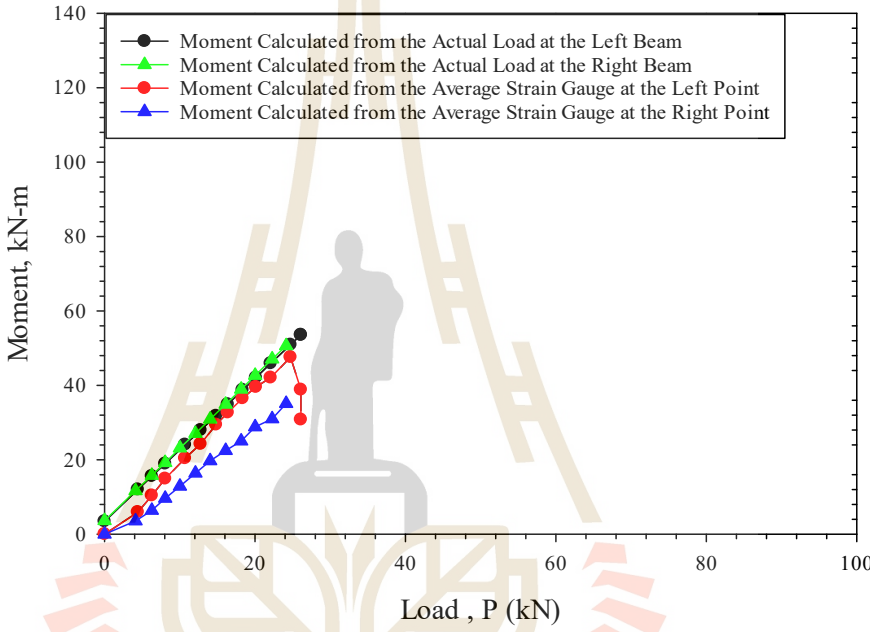

Figure 4.11 The non-overlapping without hook joint (LE4: Weak joint, L_e = 4*D*) sample: (a) Failure of the sample, (b) Relationship between the moment calculated from the average strain gauge and the applied load.

4.3.3.2 Non-overlapping with hook joint (Sample No. 3-LE4+H3)

For non-overlapping with hook joint (Weak joint, L_e = 4*D* and L_2 = 3*D*), failure occurred at the interface between the column and beam. The maximum applied loads were 22.37 kN for the left beam and 22.17 kN for the right beam, as shown in **Figure 12**. The rebars slipped out of the joint, and the UHPC material experienced fracturing and separating, indicating that the failure was due to insufficient

embedment length. To verify that Equation (1) can be used to determine the bond strength of non-overlapping rebars with hook at the joint, the maximum tensile force in rebars and the maximum bond force (F_{bond}) predicted using Equation (3) were compared. With a maximum tensile stress of 435.86 MPa and the assumed constant cross-sectional area of rebars of 201 mm², the maximum tensile force was calculated as:

$$\text{Tensile force } (F_s) = f_s \frac{\pi}{4} D^2 = (435.86)\,(201) = 87.63 \text{ kN}$$

Meanwhile, the maximum bond force predicted using Equation (3), with $\phi_1 = 1$, $\phi_2 = 1$, $k = 0.2$, $\tau_{bond} = 27.92$ MPa, $L_e/D = 3.5$, and $L_2/D = 3$, was as follows:

$$\text{Bond force } (F_{bond}) = (\phi_1 L_e + k\phi_2 L_2)\tau_{bond}\pi D$$

$$= [(1)(56) + (0.20)(1)(48)] \times (27.92)(\pi)(16)$$

$$= 92.06 \text{ kN}$$

It was evident that F_{bond} was close to F_s, with a discrepancy of 5.1%, indicating the applicability of Equation (3) in practice.

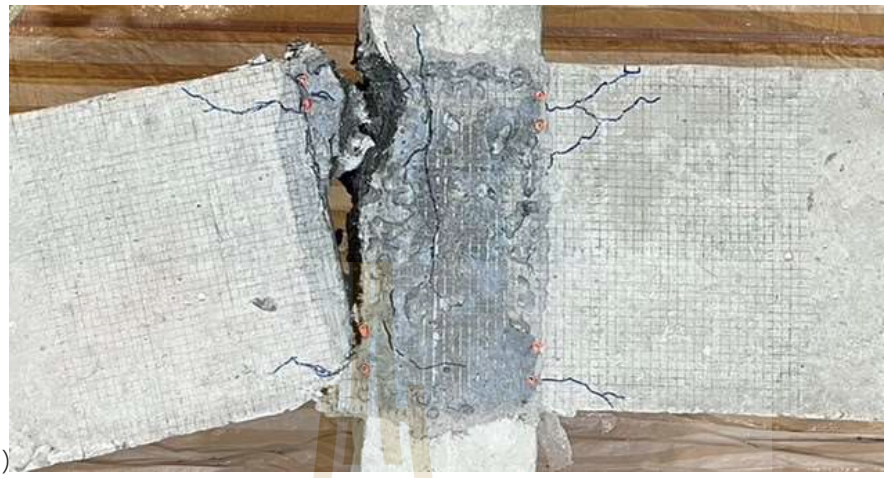

(a)

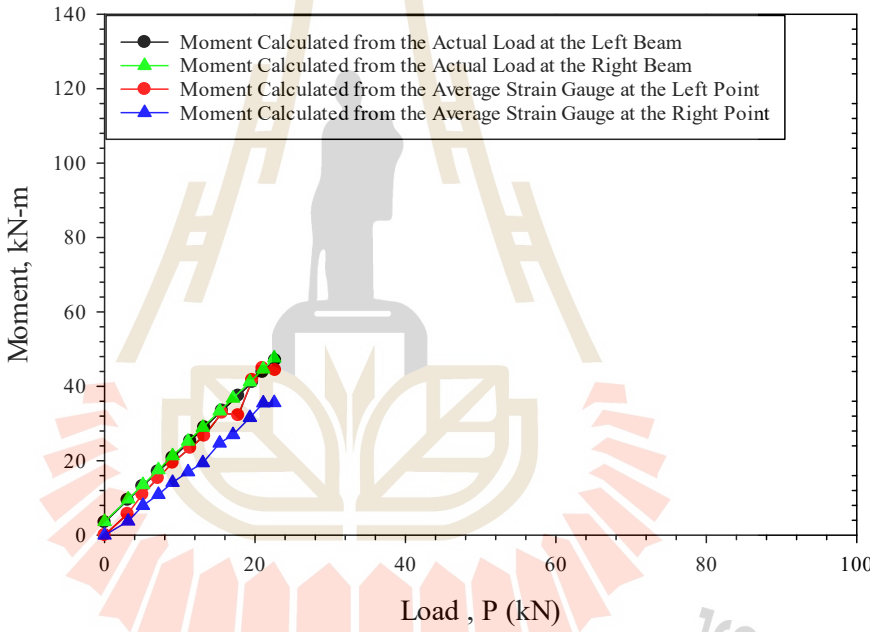

(b)

Figure 4.12 The non-overlapping with a hook joint (LE4+H3: Weak joint, L_e = 4*D* and L_2 = 3*D*) sample: (a) Failure of the sample, (b) Relationship between the moment calculated from the average strain gauge and the applied load.

4.3.4 Failure characteristics of traditional joint and UHPC strong joint

The traditional beam-column joint can withstand an average bending moment (on both sides) of 93.25 kN-m (**Figure 13(a)**). When comparing the test results

of the beam-column joints using UHPC in the case of Strong Joint (Samples 4-6), the following findings could be illustrated:

1) **Sample No. 4-LS8:** Full-scale sample of lap-splicing without hook joint (strong joint, L_1 = 8*D*): Using RB6 stirrups spaced at 0.15 meters, the joint could withstand an average bending moment (on both sides) of 91.13 kN-m (**Figure 13(b)**), which was close to the traditional beam-column joint (with a deviation of only 2.31%).

2) **Sample No. 5-LS8+H4:** Full-scale sample of lap-splicing with hook joint (strong joint, L_1 = 8*D*, L_2 = 4*D*): Using RB6 stirrups spaced at 0.15 meters, the joint could withstand an average bending moment (on both sides) of 92.8 kN-m (**Figure 13(c)**), which is close to the traditional beam-column joint (with a deviation of only 0.53%).

3) **Sample No. 6-LS9:** Full-scale sample of lap-splicing without hook joint (strong joint, L_1 = 9*D*): Using RB9 stirrups spaced at 0.10 meters, the joint could withstand an average bending moment (on both sides) of 94.76 kN-m (**Figure 13(d)**), which was close to the traditional beam-column joint (with a deviation of only 1.58%).

The beam-column joint systems in all three cases mentioned above (Strong Joint) had the capability to withstand bending moments comparable to the traditional beam-column joint, with deviations not exceeding 2.31%. All three cases were designed in the condition of under-reinforced section. The rebars at the strain gauge installation point reached the yield state and exhibited very large strain with their measured tensile stresses being greater than 599.04 MPa. These test results demonstrated that the design of rebars' lengths using the bond strength obtained from Equation (1), $\tau_{bond} = \phi 11.64\sqrt{\frac{f_c'}{D}}$, is rational and practical.

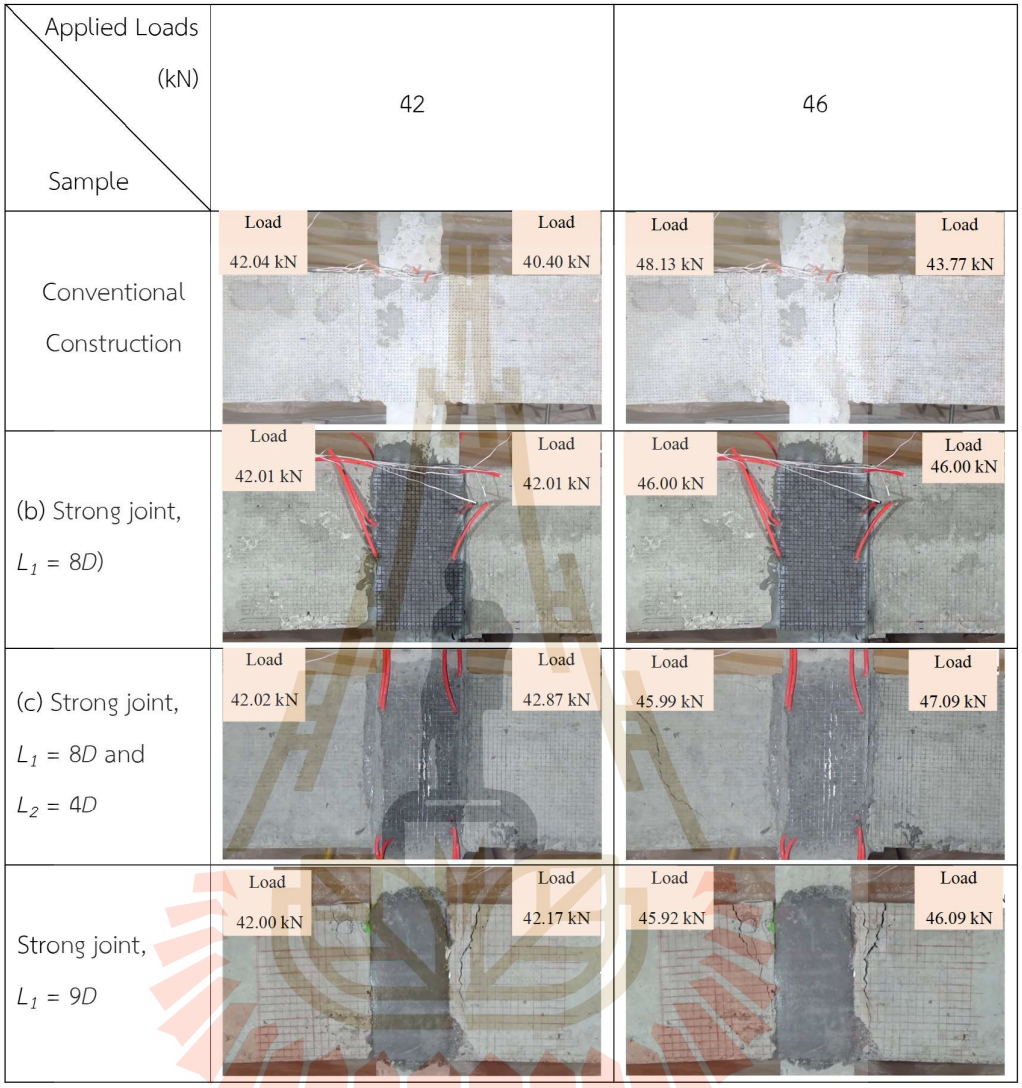

Figure 4.13 The test results of the beam-column joints using UHPC in the case of Strong Joint.

The severity of damage after failure differed significantly between the traditional beam-column joint (Sample No. 1) and UHPC joints (Samples No. 4-6), despite all being under-reinforced designs. Sample No. 1 exhibited severe and widespread damage, characterized by uncontrolled cracking at a 45-degree angle relative to the vertical plane and spalling caused by the yielding of the upper rebar, highlighting the stress distribution of traditional concrete. In contrast, UHPC joints

showed localized damage due to enhanced bond strength and confinement from steel fibers. Sample No. 4 (L_1 = 8D) demonstrated 90-degree localized damage at the beam-joint interface, with one upper rebar fracturing and the other slipping out. Sample 5 (L_1 = 8*D*, L_2 = 4*D*) exhibited 45-degree localized damage with stirrup fracture due to insufficient shear capacity from wider stirrup spacing (0.15 meters). Sample No. 6 (L_1 = 9*D*) showed improved performance with reduced stirrup spacing (0.10 meters), confining damage at a 15-degree angle to upper rebar yielding and fracture, while stirrups remained intact, indicating enhanced shear resistance and bond performance in UHPC joints compared to traditional concrete.

In the case of weak joint testing (**Figure 14**), the results indicate that Equation (1) can be used to calculate the maximum tensile stress (= bond strength) in the rebars during slippage from the concrete. The predicted maximum tensile stress closely matched the tensile stress derived from the strain gauge measurements. Therefore, it can be said that Equation (1) is highly accurate and can be used to calculate the flexural resistance for the weak beam-column joint.

Applied Loads (kN) / Sample	20	21
LE4 Non-overlapping without hook joint (Weak joint, L_e = 4D)	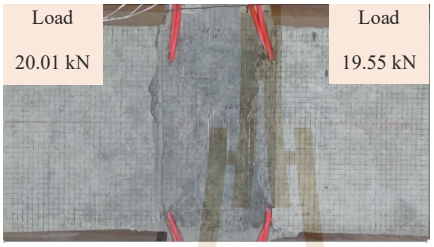	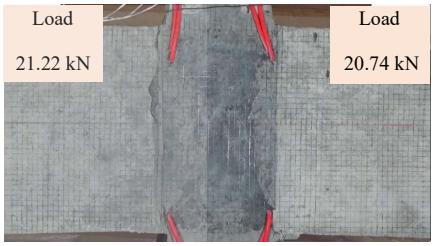
LE4+H3 Non-overlapping with a hook joint (Weak joint, L_e = 4D and L_2 = 3D)		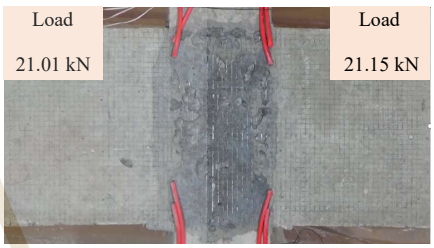

Figure 4.14 The test results of the beam-column joints using UHPC in the case of Weak Joint.

4.4 Design Scheme for Rebars' Length in UHPC Connection Joints

Based on the full-scale sample testing, this research developed a design scheme for beam cross-sections to resist target bending moments, along with determining the rebars' lengths in UHPC joints (**Figure 15**). The most economic design is the condition where the rupture of rebars and slippage of rebars happens simultaneously at the design bending moment. In other words, the rebars' length must be sufficient until the rupture of rebars (Strong Joint).

Figure 15 illustrates the suggested design steps to determine the length of rebars with various diameters to resist the target bending moment. The first step is to

determine the beam dimension, number of rebars and diameter of rebars to resist the design bending moment at the specified material properties according to ACI 318-11 standards.

The next step is to determine the development length, L_d of rebars without lap-splicing for specified yield tensile strength (f_y) using Equation (2). If the calculated L_d is less than half the width of the column, the rebars are placed without splicing or hook with $L_e > L_d$.

If the calculated L_d exceeds half the width of the column, the lap-splicing or hook (in cases where the bond strength from lap splicing is insufficient) is required. The calculation starts with determining the lap-splice length (L_1). This L_1 is then compared with the actual space available in the structural element, which refers to the physical distance or length within the joint, where the overlapping rebars can be positioned. If the calculated L_1 is less than or equal to the actual space ($L_1 \leq$ actual space), the calculated L_1 can be used directly. However, if the calculated L_1 exceeds the actual space ($L_1 >$ actual space), the hook length (L_2) is required and determined using Equation (3) to enhance the bond stress of the reinforcement. The length L_2 must be at least $3D$.

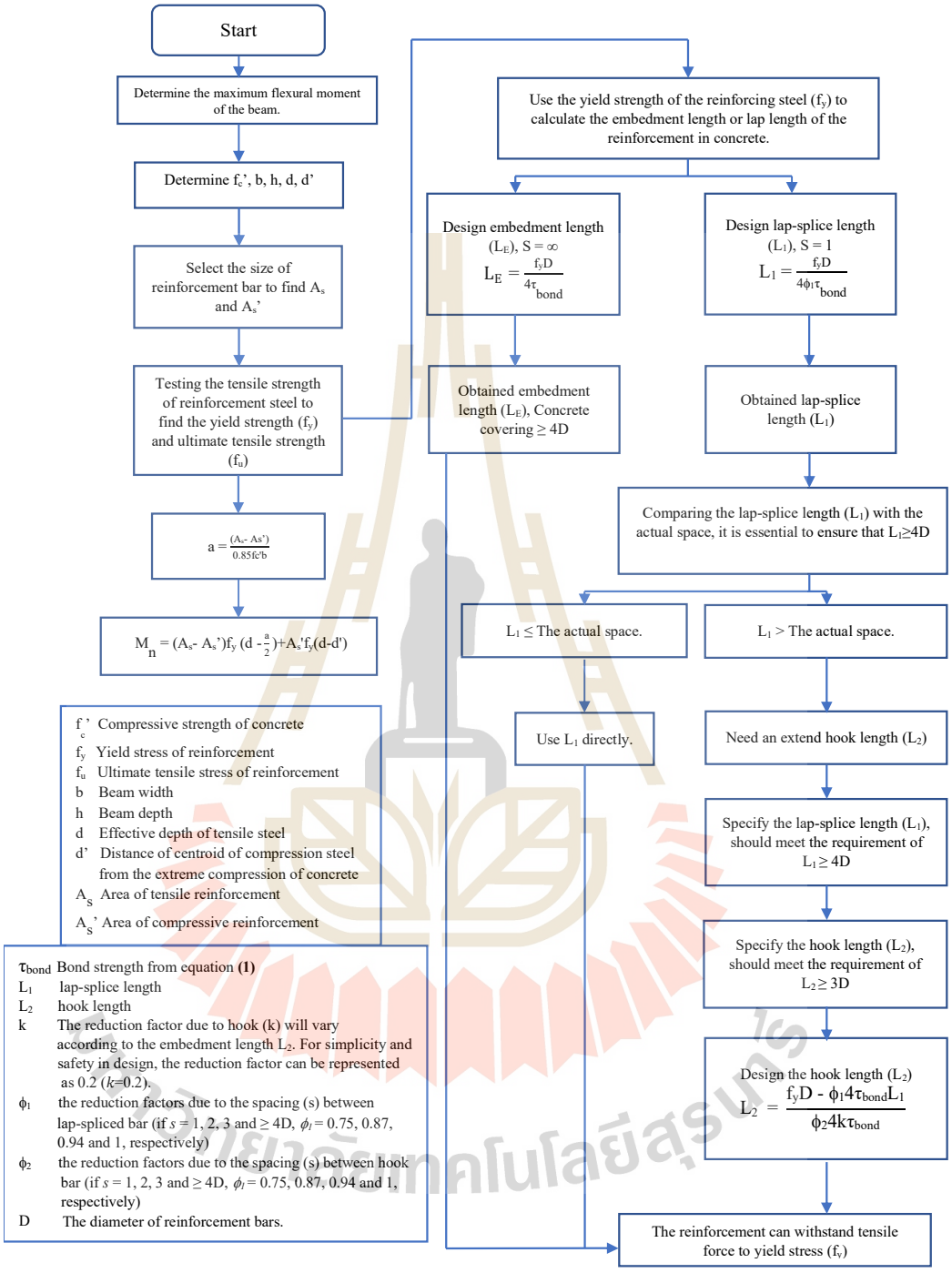

Figure 4.15. Design Scheme for Embedment Length or Lap Splice Length in UHPC Joints

4.4.1 Calculation Demonstration

4.4.1.1 Design lap-splice length without hook

f_c' = 92.05 MPa (UHPC at 7 days), b = 0.20 m, h = 0.40 m, d = 0.37 m, d' = 0.3 m

Tensile steel rebars: 2 – DB20 (As = 0.000628 m^2)

Compression steel rebars: 2 – DB20 (As' = 0.000628 m^2)

Yield strength (f_y) = 504 MPa Ultimate tensile strength (f_u) = 611 MPa

Step 1 Design lap-splice length, L_1 ($\phi_1 = 0.75$)

$$\tau_{bond} = 11.64\sqrt{\frac{f_c'}{D}} = 11.64\sqrt{\frac{92.05}{20}} = 24.97 \text{ MPa}$$

$$L_1 = \frac{f_y D}{4\phi_1 \tau_{bond}} = \frac{(504)(20)}{(4)(0.75)(24.97)} = 134.56 \text{ mm} > 4D \text{ (4x20 = 80 mm) Use } L_1 = 135 \text{ mm}$$

Step 2 Calculate the resisting moment

$$M_n = (A_s - A_s')f_y(d - \frac{a}{2}) + A_s'f_y(d-d') = (0.000628)(504x1000)(0.37-0.03) = 107.61 \text{ kN-m}$$

Check

Bond force (F_{bond}) = $\phi_1 \tau_{bond} \pi D L$ = (0.75)(26.03)(π)(20)(130) = 159.46 kN

Tensile yield force (F_y) = $f_y \frac{\pi}{4} D^2$ = (504x1000)(0.000314) = 158.26 kN < Bond force (F_{bond})

4.4.1.2 Design lap-splice length with hook

f_c' = 92.05 MPa (UHPC at 7 days), b = 0.20 m, h = 0.40 m, d = 0.37 m, d' = 0.3 m

Tensile steel rebars: 2 – DB20 (As = 0.000628 m^2)

Compression steel rebars: 2 – DB20 (As' = 0.000628 m^2)

Yield strength (f_y) = 504 MPa Ultimate tensile strength (f_u) = 611 MPa

Step 1.1 Design lap-splice length, L_1 ($\phi_1 = 0.75$)

$$\tau_{bond} = 11.64\sqrt{\frac{f_c'}{D}} = 11.64\sqrt{\frac{92.05}{20}} = 24.97 \text{ MPa}$$

$$L_1 = \frac{f_y D}{4\phi_1 \tau_{bond}} = \frac{(504)(20)}{(4)(0.75)(24.97)} = 134.56 \text{ mm} > 4D \text{ (4x20 = 80 mm)}$$

If the available space is 100 mm, Select Use L_1 = 100 mm and provide an additional hook length (L_2) to ensure sufficient bond strength.

Step 1.2 Design the hook length, L_2 ($\phi_2 = 1$)

$$L_2 = \frac{f_y D - \phi_1 4 \tau_{bond} L_1}{\phi_2 4k \tau_{bond}} = \frac{(504)(20) - (0.75)(4)(24.97)(100)}{(1)(4)(0.20)(24.97)} = 129.60 \text{ mm} > 3D \text{ (3x20 = 60 mm)}$$

Select Use L_2 = 130 mm

Step 2 Calculate the resisting moment

$$Mn = (A_s - A_s')f_y(d - \frac{a}{2}) + A_s'f_y(d-d') = (0.000628)(504x1000)(0.37-0.03) = 107.61 \text{ kN-m}$$

Check

Bond force (F_{bond}) $= (\phi_1 L_1 + k\phi_2 L_2)\tau_{bond}\pi D$

$= [(0.75)(100)+(0.20)(1)(130)](24.97x1000)(\pi)(20)$

$= 158.46$ kN

Tensile yield force (F_y) = $f_y \frac{\pi}{4} D^2$=(504x1000)(0.000314) = 158.26 kN < Bond force (F_{bond}).

The design scheme for rebars' length proposed in this study is specifically formulated for UHPC connections, taking into account the material's exceptional bond strength and mechanical properties-particularly its dense matrix and inclusion of steel fibers. These characteristics significantly enhance the bond between concrete and reinforcement, resulting in considerably shorter required development and lap splice lengths compared to conventional reinforced concrete (RC) connections. Design methods traditionally developed for RC are based on the behavior of normal-strength concrete, which exhibits relatively lower bond strength, increased porosity, and limited tensile capacity. As a result, such methods typically recommend long development and lap splice lengths to ensure adequate load transfer and structural integrity. However, directly applying these conservative RC-based design provisions to UHPC would not only be inefficient in terms of material use and construction cost, but would also fail to capture the full potential of UHPC's superior bond characteristics.

Moreover, the behavior of UHPC joints under load is fundamentally different from RC joints due to the enhanced confinement, energy absorption, and tensile performance contributed by steel fibers. These differences necessitate a separate design approach. The proposed scheme in this study is experimentally validated using full-scale testing, which captures realistic structural behavior under service conditions. It aims to achieve a ductile failure mode, in which bar rupture and bond slippage occur nearly simultaneously-a balance that optimizes both safety and material efficiency. This research is thus essential, as it provides a rational and performance-based design methodology tailored to UHPC, which has been lacking in current design codes. Without such schemes, engineers are left either overdesigning UHPC joints using outdated RC assumptions or relying on conservative empirical

judgment. The findings from this study not only close a critical knowledge gap but also support the wider adoption of UHPC in precast and cast-in-place structural systems by offering practical, safe, and cost-effective design guidance. .

To verify the accuracy and applicability of the proposed design process, the manuscript presents detailed example calculations and comparative analyses between theoretical predictions and full-scale experimental results. **Equations (1) to (3)** were employed to predict bond strength and bond force by incorporating UHPC compressive strength, rebar diameter, and embedment configurations, including lap-splice and hook lengths. The validity of these equations was assessed through direct comparison with tensile forces obtained from strain gauge measurements in full-scale specimens. In **Sample No. 2-LE4**, the calculated tensile force was 76.34 kN, while the predicted bond force was 78.58 kN, resulting in a deviation of only 2.93%. Similarly, in **Sample No. 3-LE4+H3**, the measured tensile force of 87.63 kN closely matched the predicted bond force of 92.06 kN, with a deviation of 5.1%. Furthermore, predictions of lap-splice lengths based on **Equation (2)** aligned with observed failure behaviors. For example, in **Sample No. 4-LS8**, the predicted lap-splice ratio (L_1/D = 7.86) corresponded well with the test value of 8*D*, where both rebar rupture and slippage were observed. In **Sample No. 6-LS9**, the predicted bond force (151.35 kN) exceeded the measured tensile force at rupture (132.29 kN), confirming that failure occurred through bar fracture rather than pull-out.

In addition, the shear failure observed in **Sample No. 5- LS8+H4** was investigated by comparing the experimental shear resistance with that calculated using the ACI equation. The results suggested that the ACI method, which assumes monolithic construction, may overestimate the shear capacity of precast UHPC joints. Therefore, it is recommended that the stirrup reinforcement in such joints be increased by approximately 2.5 times to ensure adequate shear resistance. The design scheme presented in **Section 4** and **Figure 15** integrates these theoretical and experimental findings into a practical and rational procedure for determining required rebar lengths

and configurations. This scheme effectively addresses structural performance requirements while maintaining construction efficiency and safety. The comparison between predictions and observed test data confirms the robustness of the proposed method across various failure modes, including rebar pull-out, rupture, and shear failure.

4.5 Conclusions

Based on the experiments conducted in this study, the following conclusions can be drawn:

The full-scale sample testing confirmed that using UHPC for beam-column joints can enable the beam-column structure to withstand loads and exhibit failure characteristics comparable to traditional construction methods. The strong joint was manufactured with two configurations of 16-mm deformed rebars including lap splicing without hook of L_1 = 9D (14.4 cm), and lap splicing with hook of L_1 = 8D and L_2 = 4D. These configurations allowed the UHPC beam-column joints to resist bending moments until the rebars reached the failure state (565.94 MPa) and subjected to large deformation, which is the ductile failure characteristic desired in reinforced concrete structure design.

However, caution should be taken for the weak joint with insufficient rebars' length. For example, the non-overlapping with hook joint (Weak Joint, L_e = 4D amd L_2 = 3D) and the non-overlapping without hook joint (Weak Joint, L_e = 4D) both exhibited sudden and hazardous failure.

The design scheme for rebars' length resulting from this project is as follows: initially, the yield tensile stress (f_y) of the rebars is used to calculate the L_d of rebars without lap-splice using Equation (1). If the calculated L_d is less than half the width of the column, the rebars are placed without lap splicing using $L_e > L_d$. However, if the

L_d exceeds half the width of the column, the lap splicing is required. If the calculated lap splice length (L_1) is less than or equal to the actual space ($L_1 \leq$ actual space), the calculated L_1 can be used in the design. If the calculated L_1 is greater than the actual space, the hook length (L_2) must be added to enhance the bond strength of the reinforcement using Equation (3); the length L_2 must be at least 3D.

The findings of this project underscore the efficacy of utilizing UHPC for precast beam-column joints. This innovative method enables the design of precast structural elements as continuous beams, rather than simple beams, thereby enhancing bending moment resistance and reducing the required amount of rebars. Manufacturing precast beam-column elements in a controlled factory setting and subsequently assembling them on-site offers several advantages. It reduces labor costs, minimizes the need for formwork and shoring, and expedites the construction process. Notably, UHPC achieves its high strength within just 7 days, compared to the traditional 28-day curing period. This significant reduction in curing time accelerates construction schedules while ensuring structural safety equivalent to conventional methods.

4.6 References

ACI Committee "Building code requirements for structural concrete (ACI 318-08) and commentary." American Concrete Institute.

Aiamsri, K., Yaowarat, T., Horpibulsuk, S., Suddeepong, A., Buritatum, A., Hiranwatthana, K., and Nitichote, K. (2024). "Bonding behavior of lap-spliced reinforcing bars embedded in ultra-high-performance concrete with steel fibers." *Developments in the Built Environment*, 20, 100585.

Aktan, A. E., Farhey, D. N., Helmicki, A. J., Brown, D. L., Hunt, V. J., Lee, K.-L., and Levi, A. (1997). "Structural identification for condition assessment: experimental arts." *Journal of structural engineering*, 123(12), 1674-1684.

Alampalli, S., Frangopol, D. M., Grimson, J., Halling, M. W., Kosnik, D. E., Lantsoght, E. O., Yang, D., and Zhou, Y. E. (2021). "Bridge load testing: State-of-the-practice." *Journal of Bridge Engineering*, 26(3), 03120002.

Alkaysi, M., and El-Tawil, S. (2017). "Factors affecting bond development between Ultra High Performance Concrete (UHPC) and steel bar reinforcement." *Construction and Building Materials*, 144, 412-422.

Anvari, B., Angeloudis, P., and Ochieng, W. Y. (2016). "A multi-objective GA-based optimisation for holistic Manufacturing, transportation and Assembly of precast construction." *Automation in Construction*, 71, 226-241.

Baek, J.-W., Park, H.-G., Lee, B.-S., and Shin, H.-M. (2018). "Shear-Friction Strength of Low-Rise Walls with 550 MPa (80 ksi) Reinforcing Bars under Cyclic Loading." *ACI Structural Journal*, 115(1).

Bahmani, H., and Mostofinejad, D. (2022). "Microstructure of ultra-high-performance concrete (UHPC)–a review study." *Journal of Building Engineering*, 50, 104118.

Bjorhovde, R., Goland, L., and Benac, D. (1999). "Tests of full-scale beam-to-column connections." *Southwest Research Institute, San Antonio, TX*.

Cabral-Fonseca, S., Correia, J., Custódio, J., Silva, H., Machado, A., and Sousa, J. (2018). "Durability of FRP-concrete bonded joints in structural rehabilitation: A review." *International Journal of Adhesion and Adhesives*, 83, 153-167.

Cai, G., and Waldmann, D. (2019). "A material and component bank to facilitate material recycling and component reuse for a sustainable construction: concept and preliminary study." *Clean Technologies and Environmental Policy*, 21, 2015-2032.

Chan, T. K. "Comparison of precast construction costs—Case studies in Australia and Malaysia." *Proc., Proceedings of the 27th Annual ARCOM Conference, Bristol, UK*, 3-12.

Choi, H.-K. (2020). "Parametric Analysis on Seismic Performance of Hybrid Precast Concrete Beam-Column Joint." *Advances in Civil Engineering*, 2020(1), 8856327.

Contento, A., Aloisio, A., Xue, J., He, J., and Briseghella, B. (2024). "Ultra-high performance concrete beam-to-beam connections in continuous bridges: Experimental full-scale tests, FE analyses and design." *Engineering Structures*, 316, 118594.

Du, J., Meng, W., Khayat, K. H., Bao, Y., Guo, P., Lyu, Z., Abu-Obeidah, A., Nassif, H., and Wang, H. (2021). "New development of ultra-high-performance concrete (UHPC)." *Composites Part B: Engineering*, 224, 109220.

Engindeniz, M., Kahn, L. F., and Abdul-Hamid, Z. (2005). "Repair and strengthening of reinforced concrete beam-column joints: State of the art." *ACI structural journal*, 102(2), 1.

Farzad, M., Shafieifar, M., and Azizinamini, A. (2019). "Experimental and numerical study on bond strength between conventional concrete and Ultra High-Performance Concrete (UHPC)." *Engineering Structures*, 186, 297-305.

Fehling, E., Schmidt, M., Walraven, J., Leutbecher, T., and Fröhlich, S. (2014). "Ultra-high performance concrete UHPC." *Ernst & Sohn: Berlin, Germany*, 25-32.

Garetti, M., and Taisch, M. (2012). "Sustainable manufacturing: trends and research challenges." *Production planning & control*, 23(2-3), 83-104.

Ghayeb, H. H., Razak, H. A., and Sulong, N. R. (2020). "Performance of dowel beam-to-column connections for precast concrete systems under seismic loads: A review." *Construction and Building Materials*, 237, 117582.

Hong, J., Shen, G. Q., Li, Z., Zhang, B., and Zhang, W. (2018). "Barriers to promoting prefabricated construction in China: A cost–benefit analysis." *Journal of cleaner production*, 172, 649-660.

Huang, Y., Grünewald, S., Schlangen, E., and Luković, M. (2022). "Strengthening of concrete structures with ultra high performance fiber reinforced concrete (UHPFRC): A critical review." *Construction and Building Materials*, 336, 127398.

Hung, C.-C., El-Tawil, S., and Chao, S.-H. (2021). "A review of developments and challenges for UHPC in structural engineering: Behavior, analysis, and design." *Journal of Structural Engineering*, 147(9), 03121001.

Kartal, S., Kalkan, I., Beycioglu, A., and Dobiszewska, M. (2021). "Load-deflection behavior of over-and under-reinforced concrete beams with hybrid FRP-steel reinforcements." *Materials*, 14(18), 5341.

Khayat, K. H., and Meng, W. (2014). "Design and performance of stay-in-place UHPC prefabricated panels for infrastructure construction." Missouri University of Science and Technology. Center for Transportation ....

Küntz, M., Jolin, M., Bastien, J., Perez, F., and Hild, F. (2006). "Digital image correlation analysis of crack behavior in a reinforced concrete beam during a load test." *Canadian Journal of Civil Engineering*, 33(11), 1418-1425.

Liu, S., Wang, X., Ali, Y. M., Su, C., and Wu, Z. (2022). "Flexural behavior and design of under-reinforced concrete beams with BFRP and steel bars." *Engineering Structures*, 263, 114386.

Lowes, L. N., and Altoontash, A. (2003). "Modeling reinforced-concrete beam-column joints subjected to cyclic loading." *Journal of Structural Engineering*, 129(12), 1686-1697.

Ma, J., Orgass, M., Dehn, F., Schmidt, D., and Tue, N. "Comparative investigations on ultra-high performance concrete with and without coarse aggregates." *Proc., International symposium on ultra high performance concrete, Kassel, Germany*, 205-212.

Maya, L., and Graybeal, B. (2017). "Experimental study of strand splice connections in UHPC for continuous precast prestressed concrete bridges." *Engineering Structures*, 133, 81-90.

Meoni, A., D'Alessandro, A., Mattiacci, M., García-Macías, E., Saviano, F., Parisi, F., Lignola, G. P., and Ubertini, F. (2024). "Structural performance assessment of full-scale masonry wall systems using operational modal analysis: Laboratory testing and numerical simulations." *Engineering Structures*, 304, 117663.

Mohammadhassani, M., Akib, S., Shariati, M., Suhatril, M., and Khanouki, M. A. (2014). "An experimental study on the failure modes of high strength concrete beams with particular references to variation of the tensile reinforcement ratio." *Engineering Failure Analysis*, 41, 73-80.

Molinari, M., Savadkoohi, A. T., Bursi, O. S., Friswell, M. I., and Zonta, D. (2009). "Damage identification of a 3D full scale steel–concrete composite structure with partial-strength joints at different pseudo-dynamic load levels." *Earthquake engineering & structural dynamics*, 38(10), 1219-1236.

Mousavi, S. S., and Dehestani, M. "Influence of mixture composition on the structural behaviour of reinforced concrete beam-column joints: A review." *Proc., Structures*, Elsevier, 29-52.

Parskiy, N., Molodtsov, M., and Molodtsova, V. "Cost effectiveness of precast reinforced concrete roof slabs." *Proc., IOP Conference Series: Materials Science and Engineering*, IOP Publishing, 012036.

Pokorný, P., Kolísko, J., Čítek, D., and Kostelecká, M. (2020). "Effect of elevated temperature on the bond strength of prestressing reinforcement in UHPC." *Materials*, 13(21), 4990.

Said, M., Shanour, A. S., Mustafa, T., Abdel-Kareem, A. H., and Khalil, M. M. (2021). "Experimental flexural performance of concrete beams reinforced with an innovative hybrid bars." *Engineering Structures*, 226, 111348.

Sev, A. (2009). "How can the construction industry contribute to sustainable development? A conceptual framework." *Sustainable Development*, 17(3), 161-173.

Shishesaz, M., and Hosseini, M. (2020). "Effects of joint geometry and material on stress distribution, strength and failure of bonded composite joints: an overview." *The Journal of Adhesion*.

Somma, G., Pieretto, A., Rossetto, T., and Grant, D. N. (2015). "RC beam to column connection failure assessment and limit state design." *Materials and Structures*, 48, 1215-1231.

Standard, A. (2003). "C33,"Standard Specification for Concrete Aggregates," ASTM international West Conshohocken, PA, USA." C.

Standard, A. "Building code requirements for structural concrete (ACI 318-11)." *Proc., American Concrete Institute*.

Supaviriyakit, T., and Pimanmas, A. (2008). "Comparative performance of sub-standard interior reinforced concrete beam–column connection with various joint reinforcing details." *Materials and Structures*, 41, 543-557.

Tack, R. (2019). *Flexural response of flat plate edge slab-column connections*, McGill University (Canada).

Ullah, R., Qiang, Y., Ahmad, J., Vatin, N. I., and El-Shorbagy, M. A. (2022). "Ultra-high-performance concrete (UHPC): A state-of-the-art review." *Materials*, 15(12), 4131.

Wang, Z., Hu, H., and Gong, J. (2018). "Framework for modeling operational uncertainty to optimize offsite production scheduling of precast components." *Automation in Construction*, 86, 69-80.

Wen, C., Zhang, P., Wang, J., and Hu, S. (2022). "Influence of fibers on the mechanical properties and durability of ultra-high-performance concrete: A review." *Journal of Building Engineering*, 52, 104370.

Xue, W., Hu, X., and Song, J. "Experimental study on seismic behavior of precast concrete beam-column joints using UHPC-based connections." *Proc., Structures*, Elsevier, 4867-4881.

Yoo, D.-Y., and Kim, M.-J. (2019). "High energy absorbent ultra-high-performance concrete with hybrid steel and polyethylene fibers." *Construction and Building Materials*, 209, 354-363.

Yoo, D.-Y., Kim, S., Kim, J.-J., and Chun, B. (2019). "An experimental study on pullout and tensile behavior of ultra-high-performance concrete reinforced with various steel fibers." *Construction and Building Materials*, 206, 46-61.

Yoo, D.-Y., Sohn, H.-K., Borges, P. H., Fediuk, R., and Kim, S. (2020). "Enhancing the tensile performance of ultra-high-performance concrete through strategic use of novel half-hooked steel fibers." *Journal of Materials Research and Technology*, 9(3), 2914-2925.

Zhang, J., Ding, C., Rong, X., Yang, H., and Li, Y. (2020). "Development and experimental investigation of hybrid precast concrete beam–column joints." *Engineering Structures*, 219, 110922.

Zhong, Y., Xiong, F., Chen, J., Deng, A., Chen, W., and Zhu, X. (2019). "Experimental study on a novel dry connection for a precast concrete beam-to-column joint." *Sustainability*, 11(17), 4543.

Zhou, Z., and Qiao, P. (2018). "Bond behavior of epoxy-coated rebar in ultra-high performance concrete." *Construction and Building Materials*, 182, 406-417.

CHAPTER V

CONCLUSIONS AND RECOMMENDATIONS

5.1 Summary and Conclusions

This thesis consists of three main objectives. The first objective is to investigate the bonding behavior of lap-spliced and embedded reinforcing steel bars in Ultra-High-Performance Concrete (UHPC), particularly in comparison to normal concrete (NC). The second objective is to develop predictive equations for bond strength and embedment length that can be used to design more efficient UHPC joints. The third objective is to verify these proposed design schemes through full-scale testing of beam-column joints, using various splice lengths and hook configurations.

5.1.1 Chapter 3: Bonding Behavior of Lap-Spliced Reinforcing Bars Embedded in Ultra-High-Performance Concrete

This chapter explores the superior bond behavior of UHPC when compared to normal concrete. The pull-out and lap-splice tests were conducted on deformed steel bars with diameters of 12, 16, 20, and 25 mm. The embedment and lap splice lengths were varied from 2D to 12D. The results revealed that UHPC specimens consistently developed higher bond strength than NC due to the presence of steel fibers, which delayed crack propagation and enhanced post-cracking tensile behavior. In many UHPC specimens, steel bar rupture was observed, indicating that the bond strength exceeded the tensile capacity of the rebar. A predictive bond strength equation was developed: $\tau_{bond,\ UHPC} = 11.64\sqrt{\frac{f_c'}{D}}$

This equation accurately predicted the bond strength for all bar sizes tested when UHPC compressive strength exceeded 70 MPa. The embedment length required to reach yield or ultimate stress was found to be significantly shorter in UHPC, with rupture occurring at L/D ratios of 4.52–6.92 depending on bar diameter.

For comparison, NC specimens showed only bond failure. The findings support the application of UHPC in joint design, particularly for precast systems where short development lengths and strong bond performance are desirable. This chapter concludes that the use of UHPC can result in more compact, efficient, and durable connection joints.

5.1.2 Chapter 4: Full-Scale Experimental Investigation on Beam-Column Connections Using UHPC

This chapter presents a full-scale experimental investigation of beam-column joints constructed with UHPC. The aim was to validate the proposed bond strength equation and splice design scheme in practical structural applications. Five UHPC connection configurations were tested under monotonic loading, focusing on different lap splice lengths (L_1 = 4D to 9D) and hook contributions (L_2 = 3D to 4D). The results indicated that joints with splice lengths of at least 8D performed well, achieving yielding and, in some cases, rupture of the steel bars without slippage. Conversely, joints with 4D splice lengths or inadequate hook lengths experienced premature bond failure. The most effective configuration (LS9) with L_1 = 9D achieved simultaneous bar rupture control, validating the theoretical model. The testing demonstrated that the proposed UHPC design scheme can reliably predict connection performance. It confirmed that conventional RC-based design approaches are not directly transferable to UHPC applications due to significant differences in bond behavior. The findings provide a rational basis for establishing UHPC-specific connection design criteria.

5.2 Recommendations

5.2.1 Development of National UHPC Design Standards

Future work should focus on incorporating the proposed design equations into Thailand's national structural design guidelines, especially regarding lap splice and embedment lengths in UHPC applications.

5.2.2 Exploration of Alternative Materials

Investigations into hybrid or synthetic fiber-reinforced UHPC, as well as the use of various rebar coatings or surface treatments, are recommended to optimize performance under different loading conditions.

5.2.3 Long-Term Durability Studies

Further testing under environmental stressors such as chloride penetration, carbonation, and freeze-thaw cycles should be conducted to validate the long-term bond performance and durability of UHPC joints.

5.2.4 Seismic and Cyclic Load Evaluation

Additional testing under cyclic and seismic loads should be conducted to assess ductility, hysteretic behavior, and energy dissipation of UHPC beam-column joints in seismic zones.

5.2.5 Extension to Other Structural Components

The findings of this study can be applied to other structural elements, including pile caps, wall panels, and bridge elements, and should be validated through further full-scale experiments.

5.2.6 Design Optimization and Economic Assessment

Comparative studies on construction speed, material savings, and life-cycle cost between UHPC and RC joints are recommended to justify the large-scale implementation of UHPC in structural applications.

APPENDIX A

LIST OF PUBLICATIONS

LIST OF PUBLICATIONS

International Journal Papers

Aiamsr, K., Yaowarat, T., Horpibulsuk, S., Suddeepong, S., Buritatum, A., Hiranwatthana, K., and Nitichote, K. (2024). "**BONDING BEHAVIOR OF LAP-SPLICED REINFORCING BARS EMBEDDED IN ULTRA-HIGH-PERFORMANCE CONCRETE WITH STEEL FIBERS.**" Journal of Developments in the Built Environment., 20(2024), 100585.

Aiamsr, K., Yaowarat, T., Horpibulsuk, S., Suddeepong, S., Buritatum, A., Udomchai, A., and Nitichote, K. (2025). "**Performance of connection joints of beam-column structure using Ultra-high-performance concrete under full-scale tests.**" Journal of Developments in the Built Environment., 22(2025), 100682.

Developments in the Built Environment 20 (2024) 100585

Contents lists available at ScienceDirect

Developments in the Built Environment

journal homepage: www.sciencedirect.com/journal/developments-in-the-built-environment

Bonding behavior of lap-spliced reinforcing bars embedded in ultra-high-performance concrete with steel fibers☆

Krairerk Aiamsri [a], Teerasak Yaowarat [a,b,*], Suksun Horpibulsuk [a,b,c,f,**], Apichat Suddeepong [a,d], Apinun Buritatum [a,b,***], Kanchana Hiranwatthana [a], Kirati Nitichote [e]

[a] Center of Excellence in Innovation for Sustainable Infrastructure Development, Suranaree University of Technology, Nakhon Ratchasima 30000, Thailand
[b] Undergraduate Program in Civil and Infrastructure Engineering, Suranaree University of Technology, Nakhon Ratchasima 30000, Thailand
[c] Academy of Science, The Royal Society of Thailand, Bangkok 10300, Thailand
[d] Institute of Research and Development, Suranaree University of Technology, Nakhon Ratchasima 30000, Thailand
[e] The Concrete Products and Aggregate Co., Ltd. Bangkok 10800, Thailand
[f] School of Civil Engineering, Suranaree University of Technology, Nakhon Ratchasima 30000, Thailand

ARTICLE INFO

Keywords:
Ultra-high performance concrete (UHPC)
Bond strength
Pull-out tests
Lap-splice tests

ABSTRACT

This study explores the bond strength of steel reinforcing bars in normal concrete (NC) and ultra-high-performance concrete (UHPC) with steel fibers, focusing on the behavior of lap-spliced rebars. Key variables such as rebar diameter (D), spacing (s), lap-splice length (L_1), and hook length (L_2) were evaluated to understand their impact on bond performance. Both NC and UHPC increase in bond strength with greater spacing and lap-splice length, with UHPC demonstrating significantly stronger bond characteristics due to its higher compressive strength. A novel predictive method for calculating bond strength is proposed, offering practical guidance for designing lap-spliced rebars in construction, and includes reduction factors tailored for realistic construction settings. This method achieves an error margin below ±16.5%, providing an accurate approach for practitioners. This rational method incorporates both engineering and economic considerations, particularly valuable for applications in precast concrete structures where enhanced bond performance and durability are essential.

1. Introduction

The precast concrete structures possess several benefits over their cast-in-place counterparts, including shorter design and construction time, cost-effectiveness, quality assurance, and improved aesthetics. Frame structures are particularly suitable for the precast concrete manufacturing due to their standardization, prefabrication, and easy assembly. As a result, the use of precast structures in infrastructure systems has garnered mounting interest in the past few years. However, under seismic attack, precast concrete structures are prone to losing their bearing capacity at the joints/connections when the plastic deformations of the frame components have not been fully mobilized, thereby impeding effective dissipation of seismic energy (Belleri et al., 2015). Stability analysis of precast buildings has shown that prefabricated beams or columns usually suffer minimal damage. Instead, structural failure primarily results from the damaged joints between structural members.

The integrity of connections in precast concrete structures is critical in ensuring their stability during seismic events. In line with this, ACI 318–19 (2019) promotes the "Strong joints and weak members" principle and sets a minimum anchorage length requirement for tensile reinforcing steel in ordinary concrete, which should be no less than 20 times its diameter. However, the installation of connection joints for precast concrete members remains a complex and challenging process in contemporary construction practices. In Europe, America, and Japan, grout sleeves are often utilized to ensure continuity of reinforcing steel

☆ NOTE: The second, third and fifth authors are the corresponding authors. Please mail communication to Prof. Suksun Horpibulsuk, School of Civil Engineering, Suranaree University of Technology, 111 University Avenue, Muang District, Nakhon Ratchasima 30,000, THAILAND.
* Corresponding author. Institute of Engineering, Suranaree University of Technology, Nakhon Ratchasima 30000, Thailand.
** Corresponding author. Institute of Engineering, Suranaree University of Technology, Nakhon Ratchasima 30000, Thailand.
*** Corresponding author. Institute of Engineering, Suranaree University of Technology, Nakhon Ratchasima 30000, Thailand.
E-mail addresses: Krairerk.ai15@gmail.com (K. Aiamsri), teerasakyaowarat@gmail.com (T. Yaowarat), suksun@g.sut.ac.th (S. Horpibulsuk), suddeepong@g.sut.ac.th (A. Suddeepong), apinun_ce@hotmail.com (A. Buritatum), kanchanahiranwatthana@gmail.com (K. Hiranwatthana), kiratini@scg.com (K. Nitichote).

https://doi.org/10.1016/j.dibe.2024.100585
Received 9 August 2024; Received in revised form 7 November 2024; Accepted 1 December 2024
Available online 4 December 2024

at connection joints, as reported by Einea et al. (1995). However, such methods necessitate high precision, and verifying the quality of grout in joints can be arduous. This may introduce potential hazards that may remain concealed within the structure, underscoring the need for safer and more efficient alternatives.

Ultra-high performance concrete (UHPC) is renowned for its extraordinary mechanical properties and workability. Offering ultra-high compressive and flexural strengths, exceptional toughness, superior durability, and a notable self-compacting factor, UHPC presents an enticing option for various structural applications requiring resilience against heavy loads, seismic activities, explosions, and impact. UHPC exists in two primary forms: with and without steel fiber reinforcement. UHPC with steel fiber reinforcement boasts enhanced mechanical properties, including improved tensile strength, ductility, and resistance to crack, making it ideal for structures necessitating heightened integrity and durability under extreme loading conditions. On the other hand, UHPC without steel fiber reinforcement relies solely on its cementitious matrix's inherent properties to achieve exceptional performance, maintaining remarkable mechanical properties and durability suitable for a diverse array of structural applications where steel fibers may not be necessary or feasible.

Notably, UHPC exhibits distinctive behavior compared to conventional concrete, as it enables the shortening lap splice length of rebars for the same bending moment requirements. The exceptional performance of UHPC is largely due to its strong bond with steel rebars, which enhances load transfer and structural integrity (Yuan and Graybeal, 2015). This attribute has opened the path for the development of innovative connection specifications for precast concrete bridges (Graybeal, 2014; Shafieifar et al., 2017) and buildings (Aarup and Jensen, 1998), highlighting the immense potential of UHPC in pushing the boundaries of structural engineering. Moreover, these connections have simplified construction procedures and minimized on-site work requirements, thanks to the significantly reduced splice length (Tosa and Salha, 2016; Ye et al., 2021).

Besides the strength of concrete, the bond strength depends on the types of rebars and stirrups. Kaufman and Fam (2024) found that Ultra High-Performance Fiber-Reinforced Concrete (UHPFRC) with Glass fiber reinforced polymer (GFRP) rebars required precise development lengths based on concrete cover and bar size, enhancing UHPC's application in beam design (Kaufman and Fam, 2024). Elsanadedy et al. (2023) studied the influence of externally attached Carbon-Fiber Reinforced Polymer (CFRP) U-wraps versus confining steel stirrups on enhancing the bond strength of lap spliced GFRP bars in concrete beams, finding CFRP U-wrapped highly effective in bond enhancement, which has implications for durability under demanding loads. Jalali and Taghizadeh, (2022), showed that strategically layering UHPFRC on beam surfaces yields superior cyclic durability and crack resistance, further emphasizing UHPC's potential in enhancing beam longevity and resilience. These findings align with UHPC's suitability for durable, load-bearing applications, especially in precast and cyclically loaded structures.

From the literature survey, the bonding mechanism in UHPC, particularly in formulations with steel fibers, exhibits a direct correlation with the increase in tensile strength, aligning closely with its compressive strength (Alkaysi and El-Tawil, 2017; Pour et al., 2016; Shen et al., 2016). Moreover, the incorporation of steel fibers into UHPC formulations notably augments the bonding mechanism by effectively delaying crack propagation and offering enhanced tensile strength, particularly after the occurrence of cracking (Lee, 2016; Yoo et al., 2015). This leads to the preservation of the concrete's bonding strength against lugs even after splitting at the lap splices. It is worthwhile noting that the concrete's bonding strength in this case is primarily influenced by the delayed crack opening induced by the steel fibers. In addition, the utilization of UHPC for joint construction provides enhanced shear capacity and reduces the necessary length of reinforcing steel within the joint. This also facilitates the attainment of greater homogeneity between columns and beams during construction, and incorporating UHPC as a connecting material for lap-spliced rebar in the joint between a beam and a column is a significant feature of precast concrete structures. This is attributed to its high flowability and self-compacting properties, which guarantee thorough consolidation and bonding around the lap-spliced rebar (Bae et al., 2016; Garcia-Taengua et al., 2016).

Despite the utilization of UHPC as a connection material for precast concrete members was found to be advantage in practice (Elliott, 2000), it is noteworthy that existing international standards, such as the ACI (American Concrete Institute) code, have inherent limitations in calculating the bond strength for concrete with compressive strength higher 70 MPa and do not provide specific provisions for concrete incorporated with steel fibers. Consequently, the incorporation of UHPC with steel fibers for precast concrete beam-column connections worldwide and in Thailand is presently limited, despite the extensively documented engineering, economic, and environmental benefits evidenced by international academic research. There exists an urgent imperative to conduct a thorough investigation and establish the applicability of UHPC within the unique context of Thailand's material standards and construction practices. Such efforts are essential for fully unlocking the potential benefits offered by this innovative technology.

This research attempted to investigate the influence of embedment length, lap-splice length and spacing between reinforcing steel in both normal concrete and UHPC, utilizing four different diameters of reinforcing steel. The lap-spliced rebars under varying lap-splice length, hook length and spacing were evaluated through pull-out tests, and the bond strength predictive formulas in terms of embedment length and lap-splice length, with and without hook, were proposed. These formulas were derived as part of the research, with a specific focus on bond strength calculations that consider engineering and economic factors. The utilization of these formulas to determine the necessary length of reinforcing steel for connecting beam-column at joint core is highly suitable, especially considering the sustainable innovation introduced by employing UHPC as the connection point for precast concrete structures. This approach not only improves the design of beam-column connections but also simplifies construction processes, minimizing the requirement for intricate construction plans and resulting in cost savings for construction projects.

Building on this investigation, the study critically addresses the gaps in current literature on bond strength of reinforcing bars in NC and UHPC, underscoring the need for predictive models that precisely account for UHPC's advanced properties, such as its high compressive strength and the reinforcing effect of steel fibers. Existing standards, such as ACI 318, are insufficient for accurately predicting bond strength in UHPC, especially for large-diameter rebars, leading to conservative design estimates that underutilize UHPC's capabilities. To address this shortfall, the study introduces a UHPC-specific predictive formula with improved accuracy, making it applicable to modern structural designs, particularly in precast concrete applications. The study's objectives include a comprehensive evaluation of bond behavior in UHPC under various configurations, such as differing rebar diameters, spacings, and lap-splice lengths, with the aim of developing a model that offers precise reduction factors and embedment length guidelines. The hypothesis of the study posits that UHPC will demonstrate substantially higher bond strength than NC, enabling the use of shorter lap-splice and embedment lengths without compromising structural integrity. This advancement supports more efficient design and construction solutions, reducing material usage and advancing sustainable, resilient infrastructure development, while simplifying the construction process and promoting cost-effective precast concrete applications.

2. Materials and methods

2.1. Material characteristics of normal concrete and UHPC

The normal concrete (NC), used as a comparison to UHPC, employed ordinary Portland cement as the cementing agent. Sand with a particle size smaller than 4.75 mm was employed as fine aggregate in accordance with ASTM C33 (2003) "Standard Specification for Concrete Aggregates", while coarse aggregates were not included in the mixture. The design goal for the NC was to attain a compressive strength >38 MPa after 28 days, achieved through the mixing weight ratio (job mix formula) of cement: sand: water in a ratio of 1:2:0.275, while maintaining a slump value within a range of 7.5 ± 2.5 cm.

The UHPC mixture utilized for casting the concrete specimens was provided by Concrete Products and Aggregate Co., Ltd. (CPAC), which is a subsidiary of Siam Cement Group (SCG), a reputable supplier of high-quality concrete products in Thailand. The maximum size of the fine aggregate was 1 mm, and the water-to-binder ratio was 0.175. A 28-day compressive strength (f_c') of this mix is > 130 MPa was achieved, while the elastic modulus was observed to be 26,455 MPa. Table 1 presents the quantities of constituent materials per cubic meter for both normal concrete (NC) and ultra-high-performance concrete (UHPC), providing a comprehensive reference for the mix design. The steel fiber in UHPC had a diameter of 0.22 mm and a length of 13 mm (Fig. 1), and exhibited an ultimate tensile strength of 2800 MPa. The laboratory tests on NC and UHPC specimens included slump flow, compression, Poisson's ratio, and elastic modulus and the testing conditions are presented in Table 2. Following the concrete casting, all test specimens were immediately wrapped with plastic sheets and kept at ambient temperature for 48 h prior to being demolded. Subsequently, the specimens were cured until the target curing time.

Reinforcing bars with four different diameters (12, 16, 20, and 25 mm) were utilized. The average yield and ultimate strengths of the four different diameters were measured as 522.24 MPa and 636.10 MPa, correspondingly, while the elastic modulus was determined to be higher than 200,000 MPa. The engineering properties of the rebars are listed in Table 3.

2.2. Test setup and procedure

2.2.1. Pull-out test

The pull-out test on rebars according to ACI-408 (2003), despite its simple and easy operation, is considered the unprecise means for measuring bond capacity in concrete. This is owing to the fact that it tends to overestimate bond capacity. In the conventional pull-out test (ACI, 2003), the tensile load applied to the rebar generates compressive stress in the surrounding concrete as it reacts against the rigid support surface holding the specimen. However, in reinforced concrete structures under flexural condition, both the rebar and concrete are under tensile loading, which differs from the traditional pull-out test method.

Table 1
The mix design for both NC and UHPC.

Ultra High Performance Concrete (UHPC)	
Materials	Materials per 1 cubic meter, kg
Cement Grout CPAC	2273
Additional admixtures PC-UP01	31
Additional admixtures Type D	22
Steel fiber	155
Water	200
Normal Concrete (NC)	
Materials	Materials per 1 cubic meter, kg
Cement type 1	585
Sand	1609
Water	190

Fig. 1. Micro steel fibers.

Table 2
Testing conditions of normal concrete and UHPC specimens.

Test item	Specimen size	Test age	Test standard	Number of specimens/mix design.
Slump flow test	Slump cone	Fresh concrete	ASTM C230	3
Initial and Final Setting Time	–	Fresh concrete	ASTM C403	3
Compressive Strength test	Φ15 cm × 30 cm	1, 3, 7, 14 and 28 days	ASTM C39	15
Flexural Strength test	10 cm × 10 cm x 40 cm	1, 3, 7, 14 and 28 days	ASTM C78	15
Poisson's ratio, and elastic modulus test	Φ15 cm × 30 cm	7 and 28 days	ASTM C469	6

Table 3
Mechanical properties of steel bars.

Diameter (mm)	Grade	Number of specimens	Yield tensile strength (MPa)	S.D. (%)	Ultimate tensile strength (MPa)	S.D. (%)
12	SD40	3	536.15	7.53	645.09	7.82
16	SD40	3	565.94	3.51	658.14	3.49
20	SD40	3	504.79	3.55	611.54	1.51
25	SD40	3	482.06	3.1	629.73	3.78

To reduce the impact of the compressive area during the testing process, a modified concrete support was employed in accordance with the Alkaysi and El-Tawil recommendation (Alkaysi and El-Tawil, 2017), as illustrated in Fig. 2. Steel rebars with nominal diameters of 12, 16, 20, and 25 mm were utilized in the experiment. A mold with a square cross-section of 150 mm and a height ranging from 150 to 300 mm was utilized to fabricate the pull-out specimen, which consisted of a single steel rebar embedded vertically along the central axis. The embedment length of 12-mm-diameter rebars was determined to be 40, 50, 75, and 100 mm, while it was determined to be 50, 75, 100, 125, 150, 175, and 200 mm for the rebars with diameters of 16, 20, and 25 mm. During the

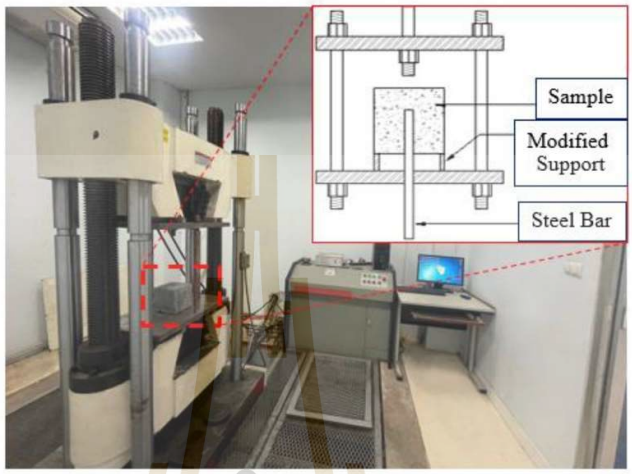

Fig. 2. Test set up details.

Table 4
Parameters and test results of lap-splice specimens.

Graphic expression (mm)	Diameter (mm)	L_1	L_2	s
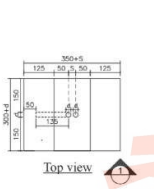	12	4d, 6d, 8d, 10d, 12d	–	1d, 1.5d, 2d, 3d
	16	3d, 4.5d, 6d, 8d, 10d, 12d		
	20	3d, 6d, 8d, 10d, 12d		
	25	3d, 4d, 6d, 8d, 10d, 12d		
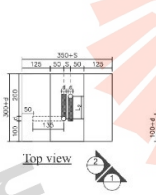	12	2d	1.5d, 2d	1d, 1.5d, 2d, 3d
		4d	1.5d, 2d, 3d, 4d	
	16	3d	1.5d, 3d	1d, 1.5d, 2d, 3d
		4d	1.5d, 3d, 4d	
		5d	1.5d, 3d, 4d, 6d	
		6d	1.5d, 3d, 4d, 6d	
	20	3d	1.5d, 3d	1d, 1.5d, 2d, 3d
		4d	1.5d, 3d, 4d	
		5.5d	1.5d, 3d, 4d, 6d	
		6d	1.5d, 3d, 4d, 6d	
	25	3d	1.5d, 3d	1d, 1.5d, 2d, 3d
		4d	1.5d, 3d, 4d	
		6d	1.5d, 3d, 4d, 6d	
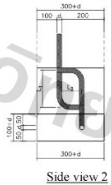				

testing, a Universal Testing Machine (UTM) with a maximum 5000-kN load capacity was adopted to apply a pull-out load via displacement control with a fixed rate at 0.5 mm per min.

The pull-out and lap-splice tests were conducted on NC and UHPC at 7 days of curing to align with ACI 347 guidelines and construction practices, which often permit formwork removal once adequate strength is achieved at this early stage (ACI 2014). At 7 days, concrete typically reaches at least 70% of its 28-day compressive strength, providing sufficient capacity for early loading and support removal, as is common in real-world scenarios. While 28-day strength remains the standard, the 7-day testing period was chosen to reflect practical construction timelines where early strength is essential for progression. This ensures meaningful comparison with ACI criteria while adapting to the early-age performance needs in construction.

2.2.2. Lap-splice test

Table 4 presents two groups of lap-splice specimens designed with different parameters of splice lengths and longitudinal bar end shape (straight or hooked). The experimental test setup employed in this study was consistent with the configuration utilized by McMullen and Haber (2019) and Yuan and Graybeal (2015). To achieve various failure modes, the splice length was ranged between 2 and 12 times the rebar diameter. The varied splice lengths (L_1) of the rebars in the concrete specimens were tailored to achieve either bonding failure or rebar rupture, with the lengths of hooked rebar ends (L_2) strategically designed to investigate the additional bond strength. The clear spacing between the two longitudinal steel bars (s) was defined in this study as ranging from 1 to 3 times the rebar diameter, measured from the center of one rebar to the center of the adjacent rebar. The lap-splice specimen was subjected to loading using a 500 kN center hole jack, as depicted in Fig. 3. This setup does provide confinement to the rebar embedded in the lower part of the specimen, which may influence bond conditions in that region. However, for the rebar being pulled out (located in the upper part of the specimen), this confinement effect does not apply, as the bond condition remains unaffected by the setup's lower part. This distinction ensures that the bond behavior of the pulled-out rebar accurately reflects the intended test conditions.

The rebars were affixed using a steel anchorage system. The magnitude of the pull-out force was measured using a digital display meter mounted on the hydraulic jack. To record the slippage between the concrete specimen and the rebars at the loaded end, an LVDT was utilized. During the loading process, the appearance and load values were measured until the specimen developed visible cracks. The pull-out test and lap-splice test were conducted with three replicates, with a standard deviation within 10% of the mean test value, to ensure reliability and accuracy of the results.

The rebar diameters (12, 16, 20, and 25 mm) represent typical sizes used in such applications in Thailand's construction. Lap lengths, ranging from 2 to 12 times the diameter, were chosen to reflect common splice configurations, and rebar spacings of 1–3 times the diameter were used to examine confinement effects typical in joint construction. These choices ensure that the study's findings are applicable to practical precast joint designs and provide relevant insights into bond performance under real-world conditions.

3. Test results

3.1. Mechanical strength of NC and UHPC

The results of the initial and final setting time tests, performed as per ASTM C403 (2009b), are presented in Fig. 4. In this test, the initial and final setting periods are calculated by measuring the compression resistance per area of 3.5 MPa and 27.6 MPa, correspondingly. The NC had initial and final setting periods of 4 h 46 min and 8 h 22 min, correspondingly, while the UHPC exhibits longer initial and final setting periods of 8 h 37 min and 14 h 16 min, respectively.

Fig. 5(a) illustrates the compressive strengths of NC and UHPC specimens at various curing times, in the manner of ASTM C39 (2001). The NC exhibited compressive strength values of 2.17, 16.16, 29.10, 35.48, and 43.91 MPa after curing for 1, 3, 7, 14, and 28 days, respectively. Conversely, the UHPC specimens displayed strength values of 5.25, 54.06, 93.86, 111.76, and 132.84 MPa for the corresponding curing periods. These findings suggested that the UHPC specimens cured for 3 days possessed a higher compressive strength than the NC specimens cured for 28 days. The elastic modulus and Poisson's ratio, carried out in the manner of ASTM C469 (2009a), are summarized in Table 5. The obtained data indicated that there was an increase in both elastic modulus and Poisson's ratio as the curing time was prolonged for both NC and UHPC. These findings are consistent with the research conducted by Huang et al. (2022). When normalizing the strength values at different curing periods by dividing them by the 28-day compressive strength value, a comparison reveals that the rate of strength development of NC and UHPC exhibits similar characteristics, as depicted in Fig. 5(b). In other words, both NC and UHPC follow a similar pattern of compressive strength development over time.

Fig. 6 illustrates the flexural strength development of NC and UHPC over a 28-day curing period. The NC exhibited flexural strength values of 0.21, 2.23, 3.62, 5.20, and 6.81 MPa after 1, 3, 7, 14, and 28 days of curing, respectively. In contrast, the UHPC specimens achieved significantly higher strength values of 1.26, 14.62, 27.21, 35.79, and 44.46

Fig. 3. Test loading device for lap-splice test.

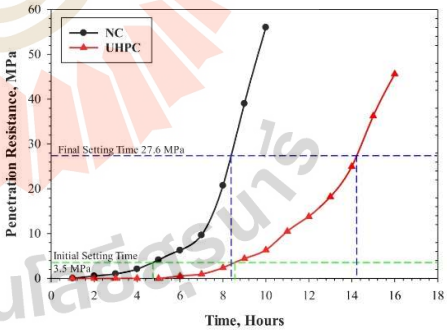

Fig. 4. Initial and Final Setting Time of Normal concrete (NC) and UHPC.

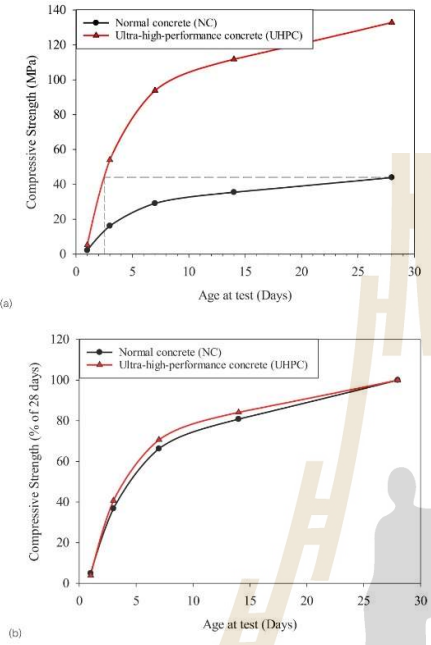

Fig. 5. NC and UHPC (a) compressive strength vs. time and (b) normalized compressive strength vs. time.

MPa at the corresponding curing intervals. This figure underscores UHPC's superior flexural performance and rapid strength gain, making it particularly suitable for applications requiring early high strength.

3.2. Pull-out test results

The failure mode of NC is observed to be the complete pull-out for all diameters of rebars, as shown in Fig. 7(a). This failure is attributed to NC's limited capacity to transfer stress through adhesion, friction, and mechanical interlock, leading to insufficient confinement. Consequently, early bond degradation and slippage occur under tensile loads, preventing the rebar from reaching its ultimate tensile strength. On the other hand, UHPC exhibits two distinct failure modes, namely the rebar's pull-out (bond failure) as depicted in Fig. 7(b), and rebar's rupture as illustrated in Fig. 7(c). UHPC's high compressive strength and the presence of steel fibers enhance confinement and mechanical interlock, allowing more effective stress transfer across the rebar-concrete interface. This robust bonding allows UHPC to mobilize the full tensile capacity of the rebar, often leading to rebar rupture rather than bond failure. The bonding equations for each size of steel rebar were generated; the tensile forces generated by the rebar rupture was not taken for the development of equations (Fig. 7(c)).

The pull-out force versus embedment length plot of the rebar was depicted in Fig. 8, where Fig. 8(a) represents all the pull-out forces data, while Fig. 8(b) shows only the pull-out forces resulting from rebar pull-out. For both NC and UHPC, the increased embedment length led to an increased pull-out force. However, in the case of UHPC, the pull-out force continued to increase with the increased embedment length until it attained the ultimate tensile strength (f_u) of the rebar. Specifically, the rebars ruptured at an embedment length of 0.05, 0.10, 0.15, and 0.175 m for DB12, DB16, DB20, and DB25, respectively.

In engineering terms, the bond strength between concrete and rebar is governed by adhesion, friction, and mechanical interlock. UHPC, with its high compressive strength and inclusion of steel fibers, significantly enhances each of these bond components. The fibers bridge potential cracks, delaying crack propagation and maintaining a high level of stress transfer across the embedment length. This results in a more effective confinement around the rebar, improving resistance to slippage and enabling higher tensile stresses to be carried by the rebar-concrete interface. Moreover, as UHPC's pull-out force continues to rise with embedment length until rebar rupture, this demonstrates a shift from bond failure (as seen in NC) to a more desirable rebar tensile failure. This shift in failure mode reflects UHPC's capacity to transfer stress along the rebar length without bond degradation, which is a critical advantage in structural applications that demand high reliability in load-bearing and seismic performance. The ability of UHPC to sustain stress transfer until the rebar's tensile strength is fully mobilized highlights its suitability for reinforced concrete structures exposed to high tensile and shear forces, where bond integrity and ultimate load resistance are paramount.

Fig. 9 displays the bond strength versus embedment length for NC and UHPC at various rebar's diameters. The bond strength obtained from pull-out test was assumed to represent the bond strength at infinite spacing ($s = \infty$); i.e., this bond strength is not influenced by the presence of neighboring rebars. The bond strengths for NC were 8.46, 7.17, 6.56,

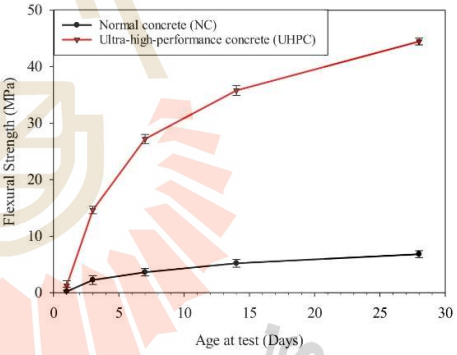

Fig. 6. The flexural strength vs. time of NC and UHPC.

Table 5
Poisson's ratio and elastic modulus of UHPC and NC.

Age (days)	Average Poisson's ratio (ν) and elastic modulus (E)							
	Normal concrete (NC)				UHPC			
	ν	S.D. (%)	E (GPa)	S.D. (%)	ν	S.D. (%)	E (GPa)	S.D. (%)
7	0.198	4.74	10.765	3.69	0.212	5.81	12.191	3.16
28	0.205	5.42	19.545	4.57	0.219	3.54	26.455	4.17

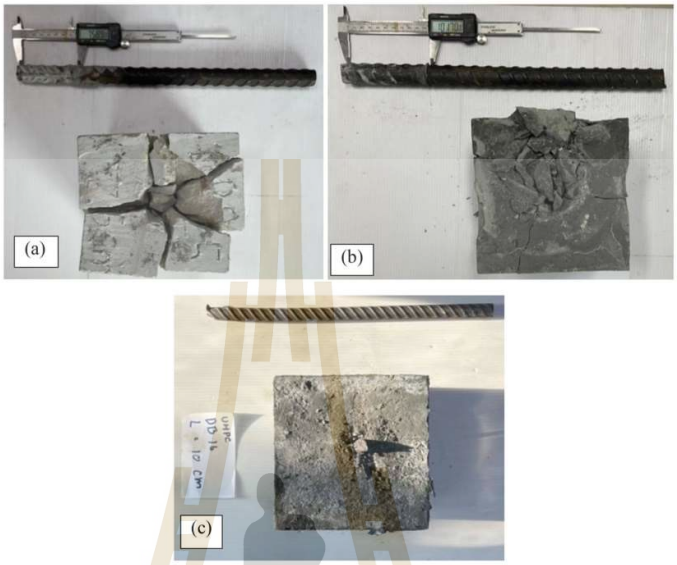

Fig. 7. Failure modes of (a) Normal concrete, (b) UHPC with bond failure and (c) UHPC with steel bar rupture.

and 6.07 MPa for DB12, DB16, DB20, and DB25, respectively. The bond strengths predicted from the ACI-318's equation (ACI, 2011) were 6.34, 4.75, 3.80, and 3.04 MPa for DB12, DB16, DB20, and DB25, respectively. It was evident that the equation underestimates the experimental results by 25.7%, 33.7%, 42.1%, and 49.9% for DB12, DB16, DB20, and DB25, respectively. The higher diversity was found for a larger diameter. The bond strength equation proposed by ACI-318 is however not capable of accurately predicting the bond strength for UHPC. This is possibly the equation is limited to compressive strength of concrete of 70 MPa (Bae et al., 2016) as suggested ACI-318 (ACI, 2011). Consequently, this research proposed a new equation for predicting the bond strength for UHPC, given by:

$$\tau_{bond,UHPC} = 11.64\sqrt{\frac{f_c'}{D}} \quad (1)$$

where $\tau_{bond,\ UHPC}$ is the bond strength for UHPC [MPa], f_c' is compressive strength of UHPC [MPa] and D is the diameter of steel rebar [mm].

The predicted bond strength of UHPC by equation (1) was found to be 32.24, 27.92, 24.97, and 22.34 MPa for DB12, DB16, DB20, and DB25, respectively. While the measured bond strengths were 34.14, 27.44, 25.53, and 23.26 MPa, indicating a small error of 5.56%, −1.74%, 2.21%, and 3.96% for DB12, DB16, DB20, and DB25, respectively. Additionally, an evaluation between the predicted and measured values at various f_c' is presented in Fig. 10. The predicted bond strengths obtained from equation (1) were highly accurate when the f_c' of UHPC exceeded 70 MPa. However, it is of interest to mention that when the f_c' of UHPC <70 MPa, the ACI-318's equation was capable of assessing the bond strength for both UHPC and NC. Furthermore, a comparison with the CEB-FIP Model Code (1993) is shown in Fig. 10. As illustrated, the CEB-FIP Model Code (1993) provided a lower-bound prediction of bond strength, particularly at higher compressive strengths, which highlights its conservative approach, especially for UHPC. This visual comparison underscores the improved accuracy of the proposed model, particularly for UHPC with compressive strengths exceeding 70 MPa, where the CEB-FIP predictions underestimate bond performance. This alignment in Fig. 10 validates the proposed model's applicability across different rebar diameters and compressive strengths, offering a more precise assessment than the CEB-FIP Model Code (1993) under certain conditions.

In addition, this research proposed an equation to predict the safe steel embedding length (development length) based on the bond strength and tension stress in the steel bar (f_s). To derive this equation, the maximum force at rebar rupture was assumed to be equal to the maximum bonding force (Max. tensile force = Max. bonding force), and the relevant equations were applied accordingly. The resulting equation for development length is as follows:

Max. tensile force ($A_b f_s$) = Max. bonding force ($\tau_{bond} A_{surface}$)

$$\tau_{bond} = \frac{f_s}{4\left(\frac{L}{D}\right)} \quad (2)$$

where τ_{bond} is the bond strength, f_s is tensile stress in rebar, A_b is the cross-section area of rebar, $A_{surface}$ is the initial surface area of embedded portion of the rebar (πDL), L/D is the embedment length to diameter ratio.

Equation (2) can be utilized to determine the boundary of the required embedment length necessary to achieve the desired bond strength between the rebar and concrete. In Fig. 11, the boundary of required embedment length is shown in terms of L/D. The tension stress in the rebar (f_s) was considered at two values: 522.24 MPa for the average yield stress and 636.1 MPa for the average ultimate stress of the rebar. Furthermore, the bond strength could be estimated using equation (1) for UHPC. It should be noted that while using equation (1) with f_s = 636.1 MPa, the predicted required L/D ratios were 4.94, 5.71, 6.39 and 7.08 for DB12, DB16, DB20, and DB25, correspondingly. However,

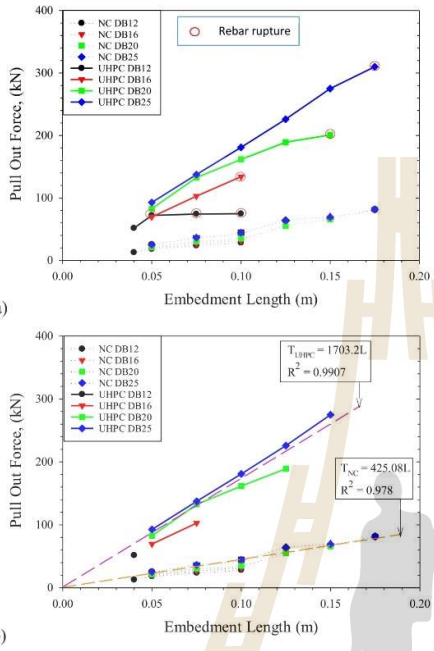

Fig. 8. Relationship between the pull-out force and embedment lengths at 7-day of fc' (a) considering all types of failures and (b) considering only types of pull-out failure.

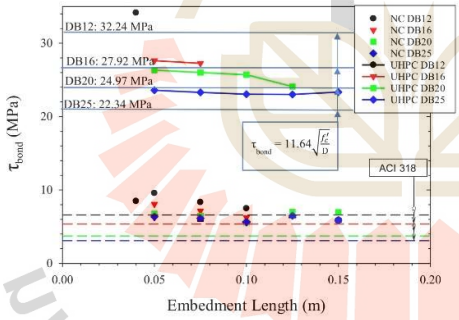

Fig. 9. Bond strength of steel rebar in NC and UHPC at 7-day of f_c'.

experimental results revealed embedment length to diameter ratios of 4.52, 5.89, 6.74 and 6.92 at the point of rebar rupture, which were lower than the predicted values by approximately 9.29%, −3.05%, −5.19% and 2.31% for the respective bar sizes.

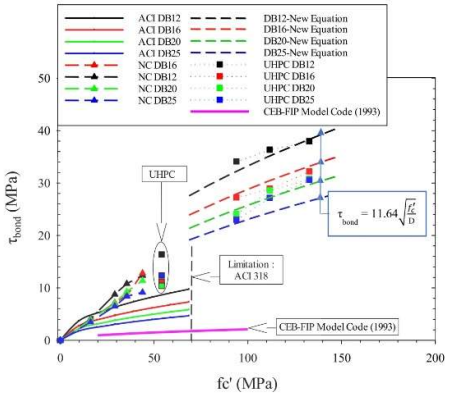

Fig. 10. Bond strength of steel rebar in NC and UHPC at varied f_c'.

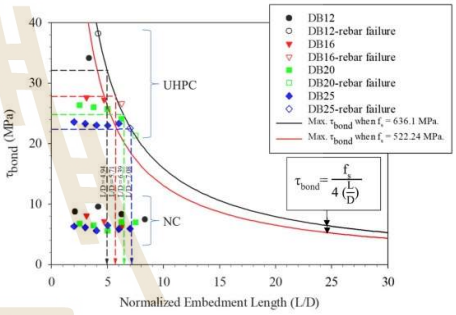

Fig. 11. Failure boundary of steel rebars of different sizes in both NC and UHP.

3.3. Lap-splice test results

The findings from the bond strength tests for lap-spliced rebars without hook in NC and UHPC, with various rebar diameters and spacings (s) and lap-splice lengths (L_1), are presented in Fig. 12. The bond strength of lap-spliced rebars increased with a rise in s for all the tested rebars, with the highest bond strength recorded at $s = 3$ and the lowest at $s = 1$. As an example, the average bond strength of DB12 (Fig. 12(a)) in NC was observed to be 5.22, 5.92, 6.72, and 7.72 MPa for the s values of 1, 1.5, 2, and 3, respectively. However, these values were found to be lower than the bond strength determined at $s = \infty$ by approximately 38.84%, 30.64%, 21.27%, and 9.55%, respectively. The lap-spliced rebars in UHPC exhibited average bond strength values of 26.52, 27.19, 30.66 and 32.18 MPa for the s values of 1, 1.5, 2, and 3, respectively. These values were observed to be lower than the bond strength obtained from $s = \infty$ by approximately 22.34%, 20.36%, 10.19%, and 5.74%, respectively.

In a similar manner, the highest bond strength was observed at $s = 3$ for DB16, DB20, and DB25 in both NC and UHPC (Fig. 12(b–d)). The average bond strengths in NC were 6.21, 6.42, and 5.03 MPa for DB16, DB20, and DB25, respectively, while in UHPC were 26.91, 24.80, and 22.47 MPa for DB16, DB20, and DB25, respectively. Conversely, when

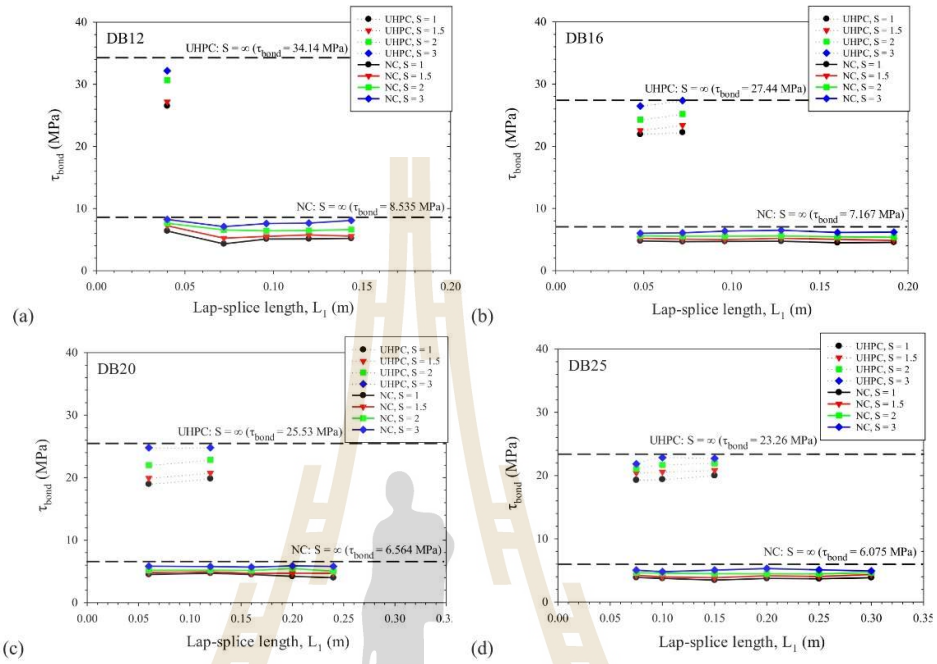

Fig. 12. Bond strength of lap-spliced bars without hook in NC and UHPC at 7-day of fc' for (a) DB12, (b) DB16, (c) DB20 and (d) DB25.

the spacing was set to 1, the average bond strength in NC was 4.65, 4.38, and 3.73 MPa for DB16, DB20, and DB25, respectively, while the average bond strength in UHPC was 22.08, 19.40, and 19.70 MPa for DB16, DB20, and DB25, respectively. The observed increase in bond strength for lap-spliced rebars in concrete with an increased rebar's spacing can be attributed to a higher level of lateral confinement forces acting on the rebars. As the spacing between the rebars increases, the rebar interference effect also decreases, hence the lateral deformation and crack formation in the surrounding concrete reduce (Harajli et al., 2004; Wang et al., 2018; Yoo et al., 2014).

The enhanced bond strength in UHPC at each spacing level is largely due to its material properties. UHPC's high compressive strength and the presence of steel fibers enable it to resist lateral deformation and control cracking more effectively than NC. The steel fibers act as crack-arresting agents, bridging cracks and limiting their propagation, even under closer rebar spacing. This increased crack control creates a more durable bond by maintaining confinement around the rebar, which is especially beneficial in densely reinforced applications where spacing is constrained. The results in UHPC demonstrate that it can sustain high bond strength even at smaller spacings, making it a superior material choice for applications requiring reliable load transfer and structural integrity under dense reinforcement configurations.

The normalized bond strength of lap-spliced rebars without hooks is presented in Fig. 13, demonstrating that a lower spacing between rebars results in a lower bond strength for both NC and UHPC when compared to $s = \infty$ for their respective concrete types. In NC, the normalized bond strength of lap-spliced rebars ranged from 0.61 to 0.66, 0.67 to 0.72, 0.74 to 0.79, and 0.82 to 0.89 for s values of 1, 1.5, 2, and 3, respectively.

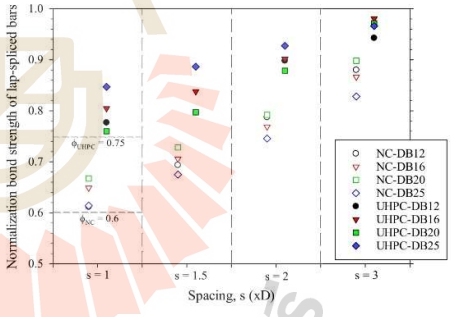

Fig. 13. Normalization of bond strength of lap-spliced bars without hook.

Meanwhile, in UHPC, the normalized bond strength of lap-spliced rebars ranged from 0.77 to 0.84, 0.79 to 0.88, 0.87 to 0.92, and 0.94 to 0.98 for s values of 1, 1.5, 2, and 3, respectively, indicting the superior bonding between rebar and UHPC. However, it is important to acknowledge that in practical construction, rebars are typically positioned close together, corresponding to a spacing of $s = 1$. Therefore, this study recommends the use of reduction factors (ϕ) of 0.6 and 0.75 for NC and UHPC, respectively, to adjust the bond strength obtained from pull-out tests

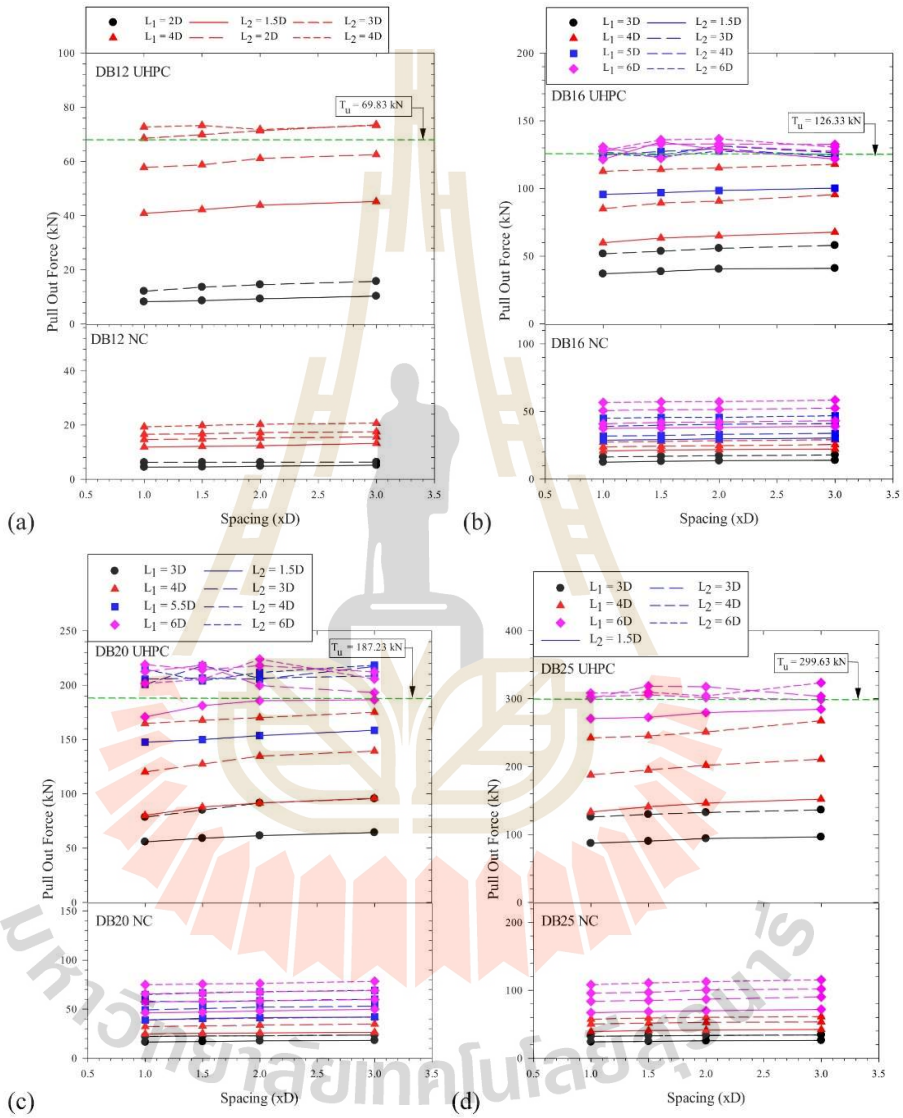

Fig. 14. Pull-out force of lap-spliced bars with hook in NC and UHPC at 7-day of fc' for (a) DB12, (b) DB16, (c) DB20 and (d) DB25.

(equation (1), $s = \infty$) to approximate the bond strength of lap-spliced rebars in practice. This approach offers a safer method for assessing bond strength and designing lap-splice lengths (L_1) as follows:

$$\frac{L_1}{D} = \frac{f_s}{4\,(\phi\tau_{bond})} \tag{3}$$

where τ_{bond} is the bond strength, L_1/D is the lap-splice length to diameter ratio, ϕ is the reduction factor obtained from Fig. 13.

The pull-out force for lap-spliced rebars with hook in NC and UHPC, with varying rebar diameters and spacings (s), lap-splice lengths (L_1) and hook lengths (L_2) are presented in Fig. 14. The green dashed line corresponds to the ultimate tensile strength of rebar (T_u) (Ma et al., 2020). The findings from the study indicate a consistent trend in both NC and UHPC, where a rise in pull-out force was observed with a rise in spacing, lap-splice length, and hook length. Particularly noteworthy was the substantial enhancement in pull-out force when $L_1 \geq 4D$, in conjunction with $L_2 \geq 3D$. This enhancement brings the pull-out force of the steel rebar closer to its ultimate tensile strength, highlighting the significant impact of these parameters on the structural performance. For instance, in the case of UHPC, when $s = 1$ and $L_1 = 4D$, the pull-out force values of DB12 were 40.84, 57.79, 68.57, and 72.72 kN for hook lengths (L_2) of 1.5D, 2D, 3D, and 4D, respectively. Conversely, for NC, the pull-out force values were 11.90, 14.68, 16.58, and 19.32 kN for L_2 of 1.5D, 2D, 3D, and 4D, respectively. In the specific scenario involving DB16, DB20, and DB25, in the case of UHPC with $s = 1$, $L_1 = 4D$, $L_2 = 4D$, the recorded pull-out force values were 114.17, 165.21, and 241.53 kN, respectively. These findings highlight a notable convergence of the pull-out force of the steel rebar with its ultimate tensile strength.

The pull-out force of lap-spliced rebars with hooks typically exceeds that of lap-spliced rebars without hooks at equivalent lap-splice lengths, primarily due to the increased length of the hook part (L_2). This L_2 provides additional surface area for bond development between the rebar and concrete, enhancing the mechanical interlock and subsequently improving bond strength (Goksu et al., 2014; Mousa, 2016; Xia et al., 2011). The extended hooks serve as effective anchorage devices, distributing applied loads more uniformly along the rebar's length and thereby reducing stress concentrations, which helps prevent premature bond failure (Mousa, 2015; Sulaiman et al., 2017 ; Yin et al., 2014; Yu and Tan, 2013). Additionally, the extended hooks offer enhanced confinement to the surrounding concrete due to their curved shape, allowing for better engagement with the concrete. This localized confinement exerts pressure, effectively restraining lateral deformation and minimizing crack formation within the concrete (Bournas and Triantafillou, 2011; Bousias et al., 2007; Ghosh and Sheikh, 2007; Tariverdilou et al., 2009).

However, for the same total embedment length, the pull-out force of the rebar without hook is higher than that with hook. The pull-out force of rebar with hooks (T) was herein assumed to be contributed from two distinct components: the bonding force in the region of the lap-spliced bars (T_1) and the bonding force specific to hooked rebar (T_2). To determine the contribution from bonding force specific to the hook part of the rebar through experimentation ($T_{2,t}$), the T_1 was subtracted from T and then compares it with the bonding force specific to the predicted hook part ($T_{2,eq}$), which is calculated with the assumption that the hook part is in the condition with $s = \infty$, as shown in the following equations:

$$T = T_1 + T_{2,t} \text{ when } T_1 = \phi\tau_{bond}\pi DL_1$$

$$T_{2,t} = T - \phi\tau_{bond}\pi DL_1$$

$$T_{2,eq} = \tau_{bond}\pi DL_2$$

where T is the pull-out force of rebar with hooks, T_1 is the bonding force in the region of the steel splice, $T_{2,t}$ is the bonding force specific to the hook part through experimentation, $T_{2,eq}$ is the bonding force specific to the hook part calculated from the analysis, τ_{bond} is the bond strength from equation (1), ϕ is the reduction factors from Fig. 13.

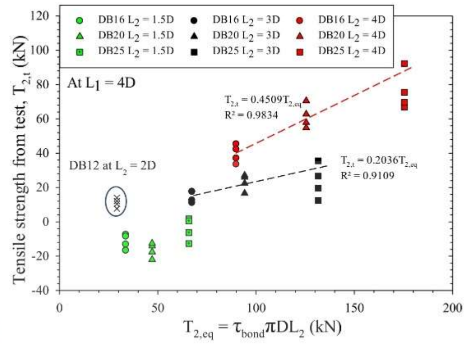

Fig. 15. A comparison of the bonding force specific to the hook part from test ($T_{2,t}$) and the bonding force specific to the hook part calculated from the analysis ($T_{2,eq}$).

Fig. 15 presents a comparison of the bonding force specific to the hook part through experimentation ($T_{2,t}$) and the bonding force specific to the hook part calculated from the analysis ($T_{2,eq}$). The ratio of $T_{2,t}/T_{2,eq}$ has values of 0.2036 and 0.4509 for L_2 of 3D and 4D, respectively. These ratios are referred to as the hook reduction factors (k). Therefore, the calculation of the bonding force for the lap-spliced rebar with hook ($T_{predict}$) can be expressed as follows:

$$T_{predict} = T_1 + T_2$$

$$T_{predict} = \phi_1\tau_{bond}\pi DL_1 + k\phi_2\tau_{bond}\pi DL_2$$

$$T_{predict} = (\phi L_1 + k\phi_2 L_2)\tau_{bond}\pi D \tag{4}$$

where ϕ_1 and ϕ_2 are the reduction factors due to the spacing between lap-spliced bars and hook rebars, respectively (Fig. 13, if $s \geq 4D$, ϕ_1 and $\phi_2 = 1$), k is the hook reduction factors (Fig. 15).

The comparison between the bonding force of lap-spliced rebars with hook from experimental testing and the predicted values from equation (4) is shown in Table 6. The study revealed a close alignment between the predicted bonding force ($T_{predict}$) for lap-spliced rebars with hooks and the corresponding bonding force observed in experimental testing. The deviation between the two did not exceed 16.49%, indicating a relatively low margin of error.

The design process for the embedment length commenced with the calculation of the development length in the form of the L/D ratio, as determined by Equations (1) and (2). In cases where the development length was determined to outstrip the certain achievable embedment length in the concrete structure, the designer is tasked with bending the rebar to form the hook length (L_2). The hook reduction factor (k) is subject to variation depending on the hook length (L_2). For the sake of simplicity and safety, it is recommended to adopt a common value for the hook reduction factor, as suggested by this research as 0.2 ($k = 0.2$). Hence, the hook length can be calculated as follows:

$$T = T_1 + T_2$$

$$f_s A_b = \phi_1\tau_{bond}\pi DL_1 + \phi_2 k\tau_{bond}\pi DL_2$$

$$L_2 = \frac{f_s D - 4\phi_1\tau_{bond}L_1}{4\phi_2 k\tau_{bond}}$$

$$\text{Taking } k = 0.2;\ L_2 = \frac{1.25 f_s D - 5\phi_1\tau_{bond}L_1}{\phi_2\tau_{bond}} \tag{5}$$

Equation (5) could have been utilized to establish the parameters

Table 6
The comparison between the bonding force of lap-spliced rebars with hooks from experimental testing (T) and the predicted values ($T_{predict}$).

DB	L_1 (xD)	L_2 (xD)	$T_1 = \phi_1\tau_{bond}\pi DL_1$ (kN)	$T_2 = k\phi_2\tau_{bond}\pi DL_2$ (kN)	$T_{predict}$ (kN)	T from pull out test (kN)	Error (%)
16	4	3	67.39	12.95	80.34	85.05	5.54
16	4	4	67.39	40.52	107.91	112.82	4.35
20	4	3	94.18	18.15	112.33	120.17	6.52
20	4	4	94.18	56.7	150.88	164.71	8.40
25	4	3	131.65	25.31	156.96	187.96	16.49
25	4	4	131.65	79.26	210.91	242.41	12.99

defining the necessary hook length for achieving the desired bond strength in UHPC. Nevertheless, it is worth emphasizing that Equation (5) was developed under the conditions where $L_1 \geq 4D$ and $L_2 \geq 3D$. Consequently, in the context of practical construction, it was recommended to meticulously set L_1 and L_2 to ensure the alignment of the bonding force for lap-spliced rebars with hooks with the predicted values, while prioritizing safety considerations.

The higher bond strength of lap-spliced bars with hooks in UHPC compared to NC possibly results from the superior engineering properties exhibited by UHPC. Owing to its higher compressive strength, UHPC inherently provides a stronger bond between the rebar and the surrounding concrete (Zhou and Qiao, 2018). The presence of steel fibers in UHPC further enhances this bond by creating an interconnected network of fibers that effectively interlock with the rebar and the concrete matrix. This improved interlocking mechanism promotes a more efficient transfer of forces, resulting in a higher bond strength (Li et al. 2018, 2019; Song et al., 2018). Moreover, the steel fibers act as effective crack bridging elements, effectively distributing stresses and impeding crack propagation, thereby contributing to the overall bond performance (Leung and Shapiro, 1999; Zhang et al., 2000). Additionally, the involvement of steel fibers enhances the ductility of concrete, allowing it to deform and absorb greater energy before experiencing failure (Balendran et al., 2002; Mohod, 2012; Oh, 1992), and hence a higher bond strength.

This study highlights the considerable bond strength advantages of UHPC over NC, especially in rebar confinement and resistance to pull-out failure, which are critical in densely reinforced, high-load-bearing elements such as beams, columns, and structural joints. However, the widespread adoption of UHPC in the field involves challenges related to cost, material availability, and scalability. The production costs of UHPC remain high due to the inclusion of premium materials like steel fibers and specialized additives, while material availability can vary regionally, potentially impacting UHPC's practical use. Future research could therefore examine optimizing UHPC mix designs to lower costs while maintaining bond performance, including exploring alternative, locally sourced materials to reduce supply chain dependency.

Additionally, field-based research is recommended to address practical limitations under different environmental and structural conditions, providing essential guidelines on aspects such as durability, installation methods, and integration with conventional construction practices. By addressing these aspects, further studies would help bridge the gap between experimental findings and field applications, making UHPC more accessible, cost-effective, and practical for engineers in high-performance structural applications.

4. Conclusions

As per the current experimental outputs, the following conclusions can be drawn.

1. In both NC and UHPC, a rise in the embedment length resulted in a rise in the pull-out force. For UHPC, this research introduced a novel equation, denoted as $\tau_{bond} = 11.64\sqrt{(f_c'/D)}$ (MPa), which offers an effective means of estimating the bond strength and the required embedment length with regard to L/D. The proposed equation demonstrated a remarkable level of accuracy, exhibiting an error margin of less than ±10%.
2. The study observed an increased bond strength for lap-spliced bars as the spacing (s) between the bars advanced, with the highest value at $s = 3$ and the lowest at $s = 1$. However, in practical construction, bars are often closely spaced ($s = 1$). To estimate the actual bond strength in such a case, reduction factors (ϕ) of 0.6 for NC and 0.75 for UHPC were recommended. These factors adjusted the experimental bond strength at infinite spacing ($s = \infty$) to the real-work lap-spliced bar condition.
3. For UHPC, in scenarios where L_1 was found to be insufficient, a practical solution for determining L_2 was available through the formula $\frac{1.25f_yD - 5\phi_1\tau_{bond}L_1}{\phi_2\tau_{bond}}$. This approach facilitated necessary adjustments when the initially planned L_1 failed to meet structural requirements. It provided a method to attain the desired bond strength while upholding safety standards in construction practices. Importantly, it should be emphasized that L_1 must be > 4D.
4. The superior bond strength of lap-spliced bars with and without hooks in UHPC compared to NC possibly results from UHPC's surpassing compressive strength, as well as the steel fibers reinforcement. The steel fibers in UHPC create an interconnected network that enhances the nexus between rebar and concrete, resulting in improved force transfer. Additionally, these fibers act as crack bridging elements, effectively distributing stresses and impeding crack propagation, thereby enhancing the overall bond performance.
5. This study presents a promising opportunity for the utilization of short-distanced lap splices embedded in UHPC structures. The experimental findings provide valuable insights into the required parameters for achieving the desired bond strength, including the embedment length, lap-spliced length, and hook length expressed in terms of L/D, L_1/D and L_2, respectively. Furthermore, this study emphasizes the potential benefits of using UHPC in combination with short-distanced lap splices, opening up possibilities for the optimization of construction processes and the realization of more efficient and sustainable structural solutions.

CRediT authorship contribution statement

Krairerk Aiamsri: Writing – original draft, Investigation, Formal analysis. **Teerasak Yaowarat:** Writing – original draft, Validation, Supervision, Project administration, Methodology, Investigation, Funding acquisition. **Suksun Horpibulsuk:** Writing – review & editing, Visualization, Supervision, Software, Resources, Project administration, Conceptualization. **Apichat Suddeepong:** Writing – original draft, Formal analysis, Data curation. **Apinun Buritatum:** Visualization, Methodology. **Kanchana Hiranwatthana:** Investigation, Data curation. **Kirati Nitichote:** Funding acquisition, Methodology.

Declaration of competing interest

The authors declare that they have no known competing financial interests or personal relationships that could have appeared to influence the work reported in this paper.

Acknowledgements

This work was financially supported by the Concrete Products and Aggregate Co., Ltd. (CPAC), Thailand, Suranaree University of Technology and Thailand Science Research and Innovation.

Data availability

Data will be made available on request.

References

Aarup, B., Jensen, B., 1998. Bond properties of high strength fiber reinforced concrete. Spec. Publ. 180, 459–472.
ACI, 2003. Development of Straight Reinforcing Bars in Tension (ACI 408R-03). American Concrete Institute, Farmington Hills, Mich.
ACI, 2011. ACI Committee 318, Building Code Requirements for Structural Concrete (ACI318-11) and Commentary. American Concrete Institute, Farmington Hills, Mich., p 391
ACI "ACI 347R-14. Guide to Formwork for Concrete." American Concrete Institute Farmington Hills, MI, USA.
Alkaysi, M., El-Tawil, S., 2017. Factors affecting bond development between Ultra High Performance Concrete (UHPC) and steel bar reinforcement. Construct. Build. Mater. 144, 412–422.
ASTM, 2001. ASTM C39: Standard Test Method for Compressive Strength of Cylindrical Concrete Specimens. ASTM international West, Conshohocken, PA, USA.
ASTM, 2003. ASTM C33: Standard Specification for Concrete Aggregates. ASTM international West, Conshohocken, PA, USA.
ASTM, 2009a. ASTM C403: Standard Test Method for Time of Setting of Concrete Mixtures by Penetration Resistance. ASTM international West, Conshohocken, PA, USA.
ASTM, 2009b. ASTM C469: Standard Test Method for Static Modulus of Elasticity and Poisson's Ratio of Concrete in Compression. ASTM international West, Conshohocken, PA, USA.
Bae, B.-I., Choi, H.-K., Choi, C.-S., 2016. Bond stress between conventional reinforcement and steel fibre reinforced reactive powder concrete. Construct. Build. Mater. 112, 825–835.
Balendran, R., Zhou, F., Nadeem, A., Leung, A., 2002. Influence of steel fibres on strength and ductility of normal and lightweight high strength concrete. Build. Environ. 37 (12), 1361–1367.
Belleri, A., Brunesi, E., Nascimbene, R., Pagani, M., Riva, P., 2015. Seismic performance of precast industrial facilities following major earthquakes in the Italian territory. J. Perform. Constr. Facil. 29 (5), 04014135.
Bournas, D., Triantafillou, T., 2011. Bond strength of lap-spliced bars in concrete confined with composite jackets. J. Compos. Construct. 15 (2), 156–167.
Bousias, S., Spathis, A.-L., Fardis, M.N., 2007. Seismic retrofitting of columns with lap spliced smooth bars through FRP or concrete jackets. J. Earthq. Eng. 11 (5), 653–674.
Code, C.F.M., 1993. Design code. Comite Euro-International du Beton.
Committee, A., 2019. Building Code Requirements for Structural Concrete and Commentary (ACI 318-319). American Concrete Institute, Farmington Hills, MI, USA, p. 623.
Einea, A., Yamane, T., Tadros, M.K., 1995. Grout filled pipe splices for precast concrete construction. PCI J. 40 (1), 82–93.
Elliott, K.S., 2000. Research and development in precast concrete framed structures. Prog. Struct. Eng. Mater. 2 (4), 405–428.
Elsanadedy, H., Alaoud, L., Abbas, H., Almusallam, T., Al-Salloum, Y., 2023. Externally bonded CFRP composites versus steel stirrups for the confinement of substandard lap spliced GFRP bars in RC beams. Compos. Struct. 306, 116602.
Garcia-Taengua, E., Martí-Vargas, J.R., Serna, P., 2016. Bond of reinforcing bars to steel fiber reinforced concrete. Construct. Build. Mater. 105, 275–284.
Ghosh, K.K., Sheikh, S.A., 2007. Seismic upgrade with carbon fiber-reinforced polymer of columns containing lap-spliced reinforcing bars. ACI Struct. J. 104 (2), 227.
Goksu, C., Yilmaz, H., Chowdhury, S., Orakcal, K., Ilki, A., 2014. The effect of lap splice length on the cyclic lateral load behavior of RC members with low strength concrete and plain bars. Adv. Struct. Eng. 17 (5), 639–658.
Graybeal, B., 2014. Design and Construction of Field-Cast UHPC Connections. Federal Highway Administration, United States.
Harajli, M.H., Hamad, B.S., Rteil, A.A., 2004. Effect of confinement of bond strength between steel. ACI Struct. J. 101 (5), 595–603.
Huang, Y., Lee, M.-G., Kan, Y.-C., Wang, W.-C., Wang, Y.-C., Pan, W.-B., 2022. Reinforced concrete beams retrofitted with UHPC or CFRP. Case Stud. Constr. Mater. 17, e01507.
Jalali, A., Taghizadeh, A., 2022. Experimental study of the effects of using ultra-high strength reinforcing rebar and UHPFRC on cyclic behavior of reinforced concrete beams. Structures. Elsevier, pp. 1383–1394.
Kaufman, L., Fam, A., 2024. Effect of GFRP bar diameter and concrete cover on bond and development length in UHPFRC. Construct. Build. Mater. 418, 135445.
Lee, J. K., 2016. Bonding behavior of lap spliced reinforcing bars embedded in ultra high strength concrete with steel fibers. KSCE J. Civ. Eng. 20, 273–281.
Leung, C.K., Shapiro, N., 1999. Optimal steel fiber strength for reinforcement of cementitious materials. J. Mater. Civ. Eng. 11 (2), 116–123.
Li, Y., Tan, K.H., Yang, E. H., 2018. Influence of aggregate size and inclusion of polypropylene and steel fibers on the hot permeability of ultra-high performance concrete (UHPC) at elevated temperature. Construct. Build. Mater. 169, 629–637.
Li, Y., Tan, K.H., Yang, E.-H., 2019. Synergistic effects of hybrid polypropylene and steel fibers on explosive spalling prevention of ultra-high performance concrete at elevated temperature. Cement Concr. Compos. 96, 174–181.
Ma, F., Deng, M., Fan, H., Yang, Y., Sun, H., 2020. Study on the lap splice behavior of post-yield deformed steel bars in ultra high performance concrete. Construct. Build. Mater. 262, 120611.
McMullen, K.F., Haber, Z., 2019. Effect of steel reinforcement type and diameter on the strength of non-contact lap splice connections using UHPC. Proc. In: International Interactive Symposium on Ultra-high Performance Concrete. Iowa State University Digital Press.
Mohod, M.V., 2012. Performance of steel fiber reinforced concrete. Int. J. Eng. Sci. 1 (12), 1–4.
Mousa, M.I., 2015. Flexural behaviour and ductility of high strength concrete (HSC) beams with tension lap splice. Alex. Eng. J. 54 (3), 551–563.
Mousa, M.I., 2016. Effect of bond loss of tension reinforcement on the flexural behaviour of reinforced concrete beams. HBRC journal 12 (3), 235–241.
Oh, B.H., 1992. Flexural analysis of reinforced concrete beams containing steel fibers. J. Struct. Eng. 118 (10), 2821–2835.
Pour, S.M., Alam, 2016. Investigation of compressive bond behavior of steel rebar embedded in concrete with partial recycled aggregate replacement. Proc., Structures. Elsevier, pp. 153–164.
Shafieifar, M., Farzad, M., Azizinamini, A., 2017. Alternative ABC Connection Utilizing UHPC.
Shen, D., Shi, X., Zhang, H., Duan, X., Jiang, G., 2016. Experimental study of early-age bond behavior between high strength concrete and steel bars using a pull-out test. Construct. Build. Mater. 113, 653–663.
Song, Q., Yu, R., Shui, Z., Rao, S., Wang, X., Sun, M., Jiang, C., 2018. Steel fibre content and interconnection induced electrochemical corrosion of Ultra High Performance Fibre Reinforced Concrete (UHPFRC). Cement Concr. Compos. 94, 191–200.
Sulaiman, M.F., Ma, C. K., Apandi, N.M., Chin, S., Awang, A.Z., Mansur, S.A., Omar, W., 2017. A review on bond and anchorage of confined high-strength concrete. In: Proc., Structures. Elsevier, pp. 97–109.
Tariverdilou, S., Farjadi, A., Barkhourdari, M., 2009. Fragility Curves for Reinforced Concrete Frames with Lap Spliced Columns.
Tosa, F.V., Salha, R., 2016. The behavior of different precast concrete structures under seismic action. Procedia Technology 22, 235–242.
Wang, F., Wu, X., Guo, C., Song, W., 2018. Experimental study on bond strength of deformed steel bars in recycled glass aggregate concrete. KSCE J. Civ. Eng. 22, 3409–3418.
Xia, J., Mackie, K.R., Saleem, M.A., Mirmiran, A., 2011. Shear failure analysis on ultra-high performance concrete beams reinforced with high strength steel. Eng. Struct. 33 (12), 3597–3609.
Ye, M., Jiang, J., Chen, H., Zhou, H., Song, D., 2021. Seismic behavior of an innovative hybrid beam-column connection for precast concrete structures. Eng. Struct. 227, 111436.
Yin, S., Xu, S., Lv, H., 2014. Flexural behavior of reinforced concrete beams with TRC tension zone cover. J. Mater. Civ. Eng. 26 (2), 320–330.
Yoo, D.-Y., Kwon, K.-Y., Park, J.-J., Yoon, Y.-S., 2015. Local bond-slip response of GFRP rebar in ultra-high-performance fiber-reinforced concrete. Compos. Struct. 120, 53–64.
Yoo, D.-Y., Shin, H.-O., Yang, J.-M., Yoon, Y.-S., 2014. Material and bond properties of ultra high performance fiber reinforced concrete with micro steel fibers. Compos. B Eng. 58, 122–133.
Yu, J., Tan, K.-H., 2013. Experimental and numerical investigation on progressive collapse resistance of reinforced concrete beam column sub-assemblages. Eng. Struct. 55, 90–106.
Yuan, J., Graybeal, B., 2015. Bond of reinforcement in ultra high performance concrete. ACI Struct. J. 112 (6).
Zhang, J., Stang, H., Li, V.C., 2000. Experimental study on crack bridging in FRC under uniaxial fatigue tension. J. Mater. Civ. Eng. 12 (1), 66–73.
Zhou, Z., Qiao, P., 2018. Bond behavior of epoxy-coated rebar in ultra-high performance concrete. Construct. Build. Mater. 182, 406–417.

the test value of 8*D*, where both rebar rupture and slippage were observed. In **Sample No. 6-LS9**, the predicted bond force (151.35 kN) exceeded the measured tensile force at rupture (132.29 kN), confirming that failure occurred through bar fracture rather than pull-out.

In addition, the shear failure observed in **Sample No. 5- LS8+H4** was investigated by comparing the experimental shear resistance with that calculated using the ACI equation. The results suggested that the ACI method, which assumes monolithic construction, may overestimate the shear capacity of precast UHPC joints. Therefore, it is recommended that the stirrup reinforcement in such joints be increased by approximately 2.5 times to ensure adequate shear resistance. The design scheme presented in Section 4 and Fig. 15 integrates these theoretical and experimental findings into a practical and rational procedure for determining required rebar lengths and configurations. This scheme effectively addresses structural performance requirements while maintaining construction efficiency and safety. The comparison between predictions and observed test data confirms the robustness of the proposed method across various failure modes, including rebar pull-out, rupture, and shear failure.

5. Conclusions

Based on the experiments conducted in this study, the following conclusions can be drawn:

The full-scale sample testing confirmed that using UHPC for beam-column joints can enable the beam-column structure to withstand loads and exhibit failure characteristics comparable to traditional construction methods. The strong joint was manufactured with two configurations of 16-mm deformed rebars including lap splicing without hook of $L_1 = 9D$ (14.4 cm), and lap splicing with hook of $L_1 = 8D$ and $L_2 = 4D$. These configurations allowed the UHPC beam-column joints to resist bending moments until the rebars reached the failure state (565.94 MPa) and subjected to large deformation, which is the ductile failure characteristic desired in reinforced concrete structure design.

However, caution should be taken for the weak joint with insufficient rebars' length. For example, the non-overlapping with hook joint (Weak Joint, $L_e = 4D$ amd $L_2 = 3D$) and the non-overlapping without hook joint (Weak Joint, $L_e = 4D$) both exhibited sudden and hazardous failure.

The design scheme for rebars' length resulting from this project is as follows: initially, the yield tensile stress (f_y) of the rebars is used to calculate the L_d of rebars without lap-splice using Equation (1). If the calculated L_d is less than half the width of the column, the rebars are placed without lap splicing using $L_e > L_d$. However, if the L_d exceeds half the width of the column, the lap splicing is required. If the calculated lap splice length (L_1) is less than or equal to the actual space ($L_1 \leq$ actual space), the calculated L_1 can be used in the design. If the calculated L_1 is greater than the actual space, the hook length (L_2) must be added to enhance the bond strength of the reinforcement using Equation (3); the length L_2 must be at least 3*D*.

The findings of this project underscore the efficacy of utilizing UHPC for precast beam-column joints. This innovative method enables the design of precast structural elements as continuous beams, rather than simple beams, thereby enhancing bending moment resistance and reducing the required amount of rebars. Manufacturing precast beam-column elements in a controlled factory setting and subsequently assembling them on-site offers several advantages. It reduces labor costs, minimizes the need for formwork and shoring, and expedites the construction process. Notably, UHPC achieves its high strength within just 7 days, compared to the traditional 28-day curing period. This significant reduction in curing time accelerates construction schedules while ensuring structural safety equivalent to conventional methods.

CRediT authorship contribution statement

Krairerk Aiamsri: Writing – original draft, Validation, Methodology, Investigation, Data curation. **Teerasak Yaowarat:** Writing – original draft, Visualization, Validation, Supervision, Resources, Project administration, Methodology, Investigation, Conceptualization. **Suksun Horpibulsuk:** Writing – review & editing, Visualization, Supervision, Resources, Project administration, Funding acquisition, Conceptualization. **Apichat Suddeepong:** Validation, Supervision, Resources, Investigation. **Apinun Buritatum:** Visualization, Validation, Resources. **Artit Udomchai:** Writing – original draft, Resources, Methodology, Investigation. **Kirati Nitichote:** Visualization, Investigation, Funding acquisition, Conceptualization.

Declaration of competing interest

The authors declare that they have no known competing financial interests or personal relationships that could have appeared to influence the work reported in this paper.

Acknowledgements

This work was financially supported by the Concrete Products and Aggregate Co., Ltd. (CPAC), Thailand, Suranaree University of Technology and Thailand Science Research and Innovation.

Data availability

Data will be made available on request.

References

A. Standard, C33, 2003. Standard Specification for Concrete Aggregates. ASTM international West, Conshohocken, PA, USA, C.

ACI Committee, 2008. Building Code Requirements for Structural Concrete (ACI 318-08) and Commentary. American Concrete Institute.

Aiamsri, K., Yaowarat, T., Horpibulsuk, S., Suddeepong, A., Buritatum, A., Hiranwatthana, K., Nitichote, K., 2024. Bonding behavior of lap-spliced reinforcing bars embedded in ultra high-performance concrete with steel fibers. Developments in the Built Environment 20, 100585.

Aktan, A.E., Farhey, D.N., Helmicki, A.J., Brown, D.L., Hunt, V.J., Lee, K.-L., Levi, A., 1997. Structural identification for condition assessment: experimental arts. J. Struct. Eng. 123 (12), 1674–1684.

Alampalli, S., Frangopol, D.M., Grimson, J., Halling, M.W., Kosnik, D.E., Lantsoght, E.O., Yang, D., Zhou, Y.E., 2021. Bridge load testing: state of the practice. J. Bridge Eng. 26 (3), 03120002.

Alkaysi, M., El-Tawil, S., 2017. Factors affecting bond development between Ultra High Performance Concrete (UHPC) and steel bar reinforcement. Constr. Build. Mater. 144, 412–422.

Anvari, B., Angeloudis, P., Ochieng, W.Y., 2016. A multi-objective GA-based optimisation for holistic Manufacturing, transportation and Assembly of precast construction. Autom. ConStruct. 71, 226–241.

Baek, J.-W., Park, H.-G., Lee, B.-S., Shin, H.-M., 2018. Shear-friction strength of low-rise walls with 550 MPa (80 ksi) reinforcing bars under cyclic loading. ACI Struct. J. 115 (1).

Bahmani, H., Mostofinejad, D., 2022. Microstructure of ultra-high-performance concrete (UHPC)–a review study. J. Build. Eng. 50, 104118.

Bjorhovde, R., Goland, L., Benac, D., 1999. Tests of Full Scale Beam To Column Connections. Southwest Research Institute, San Antonio, TX.

Cabral-Fonseca, S., Correia, J., Custódio, J., Silva, H., Machado, A., Sousa, J., 2018. Durability of FRP concrete bonded joints in structural rehabilitation: a review. Int. J. Adhesion Adhes. 83, 153–167.

Cai, G., Waldmann, D., 2019. A material and component bank to facilitate material recycling and component reuse for a sustainable construction: concept and preliminary study. Clean Technol. Environ. Policy 21, 2015–2032.

Chan, T.K., 2011. Comparison of precast construction costs—case studies in Australia and Malaysia. Proceedings of the 27th Annual ARCOM Conference, pp. 3–12. Bristol, UK.

Choi, H. K., 2020. Parametric analysis on seismic performance of hybrid precast concrete beam-column joint. Adv. Civ. Eng. 2020 (1), 8856327.

Contento, A., Aloisio, A., Xue, J., He, J., Briseghella, B., 2024. Ultra high performance concrete beam-to-beam connections in continuous bridges: experimental full-scale tests, FE analyses and design. Eng. Struct. 316, 118594.

Du, J., Meng, W., Khayat, K.H., Bao, Y., Guo, P., Lyu, Z., Abu-Obeidah, A., Nassif, H., Wang, H., 2021. New development of ultra high performance concrete (UHPC). Compos. B Eng. 224, 109220.

Engindeniz, M., Kahn, L.F., Abdul-Hamid, Z., 2005. Repair and strengthening of reinforced concrete beam-column joints: state of the art. ACI Struct. J. 102 (2), 1.

Farzad, M., Shafieifar, M., Azizinamini, A., 2019. Experimental and numerical study on bond strength between conventional concrete and Ultra High-Performance Concrete (UHPC). Eng. Struct. 186, 297–305.

Fehling, E., Schmidt, M., Walraven, J., Leutbecher, T., Fröhlich, S., 2014. Ultra-high Performance Concrete UHPC. Ernst & Sohn, Berlin, Germany, pp. 25–32.
Garetti, M., Taisch, M., 2012. Sustainable manufacturing: trends and research challenges. Prod. Plann. Control 23 (2–3), 83–104.
Ghayeb, H.H., Razak, H.A., Sulong, N.R., 2020. Performance of dowel beam-to-column connections for precast concrete systems under seismic loads: a review. Constr. Build. Mater. 237, 117582.
Hong, J., Shen, G.Q., Li, Z., Zhang, B., Zhang, W., 2018. Barriers to promoting prefabricated construction in China: a cost–benefit analysis. J. Clean. Prod. 172, 649–660.
Huang, Y., Grünewald, S., Schlangen, E., Luković, M., 2022. Strengthening of concrete structures with ultra high performance fiber reinforced concrete (UHPFRC): a critical review. Constr. Build. Mater. 336, 127398.
Hung, C.-C., El-Tawil, S., Chao, S.-H., 2021. A review of developments and challenges for UHPC in structural engineering: behavior, analysis, and design. J. Struct. Eng. 147 (9), 03121001.
Kartal, S., Kalkan, I., Beycioglu, A., Dobiszewska, M., 2021. Load-deflection behavior of over-and under-reinforced concrete beams with hybrid FRP-steel reinforcements. Materials 14 (18), 5341.
Khayat, K.H., Meng, W., 2014. Design and Performance of Stay-In-Place UHPC Prefabricated Panels for Infrastructure Construction, Missouri University of Science and Technology. Center for Transportation ….
Küntz, M., Jolin, M., Bastien, J., Perez, F., Hild, F., 2006. Digital image correlation analysis of crack behavior in a reinforced concrete beam during a load test. Can. J. Civ. Eng. 33 (11), 1418–1425.
Liu, S., Wang, X., Ali, Y.M., Su, C., Wu, Z., 2022. Flexural behavior and design of under-reinforced concrete beams with BFRP and steel bars. Eng. Struct. 263, 114386.
Lowes, L.N., Altoontash, A., 2003. Modeling reinforced-concrete beam-column joints subjected to cyclic loading. J. Struct. Eng. 129 (12), 1686–1697.
Ma, J., Orgass, M., Dehn, F., Schmidt, D., Tue, N., 2004. Comparative investigations on ultra-high performance concrete with and without coarse aggregates. International Symposium on Ultra High Performance Concrete, pp. 205–212. Kassel, Germany.
Maya, L., Graybeal, B., 2017. Experimental study of strand splice connections in UHPC for continuous precast prestressed concrete bridges. Eng. Struct. 133, 81–90.
Meoni, A., D'Alessandro, A., Mattiacci, M., García Macías, E., Saviano, F., Parisi, F., Lignola, G.P., Ubertini, F., 2024. Structural performance assessment of full scale masonry wall systems using operational modal analysis: laboratory testing and numerical simulations. Eng. Struct. 304, 117663.
Mohammadhassani, M., Akib, S., Shariati, M., Suhatril, M., Khanouki, M.A., 2014. An experimental study on the failure modes of high strength concrete beams with particular references to variation of the tensile reinforcement ratio. Eng. Fail. Anal. 41, 73–80.
Molinari, M., Savadkoohi, A.T., Bursi, O.S., Friswell, M.I., Zonta, D., 2009. Damage identification of a 3D full scale steel–concrete composite structure with partial-strength joints at different pseudo-dynamic load levels. Earthq. Eng. Struct. Dynam. 38 (10), 1219–1236.
Mousavi, S.S., Dehestani, M., 2022. Influence of mixture composition on the structural behaviour of reinforced concrete beam-column joints. A Review, Structures. Elsevier, pp. 29–52.
Parskiy, N., Molodtsov, M., Molodtsova, V., 2017. Cost effectiveness of precast reinforced concrete roof slabs. IOP Conference Series: Materials Science and Engineering. IOP Publishing, 012036.
Pokorný, P., Kolísko, J., Čítek, D., Kostelecká, M., 2020. Effect of elevated temperature on the bond strength of prestressing reinforcement in UHPC. Materials 13 (21), 4990.
Said, M., Shanour, A.S., Mustafa, T., Abdel-Kareem, A.H., Khalil, M.M., 2021. Experimental flexural performance of concrete beams reinforced with an innovative hybrid bars. Eng. Struct. 226, 111348.
Sev, A., 2009. How can the construction industry contribute to sustainable development? A conceptual framework. Sustain. Dev. 17 (3), 161–173.
Shishesaz, M., Hosseini, M., 2020. Effects of joint geometry and material on stress distribution, strength and failure of bonded composite joints: an overview. J. Adhes. 96, 1053–1121.
Somma, G., Pieretto, A., Rossetto, T., Grant, D.N., 2015. RC beam to column connection failure assessment and limit state design. Mater. Struct. 48, 1215–1231.
Standard, A., 2011. Building Code Requirements for Structural Concrete (ACI 318-11). American Concrete Institute.
Supaviriyakit, T., Pimanmas, A., 2008. Comparative performance of sub-standard interior reinforced concrete beam–column connection with various joint reinforcing details. Mater. Struct. 41, 543–557.
Tack, R., 2019. Flexural Response of Flat Plate Edge Slab-Column Connections. McGill University, Canada.
Ullah, R., Qiang, Y., Ahmad, J., Vatin, N.I., El-Shorbagy, M.A., 2022. Ultra-high-performance concrete (UHPC): a state-of-the-art review. Materials 15 (12), 4131.
Wang, Z., Hu, H., Gong, J., 2018. Framework for modeling operational uncertainty to optimize offsite production scheduling of precast components. Autom. ConStruct. 86, 69–80.
Wen, C., Zhang, P., Wang, J., Hu, S., 2022. Influence of fibers on the mechanical properties and durability of ultra-high-performance concrete: a review. J. Build. Eng. 52, 104370.
Xue, W., Hu, X., Song, J., 2021. Experimental study on seismic behavior of precast concrete beam column joints using UHPC based connections. Structures. Elsevier, pp. 4867–4881.
Yoo, D. Y., Kim, M. J., 2019. High energy absorbent ultra high performance concrete with hybrid steel and polyethylene fibers. Constr. Build. Mater. 209, 354–363.
Yoo, D.-Y., Kim, S., Kim, J.-J., Chun, B., 2019. An experimental study on pullout and tensile behavior of ultra-high-performance concrete reinforced with various steel fibers. Constr. Build. Mater. 206, 46–61.
Yoo, D. Y., Sohn, H. K., Borges, P.H., Fediuk, R., Kim, S., 2020. Enhancing the tensile performance of ultra-high-performance concrete through strategic use of novel half-hooked steel fibers. J. Mater. Res. Technol. 9 (3), 2914–2925.
Zhang, J., Ding, C., Rong, X., Yang, H., Li, Y., 2020. Development and experimental investigation of hybrid precast concrete beam–column joints. Eng. Struct. 219, 110922.
Zhong, Y., Xiong, F., Chen, J., Deng, A., Chen, W., Zhu, X., 2019. Experimental study on a novel dry connection for a precast concrete beam-to-column joint. Sustainability 11 (17), 4543.
Zhou, Z., Qiao, P., 2018. Bond behavior of epoxy-coated rebar in ultra-high performance concrete. Constr. Build. Mater. 182, 406–417.

Developments in the Built Environment 22 (2025) 100682

Contents lists available at ScienceDirect

Developments in the Built Environment

journal homepage: www.sciencedirect.com/journal/developments-in-the-built-environment

Performance of connection joints of beam-column structure using Ultra-high-performance concrete under full-scale tests

Krairerk Aiamsri [a], Teerasak Yaowarat [b,c,*], Suksun Horpibulsuk [d,c,e,**], Apichat Suddeepong [f], Apinun Buritatum [b,c], Artit Udomchai [c], Kirati Nitichote [g]

[a] School of Civil Engineering and Construction Management, Suranaree University of Technology, 111 University Avenue, Muang District, Nakhon Ratchasima, 30000, Thailand
[b] Undergraduate Program in Civil and Infrastructure Engineering, Suranaree University of Technology, Nakhon Ratchasima, 30000, Thailand
[c] Center of Excellence in Innovation for Sustainable Infrastructure Development, Suranaree University of Technology, Nakhon Ratchasima, 30000, Thailand
[d] School of Civil Engineering, Suranaree University of Technology, Nakhon Ratchasima 30000, Thailand
[e] Academy of Science, The Royal Society of Thailand, Bangkok, 10300, Thailand
[f] Institute of Research and Development, Suranaree University of Technology, Nakhon Ratchasima, 30000, Thailand
[g] The Concrete and Aggregate Products Co., Ltd., Bangkok, 10800, Thailand

ARTICLE INFO

Keywords:
Ultra-high performance concrete (UHPC)
Precast concrete joints
Embedment length
Lap splice length
Full scale testing

ABSTRACT

This study examines the application of Ultra-High Performance Concrete (UHPC) in precast beam-column joints to improve structural performance. The studied joints included both adequately and inadequately reinforced conditions (strong and weak joints), constructed using UHPC and deformed rebars. The strong joints allowed the rebars to reach their yield strength under the design bending moment, effectively transferring loads and maintaining structural integrity during service conditions. These well-detailed joints exhibited ductile failure behavior, which is a desired characteristic in reinforced concrete design. In contrast, the weak joints experienced premature and brittle failures, underscoring the importance of proper detailing and reinforcement length. Finally, a practical design scheme was developed to determine the appropriate rebar lengths in UHPC connections to ensure structural integrity and safety. Overall, the integration of UHPC into precast concrete joints significantly enhanced bond performance, improved load transfer mechanisms, and contributed to more resilient and reliable construction practices.

1. Introduction

The use of precast concrete technology has revolutionized modern construction practices, providing significant advantages in terms of construction speed, quality control, and cost-effectiveness (Chan, 2011; Parskiy et al., 2017). Precast concrete involves casting concrete elements in a controlled factory environment and then transporting them to the construction site for assembly. This method ensures that each component is produced under optimal conditions, leading to high-quality, consistent products (Hong et al., 2018). The precast approach allows for rapid assembly on-site, reducing construction time and labor costs (Anvari et al., 2016; Wang et al., 2018). Additionally, the ability to produce components in a factory setting allows for better resource management and waste reduction, contributing to more sustainable construction practices (Cai and Waldmann, 2019; Garetti and Taisch, 2012; Sev, 2009). However, despite its many benefits, precast concrete technology faces several challenges, particularly concerning the performance of joints in precast column-beam structures (Choi, 2020; Ghayeb et al., 2020; Xue et al., 2021; Zhang et al., 2020; Zhong et al., 2019).

One of the main issues with precast concrete structures is the performance of the joints that connect the various elements. These joints are critical to the structural integrity and overall stability of the structure. They must efficiently transfer loads, including axial loads, shear forces, and bending moments, between the connected elements (Cabral-Fonseca et al., 2018; Engindeniz et al., 2005; Mousavi and

* Corresponding author. Undergraduate Program in Civil and Infrastructure Engineering, Suranaree University of Technology, Nakhon Ratchasima, 30000, Thailand.
** Corresponding author. School of Civil Engineering, Suranaree University of Technology, Nakhon Ratchasima, 30000, Thailand.
E-mail addresses: Krairerk.ai15@gmail.com (K. Aiamsri), teerasakyaowarat@gmail.com (T. Yaowarat), suksun@g.sut.ac.th (S. Horpibulsuk), suddeepong@g.sut.ac.th (A. Suddeepong), apinun.ce@hotmail.com (A. Buritatum), artit.u@g.sut.ac.th (A. Udomchai), kiratin@scg.com (K. Nitichote).

https://doi.org/10.1016/j.dibe.2025.100682
Received 19 February 2025; Received in revised form 16 May 2025; Accepted 17 May 2025
Available online 19 May 2025

Table 1
Mix design for UHPC.

UHPC		Materials per 1 cubic meter, kg
Cement Grout CPAC	Cement Grout	1143
	Sand	1130
Additional admixtures PC-UP01		31
Additional admixtures Type D		22
Steel fiber		155
Water		200

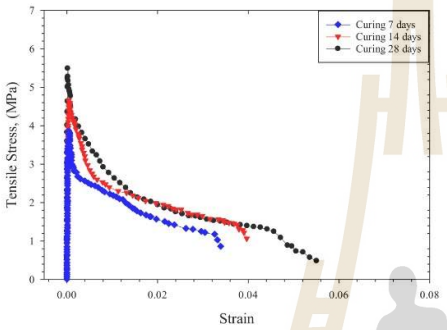

Fig. 1. Tensile stress–strain behavior of UHPC at various curing ages.

Fig. 2. Steel fibers in the UHPC.

Dehestani, 2022). Poorly designed or constructed joints can become weak points in the structure, leading to potential failure under load. Common problems include inadequate bonding between the precast elements, insufficient load transfer capabilities, and susceptibility to cracking and other forms of deterioration over time (Lowes and Altoontash, 2003; Shishesaz and Hosseini, 2020). Addressing these issues is crucial for ensuring the long-term durability and safety of precast concrete structures.

In addition to the common challenges found in precast systems, reinforced concrete (RC) beam-column joints in traditional construction also have important weaknesses, especially when the design details are not carefully considered. These joints must transfer different types of

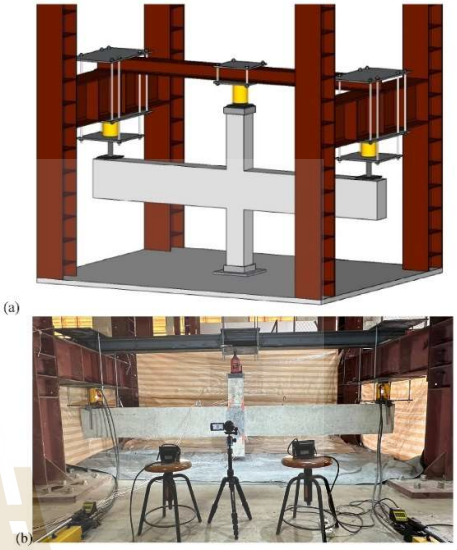

Fig. 3. (a) The full-scale test model and (b) the actual test conditions.

forces such as shear and tension within a small area, making the force transfer process quite complicated. If the steel rebars inside the joint are not properly anchored or if there is insufficient reinforcement, the joint can fail early, even under normal loading conditions. Supaviriyakit and Pimanmas (2008) found that joints without horizontal reinforcement or with weak rebar connections failed in brittle ways, like cracking along diagonals or splitting the beam, and they could not absorb much energy. Their research also showed that simply adding more reinforcement does not always improve performance if the joint's shape or detailing is still poor. Similarly, Somma et al. (2015) pointed out that problems like weak concrete confinement, short rebar anchorage, and poor coordination between the concrete and steel parts of the joint can also lead to failure. They explained that these parts need to work together, and if one fails, the others may not work properly either. For example, when stirrups (the small steel loops) inside the joint give way, the joint quickly loses its ability to resist shear forces. These issues highlight the importance of using well-rounded design approaches that consider all key factors like bonding, support, and shear resistance to ensure RC joints are strong and reliable.

Ultra-High-Performance Concrete (UHPC) has emerged as a promising solution to the challenges associated with joints in precast concrete structures. UHPC is an advanced cementitious material known for its exceptional mechanical properties and durability. It typically exhibits compressive strengths exceeding 150 MPa, significantly higher than conventional concrete (Du et al., 2021; Fehling et al., 2014; Ullah et al., 2022). UHPC's dense microstructure provides excellent resistance to environmental degradation, such as freeze-thaw cycles, chemical attacks, and abrasion (Bahmani and Mostofinejad, 2022). Additionally, UHPC includes steel fibers, which enhance its tensile strength and ductility, allowing it to absorb and dissipate energy more effectively (Wen et al., 2022; Yoo and Kim, 2019; Yoo et al., 2019, 2020). These properties make UHPC an ideal material for improving the performance of precast concrete joints, addressing the weaknesses that commonly arise in these critical areas.

Table 2
Summary of test specimens and connection Configurations.

No.	Name	Concrete at joint	Embedment length (L_e)	Splice length (L_1)	Hook length (L_2)	Remark
1	Traditional cast-in-place beam-column joint (**TCIP**)	Normal Concrete	–	–	–	Strong joint
2	Non-overlapping without hook joint (**LE4**)	UHPC	4D	–	–	Weak joint
3	Non-overlapping with hook joint (**LE4+H3**)	UHPC	4D	–	3D	Weak joint
4	Lap-splicing without hook joint (**LS8**)	UHPC	–	8D	–	Strong joint
5	Lap-splicing with hook joint (**LS8+H4**)	UHPC	–	8D	4D	Strong joint
6	Lap-splicing without hook joint (**LS9**)	UHPC	–	9D	–	Strong joint

TCIP: Traditional Cast-In-Place, **LE4**: Embedment length with 4D, **LS8/LS9**: Lap Splice with 8D or 9D.
H3/H4: Hook with 3D or 4D.

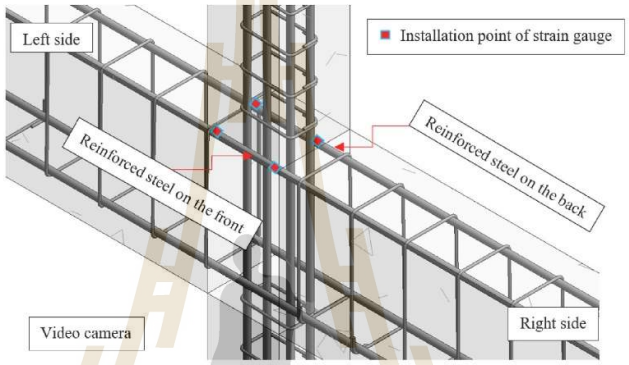

Fig. 4. Detailed specifications of the steel reinforcement and locations of strain-gauge installation.

The high compressive strength of UHPC has a significant impact on the bond strength between rebar and concrete (Alkaysi and El-Tawil, 2017; Farzad et al., 2019; Pokorný et al., 2020). UHPC's superior bonding capabilities ensure that the rebar can effectively anchor within the concrete, providing enhanced load transfer and structural stability (Huang et al., 2022; Hung et al., 2021). This characteristic is particularly beneficial for the design of joints in precast concrete structures, where effective load transfer is essential for maintaining the overall integrity of the structure. The enhanced bond strength provided by UHPC helps prevent issues such as slippage or pull-out of the reinforcing bars, which can compromise the joint's performance (Khayat and Meng, 2014; Maya and Graybeal, 2017; Zhou and Qiao, 2018).

Aiamsri et al. (2024) conducted a laboratory test and proposed a new equation to predict the bond strength of rebar in UHPC:

$$\tau_{bond} = \phi 11.64\sqrt{\frac{f'_c}{D}} \quad (1)$$

where τ_{bond} is the bond strength for UHPC [MPa], ϕ is the reduction factor due to a spacing (s) between rebars ($s = 1, 2, 3$ and $\geq 4D$, $\phi = 0.75$, 0.87, 0.94 and 1, respectively), f'_c is the compressive strength of UHPC [MPa] and D is the diameter of steel rebar [mm].

Therefore, the development length of rebars in UHPC can be determined:

$$\frac{L_d}{D} = \frac{f_s}{4\,(\tau_{bond})} \quad (2)$$

where f_s is tensile stress in rebar, L_d/D is the development length to diameter ratio.

Furthermore, Aiamsri et al. (Maya and Graybeal, 2017) proposed an equation to determine the bond force of lap-splice rebar with hook (F_{bond}) could be expressed as follows:

$$F_{bond} = (\phi_1 L_1 + k\phi_2 L_2)\tau_{bond}\pi D \quad (3)$$

where ϕ_1 and ϕ_2 are the reduction factors due to the spacing (s) between lap-spliced rebars and hooks, respectively (if $s = 1, 2, 3$ and $\geq 4D$, ϕ_1 and $\phi_2 = 0.75$, 0.87, 0.94 and 1, respectively), L_1 and L_2 are lap-splice length and hook length, respectively, and k = reduction factor due to hook length (for simplicity and safety in design, the reduction factor was recommended as 0.2). τ_{bond} can be obtained from Equation (1).

To thoroughly evaluate the performance of UHPC in precast concrete joints, full-scale testing under loading conditions is essential. Static load tests involve applying gradual, controlled loads to the structure to assess its behavior under typical service conditions (Küntz et al., 2006; Aktan et al., 1997; Alampalli et al., 2021). This type of testing provides valuable insights into the structural performance of the joints, including their load-carrying capacity, deformation characteristics, and failure modes. These tests are crucial for validating theoretical models and ensuring that the joints perform as expected in real-world applications (Contento et al., 2024; Meoni et al., 2024; Molinari et al., 2009).

In this research, two types of lap-spliced rebars embedded in UHPC are investigated: lap-splice without hook (L_1) and lap-splice with a 90-degree hook. Lap splicing is a common method of connecting rebars in concrete structures, where the ends of 2 bars overlap for a certain length to transfer load between them. The inclusion of a 90-degree hook (L_2) provides additional anchorage (Baek et al., 2018; Tack, 2019), potentially enhancing the bond strength and overall performance of the joint. Comparing the performance of these two configurations under static load conditions will provide insights into the most effective reinforcement strategies for UHPC joints in precast concrete structures. A key objective of this research is to validate the rebar length predicted by previous equations (Maya and Graybeal, 2017) for use in UHPC joints at

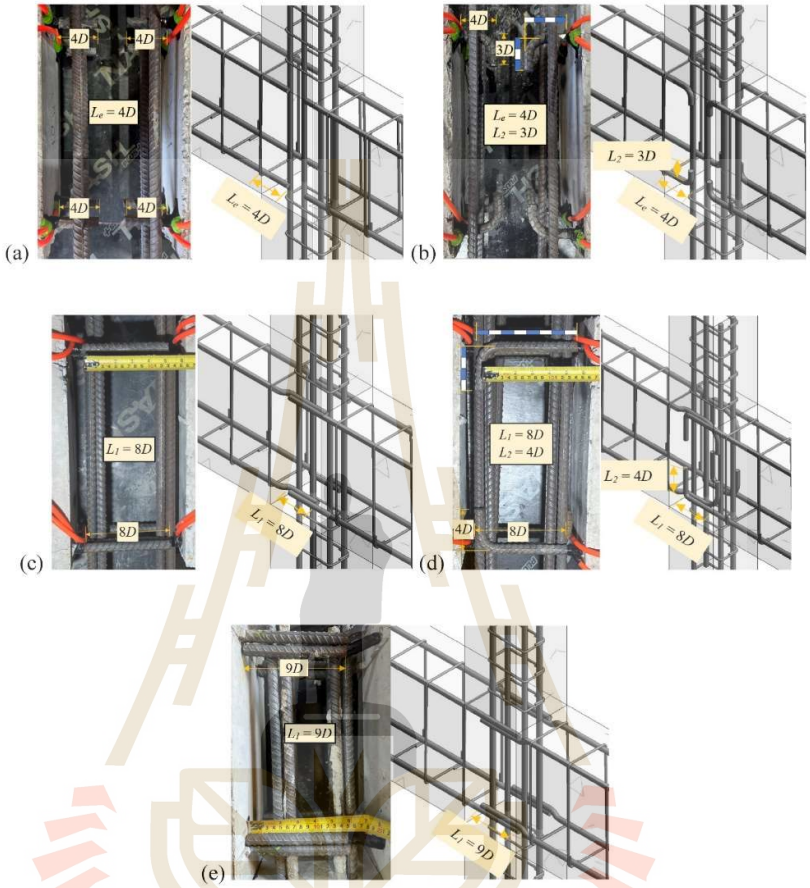

Fig. 5. Type of joint for each sample (a) LE4, (b) LE4+I13, (c) LS8, (d) LS8+I14 and (e) LS9.

full scale. The failure behavior at the connection joint would moreover be investigated. Understanding this failure behavior is crucial for designing joints that have comparable or superior performance to the conventional concrete joints. The research finally aimed to establish guidelines for determining the required embedment length of rebars in UHPC, ensuring effective load transfer and maintaining structural integrity under service conditions.

Integrating UHPC into precast concrete joints holds substantial significant for enhancing the performance of the precast concrete elements. The superior mechanical properties of UHPC address many common issues associated with precast concrete joints, such as inadequate bonding and load transfer. The full-scale testing under static load conditions provides essential data to validate the effectiveness of UHPC in the connection application, thereby informing the development of improved design practices and standards. By exploring various configurations of lap-splice rebars and determining the optimal embedment length, this research seeks to advance the understanding of UHPC's role in strengthening the structural integrity of precast column-beam assemblies, ultimately contributing to more resilient and reliable construction practices.

2. Materials and methods

2.1. Material characteristics of normal concrete and UHPC

The normal concrete (NC), used as a benchmark for UHPC, employed ordinary Portland cement as its binding agent. Fine aggregate consisted of sand with a grain size smaller than 4.75 mm, adhered to the ASTM C33 (A. Standard and C33, 2003). The NC achieved a compressive strength exceeding 38 MPa after 28 days, using a mix ratio (job mix formula) of cement to sand to water at 1:2:0.275, while maintaining a slump value within the range of 50–100 mm.

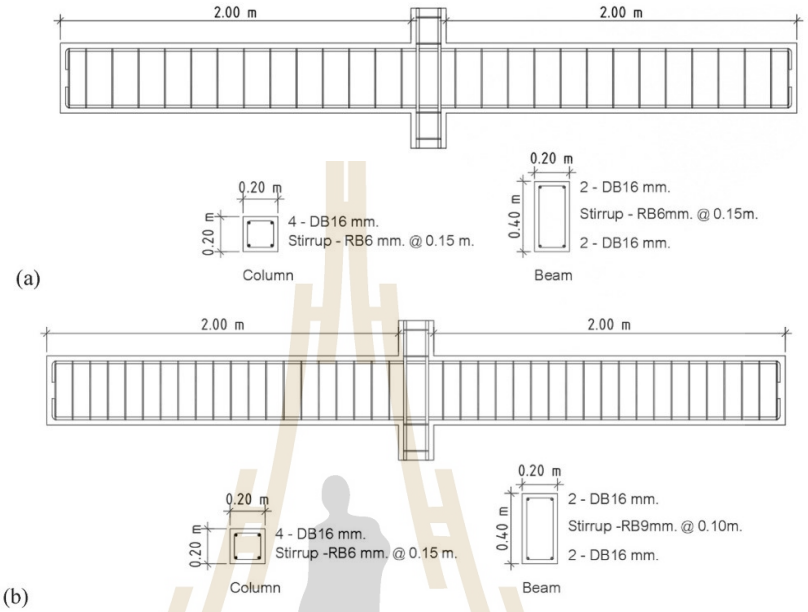

Fig. 6. Reinforcement arrangement details for the beam-column of (a) TCIP, LE4, LE4+H3, LS8, LS8+H4 and (b) LS9.

Table 3
Measured parameters from full-scale sample.

Parameter	Position	No.1 TCIP	No. 2 LE4	No. 3 LE4+H3	No. 4 LS8	No. 5 LS8+H4	No. 6 LS9
Applied Load (kN)	At the Left side	47.37	25.11	22.37	45.7	45.11	47.27
	At the Right side	46.09	25.70	22.17	45.6	47.37	47.76
Moment Calculated from the Applied Load (kN-m)	At the Left side	94.44	51.70	46.39	91.2	91.01	94.24
	At the Right side	96.4	52.78	45.99	91.01	94.44	95.12
Strain value	Strain front at the Left side	6073	663	762	9737	17872	13380
	Strain behind at the Left side	12404	625	437	9735	18293	3404
	Strain front at the Right side	16906	444	430	15400	14716	20277
	Strain behind at the Right side	16630	507	482.5	22230	18532	20126
Stress value, f_s (MPa)	Stress front at the Left side	588.14	379.57	435.86	610.97	643.6	622.46
	Stress behind at the Left side	617.9	357.81	250.56	599.75	645.58	575.6
	Stress front at the Right side	639.06	254.19	306.29	658.18	649.83	658.18
	Stress behind at the Right side	637.76	290.25	246.17	658.18	625.63	658.18
Average Stress, σ_{av} (MPa)	At the Left side	603.01	368.69	343.21	605.35	644.58	599.03
	At the Right side	638.4	272.22	276.23	658.14	637.72	658.14
Moment Calculated from the Average Strain Gauge (kN-m)	At the Left side	77.77	47.56	44.33	78.16	83.16	77.28
	At the Right side	82.38	35.11	35.6	83.65	82.28	84.44

The UHPC mixture (ready-mix) used for casting the concrete specimens was supplied by Concrete Products and Aggregate Co., Ltd. (CPAC), a subsidiary of Siam Cement Group (SCG), a well-known provider of high-quality concrete products in Thailand. The mixing procedure for UHPC began by adding CPAC Cement Grout into the mixer and mixed it for 2 min. Next, water and the admixture PC-UP01 were added, followed by an additional 1 min of mixing. Then, the Type D admixture was introduced, and the mixing continued for another 5 min. Steel fibers were gradually added to the mix by sprinkling them in with a scoop to prevent clumping, and the mixing proceeded for an additional 3 min. Finally, the flowability of the UHPC was checked either visually or by measuring the flow diameter, which should range between 80 and 95 cm.

Table 1 presents the constituent material proportions per cubic meter for UHPC, offering a detailed reference for its mix design. The fine aggregate had a maximum size of 1 mm, and the water-to-binder ratio was 0.175. This mix design achieved compressive strengths (f_c') of 92.05, 111.76 and 132.84 MPa at 7, 14 and 28 days, respectively. The

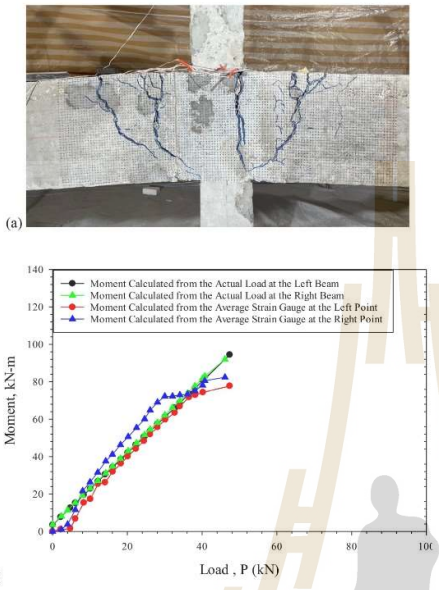

Fig. 7. Traditional cast-in-place beam-column joint (TCIP) sample: (a) Failure of the sample, (b) Relationship between the moment calculated from the average strain gauge and the applied load.

corresponding tensile strengths, as illustrated in Fig. 1, were 3.87 MPa, 4.66 MPa, and 5.49 MPa. The elastic modulus was 19.54 and 26.46 GPa at 7 and 28 days of curing, respectively, The straight steel fibers in the UHPC measured 0.22 mm in diameter and 13 mm in length (Fig. 2) and had an ultimate tensile strength of 2800 MPa.

The relatively low modulus of elasticity (26.46 GPa) observed in this study's UHPC mix can be attributed to the absence of coarse aggregate, as the mixture was composed solely of fine aggregate (maximum size 1 mm) and a high binder content. Although UHPC typically exhibits superior compressive strength compared to conventional concrete, its elastic modulus is more strongly influenced by the stiffness and volume fraction of the aggregates than by compressive strength alone. Previous studies have shown that UHPC containing only fine quartz sand can have a modulus of around 48 GPa, while the inclusion of stiffer coarse aggregates such as basalt or bauxite split can increase the modulus by approximately 21 %–46 %, reaching up to 70 GPa (Ma et al., 2004). Thus, the use of only fine aggregate in the current mix resulted in a more deformable matrix, explaining the lower measured elastic modulus.

16-mm deformed rebars (DB16) were used to manufacture the beam. The average yield and ultimate loads for this rebar were measured at 108.63 kN and 126.33 kN, respectively. The average yield stress (f_y) and ultimate stress (f_u) were thus 565.94 MPa and 658.13 MPa, respectively, with an elastic modulus equal to 201,830 MPa.

2.2. Preparation of full-scale samples

The full-scale test involved evaluating the connection joints of precast concrete beam-column members under static loads. The test began with the casting of a column specimen and 2 cantilever beam specimens. The column had a cross-section of 0.20 × 0.20 m^2 and a height of 0.40 m, and the beam had a cross-section of 0.20 × 0.40 m^2, extending 2.00 m from the column, as illustrated in Fig. 3. The test comprised six connection conditions, including one with a traditional beam-column concrete connection and five with specialized UHPC connections, as summarized in Table 2.

For the five UHPC connection conditions, after casting the beam and column specimens by normal concrete, all test specimens were immediately covered with plastic sheets and cured at room temperature for 48 h before being demolded. The specimens were then stored at room temperature until the target curing time was reached. The beam and column specimens were cured more for 19 days using water sprinkling before being assembled at connections filled with UHPC. The entire assembly was then cured for an additional 7 days, ensuring that the beam-column specimens were cured for a total of 28 days and the UHPC was cured for 7 days. The rebars of the beam specimens embedded in the UHPC connection joints were configured with varying lap-splice lengths (L_1) and hook lengths (L_2), maintaining a spacing (s) of 1 (measured as the center-to-center distance between bars). In cases where the rebars are non-overlapping ($s \geq 4D$), the embedment length (L_e) was evaluated both with and without hook lengths (L_2). Variations in the L_e, L_1 and L_2 configurations resulted in different failure modes, which were classified into two categories: Weak Joint (Samples No. 2–3) and Strong Joint (Samples No. 4–6). Weak Joints are characterized by insufficient lap-splice and hook lengths, leading to premature bond failure and reduced load-carrying capacity. In contrast, Strong Joints exhibit adequate lap-splice and hook lengths, providing superior bond performance and enabling the rebars to reach their failure tensile strength before failure.

For the full-scale tests, strain gauges were installed on the upper and lower rebars at the beam-column interface, with four points on each side. These gauges were used in every test to measure strain variations, which were then converted into tensile stresses to calculate the flexural moment capacity of the cross-section, as detailed in ACI-318 (ACI Committee, 2008). The steel rebars exhibited an average failure tensile strength (f_u) of 658.13 MPa. The test procedure involved the application of vertical static loads simultaneously at both ends of the cantilever beams using two 500 kN hydraulic jacks, each precisely controlled to increment the load by approximately 1 kN. As shown in Fig. 3, the experimental setup included three hydraulic jacks. The two side jacks were actively engaged in applying the test loads, while the central 200 kN hydraulic jack, positioned above the column, functioned solely as a support mechanism to stabilize the specimen and maintain the vertical alignment of the beam-column assembly under its self-weight. This central jack did not apply any active load during the test, thereby allowing the structural response of the beam-column connections to be assessed under well-defined loading conditions. The deliberate omission of axial loading on the column was intended to isolate the mechanical behavior and failure mechanisms of the connection itself, independent of axial force effects (Bjorhovde et al., 1999). Following each load increment, the test was paused for approximately 1 min to allow strain readings to stabilize and for data acquisition to be completed. This controlled, step-by-step loading protocol ensured accurate and consistent monitoring of strain distribution within the reinforcement. The following comparisons were then made.

- The actual flexural moment obtained from the test (calculated as force multiplied by the distance from the edge of the column to the point of loading) was compared with the flexural moment calculated from the tensile force of the rebars, as measured by the strain gauges.
- The bond strength of the rebars obtained from the full-scale test was compared with the predicted bond strength calculated using Equations (1)–(3).

The beam-column connection test comprised six samples, defined as follows.

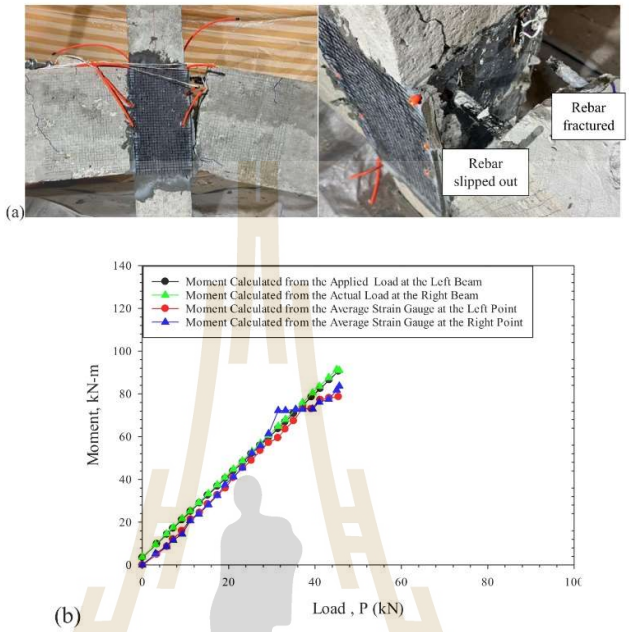

Fig. 8. Lap-splicing without hook joint (LS8: Strong joint, $L_1 = 8D$) sample: (a) Failure of the sample, (b) Relationship between the moment calculated from the average strain gauge and the applied load.

- **Sample No.1-TCIP:** Traditional cast-in-place beam-column joint

The sample was fabricated by casting beam-column specimens in a standard construction manner, with the beam's rebars passing through the column. The sample was constructed from concrete cast uniformly through the entire sample. Following a 28-day curing period, testing commenced. Details of the steel reinforcement and strain-gauge installation are illustrated in Fig. 4.

- **Sample No. 2-LE4:** Non-overlapping without hook joint (Weak joint, $L_e = 4D$)

A full-scale test sample was cast and assembled, without any lap-splicing in the joint area (rebars embedded in the joint were shorter than half of the column width). The embedded length of the beam's rebars in the joint (L_e) was 64 mm (4*D* of DB16). Details are shown in Fig. 5(a).

- **Sample No. 3-LE4+H3:** Non-overlapping with hook joint (Weak joint, $L_e = 4D$ and $L_2 = 3D$)

The test sample was prepared by casting separate beam and column components and then assembling them, with hook rebars embedded into the beam-column joint area. The embedded straight length of the beam's rebars (L_e) was 64 mm (4*D* of DB16), and the hook length (L_2) was 48 mm (3*D* of DB16). Details are shown in Fig. 5(b).

- **Sample No. 4-LS8:** Lap-splicing without hook joint (Strong joint, $L_1 = 8D$)

The test sample was cast and assembled with straight lap-splicing of the rebars in the joint area. The lap splice length of the beam's rebars was 128 mm (8*D* of DB16). Details are shown in Fig. 5(c).

- **Sample No. 5-LS8+H4:** Lap-splicing with hook joint (Strong joint, $L_1 = 8D$ and $L_2 = 4D$)

The samples were cast and assembled with lap-splice and hook rebars in the joint area. The lap splice length of the beam's rebars (L_1) was 128 mm (8*D* of DB16), and the hook length (L_2) was 64 mm (4*D* of DB16). Details of the reinforcement and lap-splicing are shown in Fig. 5(d).

- **Sample No. 6-LS9:** Lap-splicing without hook joint (Strong joint, $L_1 = 9D$)

The test sample was prepared by casting separate beam and column components and then assembling them with straight lap-splicing of the rebars in the beam-column joint area. The lap splice length of the beam's rebars (L_1) was 144 mm (9*D* of DB16). Details of the reinforcement are shown in Fig. 5(e).

In the UHPC joint (Fig. 5), specific portions of the rebars were either embedded without overlapping or lap spliced, while other sections were intentionally insulated using black Scotch VM Tape. This insulation ensures that no bond occurs between the rebars and the surrounding UHPC in the taped regions. By isolating these areas, the study focused on the bond performance only in the designated sections, allowing for a controlled and accurate analysis of the bond behavior as scheduled. This approach prevented unintended bonding outside the target area and ensured the reliability of the experimental results. The reinforcement

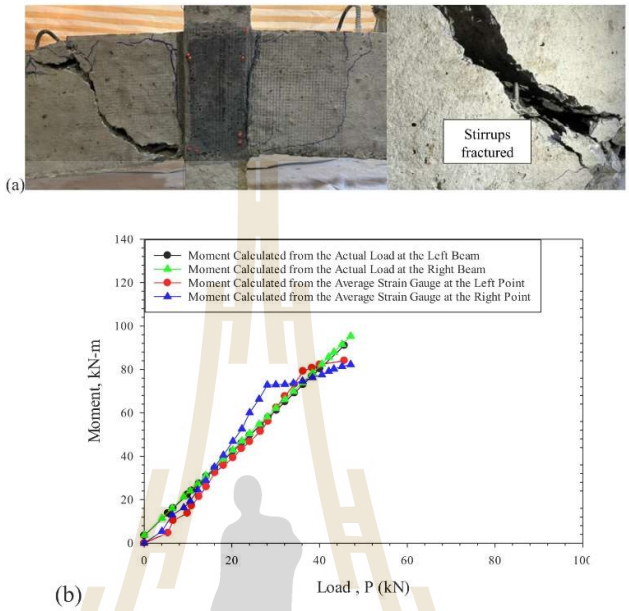

Fig. 9. Lap-splicing with a hook joint (LS8–H4: Strong joint, $L_1 = 8D$ and $L_2 = 4D$) sample: (a) Failure of the sample, (b) Relationship between the moment calculated from the average strain gauge and the applied load.

arrangement details for the beam-column samples No. 1–5 are shown in Fig. 6(a), featuring RB6 stirrups spaced at 0.15 m for both the beam and column. In contrast, Fig. 6(b) depicts the reinforcement arrangement to prevent shear failure in the beams of sample No. 6, with RB6 stirrups at 0.15 m for the column and RB9 stirrups at 0.10 m for the beam.

3. Results

Table 3 provides a comprehensive summary of the measured parameters from all full-scale samples (Samples No. 1–6), including applied loads, tensile strains, and bending moments calculated from applied loads and strains. The moment calculated from the maximum applied load indicates the corresponding maximum bending moment at the critical section of the beam-column connection. Measured strains using stain gauges display the deformation in the tested rebars, and the corresponding stresses in the rebars are converted from the measured strain. Finally, the bending moments were calculated using the ACI equation (ACI Committee, 2008); they provides valuable insights into the structural behavior of the connections under applied loads, enhancing the understanding of the integrity and failure mechanisms for each test condition.

3.1. Traditional cast-in-place beam-column joint (Sample No. 1-TCIP)

The failure at the connection, depicted in Fig. 7(a), was notably attributed to flexural moment with no track of shear failure, due to insufficient number of tensile rebars. The comparison of moments calculated from the applied loads and strain measurements, from the initial application of the loads to their maximum, is depicted in Fig. 7(b). The results revealed that the average maximum flexural moments calculated from the maximum load and strain were 93.25 kN-m and 80.10 kN-m, respectively. Though the rupture of rebars were not observed, the tensile stress in all four rebars exceeded the yield point with large deformation. This indicates that the test beam was designed under under-reinforced condition (Kartal et al., 2021; Liu et al., 2022; Mohammadhassani et al., 2014; Said et al., 2021), where failure did not occur due to the compression rupture of concrete, but rather due to the large elongation of the rebars beyond their yield limit. This caused the concrete above the top rebars, which has a low tensile strength, to crack and ultimately fail.

3.2. Strong joint configuration

3.2.1. Lap-splicing without hook joint (Sample No. 4-LS8)

For lap-splicing without hook joint (Strong joint, $L_1 = 8D$) sample, the observed failure after the test and the moments calculated from the applied loads and measured strains during the test are depicted in Fig. 8. One of the tensile rebars was found to fail, while another had slipped out. Since the test was conducted until the rebars failed, the tensile stress used in calculating the threshold lap-splice length without hook joint is the value at the rupture ($f_{it} = 658.13$ MPa). Using Equation (1) with $s = 1$, $\phi = 0.75$, and $\tau_{bond} = 0.75 \times 27.92 = 20.94$ MPa and applying Equation (2), the threshold lap-splicing length of rebars at rupture state was determined as follows:

$$\frac{L_1}{D} = \frac{f_s}{4\,(\tau_{bond})} = \frac{658.18}{4\,(20.94)} = 7.86$$

In this experiment, $L_1/D = 8$ was used, which is close to the value obtained from Equation (2). This length resulted in slippage and rupture of rebars occurring simultaneously. It was evident that this calculation was

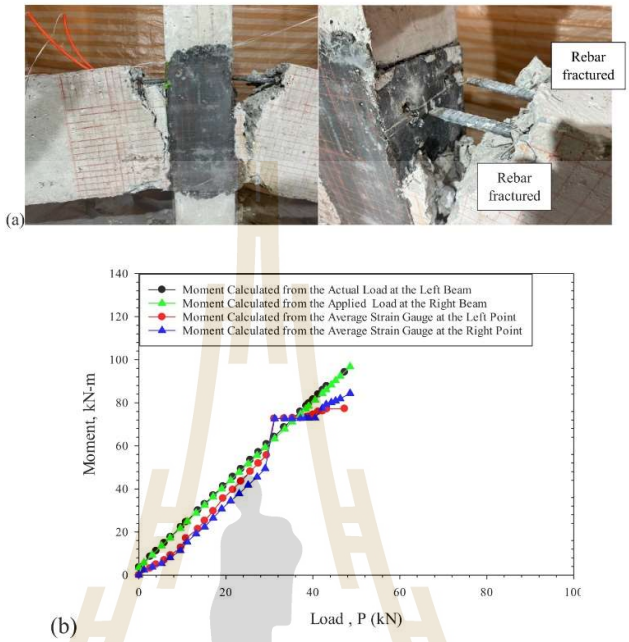

Fig. 10. Lap-splicing without hook joint (LS9: Strong joint, $L_1 = 9D$) sample: (a) Failure of the sample, (b) Relationship between the moment calculated from the average strain gauge and the applied load.

consistent with the failure of the joint, where one rebar slipped out and another one fractured.

3.2.2. Lap-splicing with hook joint (Sample No. 5-LS8+H4)

For lap-splicing with hook joint (Strong joint, $L_1 = 8D$ and $L_2 = 4D$), the observed failure after the test and the bending moments generated at the joint interface during the test are depicted in Fig. 9. Unlike the previous observations, the failure occurred in the beam rather than at the joint interface, attributed to the shear failure. The failure initiated with a shear at the junction between the beam and column, which was subsequently followed by the failure of the stirrups. The inclusion of the hook (L_2) in this case where the lap splice length exceeded the development length would typically indicate the rupture failure of rebars if the bending moment was dominant. In other words, in this experiment, shear failure was observed to be dominant without the rupture of rebars. The shear resistance of the beam can be calculated using the ACI (Standard, 2011) equation as follows:

$$V_n = V_c + V_s = 0.53bd\sqrt{fc'} + A_v f_y d/s$$

The properties of the stirrups used in the research, RB6-SR24, included a cross-sectional area of 28.2 mm^2, a yield tensile stress (f_y) of 240 MPa, and a stirrup spacing (s) of 150 mm.

Thus, $V_n = 0.17(200)(361)(\sqrt{43.91}) + (2)(28.2)(240)(361)/(150)$

$$V_n = 81.33 + 32.58 = 113.91 \text{ kN}$$

The calculated shear resistance was greater than the shear force applied at the beam-column interface, which was 45.62 kN. Initial shear failure occurred at the beam-column joint, followed by stirrup failure (Fig. 9(a)). This implied that the ACI's equation to calculate the shear resistance was overestimated. This might be because the ACI's equation assumes monolithic casting of beams and columns, which does not account for the weakness at the joint. This suggests that using UHPC for beam connections requires stirrups with approximately 2.5 times greater cross-sectional area than what is calculated using the ACI equation.

3.2.3. Lap-splicing without hook joint (Sample No. 6-LS9)

In this test, the size of the stirrups was increased to RB9 and the spacing was reduced to 100 mm. The lap splice length (L_1) was 144 mm (9D of DB16). After completing the test, the observed failure, shown in Fig. 10(a), indicated that both top rebars fractured under tensile stress without any stirrup failure. According to Equation (1), the bond strength of the rebar ($\phi_1 = 0.75$) could be calculated as follows:

$$\tau_{bond} = 0.75 \text{ x } 11.64\sqrt{\frac{fc'}{D}} = 0.75 \text{ x } 11.64\sqrt{\frac{92.05}{16}} = 20.94 \text{ MPa}$$

Therefore, the maximum bond force was:

$$\text{Bond force } (F_{bond}) = \tau_{bond}\, \pi\, D\, L = (20.94)(\pi)(16)(16\text{x}9) = 151.35 \text{ kN}$$

which was greater than the tensile force at the point of failure of the rebars:

$$\text{Tensile force } (F_s) = f_s \frac{\pi}{4} D^2 = (658.13)(201) = 132.29 \text{ kN}$$

This calculation is consistent with the test results, indicating that the reinforcement failed without slipping out of the concrete.

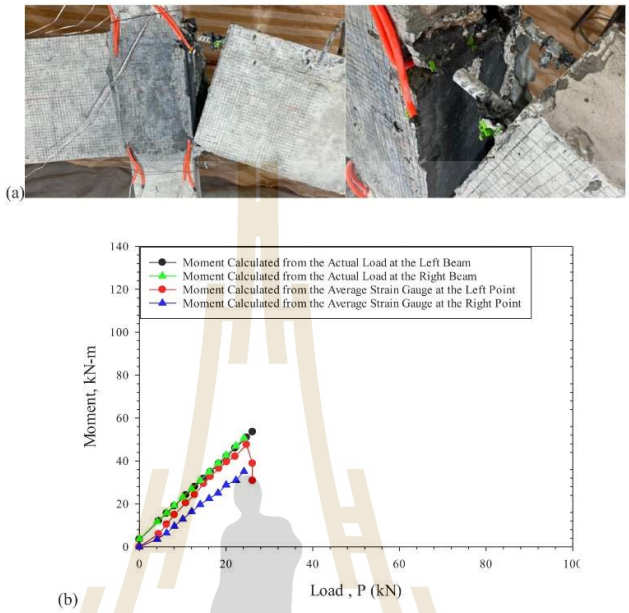

Fig. 11. Non-overlapping without hook joint (LE4: Weak joint, $L_e = 4D$) sample: (a) Failure of the sample, (b) Relationship between the moment calculated from the average strain gauge and the applied load.

3.3. Weak joint configuration

3.3.1. Non-overlapping without hook joint (Sample No. 2-LE4)

For non-overlapping without hook joint (Weak joint, L_e = 4D) sample, failure occurred at the interface between the column and beam (Fig. 11(a)), where both top rebars slipped out from the UHPE connection. In other words, the failure was due to insufficient embedment length of the rebars. The comparison of moments derived from the applied loads and measured strains, spanning from the initial loading to the peak load, is illustrated in Fig. 11(b). To verify the applicability of the bond strength equation, the tensile force (Fs) in the rebars calculated from the measured strain (data from Table 3) was compared with the maximum bond force (F_{bond}) calculated using Equation (1). At a measured maximum f_s = 379.57 MPa, and with a cross-sectional area of the rebars during applied loading being assumed to be constant and equal to 201 mm^2, F_s was then calculated as:

$$\text{Tensile force } (Fs) = f_s \frac{\pi}{4} D^2 = (379.57)(201) = 76.34 \text{ kN}$$

τ_{bond} predicted from Equation (1) was 27.92 MPa (f_c' of UHPC at 7-day = 92.05 MPa) using an L_e/D ratio of 3.5, instead of 4.0. This reduction in input L_e/D was the correction due to the placement of the column's rebars passing through the beam's rebars at the joint caused the beam's rebars on either side to be positioned closer to the column's rebars, resulting in a reduced bonding surface between the beam's rebars and the UHPC. Therefore,

$$\text{Bond force } (F_{bond}) = \tau_{bond}\, \pi\, D\, L_e = (27.92)(\pi)(16)(16\text{x}3.5) = 78.58 \text{ kN}$$

It was observed that the F_{bond} predicted by Equation (1) was very close to the F_s calculated from the measured strain, with a discrepancy of only 2.93 %. In addition, the predicted F_{bond} was found to be less than the rupture tensile force of the rebars (126.33 kN), indicating the reinforcement being failed by slipping out due to insufficient bond resistance.

3.3.2. Non-overlapping with hook joint (Sample No. 3-LE4+H3)

For non-overlapping with hook joint (Weak joint, $L_e = 4D$ and $L_2 = 3D$), failure occurred at the interface between the column and beam. The maximum applied loads were 22.37 kN for the left beam and 22.17 kN for the right beam, as shown in Fig. 12. The rebars slipped out of the joint, and the UHPC material experienced fracturing and separating, indicating that the failure was due to insufficient embedment length. To verify that Equation (1) can be used to determine the bond strength of non-overlapping rebars with hook at the joint, the maximum tensile force in rebars and the maximum bond force (F_{bond}) predicted using Equation (3) were compared. With a maximum tensile stress of 435.86 MPa and the assumed constant cross-sectional area of rebars of 201 mm^2, the maximum tensile force was calculated as:

$$\text{Tensile force } (F_s) = f_s \frac{\pi}{4} D^2 = (435.86)\,(201) = 87.63 \text{ kN}$$

Meanwhile, the maximum bond force predicted using Equation (3), with $\phi_1 = 1$, $\phi_2 = 1$, $k = 0.2$, τ_{bond} = 27.92 MPa, $L_e/D = 3.5$, and $L_2/D = 3$, was as follows:

$$\text{Bond force } (F_{bond}) = (\phi_1 L_e + k\phi_2 L_2)\tau_{bond}\pi D$$
$$= [(1)(56) + (0.20)(1)(48)]\text{x}\,(27.92)(\pi)(16)$$
$$= 92.06 \text{ kN}$$

It was evident that F_{bond} was close to F_s, with a discrepancy of 5.1 %, indicating the applicability of Equation (3) in practice.

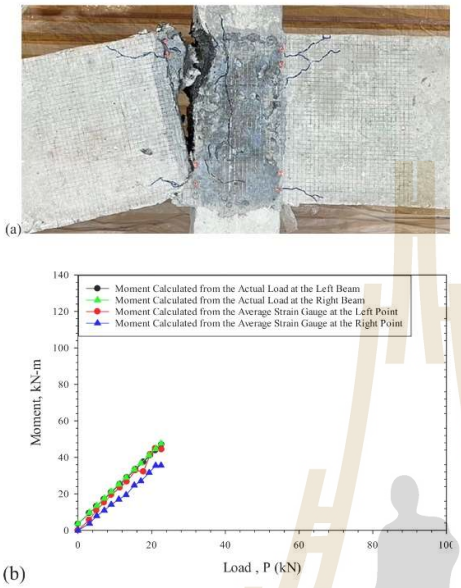

Fig. 12. Non-overlapping with a hook joint (LE4+H3: Weak joint, $L_e = 4D$ and $L_2 = 3D$) sample: (a) Failure of the sample, (b) Relationship between the moment calculated from the average strain gauge and the applied load.

3.4. Failure characteristics of traditional joint and UHPC strong joint

The traditional beam-column joint can withstand an average bending moment (on both sides) of 93.25 kN-m (Fig. 13(a)). When comparing the test results of the beam-column joints using UHPC in the case of Strong Joint (Samples 4–6), the following findings could be illustrated.

1. **Sample No. 4-LS8:** Full-scale sample of lap-splicing without hook joint (strong joint, $L_1 = 8D$): Using RB6 stirrups spaced at 0.15 m, the joint could withstand an average bending moment (on both sides) of 91.13 kN-m (Fig. 13(b)), which was close to the traditional beam-column joint (with a deviation of only 2.31 %).
2. **Sample No. 5-LS8+H4:** Full-scale sample of lap-splicing with hook joint (strong joint, $L_1 = 8D$, $L_2 = 4D$): Using RB6 stirrups spaced at 0.15 m, the joint could withstand an average bending moment (on both sides) of 92.8 kN-m (Fig. 13(c)), which is close to the traditional beam-column joint (with a deviation of only 0.53 %).
3. **Sample No. 6-LS9:** Full-scale sample of lap-splicing without hook joint (strong joint, $L_1 = 9D$): Using RB9 stirrups spaced at 0.10 m, the joint could withstand an average bending moment (on both sides) of 94.76 kN-m (Fig. 13(d)), which was close to the traditional beam-column joint (with a deviation of only 1.58 %).

The beam-column joint systems in all three cases mentioned above (Strong Joint) had the capability to withstand bending moments comparable to the traditional beam-column joint, with deviations not exceeding 2.31 %. All three cases were designed in the condition of under-reinforced section. The rebars at the strain gauge installation point reached the yield state and exhibited very large strain with their measured tensile stresses being greater than 599.04 MPa. These test results demonstrated that the design of rebars' lengths using the bond strength obtained from Equation (1), $\tau_{bond} = \phi 11.64\sqrt{\frac{f'_c}{D}}$, is rational and practical.

The severity of damage after failure differed significantly between the traditional beam-column joint (Sample No. 1) and UHPC joints (Samples No. 4–6), despite all being under-reinforced designs. Sample No. 1 exhibited severe and widespread damage, characterized by uncontrolled cracking at a 45-degree angle relative to the vertical plane and spalling caused by the yielding of the upper rebar, highlighting the stress distribution of traditional concrete. In contrast, UHPC joints showed localized damage due to enhanced bond strength and confinement from steel fibers. Sample No. 4 ($L_1 = 8D$) demonstrated 90-degree localized damage at the beam-joint interface, with one upper rebar fracturing and the other slipping out. Sample 5 ($L_1 = 8D$, $L_2 = 4D$) exhibited 45-degree localized damage with stirrup fracture due to insufficient shear capacity from wider stirrup spacing (0.15 m). Sample No. 6 ($L_1 = 9D$) showed improved performance with reduced stirrup spacing (0.10 m), confining damage at a 15-degree angle to upper rebar yielding and fracture, while stirrups remained intact, indicating enhanced shear resistance and bond performance in UHPC joints compared to traditional concrete.

In the case of weak joint testing (Fig. 14), the results indicate that Equation (1) can be used to calculate the maximum tensile stress (= bond strength) in the rebars during slippage from the concrete. The predicted maximum tensile stress closely matched the tensile stress derived from the strain gauge measurements. Therefore, it can be said that Equation (1) is highly accurate and can be used to calculate the flexural resistance for the weak beam-column joint.

4. Design scheme for rebars' length in UHPC connection joints

Based on the full-scale sample testing, this research developed a design scheme for beam cross-sections to resist target bending moments, along with determining the rebars' lengths in UHPC joints (Fig. 15). The most economic design is the condition where the rupture of rebars and slippage of rebars happens simultaneously at the design bending moment. In other words, the rebars' length must be sufficient until the rupture of rebars (Strong Joint).

Fig. 15 illustrates the suggested design steps to determine the length of rebars with various diameters to resist the target bending moment. The first step is to determine the beam dimension, number of rebars and diameter of rebars to resist the design bending moment at the specified material properties according to ACI 318-11 standards.

The next step is to determine the development length, L_d of rebars without lap-splicing for specified yield tensile strength (f_y) using Equation (2). If the calculated L_d is less than half the width of the column, the rebars are placed without splicing or hook with $L_e > L_d$.

If the calculated L_d exceeds half the width of the column, the lap-splicing or hook (in cases where the bond strength from lap splicing is insufficient) is required. The calculation starts with determining the lap-splice length (L_1). This L_1 is then compared with the actual space available in the structural element, which refers to the physical distance or length within the joint, where the overlapping rebars can be positioned. If the calculated L_1 is less than or equal to the actual space ($L_1 \leq$ actual space), the calculated L_1 can be used directly. However, if the calculated L_1 exceeds the actual space ($L_1 >$ actual space), the hook length (L_2) is required and determined using Equation (3) to enhance the bond stress of the reinforcement. The length L_2 must be at least $3D$.

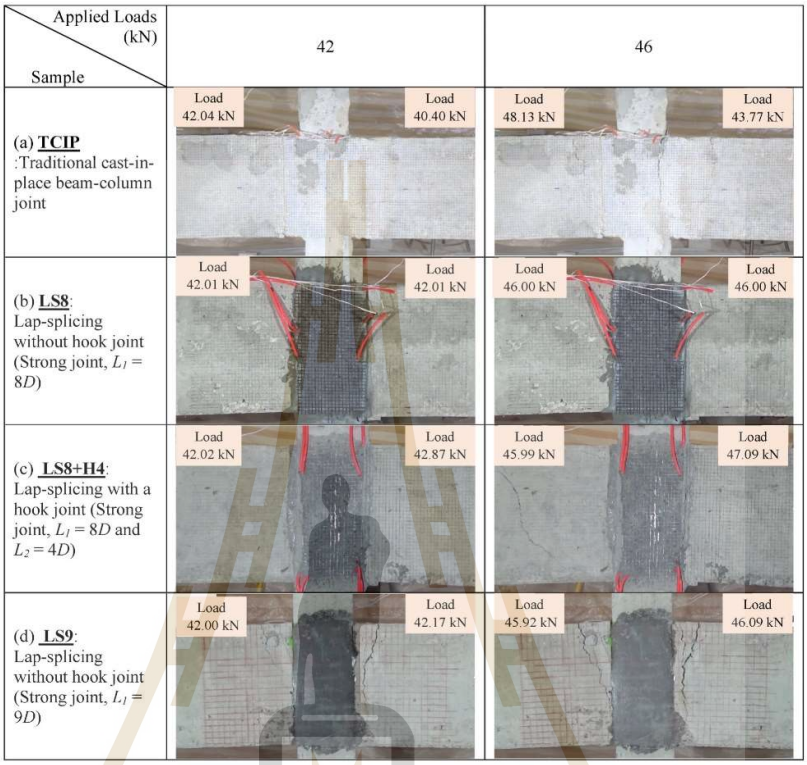

Fig. 13. Test results of the beam-column joints using UHPC in the case of Strong Joint.

4.1. Calculation Demonstration

4.1.1. Design lap-splice length without hook

f_c' = 92.05 MPa (UHPC at 7 days),
b = 0.20 m,
h = 0.40 m,
d = 0.37 m.
d' = 0.3 m

Tensile steel rebars: 2 – DB20 (As = 0.000628 m^2)
Compression steel rebars: 2 – DB20 (As' = 0.000628 m^2)
Yield strength (f_y) = 504 MPa.
Ultimate tensile strength (f_u) = 611 MPa.

Step 1 Design lap-splice length, L_1 (ϕ_1 = 0.75)

$$\tau_{bond} = 11.64\sqrt{\frac{f_c'}{D}} = 11.64\sqrt{\frac{92.05}{20}} = 24.97 \text{ MPa}$$

$$L_1 = \frac{f_y D}{4\phi_1 \tau bond} = \frac{(504)(20)}{(4)(0.75)(24.97)}$$

= 134.56 mm > 4D (4x20 = 80 mm)
Use L_1 = 135 mm

Step 2 Calculate the resisting moment

$$M_n = (A_s - A_s')f_y\left(d - \frac{a}{2}\right) + A_s' f_y (d - d')$$

$$= (0.000628)(504\text{x}1000)(0.37\text{-}0.03) = 107.61 \text{ kN} - \text{m}$$

Check

Bond force (F_{bond}) = $\phi_1 \tau_{bond} \pi D L$ = (0.75)(26.03)(π)(20)(130) = 159.46 kN

Tensile yield force (F_y) = $f_y \frac{\pi}{4} D^2$

= (504x1000)(0.000314)

= 158.26 kN < Bond force (F_{bond})

4.1.2. Design lap-splice length with hook

f_c' = 92.05 MPa (UHPC at 7 days),
b = 0.20 m,
h = 0.40 m,
d = 0.37 m,
d' = 0.3 m

Tensile steel rebars: 2 – DB20 (As = 0.000628 m^2)
Compression steel rebars: 2 – DB20 (As' = 0.000628 m^2)

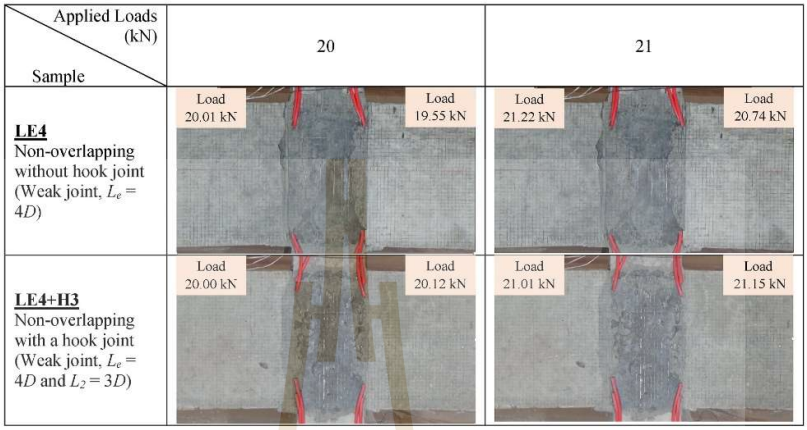

Fig. 14. Test results of the beam-column joints using UHPC in the case of Weak Joint.

Yield strength (f_y) = 504 MPa.
Ultimate tensile strength (f_u) = 611 MPa.

Step 1.1 Design lap-splice length, L_1 ($\phi_1 = 0.75$)

$$\tau_{bond} = 11.64\sqrt{\frac{f_c}{D}} = 11.64\sqrt{\frac{92.05}{20}} = 24.97 \text{ MPa}$$

$$L_1 = \frac{f_y D}{4\phi_1 \tau bond} = \frac{(504)(20)}{(4)(0.75)(24.97)}$$
$$= 134.56 \text{ mm} > 4D \text{ (4x20 = 80 mm)}$$

If the available space is 100 mm, Select Use L_1 = 100 mm and provide an additional hook length (L_2) to ensure sufficient bond strength.

Step 1.2 Design the hook length, L_2 ($\phi_2 = 1$)

$$L_2 = \frac{f_y D - \phi_1 4\tau_{bond} L_1}{\phi_2 4k\tau_{bond}} = \frac{(504)(20) - (0.75)(4)(24.97)(100)}{(1)(4)(0.20)(24.97)}$$
$$= 129.60 \text{ mm} > 3D \text{ (3x20 = 60 mm)}$$

Use L_2 = 130 mm.

Step 2 Calculate the resisting moment

$$Mn = (A_s\text{-}A_s')f_y\left(d - \frac{a}{2}\right) + A_s' f_y (d\text{-}d')$$
$$= (0.000628)(504x1000)(0.37\text{-}0.03)$$
$$= 107.61 \text{ kN} - \text{m}$$

Check

Bond force (F_{bond}) = $(\phi_1 L_1 + k\phi_2 L_2)\tau_{bond}\pi D$
$$= [(0.75)(100) + (0.20)(1)(130)](24.97x1000)(\pi)(20)$$
$$= 158.46 \text{ kN}$$

Tensile yield force (F_y) = $f_y \frac{\pi}{4} D^2$
$$= (504x1000)(0.000314)$$
$$= 158.26 \text{ kN} < \text{Bond force } (F_{bond}).$$

The design scheme for rebars' length proposed in this study is specifically formulated for UHPC connections, taking into account the material's exceptional bond strength and mechanical properties-particularly its dense matrix and inclusion of steel fibers. These characteristics significantly enhance the bond between concrete and reinforcement, resulting in considerably shorter required development and lap splice lengths compared to conventional reinforced concrete (RC) connections. Design methods traditionally developed for RC are based on the behavior of normal-strength concrete, which exhibits relatively lower bond strength, increased porosity, and limited tensile capacity. As a result, such methods typically recommend long development and lap splice lengths to ensure adequate load transfer and structural integrity. However, directly applying these conservative RC-based design provisions to UHPC would not only be inefficient in terms of material use and construction cost, but would also fail to capture the full potential of UHPC's superior bond characteristics.

Moreover, the behavior of UHPC joints under load is fundamentally different from RC joints due to the enhanced confinement, energy absorption, and tensile performance contributed by steel fibers. These differences necessitate a separate design approach. The proposed scheme in this study is experimentally validated using full-scale testing, which captures realistic structural behavior under service conditions. It aims to achieve a ductile failure mode, in which bar rupture and bond slippage occur nearly simultaneously-a balance that optimizes both safety and material efficiency. This research is thus essential, as it provides a rational and performance-based design methodology tailored to UHPC, which has been lacking in current design codes. Without such schemes, engineers are left either overdesigning UHPC joints using outdated RC assumptions or relying on conservative empirical judgment. The findings from this study not only close a critical knowledge gap but also support the wider adoption of UHPC in precast and cast-in-place structural systems by offering practical, safe, and cost-effective design guidance.

To verify the accuracy and applicability of the proposed design process, the manuscript presents detailed example calculations and comparative analyses between theoretical predictions and full-scale experimental results. Equations (1)–(3) were employed to predict bond strength and bond force by incorporating UHPC compressive strength, rebar diameter, and embedment configurations, including lap-splice and hook lengths. The validity of these equations was assessed through direct comparison with tensile forces obtained from strain

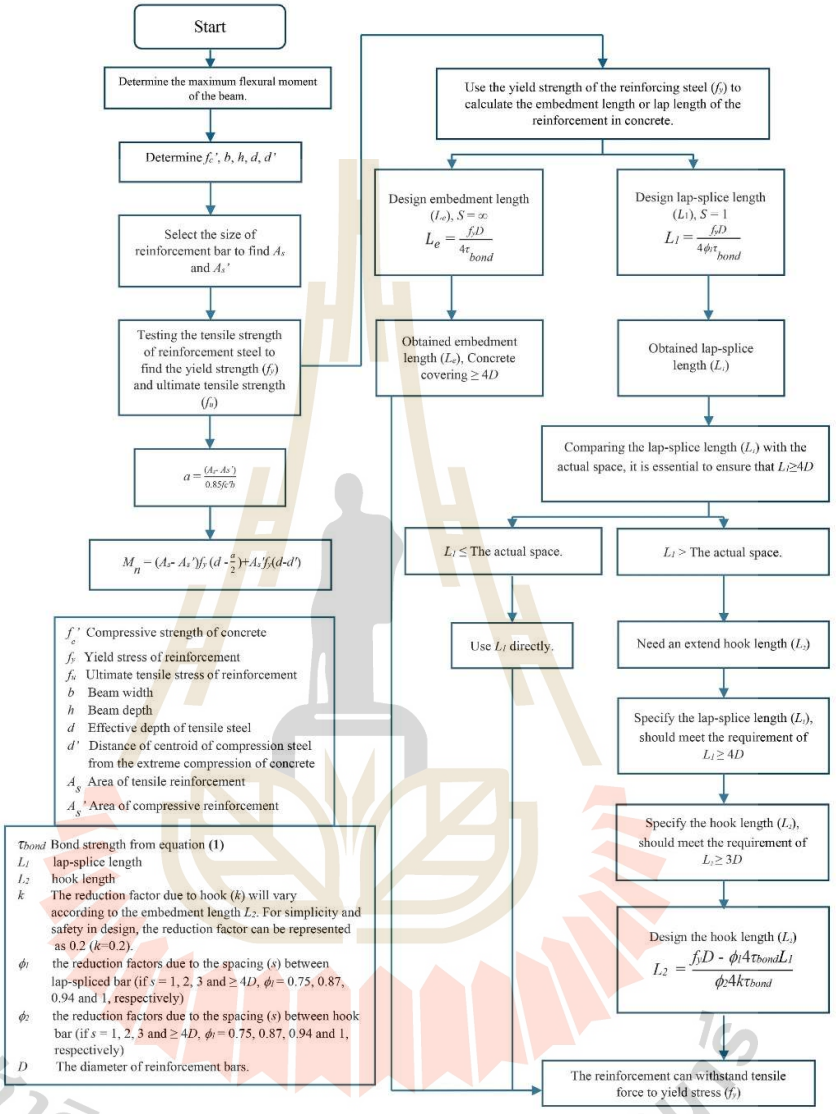

Fig. 15. Design scheme for embedment length or lap splice length in UHPC joints.

gauge measurements in full-scale specimens. In **Sample No. 2-LE4**, the calculated tensile force was 76.34 kN, while the predicted bond force was 78.58 kN, resulting in a deviation of only 2.93 %. Similarly, in **Sample No. 3-LE4+H3**, the measured tensile force of 87.63 kN closely matched the predicted bond force of 92.06 kN, with a deviation of 5.1 %. Furthermore, predictions of lap-splice lengths based on Equation (2) aligned with observed failure behaviors. For example, in **Sample No. 4-LS8**, the predicted lap-splice ratio (L_1/D = 7.86) corresponded well with

the test value of 8*D*, where both rebar rupture and slippage were observed. In **Sample No. 6-LS9**, the predicted bond force (151.35 kN) exceeded the measured tensile force at rupture (132.29 kN), confirming that failure occurred through bar fracture rather than pull-out.

In addition, the shear failure observed in **Sample No. 5- LS8+H4** was investigated by comparing the experimental shear resistance with that calculated using the ACI equation. The results suggested that the ACI method, which assumes monolithic construction, may overestimate the shear capacity of precast UHPC joints. Therefore, it is recommended that the stirrup reinforcement in such joints be increased by approximately 2.5 times to ensure adequate shear resistance. The design scheme presented in Section 4 and Fig. 15 integrates these theoretical and experimental findings into a practical and rational procedure for determining required rebar lengths and configurations. This scheme effectively addresses structural performance requirements while maintaining construction efficiency and safety. The comparison between predictions and observed test data confirms the robustness of the proposed method across various failure modes, including rebar pull-out, rupture, and shear failure.

5. Conclusions

Based on the experiments conducted in this study, the following conclusions can be drawn:

The full-scale sample testing confirmed that using UHPC for beam-column joints can enable the beam-column structure to withstand loads and exhibit failure characteristics comparable to traditional construction methods. The strong joint was manufactured with two configurations of 16-mm deformed rebars including lap splicing without hook of $L_1 = 9D$ (14.4 cm), and lap splicing with hook of $L_1 = 8D$ and $L_2 = 4D$. These configurations allowed the UHPC beam-column joints to resist bending moments until the rebars reached the failure state (565.94 MPa) and subjected to large deformation, which is the ductile failure characteristic desired in reinforced concrete structure design.

However, caution should be taken for the weak joint with insufficient rebars' length. For example, the non-overlapping with hook joint (Weak Joint, $L_e = 4D$ amd $L_2 = 3D$) and the non-overlapping without hook joint (Weak Joint, $L_e = 4D$) both exhibited sudden and hazardous failure.

The design scheme for rebars' length resulting from this project is as follows: initially, the yield tensile stress (f_y) of the rebars is used to calculate the L_d of rebars without lap-splice using Equation (1). If the calculated L_d is less than half the width of the column, the rebars are placed without lap splicing using $L_e > L_d$. However, if the L_d exceeds half the width of the column, the lap splicing is required. If the calculated lap splice length (L_1) is less than or equal to the actual space ($L_1 \leq$ actual space), the calculated L_1 can be used in the design. If the calculated L_1 is greater than the actual space, the hook length (L_2) must be added to enhance the bond strength of the reinforcement using Equation (3); the length L_2 must be at least 3*D*.

The findings of this project underscore the efficacy of utilizing UHPC for precast beam-column joints. This innovative method enables the design of precast structural elements as continuous beams, rather than simple beams, thereby enhancing bending moment resistance and reducing the required amount of rebars. Manufacturing precast beam-column elements in a controlled factory setting and subsequently assembling them on-site offers several advantages. It reduces labor costs, minimizes the need for formwork and shoring, and expedites the construction process. Notably, UHPC achieves its high strength within just 7 days, compared to the traditional 28-day curing period. This significant reduction in curing time accelerates construction schedules while ensuring structural safety equivalent to conventional methods.

CRediT authorship contribution statement

Krairerk Aiamsri: Writing – original draft, Validation, Methodology, Investigation, Data curation. **Teerasak Yaowarat:** Writing – original draft, Visualization, Validation, Supervision, Resources, Project administration, Methodology, Investigation, Conceptualization. **Suksun Horpibulsuk:** Writing – review & editing, Visualization, Supervision, Resources, Project administration, Funding acquisition, Conceptualization. **Apichat Suddeepong:** Validation, Supervision, Resources, Investigation. **Apinun Buritatum:** Visualization, Validation, Resources. **Artit Udomchai:** Writing – original draft, Resources, Methodology, Investigation. **Kirati Nitichote:** Visualization, Investigation, Funding acquisition, Conceptualization.

Declaration of competing interest

The authors declare that they have no known competing financial interests or personal relationships that could have appeared to influence the work reported in this paper.

Acknowledgements

This work was financially supported by the Concrete Products and Aggregate Co., Ltd. (CPAC), Thailand, Suranaree University of Technology and Thailand Science Research and Innovation.

Data availability

Data will be made available on request.

References

A. Standard, C33, 2003. Standard Specification for Concrete Aggregates. ASTM international West, Conshohocken, PA, USA, C.

ACI Committee, 2008. Building Code Requirements for Structural Concrete (ACI 318-08) and Commentary. American Concrete Institute.

Aiamsri, K., Yaowarat, T., Horpibulsuk, S., Suddeepong, A., Buritatum, A., Hiranwatthana, K., Nitichote, K., 2024. Bonding behavior of lap-spliced reinforcing bars embedded in ultra high-performance concrete with steel fibers. Developments in the Built Environment 20, 100585.

Aktan, A.E., Farhey, D.N., Helmicki, A.J., Brown, D.L., Hunt, V.J., Lee, K.-L., Levi, A., 1997. Structural identification for condition assessment: experimental arts. J. Struct. Eng. 123 (12), 1674–1684.

Alampalli, S., Frangopol, D.M., Grimson, J., Halling, M.W., Kosnik, D.E., Lantsoght, E.O., Yang, D., Zhou, Y.E., 2021. Bridge load testing: state-of-the-practice. J. Bridge Eng. 26 (3), 03120002.

Alkaysi, M., El-Tawil, S., 2017. Factors affecting bond development between Ultra High Performance Concrete (UHPC) and steel bar reinforcement. Constr. Build. Mater. 144, 412–422.

Anvari, B., Angeloudis, P., Ochieng, W.Y., 2016. A multi-objective GA based optimisation for holistic Manufacturing, transportation and Assembly of precast construction. Autom. ConStruct. 71, 226–241.

Back, J. W., Park, H. G., Lee, B. S., Shin, H. M., 2018. Shear friction strength of low rise walls with 550 MPa (80 ksi) reinforcing bars under cyclic loading. ACI Struct. J. 115 (1).

Bahmani, H., Mostofinejad, D., 2022. Microstructure of ultra-high-performance concrete (UHPC)–a review study. J. Build. Eng. 50, 104118.

Bjorhovde, R., Goland, L., Benac, D., 1999. Tests of Full-Scale Beam-To-Column Connections. Southwest Research Institute, San Antonio, TX.

Cabral-Fonseca, S., Correia, J., Custódio, J., Silva, H., Machado, A., Sousa, J., 2018. Durability of FRP concrete bonded joints in structural rehabilitation: a review. Int. J. Adhesion Adhes. 83, 153–167.

Cai, G., Waldmann, D., 2019. A material and component bank to facilitate material recycling and component reuse for a sustainable construction: concept and preliminary study. Clean Technol. Environ. Policy 21, 2015–2032.

Chan, T.K., 2011. Comparison of precast construction costs—case studies in Australia and Malaysia. Proceedings of the 27th Annual ARCOM Conference, pp. 3–12. Bristol, UK.

Choi, H.-K., 2020. Parametric analysis on seismic performance of hybrid precast concrete beam-column joint. Adv. Civ. Eng. 2020 (1), 8856327.

Contento, A., Aloisio, A., Xue, J., He, J., Baseglielle, B., 2024. Ultra-high performance concrete beam-to-beam connections in continuous bridges: experimental full-scale tests, FE analyses and design. Eng. Struct. 316, 118594.

Du, J., Meng, W., Khayat, K.H., Bao, Y., Guo, P., Lyu, Z., Abu Obeidah, A., Nassif, H., Wang, H., 2021. New development of ultra-high-performance concrete (UHPC). Compos. B Eng. 224, 109220.

Engindeniz, M., Kahn, L.F., Abdul-Hamid, Z., 2005. Repair and strengthening of reinforced concrete beam column joints: state of the art. ACI Struct. J. 102 (2), 1.

Farzad, M., Shafieifar, M., Azizinamini, A., 2019. Experimental and numerical study on bond strength between conventional concrete and Ultra High-Performance Concrete (UHPC). Eng. Struct. 186, 297–305.

Fehling, E., Schmidt, M., Walraven, J., Leutbecher, T., Fröhlich, S., 2014. Ultra-high Performance Concrete UHPC. Ernst & Sohn, Berlin, Germany, pp. 25–32.
Garetti, M., Taisch, M., 2012. Sustainable manufacturing: trends and research challenges. Prod. Plann. Control 23 (2–3), 83–104.
Ghayeb, H.H., Razak, H.A., Sulong, N.R., 2020. Performance of dowel beam-to-column connections for precast concrete systems under seismic loads: a review. Constr. Build. Mater. 237, 117582.
Hong, J., Shen, G.Q., Li, Z., Zhang, B., Zhang, W., 2018. Barriers to promoting prefabricated construction in China: a cost–benefit analysis. J. Clean. Prod. 172, 649–660.
Huang, Y., Grünewald, S., Schlangen, E., Luković, M., 2022. Strengthening of concrete structures with ultra high performance fiber reinforced concrete (UHPFRC): a critical review. Constr. Build. Mater. 336, 127398.
Hung, C. C., El Tawil, S., Chao, S. H., 2021. A review of developments and challenges for UHPC in structural engineering: behavior, analysis, and design. J. Struct. Eng. 147 (9), 03121001.
Kartal, S., Kalkan, I., Beycioglu, A., Dobiszewska, M., 2021. Load-deflection behavior of over-and under-reinforced concrete beams with hybrid FRP-steel reinforcements. Materials 14 (18), 5341.
Khayat, K.H., Meng, W., 2014. Design and Performance of Stay-In-Place UHPC Prefabricated Panels for Infrastructure Construction, Missouri University of Science and Technology. Center for Transportation ….
Küntz, M., Jolin, M., Bastien, J., Perez, F., Hild, F., 2006. Digital image correlation analysis of crack behavior in a reinforced concrete beam during a load test. Can. J. Civ. Eng. 33 (11), 1418–1425.
Liu, S., Wang, X., Ali, Y.M., Su, C., Wu, Z., 2022. Flexural behavior and design of under reinforced concrete beams with BFRP and steel bars. Eng. Struct. 263, 114386.
Lowes, L.N., Altoontash, A., 2003. Modeling reinforced concrete beam-column joints subjected to cyclic loading. J. Struct. Eng. 129 (12), 1686–1697.
Ma, J., Orgass, M., Dehn, F., Schmidt, D., Tue, N., 2004. Comparative investigations on ultra-high performance concrete with and without coarse aggregates. International Symposium on Ultra High Performance Concrete, pp. 205–212. Kassel, Germany.
Maya, L., Graybeal, B., 2017. Experimental study of strand splice connections in UHPC for continuous precast prestressed concrete bridges. Eng. Struct. 133, 81–90.
Meoni, A., D'Alessandro, A., Mattiacci, M., García-Macías, E., Saviano, F., Parisi, F., Lignola, G.P., Ubertini, F., 2024. Structural performance assessment of full-scale masonry wall systems using operational modal analysis: laboratory testing and numerical simulations. Eng. Struct. 304, 117663.
Mohammadhassani, M., Akib, S., Shariati, M., Suhatril, M., Khanouki, M.A., 2014. An experimental study on the failure modes of high strength concrete beams with particular references to variation of the tensile reinforcement ratio. Eng. Fail. Anal. 41, 73–80.
Molinari, M., Savadkoohi, A.T., Bursi, O.S., Friswell, M.I., Zonta, D., 2009. Damage identification of a 3D full scale steel–concrete composite structure with partial-strength joints at different pseudo-dynamic load levels. Earthq. Eng. Struct. Dynam. 38 (10), 1219–1236.
Mousavi, S.S., Dehestani, M., 2022. Influence of mixture composition on the structural behaviour of reinforced concrete beam column joints. A Review, Structures. Elsevier, pp. 29–52.
Parskiy, N., Molodtsov, M., Molodtsova, V., 2017. Cost effectiveness of precast reinforced concrete roof slabs. IOP Conference Series: Materials Science and Engineering. IOP Publishing, 012036.
Pokorný, P., Kolísko, J., Čítek, D., Kostelecká, M., 2020. Effect of elevated temperature on the bond strength of prestressing reinforcement in UHPC. Materials 13 (21), 4990.
Said, M., Shanour, A.S., Mustafa, T., Abdel-Kareem, A.H., Khalil, M.M., 2021. Experimental flexural performance of concrete beams reinforced with an innovative hybrid bars. Eng. Struct. 226, 111348.
Sev, A., 2009. How can the construction industry contribute to sustainable development? A conceptual framework. Sustain. Dev. 17 (3), 161–173.
Shishesaz, M., Hosseini, M., 2020. Effects of joint geometry and material on stress distribution, strength and failure of bonded composite joints: an overview. J. Adhes. 96, 1053–1121.
Somma, G., Pieretto, A., Rossetto, T., Grant, D.N., 2015. RC beam to column connection failure assessment and limit state design. Mater. Struct. 48, 1215–1231.
Standard, A., 2011. Building Code Requirements for Structural Concrete (ACI 318-11). American Concrete Institute.
Supaviriyakit, T., Pimanmas, A., 2008. Comparative performance of sub-standard interior reinforced concrete beam–column connection with various joint reinforcing details. Mater. Struct. 41, 543–557.
Tack, R., 2019. Flexural Response of Flat Plate Edge Slab-Column Connections. McGill University, Canada.
Ullah, R., Qiang, Y., Ahmad, J., Vatin, N.I., El-Shorbagy, M.A., 2022. Ultra-high-performance concrete (UHPC): a state of the art review. Materials 15 (12), 4131.
Wang, Z., Hu, H., Gong, J., 2018. Framework for modeling operational uncertainty to optimize offsite production scheduling of precast components. Autom. ConStruct. 86, 69–80.
Wen, C., Zhang, P., Wang, J., Hu, S., 2022. Influence of fibers on the mechanical properties and durability of ultra-high-performance concrete: a review. J. Build. Eng. 52, 104370.
Xue, W., Hu, X., Song, J., 2021. Experimental study on seismic behavior of precast concrete beam-column joints using UHPC-based connections. Structures. Elsevier, pp. 4867–4881.
Yoo, D.-Y., Kim, M.-J., 2019. High energy absorbent ultra-high-performance concrete with hybrid steel and polyethylene fibers. Constr. Build. Mater. 209, 354–363.
Yoo, D. Y., Kim, S., Kim, J. J., Chun, B., 2019. An experimental study on pullout and tensile behavior of ultra-high-performance concrete reinforced with various steel fibers. Constr. Build. Mater. 206, 46–61.
Yoo, D. Y., Sohn, H. K., Borges, P.H., Fediuk, R., Kim, S., 2020. Enhancing the tensile performance of ultra-high-performance concrete through strategic use of novel half-hooked steel fibers. J. Mater. Res. Technol. 9 (3), 2914–2925.
Zhang, J., Ding, C., Rong, X., Yang, H., Li, Y., 2020. Development and experimental investigation of hybrid precast concrete beam–column joints. Eng. Struct. 219, 110922.
Zhong, Y., Xiong, F., Chen, J., Deng, A., Chen, W., Zhu, X., 2019. Experimental study on a novel dry connection for a precast concrete beam-to-column joint. Sustainability 11 (17), 4543.
Zhou, Z., Qiao, P., 2018. Bond behavior of epoxy-coated rebar in ultra-high performance concrete. Constr. Build. Mater. 182, 406–417.

BIOGRAPHY

Mr.Kairerk Aiamsri was born on June 19, 1995. He obtained a Vocational Certificate in Construction and a Higher Vocational Certificate in Construction Technology from Nakhon Ratchasima Technical College. He later earned a Bachelor of Engineering degree in Civil Engineering from the Faculty of Engineering and Architecture, Rajamangala University of Technology Isan in 2018. In 2021, he completed a Master of Engineering degree in Civil Engineering at Suranaree University of Technology. Currently, he is pursuing a Doctor of Philosophy (Ph.D.) in Civil Engineering and Construction Management.